Exploring Block and Permeation of *N*-methyl-D-Aspartate (NMDA) Receptor Channels for Treatment of Neurodegenerative Disorders

Izuddin Fahmy Abu, BSc, MSc.

Thesis submitted to the University of Nottingham for the degree of

Doctor of Philosophy

November 2016

Abstract

N-methyl-D-aspartate receptors (NMDAR) are ionotropic glutamate receptors which can be blocked by Mg^{2+} in a voltage-dependent manner and are highly permeable to Ca^{2+}, hence they represent a medically relevant target for neurodegenerative disorders caused by excitotoxicity. The two main objectives of this study were, (i) to determine the impact of Q/R/N, +1 and -8 sites modification in the M2 pore region of GluN2A NMDAR subunit on Mg^{2+} block and other open channel blockers; and (ii) to evaluate novel multi-target-directed ligands (MTDL) for Alzheimer's disease therapy. The *Xenopus laevis* oocyte expression system was employed where NMDAR subunit cRNAs were injected into the oocytes and responses to NMDA/glycine and channel blockers were recorded using two-electrode voltage clamp (TEVC) electrophysiology.

Pore region mutations to investigate the impact of Q/R/N and adjacent sites were characterized using Mg^{2+}, memantine, MK-801, philanthotoxin analogues and an MTDL compound, CR18. NN at the Q/R/N and +1 sites in GluN2A subunits were mutated to GR and RR, while W at the -8 position (in relation to the Q/R/N site), was mutated to N. Wild type and mutated GluN2A were co-expressed with GluN1-1a in *Xenopus* oocytes and antagonistic responses by channel blockers were recorded with TEVC. At -75 mV, the RR mutation significantly increased IC_{50}s of Mg^{2+}, memantine and MK-801 by 27-, 42- and 325-fold respectively, compared to wild-type. As for the GR mutation, IC_{50}s were also significantly increased for memantine and MK-801 by 5- and 132-fold respectively, compared to wild type. W to N mutation at the -8 position did not significantly affect blocking potencies for all channel blockers. Blocking potency for PhTX-343 was not significantly altered by any mutations. This study provided evidence that the presence of G and R at the Q/R/N and +1 sites are likely responsible for the changes in blocking sensitivity and play important roles in ion permeability. The fact that PhTX-343 remained potent despite the mutations suggest that this compound might have a different mode of action or different binding site other than the M2 region and should be further characterized.

In the MTDL study, twenty one novel compounds were tested on GluN1-1a/GluN2A NMDAR subunits. Thirteen were memantine-derivatives (MAB) incorporated with antioxidant moieties, three were spermine-derived polyamines also incorporated with antioxidants, and five were combinatorial forms of donepezil and carvedilol. The antagonistic properties of the compounds were tested electrophysiologically at -60 mV and compared with Mg^{2+} and memantine. The MAB series were found to be weak NMDAR channel blockers suggesting the loss of memantine functionality due to attachment of the antioxidant structure to its amine group. Subsequently, modification of the linker point to memantine moieties to free its amine group eventually resulted in weaker NMDAR channel blockers with IC_{50}s of more than 100 µM. The spermine-derived polyamines (CR compounds) were potent NMDAR blockers with IC_{50}s (0.69 to 2.35 µM) comparable to memantine (2.28 µM) and significantly lower than Mg^{2+} (10.1 µM) and also exhibited voltage-dependence block.

Our mutation study revealed that CR18, the most potent MTDL compound was less sensitive in NMDAR containing GR or RR mutation in GluN2A subunits. This is a favourable property of an NMDAR blocker for potential Alzheimer's disease treatment since GluN3 subunits containing GR or RR at the Q/R/N and +1 sites are less permeable to Ca^{2+} influx and has been shown to exert neuroprotective effects.

Acknowledgements

First and foremost, I would like to thank my primary supervisor, Dr. Ian Mellor for his time, invaluable guidance, constant motivation and excellent supervision. I will forever be grateful for the skills he has helped me develop. *Ian, you are a remarkable individual and I am extremely thankful for the chance to work with you*. *You really are a great mentor and I couldn't have done this without you!*

I am hugely indebted to Dr. Helen Miranda Knight for her tireless effort throughout the writing phase of my PhD. I would also like to thank Dr. Ian Duce and Prof. Dr. David Wyllie for providing me with great advice and useful feedbacks for this thesis.

Thank you to our collaborators, Dr. Michela Rosini and colleagues from the University of Bologna, Italy for synthesizing the novel MTDL compounds; Prof. Dr. Kristian Strømgaard and Dr. Henrik Franzyk from the University of Copenhagen, Denmark for providing the philanthotoxin analogues; Tim Smith and Declan Brady for their technical support; past and present members of the A70 Electrophysiology group - Dr. Hamid Kachel, Dr. David Richards, Dr. Saleh Alhewairini, John Grzeskowiak, Rohit Patel, Neville Ngum, Maria Koromina, Alexandria Blockley, James Addy, Zhu Bin, Mahmoud Sherif and countless MSci, MRes, and intern students for all their help and making the lab a great place to work in.

I wish to thank my wife, Dr. Nur Aqilah Tajul Lile, for her unwavering love, encouragement and most importantly for patiently bearing with me throughout the last year of my PhD journey. My sincere appreciation goes to my parents, family and friends for their never-ending support.

Finally, I wish to express my gratitude to Universiti Kuala Lumpur and Malaysia's government sponsoring body, Majlis Amanah Rakyat for the financial assistance, without which I would not be able to pursue my PhD studies here in Nottingham, UK.

Table of Contents

Abstract i

Acknowledgements iii

Table of Contents iv

List of Abbreviations viii

List of Amino Acid Codes xi

List of Tables xii

List of Figures xiii

CHAPTER 1 1

INTRODUCTION 1

1.1 THE GLUTAMATE RECEPTOR FAMILY 1

1.1.1 AMPA Receptors 5

1.1.2 Kainate Receptors 6

1.1.3 NMDA Receptors 6

1.2 NMDAR STRUCTURES AND SUBUNITS 8

1.2.1 GluN1 9

1.2.2 GluN2 10

1.2.3 GluN3 11

1.2.4 The Q/R/N Site and mRNA Editing 14

1.3 NMDA RECEPTOR CHANNEL BLOCK 16

1.3.1 Mg^{2+} 17

1.3.2 Memantine 18

1.3.3 MK-801 19

1.3.4 Polyamines: Spermine and Spermidine 21

1.3.5 Philanthotoxin Analogues 21

1.4 ALZHEIMER'S DISEASE (AD) AND NMDA RECEPTORS 24

1.4.1 Epidemiology of Dementia and AD 24

1.4.2 Pathogenesis of AD 26

1.4.3 NMDAR-Implicated Pathogenesis 32

1.4.4 AD Treatments 36

1.4.5 Multi-Target-Directed Ligands (MTDL) 40

1.5 *XENOPUS LAEVIS* OOCYTE EXPRESSION SYSTEM FOR STUDYING ION CHANNELS ... 45

1.6 THESIS PROJECT OBJECTIVES 48

CHAPTER 2 49
METHODOLOGY 49
2.1 DNA CLONING AND mRNA PREPARATION 49
2.1.1 Preparation of Chemically Competent Cells 49
2.1.2 Plasmid DNA 49
2.1.3 Bacterial Transformation 52
2.1.4 Plasmid Purification 52
2.1.5 DNA Restriction Digest 53
2.1.6 Agarose Gel Electrophoresis 54
2.1.7 mRNA Transcription 55
2.2 SITE-DIRECTED MUTAGENESIS 55
2.2.1 Primer Design 55
2.2.2 PCR Reaction 56
2.3 *XENOPUS* OOCYTE EXPRESSION SYSTEM 58
2.3.1 Oocyte Preparation 58
2.3.2 Oocyte Microinjection 59
2.4 ELECTROPHYSIOLOGICAL MEASUREMENT 60
2.4.1 Two-Electrode Voltage-Clamp (TEVC) 60
2.4.2 Determination of NMDA and Glycine EC_{50} 62
2.4.3 Determination of Antagonists IC_{50} 63
2.5 MULTI-TARGET-DIRECTED LIGANDS 64
2.5.1 Electrophysiology of MTDL Compounds 68
2.6 DATA ANALYSIS 70
CHAPTER 3 72
NMDA RECEPTOR CHARACTERIZATION 72
3.1 SUMMARY 72
3.2 NMDA RECEPTOR AGONISM 72
3.2.1 NMDA and Glycine Activation 72
3.2.2 EC_{50} of NMDA 73
3.2.3 EC_{50} of Glycine 75
3.3 NMDA RECEPTOR ANTAGONISM BY OPEN CHANNEL BLOCKERS 76
3.3.1 Mg^{2+} 76
3.3.2 Memantine 77
3.3.3 MK-801 78

3.3.4 Philanthotoxin-343 79
3.3.5 Cha-PhTX-343 80
3.3.6 Bn-Cha-PhTX-343 81
3.3.7 CR18 82
3.3.8 δ Value 83
3.4 DISCUSSION 84
3.4.1 NMDA Receptor Agonism 84
3.4.2 NMDA Receptor Antagonism 85
3.4.2.1 Mg^{2+} 85
3.4.2.2 Memantine 86
3.4.2.3 MK-801 88
3.4.2.4 Philanthotoxin Analogues 89
3.4.2.5 CR18 91
CHAPTER 4 93
PORE REGION (M2) MUTATION STUDY 93
4.1 SUMMARY 93
4.2 GLUN3 SITE-DIRECTED MUTAGENESIS 93
4.2.1 Validation of GluN3 Expression by Glycine Sensitivity Testing 98
4.3 GLUN2A SITE-DIRECTED MUTAGENESIS 100
4.4 NMDAR ANTAGONISM ON MUTATED GLUN2A 102
4.4.1 Mg^{2+} 102
4.4.2 Memantine 104
4.4.3 MK-801 106
4.4.4 Philanthotoxin-343 108
4.4.5 CR18 110
4.5 VOLTAGE-DEPENDENCE OF INHIBITION 112
4.5.1 $GluN2A_{(W606N)}$ Mutation 112
4.5.2 $GluN2A_{(N614G/N615R)}$ Mutation 114
4.5.3 $GluN2A_{(N614R/N615R)}$ Mutation 116
4.6 DISCUSSION 120

CHAPTER 5 128
MULTI-TARGET-DIRECTED LIGANDS STUDY 128
5.1 SUMMARY 128
5.2 CONTROL CHANNEL BLOCKERS 129
5.2.1 Mg^{2+} 129
5.2.2 Memantine 131
5.3 MEMANTINE-DERIVATIVE (MAB) COMPOUNDS (i) 133
5.3.1 Concentration-Inhibition of Methoxyphenol-Containing MAB Compounds 133
5.3.2 Concentration-Inhibition of Lipoic Acid-Containing MAB Compounds 135
5.3.3 Voltage-Dependence of MAB Compounds 137
5.4 MEMANTINE-DERIVATIVE (FC/GB) COMPOUNDS (ii) 139
5.4.1 Concentration-Inhibition of Methoxyphenol-Containing FC Compounds ... 139
5.4.2 Concentration-Inhibition of Catechol-Containing FC/GB Compounds 140
5.5 SPERMINE-DERIVED POLYAMINE (CR) COMPOUNDS 142
5.5.1 Concentration-Inhibition of CR Compounds 142
5.5.2 Voltage-Dependence of CR Compounds 144
5.6 DONEPEZIL-DERIVED (MGM) COMPOUNDS 146
5.6.1 Antagonistic Responses on NMDA Receptor 146
5.6.2 Responses on Nicotinic Receptors 150
5.6.2.1 Agonistic Responses on Nicotinic Receptors 150
5.6.2.2 Antagonistic Responses on α4β2 Nicotinic Receptors 152
5.6.2.3 Antagonistic Responses on α7 Nicotinic Receptors 156
5.7 DISCUSSION 161
CHAPTER 6 168
GENERAL DISCUSSION 168
6.1 PORE-REGION (M2) MUTATION STUDIES 168
6.2 MTDL AS POTENTIAL THERAPEUTICS FOR AD 170
6.3 FUTURE WORKS AND RECOMMENDATIONS 172
6.4 CONCLUSION 174
Bibliography 176
Appendix 196

List of Abbreviations

Aβ	beta-amyloid
ACh	acetylcholine
AChE	acetylcholinesterase
AChEI	acetylcholinesterase inhibitors
AD	Alzheimer's disease
AIDS	acquired immune deficiency syndrome
ALA	alpha lipoic acid
AMPA	2-amino-3-(3-hydroxy-5-methyl-isoxazol-4-yl)propanoic acid
AMPAR	AMPA receptor
AP5	2-amino-5-phosphonopentanoate
ApoE4	apolipoprotein E4
APP	amyloid precursor protein
AQ	anthraquinone
ATD	amino terminal domain
Ba^{2+}	barium ion
Bn-Cha-PhTX-343	benzyl-cyclohexylalanine-philanthotoxin-343
BSA	bovine serum albumin
Ca^{2+}	calcium ion
$CaCl_2$	calcium chloride
CDK5	cyclin-dependent kinase 5
cDNA	complementary deoxyribonucleic acid
ChEI	cholinesterase inhibitors
CHF	congestive heart failure
ChAT	choline acetyltransferase
CNS	central nervous system
CoQ	coenzyme Q
cRNA	complementary ribonucleic acid
Cha-PhTX-343	cyclohexylalanine-philanthotoxin-343
DBA	dibenzylamino
ddH_2O	double distilled water
DMSO	dimethyl sulfoxide
DNA	deoxyribonucleic acid
dNTP	deoxynucleotides
dsDNA	double stranded deoxyribonucleic acid

E. coli	*Escherichia coli*
EC_{50}	half maximal effective concentration
ED_{50}	median effective dose
EDTA	ethylenediaminetetraacetic acid
EOAD	early onset Alzheimer's disease
FAD	familial Alzheimer's disease
FAK	focal adhesion kinase
FDA	US Food and Drug Administration
GFP	green fluorescent protein
GSK3β	glycogen synthase kinase 3 beta
GTP	gentamicin theophylline pyruvate
H_2O_2	hydrogen peroxide
HEK	human embryonic kidney
HEPES	4-(2-hydroxyethyl)-1-piperazineethanesulfonic acid
HF	high-fidelity
HOCl	hypochlorous acid
IC_{50}	half maximal inhibitory concentration
IDE	insulin-degrading enzyme
iGluR	ionotropic glutamate receptor
IPTG	isopropyl β-D-1-thiogalactopyranoside
IU	international unit
KA	kainate
KAR	kainate receptor
KCl	potassium chloride
LB	lysogeny broth
LBD	ligand-binding domain
LDL	low-density lipoprotein
LOAD	late onset Alzheimer's disease
LTD	long-term depression
LTP	long-term potentiation
MAO	monoamine oxidase
Mg^{2+}	magnesium ion
$MgCl_2$	magnesium chloride
mGluR	metabotropic glutamate receptor
MK-801	(+)-5-methyl-10, 1 1-dihydro-5*H*-dibenzo[*a,d*]cyclohepten-5,10-imine maleate

mRNA	messenger ribonucleic acid
MS	multiple sclerosis
MTDL	multi-target directed ligands
MW	molecular weight
NaCl	sodium chloride
nAChR	nicotinic acetylcholine receptor
NaOH	sodium hydroxide
NC-IUPHAR	The International Union of Pharmacology Committee on Receptor Nomenclature and Drug Classification
NEP	neprilysin
NFT	neurofibrillary tangle
NMDA	*N*-methyl-D-aspartate
NMDAR	NMDA receptor
NTD	N-terminal domain
PCP	phencyclidine
PCR	polymerase chain reaction
pDNA	plasmid DNA
PhTX	philanthotoxin
PS-1	presenilin-1
PS-2	presenilin-2
ROS	reactive oxygen species
SAD	sporadic Alzheimer's disease
SEM	standard error of the mean
SOC	super optimal broth with catabolite repression
STN	subthalamic nucleus
TAE	tris-acetate-ethylenedia minetetraacetic acid
TARPs	transmembrane AMPAR regulatory protein
TB-3-4	N1,N4,N8-tri-benzyl-spermidine
TEVC	two-electrode voltage clamp
TMD	transmembrane domain
X-gal	5-bromo-4-chloro-3-indolyl-β-D-galactopyranoside

List of Amino Acid Codes

Amino Acid	Three-Letter Code	One-Letter Code
Alanine	Ala	A
Arginine	Arg	R
Asparagine	Asn	N
Aspartate	Asp	D
Cysteine	Cys	C
Glutamate	Glu	E
Glutamine	Gln	Q
Glycine	Gly	G
Histidine	His	H
Isoleucine	Ile	I
Leucine	Leu	L
Lysine	Lys	K
Methionine	Met	M
Phenylalanine	Phe	F
Proline	Pro	P
Serine	Ser	S
Threonine	Thr	T
Tryptophan	Trp	W
Tyrosine	Tyr	Y
Valine	Val	V

List of Tables

Table 1: Ionotropic glutamate receptor classification by NC-IUPHAR..... 2
Table 2: Major agonists and co-agonists of ionotropic glutamate receptors..... 4
Table 3: IC_{50} for several channel blockers tested on NMDA receptors containing GluN1-1a and GluN2A compared to NMDAR incorporated with GluN3A or GluN3B at three holding potentials. 12
Table 4: Genetic predisposition to Alzheimer's disease in relation to Aβ expression..... 27
Table 5: List of acetylcholinesterase inhibitors (AChEI). 37
Table 6: Antioxidants used in the multi-target-directed ligands study. 42
Table 7: Primers used to produce mutations in NMDA receptor subunits using site-directed mutagenesis protocol. 56
Table 8: PCR cycling parameters for site-directed mutagenesis experiments. 57
Table 9: Primers designed for DNA sequencing of NMDA receptor subunits containing the mutations produced via site-directed mutagenesis. 57
Table 10: Novel memantine-derivative (MAB) MTDL compounds incorporated with a methoxyphenol or lipoic acid moiety assessed in this study. 65
Table 11: Novel memantine-derivative (FC/GB) MTDL compounds incorporated with methoxyphenol or catechol moiety assessed in this study. 66
Table 12: Novel spermine-derived polyamine MTDLs (CR) assessed in this study. 67
Table 13: Donepezil-derived MTDL compounds assessed in this study. 68
Table 14: IC_{50} values for Mg^{2+} on NMDARs containing GluN2A mutations and compared with IC_{50} on wild type GluN1-1a/GluN2A. 102
Table 15: IC_{50} values for memantine on NMDARs containing GluN2A mutations and compared with IC_{50} on wild type GluN1-1a/GluN2A. 104
Table 16: IC_{50} values for MK-801 on NMDARs containing GluN2A mutations and compared with IC_{50} on wild type GluN1-1a/GluN2A. 106
Table 17: IC_{50} values for philanthotoxin-343 on NMDARs containing GluN2A mutations and compared with IC_{50} on wild type GluN1-1a/GluN2A. 108
Table 18: IC_{50} values for CR18 compound on NMDARs containing GluN2A mutations and compared with IC_{50} on wild type GluN1-1a/GluN2A. 110
Table 19: Comparison of IC_{50} values for channel blockers on NMDARs containing $GluN2A_{W606N}$ mutation across three different holding potentials. 112
Table 20: Comparison of IC_{50} values for channel blockers on NMDARs containing $GluN2A_{N614G/N615R}$ mutation across three different holding potentials. 114
Table 21: Comparison of IC_{50} values for channel blockers on NMDARs containing $GluN2A_{N614R/N615R}$ mutation across three different holding potentials. 116
Table 22: Calculated δ values from the Woodhull equation for channel blockers tested on GluN1-1a/2A, GluN1-1a/$2A_{(W606N)}$, GluN1-1a/$2A_{(N614G/N615R)}$ and GluN1-1a/$2A_{(N614R/N615R)}$ subunit combinations. 118

List of Figures

Figure 1: Modular structure of glutamate receptors. 3
Figure 2: Diagram of NMDA receptor showing its main distinct characteristics. 7
Figure 3: NMDA receptor heterotetrameric modular structure. 8
Figure 4: Model structure of GluN1/GluN2/GluN3 assembly. 9
Figure 5: NMDAR subunit diversity, structure and expression. 13
Figure 6: Amino acid sequences of NMDAR subunits aligned with AMPAR subunits, GluA1 and GluA2 at the major pore lining regions (M2-M3) in rat and human. 14
Figure 7: A simplified schematic showing activated NMDAR and the mechanism of NMDAR block by various types of antagonists. 16
Figure 8: Chemical structure of memantine. 18
Figure 9: Chemical structure of MK-801. 19
Figure 10: Chemical structures of (A) spermine and (B) spermidine. 21
Figure 11: Chemical structures of (A) PhTX-433 and (B) PhTX-343. 22
Figure 12: Structure of philanthotoxin analogues. (A) Cyclohexylalanine-philanthotoxin-343 (Cha-PhTX-343), (B) Benzyl-cyclohexylalanine-philanthotoxin-343 (Bz-Cha-PhTX-343). 24
Figure 13: Global incidence of people living with dementia. 25
Figure 14: Senile plaques and neurofibrillary tangles observed in the cortex of an Alzheimer's disease patient. 27
Figure 15: Schematic diagram of the amyloid cascade hypothesis underlying AD pathogenesis. 30
Figure 16: Proposed neurochemical alterations in AD cortical synaptic transmission. 32
Figure 17: Proposed action of Aβ oligomers on hippocampal synaptic plasticity and neurotransmission leading to the development of cognitive decline seen in dementia. 35
Figure 18: Structure of carvedilol. 44
Figure 19: Genetic processing of injected DNA/RNA in *Xenopus laevis* oocytes into ion channels/receptors. 45
Figure 20: A microscopic visual of *Xenopus* oocyte in the bath chamber with two glass electrodes impaling the cell. 47
Figure 21: Schematic diagram of the oocyte expression system and utilisation of two-electrode voltage clamp (TEVC). 47
Figure 22: Vector maps for (A) GluN1-1a and (B) GluN2A in pRK7. 50
Figure 23: Vector maps for (A) GluN3A and (B) GluN3B in pcDNA3.1(+). 51
Figure 24: Agarose gel electrophoresis of uncut and linearized pDNA of GluN1-1a, GluN2A, GluN3A and GluN3B NMDA receptor subunits. 54
Figure 25: The *Xenopus laevis* frog and oocytes. 58
Figure 26: Developmental stages (I – VI) of *Xenopus laevis* oocytes. 59
Figure 27: Nanoinjector used for injection of cRNAs into *Xenopus laevis* oocytes. 59
Figure 28: Diagram representation of two-electrode voltage clamp. 61
Figure 29: Electrophysiology set-up to record drug/test compound responses on receptor channels expressed on *Xenopus laevis* oocytes. 62
Figure 30: TEVC recordings of NMDA and glycine activation mediated by GluN1-1a/GluN2A-containing NMDA receptors at -75 mV. 73

Figure 31: Concentration-response relationship for NMDA co-applied with glycine mediated by GluN1-1a/GluN2A-containing receptors. 74
Figure 32: Concentration-response relationship for glycine co-applied with NMDA mediated by GluN1-1a/GluN2A-containing receptors. 75
Figure 33: Mg^{2+} block of NMDA/glycine responses in GluN1-1a/GluN2A-containing NMDA receptors. 76
Figure 34: Memantine block of NMDA/glycine responses in GluN1-1a/GluN2A-containing NMDA receptors. 77
Figure 35: MK-801 block of NMDA/glycine responses in GluN1-1a/GluN2A-containing NMDA receptors. 78
Figure 36: PhTX-343 block of NMDA/glycine responses in GluN1-1a/GluN2A-containing NMDA receptors. 79
Figure 37: Cha-PhTX-343 block of NMDA/glycine responses in GluN1-1a/GluN2A-containing NMDA receptors. 80
Figure 38: Bn-Cha-PhTX-343 block of NMDA/glycine responses in GluN1-1a/GluN2A-containing NMDA receptors. 81
Figure 39: CR18 block of NMDA/glycine responses in GluN1-1a/GluN2A-containing NMDA receptors. 82
Figure 40: Voltage-dependence of inhibition for all compounds mediated by GluN1-1a/GluN2A-containing NMDA receptors. 83
Figure 41: A model of philanthotoxin docking in the GluA1 receptor channel. 90
Figure 42: Site-Directed QuickChange II XL Mutagenesis control and sample plates. 95
Figure 43: Chromatograms of nucleotide sequence from the site-directed mutagenesis PCR products showing the mutations generated in GluN3A subunits. 96
Figure 44: Chromatograms of nucleotide sequence from the site-directed mutagenesis PCR products showing the mutations generated in GluN3B subunits. 97
Figure 45: TEVC recordings of 100 µM NMDA-evoked currents co-applied with tenfold increasing concentration of glycine (0.1–100 µM) tested at -75 mV on GluN1-1a/2A, GluN1-1a/2A/‘3A’ and GluN1-1a/2A/‘3B’. 98
Figure 46: Concentration-response relationship for glycine co-applied with NMDA tested against GluN1-1a/2A, GluN1-1a/2A/‘3A’ and GluN1-1a/2A/‘3B’. 99
Figure 47: Chromatograms of nucleotide sequence from the site-directed mutagenesis PCR products showing the mutations generated in GluN2A subunits. 101
Figure 48: Concentration-inhibition relationship for Mg^{2+} block of NMDA/glycine on NMDARs containing GluN2A mutations compared with block on wild type GluN1-1a/GluN2A subunits. 103
Figure 49: Concentration-inhibition relationship for memantine block of NMDA/glycine on NMDARs containing GluN2A mutations compared with block on wild type GluN1-1a/GluN2A subunits. 105
Figure 50: Concentration-inhibition relationship for MK-801 block of NMDA/glycine on NMDARs containing GluN2A mutations compared with block on wild type GluN1-1a/GluN2A subunits. 107
Figure 51: Concentration-inhibition relationship for Philanthotoxin-343 block of NMDA/glycine on NMDARs containing GluN2A mutations compared with block on wild type GluN1-1a/GluN2A subunits. 109

Figure 52: Concentration-inhibition relationship for CR18 block of NMDA/glycine on NMDARs containing GluN2A mutations compared with block on wild type GluN1-1a/GluN2A subunits. 111
Figure 53: Concentration-inhibition curves showing voltage-dependent block of NMDA/glycine responses by open channel blockers mediated by GluN1-1a/GluN2A$_{(W606N)}$ receptor combination at -50, -75 and -100 mV. 113
Figure 54: Concentration-inhibition curves showing voltage-dependent block of NMDA/glycine responses by open channel blockers mediated by GluN1-1a/GluN2A$_{(N614G/N615R)}$ receptor combination at -50, -75 and -100 mV..... 115
Figure 55: Concentration-inhibition curves showing voltage-dependent block of NMDA/glycine responses by open channel blockers mediated by GluN1-1a/GluN2A$_{(N614R/N615R)}$ receptor combination at -50, -75 and -100 mV..... 117
Figure 56: Voltage-dependence of IC_{50} for channel block of NMDA/glycine responses on all NMDA receptor combinations fitted with the Woodhull equation..... 119
Figure 57: Chemical structures of (A) AQ343 and (B) AQ444. 124
Figure 58: Concentration-dependent Mg^{2+} block of NMDA/glycine responses in GluN1-1a/GluN2A NMDA receptors. 129
Figure 59: Voltage-dependent Mg^{2+} (10 μM) block of NMDA/glycine in GluN1-1a/GluN2A-containing NMDA receptors. 130
Figure 60: Concentration-dependent memantine block of NMDA/glycine responses in GluN1-1a/GluN2A-containing NMDA receptors. 131
Figure 61: Voltage-dependent memantine (3 μM) block of NMDA/glycine in GluN1-1a/GluN2A-containing NMDA receptors. 132
Figure 62: TEVC recordings for MAB23(2), MAB14, MAB22 and MAB30 (0.01–100 μM) block of NMDA/glycine responses at -60 mV on single oocytes. 133
Figure 63: Comparison of concentration-inhibition for MAB compounds (containing methoxyphenol moiety), Mg^{2+} and memantine block of NMDA/glycine responses in GluN1-1a/GluN2A NMDA receptors at -60 mV. 134
Figure 64: TEVC recordings for MAB7, MAB15, MAB21 and MAB32 (0.01–100 μM) block of NMDA/glycine responses at -60 mV on single oocytes. 135
Figure 65: Comparison of concentration-inhibition for MAB compounds (containing lipoic acid moiety), Mg^{2+} and memantine block of NMDA/glycine responses in GluN1-1a/GluN2A NMDA receptors at -60 mV..... 136
Figure 66: TEVC recordings of MAB compounds (MAB14, MAB22, MAB30 and MAB7) voltage-dependent block of NMDA/glycine responses in GluN1-1a/GluN2 NMDA receptors tested at -100, -80, -60 and -40 mV on single oocytes. 137
Figure 67: Comparison of voltage-dependent inhibition of MAB compounds (containing methoxyphenol moiety), Mg^{2+} and memantine block of NMDA/glycine responses in GluN1-1a/GluN2A NMDA receptors. 138
Figure 68: TEVC recordings of FC7, FC12 and FC17 (0.01–100 μM) block of NMDA/glycine responses at -60 mV on single oocytes..... 139
Figure 69: TEVC recordings of FC20 and GB13 (0.01–100 μM) block of NMDA/glycine responses at -60 mV on single oocytes..... 140

Figure 70: Comparison of concentration-inhibition relationship for FC/GB compounds, Mg^{2+} and memantine block of NMDA/glycine responses in GluN1-1a/GluN2A NMDA receptors at -60 mV. 141
Figure 71: TEVC recordings of CR8, CR18 and CR24 (0.01–100 μM) block of NMDA/glycine responses at -60 mV on single oocytes. 142
Figure 72: Comparison of concentration-inhibition for CR compounds, Mg^{2+} and memantine block of NMDA/glycine responses in GluN1-1a/GluN2A NMDA receptors at -60 mV. 143
Figure 73: TEVC recordings of CR compounds (CR8, CR18 and CR24) voltage-dependent block of NMDA/glycine responses in GluN1-1a/GluN2 NMDA receptors tested at -100, -80, -60 and -40 mV on single oocytes. 144
Figure 74: Comparison of voltage-dependent inhibition for CR compounds block of NMDA/glycine in GluN1-1a/GluN2A-containing NMDA receptors. 145
Figure 75: Concentration-inhibition relationship of MGM2 block on GluN1-1a/GluN2A-containing NMDA receptors. 146
Figure 76: Concentration-inhibition relationship of MGM3 block on GluN1-1a/GluN2A-containing NMDA receptors. 147
Figure 77: Concentration-inhibition relationship of MGM11 block on GluN1-1a/GluN2A-containing NMDA receptors. 147
Figure 78: MGM10 block of NMDA/glycine responses in GluN1-1a/GluN2A-containing NMDA receptors. 148
Figure 79: MGM12 block of NMDA/glycine responses in GluN1-1a/GluN2A-containing NMDA receptors. 149
Figure 80: Agonistic responses of MGM compounds (10 μM) on α4β2 nicotinic receptor. 151
Figure 81: Agonistic responses of MGM compounds (100 μM) on α4β2 nicotinic receptor 152
Figure 82: MGM2 block of ACh responses on α4β2 nicotinic receptor. 153
Figure 83: MGM3 block of ACh responses on α4β2 nicotinic receptor. 153
Figure 84: MGM10 block of ACh responses on α4β2 nicotinic receptor. 154
Figure 85: MGM11 block of ACh responses on α4β2 nicotinic receptor. 154
Figure 86: MGM12 block of ACh responses on α4β2 nicotinic receptor. 155
Figure 87: MGM2 block of ACh responses on α7 nicotinic receptor. 156
Figure 88: MGM3 block of ACh responses on α7 nicotinic receptor. 157
Figure 89: MGM10 block of ACh responses on α7 nicotinic receptor. 158
Figure 90: MGM11 block of ACh responses on α7 nicotinic receptor. 159
Figure 91: MGM12 block of ACh responses on α7 nicotinic receptor. 160
Figure 92: Chemical structures of (A) memoquin, (B) lipocrine and (C) carbacrine. 164
Figure 93: Amino acid sequence alignment for human NMDAR subtypes. 169
Figure 94: Potential roles of NMDA receptors in Aβ-related mechanism. 170

CHAPTER 1

INTRODUCTION

1.1 THE GLUTAMATE RECEPTOR FAMILY

Glutamate receptors mediate excitatory neurotransmission in the vertebrate CNS (Kumar and Mayer, 2013). They are known to have a key role in memory and learning and have been associated with a role in neurodegenerative disorders (Traynelis et al., 2010). Ever since the first glutamate receptor subunit was cloned in rat by Hollmann and colleagues, there have been important discoveries leading to the identification of different glutamate receptor subunits (Hollmann et al., 1989).

Glutamate receptors are classified into metabotropic (mGluR) or ionotropic glutamate receptors (iGluR). The former transmit signals via intracellular G proteins while the latter open ion channels directly after agonist binding (Erreger et al., 2004; Niswender and Conn, 2010). To date, 18 human iGluR genes have been cloned giving rise to four main classes of iGluRs characterized based on their pharmacological properties, selective agonists, structural homology and DNA sequences (Mayer, 2011a). The three major families are 2-amino-3-(3-hydroxy-5-methyl-isoxazol-4-yl)propanoic acid (AMPA), kainate (KA) and *N*-methyl-D-aspartate (NMDA) receptors which all mediate excitatory synaptic neurotransmission in brain (Mayer, 2011b). The remaining orphan class, GluD consisting of GluD1 and GluD2 does not form functional ion channels although they share similar overall structure with other types of iGluR (Collingridge et al., 2009; Mayer, 2011a). Although abundantly expressed in the brain cerebellum, and may also be found in numerous regions of the brain, their function in neurotransmission is yet to be established (Kumar and Mayer, 2013).

Table 1 shows the classification and nomenclature of iGluRs as established by The International Union of Pharmacology Committee on Receptor Nomenclature and Drug Classification (NC-IUPHAR).

Table 1: Ionotropic glutamate receptor classification by NC-IUPHAR

Receptor Family	NC-IUPHAR Subunit Nomenclature	Human Gene Name	Human Chromosomal Location
AMPA	GluA1	*GRIA1*	5q31.1
	GluA2	*GRIA2*	4q32–q33
	GluA3	*GRIA3*	Xq25–q26
	GluA4	*GRIA4*	11q22
Kainate	GluK1	*GRIK1*	21q22.11
	GluK2	*GRIK2*	6q16.3–q21
	GluK3	*GRIK3*	1p34–p33
	GluK4	*GRIK4*	11q22.3
	GluK5	*GRIK5*	19q13.2
NMDA	GluN1	*GRIN1*	9q34.3
	GluN2A	*GRIN2A*	16p13.2
	GluN2B	*GRIN2B*	12p12
	GluN2C	*GRIN2C*	17q25
	GluN2D	*GRIN2D*	19q13.1
	GluN3A	*GRIN3A*	9q31.1
	GluN3B	*GRIN3B*	19p13.3
'Orphan' (GluD)	GluD1	*GRID1*	10q22
	GluD2	*GRID2*	4q22

Table 1 presents the classification and nomenclature for ligand-gated ion channels for the glutamate receptor family that are expressed in humans. Adapted from Collingridge et al. (2009).

Each of the classes demonstrates a common modular structure which is conserved throughout the iGluR family and differentiates them from other neurotransmitter receptors and ion channels (Kumar and Mayer, 2013; Suzuki et al., 2013). They form ligand-gated ion channels which allow cations to pass through the channel pore (Meldrum, 2000). Sequence homology shared between the iGluRs suggest that they share a similar structure. All iGluR subunits consists of four domains (i) extracellular amino-terminal domain (ATD), (ii) extracellular ligand-binding domain (LBD), (iii) transmembrane domain (TMD), and (iv) intracellular carboxyl-terminal domain (CTD) (Traynelis et al., 2010). Figure 1 shows the common modular structure and domain organization of glutamate receptors.

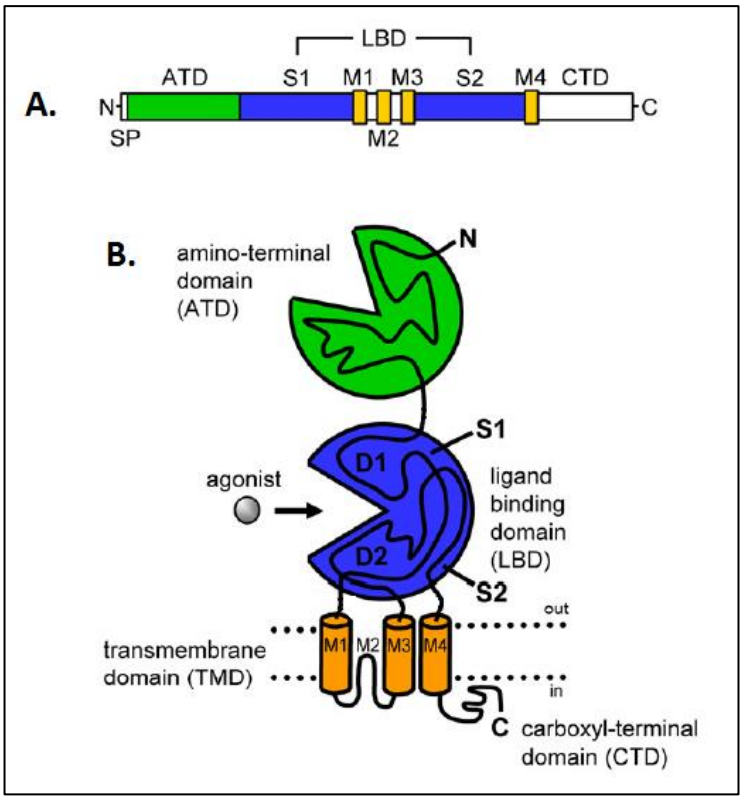


Figure 1: Modular structure of glutamate receptors.

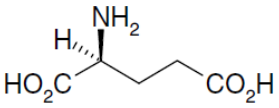
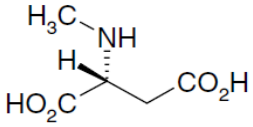
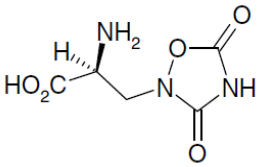
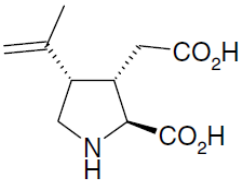
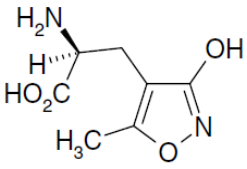
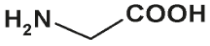
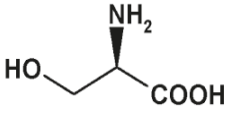
(A) Linear representation of the subunit polypeptide chain. (B) Schematic illustration of the subunit topology comprising of (i) extracellular ATD (green), (ii) extracellular LBD (blue) formed by two amino acid segments, S1 and S2, (iii) TMD (orange) comprised of three membrane-spanning helices (M1, M3, and M4) and a membrane re-entrant loop (M2) which forms part of the channel pore, and (iv) intracellular CTD. Source: Traynelis et al. (2010)

Despite sharing similarities, the different classes of receptors also display individual developmental and cell-specific expression profiles, varied cation permeability to Ca^{2+} and distinct roles in brain physiology conferred by different subunit combinations and RNA editing (Meldrum, 2000; Traynelis et al., 2010).

iGluRs are inducible by L-glutamate as the primary neurotransmitter that mediates mammalian excitatory neurotransmission in the CNS (Traynelis et al., 2010). L-aspartate (Patneau and Mayer, 1990) and NMDA are agonists which specifically stimulate NMDA receptors (NMDAR) (Mayer and Westbrook, 1987). The activation of NMDAR, however, requires glycine or D-serine as the essential co-agonist (Kleckner and Dingledine, 1988). Glycine was reported to be more potent with three to four times lower ED_{50} than that of D-serine (Matsui et al., 1995), although later

studies have shown that D-serine is also a potent co-agonist (Chen et al., 2008). AMPA and KA receptors (AMPAR and KAR, respectively) can be activated by their respective specific agonists of glutamate analogues, although early reports have suggested that certain assemblies of these receptor subunits may also be triggered by both amino acids to a certain extent (Dingledine et al., 1999). AMPARs are also stimulated by quisqualate by which the receptor was previously named until AMPA was found to be more potent and selective (Watkins and Jane, 2006). Some of the major agonists and co-agonists of ionotropic glutamate receptors are presented in table 2.

Table 2: Major agonists and co-agonists of ionotropic glutamate receptors.

Compound	Chemical Structure
L-Glutamate	
NMDA	
Quisqualate	
Kainate	
AMPA	
Glycine	
D-Serine	

Adapted from Watkins and Jane (2006) and Urwyler et al. (2009).

1.1.1 AMPA Receptors

The AMPAR subtype which is found abundantly in the brain has pivotal roles in excitatory neurotransmission and synaptic plasticity (Chang et al., 2012). AMPARs are also important in maintaining dendritic spines to ensure functional neural circuit connectivity. Synaptic responses can affect changes to AMPAR density which in turn affect the synaptic structure and actin cytoskeleton conferring the spine shape (Chang et al., 2012). Structurally, AMPARs can form homomers but are generally found to be heterotetramers assembled from the possible combinations of GluA1, GluA2, GluA3 or GluA4 subunits that form ligand-gated ion channels (Collingridge et al., 2009; Geiger et al., 1995; Traynelis et al., 2010). These AMPAR subunits are found to be equally abundant but differentially distributed in specific parts of the brain (Chang et al., 2012; Hollmann and Heinemann, 1994).

Heteromeric receptors, may be assembled from two GluA2 subunits and two of either the GluA1, GluA3, or GluA4 subunits (i.e., GluA1A2, GluA2A3, GluA2A4) and are the principal subtypes expressed on excitatory neurons (Sans et al., 2003; Wenthold et al., 1996). Subunit composition varies depending on the brain region, but at the hippocampal CA3–CA1 synapse most AMPARs are heteromers comprised of GluA2 plus GluA1 or GluA3 subunits (Derkach et al., 2007). Homomeric receptors are more dispersed throughout the nervous system, with GluA1 receptors mainly found on inhibitory neurons (Geiger et al., 1995). Subunit compositions of the receptor distinguished the characteristics and pharmacological properties of AMPARs such as channel conductance, ion permeability, gating kinetics and trafficking (Jonas and Burnashev, 1995; Washburn et al., 1997). In the adult brain, majority of the AMPARs are co-assembled with an alternative form of the GluA2 subunit produced by RNA editing which confers the ion channel Ca^{2+}-impermeable characteristics (Henley and Wilkinson, 2016).

More recently, the transmembrane AMPAR regulatory proteins (TARPs) have been characterized which form associations with AMPARs as auxiliary subunits. TARPs modulate trafficking and biophysical functions of the receptor playing a key role in

synaptic plasticity especially in long-term potentiation (LTP) and long-term depression (LTD) (Bats et al., 2013; Payne, 2008). Further studies have shown that TARPs bind directly to AMPARs, and target the receptors to synapses via binding to the scaffolding protein postsynaptic density-95 (PSD95) and dramatically alter the gating and pharmacological properties of AMPARs (Shi et al., 2010).

1.1.2 Kainate Receptors

There are five types of KAR s subunits, GluK1 to GluK5 (previously termed GluR5, GluR6, GluR7, KA1 and KA2) which are approximately 100 kDa (MW) in size (Lerma et al., 2001). Similar to AMPAR subunits, GluK1, GluK2 and GluK3 subunits can assemble into heteromers or homomers. However, GluK4 and GluK5 can only function as ion channels if co-assembled with GluK1 to GluK3 (Traynelis et al., 2010). The expression of KAR are ubiquitous throughout the nervous system with each subunit heterogeneously concentrated in certain areas of the brain (Lerma et al., 2001). Studies concerning KAR function are relatively limited compared to AMPAR and NMDAR. However, research has shown that KAR are involved in both excitatory and inhibitory neurotransmission (Koga et al., 2012), nociception (Bhangoo and Swanson, 2013), and may underlie the neuropathophysiology of neurospsychiatric disorders (Knight et al., 2012; Pickard et al., 2008) and epilepsy (Bowie, 2008). In addition, researchers have identified two auxiliary subunits, termed as Neto1 and Neto2 which co-assemble with KARs to modulate their functions. It has been indicated that Neto's affect how KAR respond when glutamate binds to them (Sheng et al., 2015; Wyeth et al., 2014).

1.1.3 NMDA Receptors

NMDARs are ionotropic glutamate receptors activated by glutamate or NMDA as the agonist and glycine or D-serine as the co-agonist. Two of the main characteristics which distinguish NMDARs from other iGluRs are their susceptibility to voltage-dependent block by Mg^{2+} and high permeability for Ca^{2+} especially in GluN2A and

GluN2B-containing receptors as depicted in figure 2 (Sanz-Clemente et al., 2013; Traynelis et al., 2010).

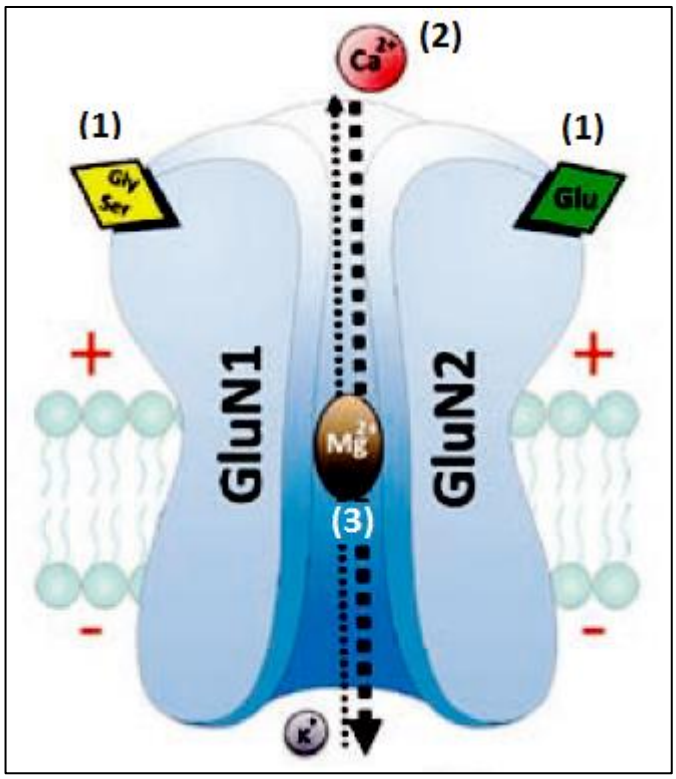


Figure 2: Diagram of NMDA receptor showing its main distinct characteristics.

NMDA receptors require glutamate (Glu) which binds to GluN2 and glycine (Gly) or D-serine (Ser) as the co-agonist binding to GluN1 to be activated (1). They are highly permeable to Ca^{2+} (2). They can be blocked by Mg^{2+} which is dependent on the membrane potential (3). Adapted from Sanz-Clemente et al. (2013).

The opening of NMDAR channels occur with the binding of glutamate bound to the receptor, and when the postsynaptic cell is depolarized which removes the Mg^{2+} from blocking the channel (Dale et al., 2008). They are distributed ubiquitously throughout the CNS (Wollmuth et al., 1996) where they are involved in synaptic plasticity and long-term potentiation which underlie learning and memory (Takatsuki et al., 2001; Zimmer et al., 1995). They also play critical roles in spatial learning, synaptogenesis and contextual fear memory acquisition (Lynch, 2004; Traynelis et al., 2010). Due to their functionality, NMDAR impairment is implicated in multiple neurological and psychiatric diseases such as Alzheimer's disease, schizophrenia and chronic pain (Malinow, 2012; Suzuki et al., 2013).

1.2 NMDAR STRUCTURES AND SUBUNITS

The first rat NMDAR gene was cloned and characterized by Moriyoshi and colleagues in 1991. It is now known that NMDARs are encoded by seven genes and form obligatory heterotetramers (figure 3) comprised from the combination of three subunits; GluN1, GluN2 and the most recently cloned GluN3 (Chaffey and Chazot, 2008). Numerous studies have established that the majority of NMDARs are comprised of two GluN1 and two GluN2 subunits. Both of these subunits are essential to form a functional NMDA/glutamate-gated receptor channels in the mammalian nervous system (Furukawa et al., 2005).

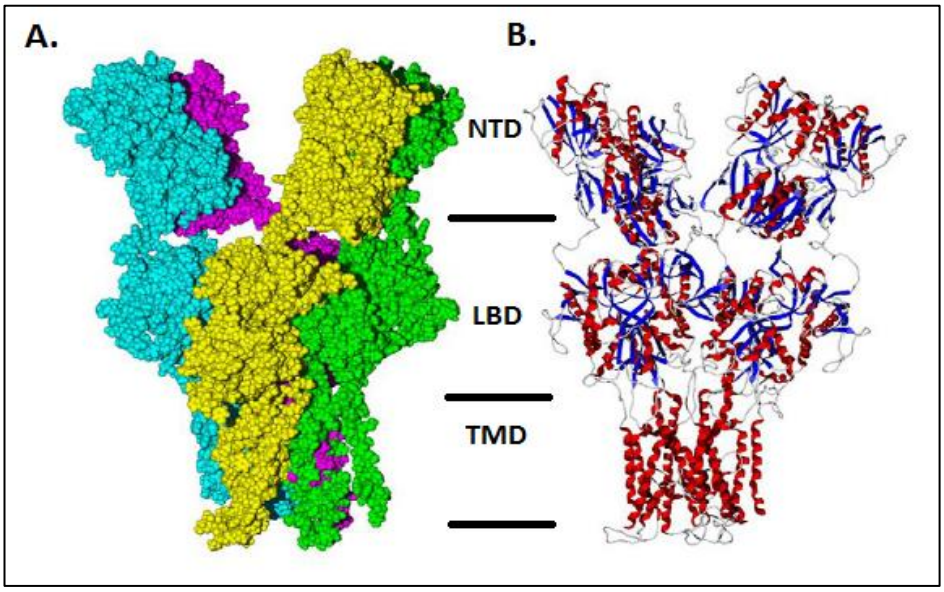


Figure 3: NMDA receptor heterotetrameric modular structure.
(A) Crystallographic space-filling homology model of two GluN1 (green and blue) and two GluN2 (yellow and magenta) subunits forming a heterotetrameric assembly, showing the major regions (N-terminal domain, ligand-binding domain and transmembrane domain) of the protein, (B) The corresponding backbone ribbon structure. Adapted from Monaghan et al. (2012).

Each of the NMDAR subunits contain an N-terminal domain (NTD), an extracellular agonist binding domain for glutamate/NMDA or glycine binding (ligand binding domain, LBD) consisting of S1 (pre-M1) and S2 (between M3 and M4) regions, a transmembrane domains (TMD) consisting of three transmembrane helices (M1, M3, and M4) and a re-entrant loop (M2) which forms the selectivity filter region, and an intracellular C-terminal domain as shown in figure 4 (Beck et al., 1999; Traynelis et al., 2010).

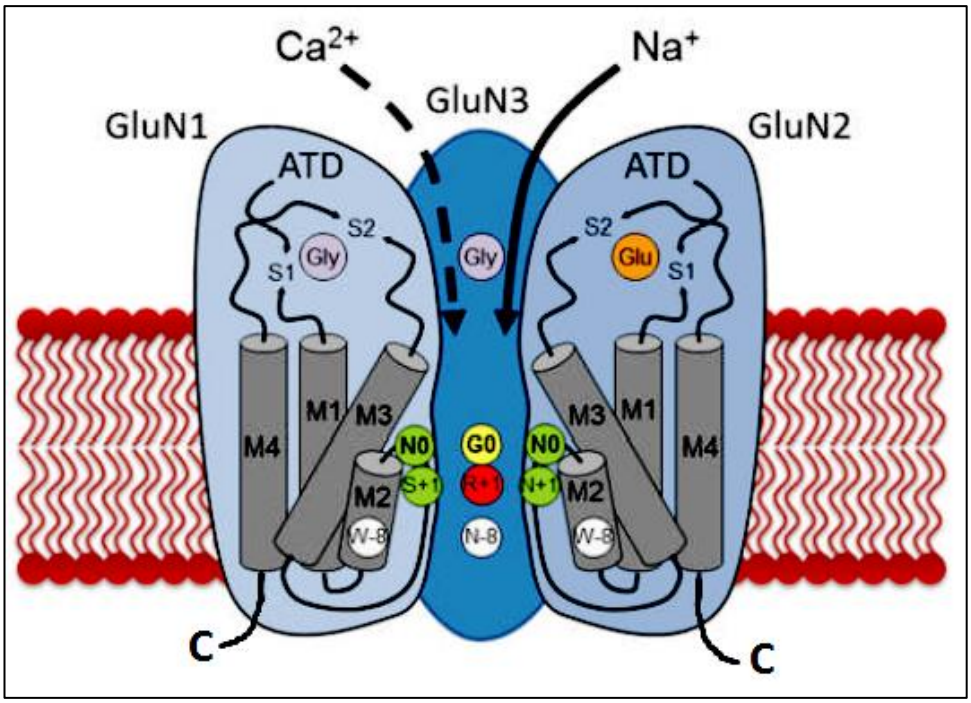


Figure 4: Model structure of GluN1/GluN2/GluN3 assembly.

Only three subunits are shown for clarity. Each subunit consists of an extracellular N-terminal region containing the amino-terminal domain (ATD) and part of the agonist binding site (S1) for glutamate (Glu) or glycine (Gly), a region containing four membrane domains; three transmembrane regions (M1, M3, M4) and a cytoplasmic re-entrant loop (M2) and an intracellular C-terminal domain. Between M3 and M4 is a large extracellular loop that contains the other part of the agonist binding site (S2). Also shown is the Q/R/N site which is the amino acid residue thought to regulate ion selectivity marked by N/G0 (green/yellow circle) as well as +1 (green/red circle) and -8 (white circle) sites. These are all sites of interest in this study.

1.2.1 GluN1

The *Grin1* gene which encodes for the GluN1 subunit is subjected to alternative splicing. This gives rise to eight variants of GluN1 which are differentially distributed and expressed within the CNS (Cull-Candy et al., 2001; Kristiansen et al., 2007). The eight GluN1 variants are GluN1-1a, GluN1-1b, GluN1-2a, GluN1-2b, GluN1-3a, GluN1-3b, GluN1-4a and GluN1-4b. GluN1-1a is the most abundant form and the most extensively characterized (Cavara et al., 2009; Patil et al., 2012; Stephenson, 2006). The GluN1 subunit is fundamental for the functionality of NMDA receptors. It contributes towards channel pore formation and provides the binding site for glycine, the essential co-agonist for glutamate or NMDA (Traynelis et al., 2010; Vrajova et al., 2010). This corresponds with findings that *Xenopus* oocytes expressing just GluN1 are

only faintly stimulated by NMDAR agonists (Moriyoshi et al., 1991) while there is no response recorded in mammalian cells transfected with GluN1 alone (Traynelis et al., 2010).

1.2.2 GluN2

Within a year after GluN1 was cloned, GluN2 subunits were identified as being comprised of four subtypes encoded by four different genes; GluN2A, GluN2B, GluN2C and GluN2D (Ikeda et al., 1992; Kutsuwada et al., 1992; Meguro et al., 1992; Monyer et al., 1992). The GluN2 subunits provide the site for agonist binding (NMDA or glutamate) for activation to occur (Vrajova et al., 2010). The expression of GluN2 subunits, primarily GluN2A and GluN2B, are found abundantly in the forebrain especially in the cortex and hippocampus (Traynelis et al., 2010). Although GluN2B is prominent in the early postnatal brain, this isoform eventually decreases during development while GluN2A increases until they become more abundant than GluN2B. This GluN2B-GluN2A switch occurring during development is postulated to underlie the functional changes in NMDA receptor properties (Liu et al., 2004). GluN2C are found mainly in the cerebellum, and GluN2D subunits are expressed in basal ganglia and associated brainstem nuclei, including the subthalamic nucleus (STN), globus pallidus, striatum, and substantia nigra (Brothwell et al., 2008; Swanger et al., 2015).

GluN2 subunits are critical for the functionality of NMDA receptors and are believed to distinguish the characteristics of the receptor assembly (Saiki et al., 2013; Sanz-Clemente et al., 2013). GluN2 subunits have been demonstrated to control and confer NMDAR pharmacological and kinetic properties (Chen and Wyllie, 2006; Gielen et al., 2009; Yuan et al., 2009). The combination of different GluN2 subunits with GluN1 renders the NMDAR variable in its sensitivity towards block by Mg^{2+} and other antagonists as well potency of agonists and co-agonists (Ishii et al., 1993; Kutsuwada et al., 1992; Monyer et al., 1992; Wyllie et al., 2013) . For example, a study by Wrighton et al. (2008) revealed that the sensitivity to Mg^{2+} block was much less in

GluN2D compared to in GluN2A, by which the effects are mediated not only by the channel pore region but also the ligand binding domain.

1.2.3 GluN3

GluN3A and GluN3B were the final subtypes of NMDAR subunits discovered in 1995 and are of particular interest to this study (Ciabarra et al., 1995; Forcina et al., 1995; Sevarino et al., 1996; Sucher et al., 1995). Rat GluN3A is composed of 1115 amino acids while GluN3B is composed of 1002 amino acids (Pachernegg et al., 2012). Akin to GluN1, GluN3 subunits provide a binding site for glycine but with a stronger affinity compared to the former (Nilsson et al., 2007). On their own, GluN3 subunits are not functional and even when co-expressed with the GluN1 subunit, the combination have not been convincingly proven functional in mammalian neurons (Cull-Candy et al., 2001). However, Chatterton et al. (2002) have reported that *Xenopus* oocytes co-injected with both GluN1 and GluN3 may be stimulated by glycine. So far, receptor assemblies containing GluN3 subunits together with the original composition of GluN1/GluN2A/B subunits have been found in specific areas of the CNS and also expressed in *Xenopus* oocytes or cell lines such as the human embryonic kidney (HEK)-293 cells (Sasaki et al., 2002).

GluN3A has a unique developmental expression pattern distributed across several brain regions (Wong et al., 2002). It is initially expressed in the thalamus, entorhinal cortex, subiculum and several layers of the neocortex. It is elevated during the first postnatal weeks in the CA1 field of the hippocampus and in the thalamus. It has also been detected in the spinal cord, medulla, pons, tegmentum and hypothalamus at varying degrees (Ciabarra et al., 1995; Sucher et al., 1995; Sun et al., 1998). The expression level will eventually decline but remain low in specific areas of the brain throughout adulthood. Therefore it was suggested that GluN3A could control NMDAR function in a time-dependent manner during critical periods of development (Kehoe et al., 2013). GluN3B has a different spatial and temporal expression pattern and can act independently of GluN3A (Cavara et al., 2009; Chatterton et al., 2002; Matsuda et al., 2002; McClymont et al., 2012). The expression of GluN3B mRNA levels

rise throughout the development and is maintained into adulthood, with a distribution in the pons, midbrain, medulla and spinal cord (Matsuda et al., 2002).

Although GluN3 receptor subunit functions are yet to be clearly distinguished, previous studies have demonstrated that they are responsible for: (i) reduced susceptibility to be blocked by Mg^{2+} and reduced Ca^{2+} permeability (Matsuda et al., 2002; McClymont et al., 2012; Sasaki et al., 2002); (ii) reduced single channel conductance thus downregulating the channel current (Das et al., 1998; Sasaki et al., 2002); and (iii) forming excitatory glycine-gated receptor complex with GluN1 (Chatterton et al., 2002; Stephenson, 2006).

A study by McClymont et al. (2012) demonstrated that the incorporation on GluN3 subunits in the original composition of NMDAR impaired the blocking efficacy of several well-known antagonists. More interesting is that NMDAR complexes containing GluN3B generally confer higher resistance to antagonist block compared to GluN3A across different membrane potentials as presented in table 3.

Table 3: IC_{50} for several channel blockers tested on NMDA receptors containing GluN1-1a and GluN2A compared to NMDAR incorporated with GluN3A or GluN3B at three holding potentials.

	-50 mV			-75 mV			-100 mV		
	1/2A	+3A	+3B	1/2A	+3A	+3B	1/2A	+3A	+3B
Mg^{2+}	16.0	**25.8**	**71.6**	4.23	**22.4**	**40.1**	1.74	**5.83**	**15.7**
Memantine	3.94	**15.9**	**18.2**	2.48	**7.54**	**17.5**	0.80	**2.55**	**17.8**
MK-801	0.50	0.49	**5.56**	0.21	0.31	**2.19**	0.19	**0.46**	**0.68**
PhTX-343	17.2	17.3	**62.8**	2.95	4.64	5.74	0.30	**1.40**	**0.93**

IC_{50}s are in µM. Values in bold are significantly different compared to 1/2A (GluN1-1a/GluN2A). Values underlined are significantly different between +3A (GluN1-1a/GluN2A/GluN3A) and +3B (GluN1-1a/GluN2A/GluN3B). Adapted from McClymont et al. (2012).

The study by McClymont et al. (2012) provided evidence that NMDARs containing GluN3 subunits generally cause reduced Mg^{2+} block resulting in significant increase of IC_{50} for Mg^{2+} and several other open channel blockers tested. It was strongly postulated that the amino acid residue, glycine (G) located at the selectivity filter in the M2 pore region might be the reason for this phenomena since this site is known to be responsible for ion permeation and Mg^{2+} block. The site termed 'Q/R/N' is further discussed in the next section. A summary of the NMDAR subunit diversity, structure and expression is presented in figure 5.

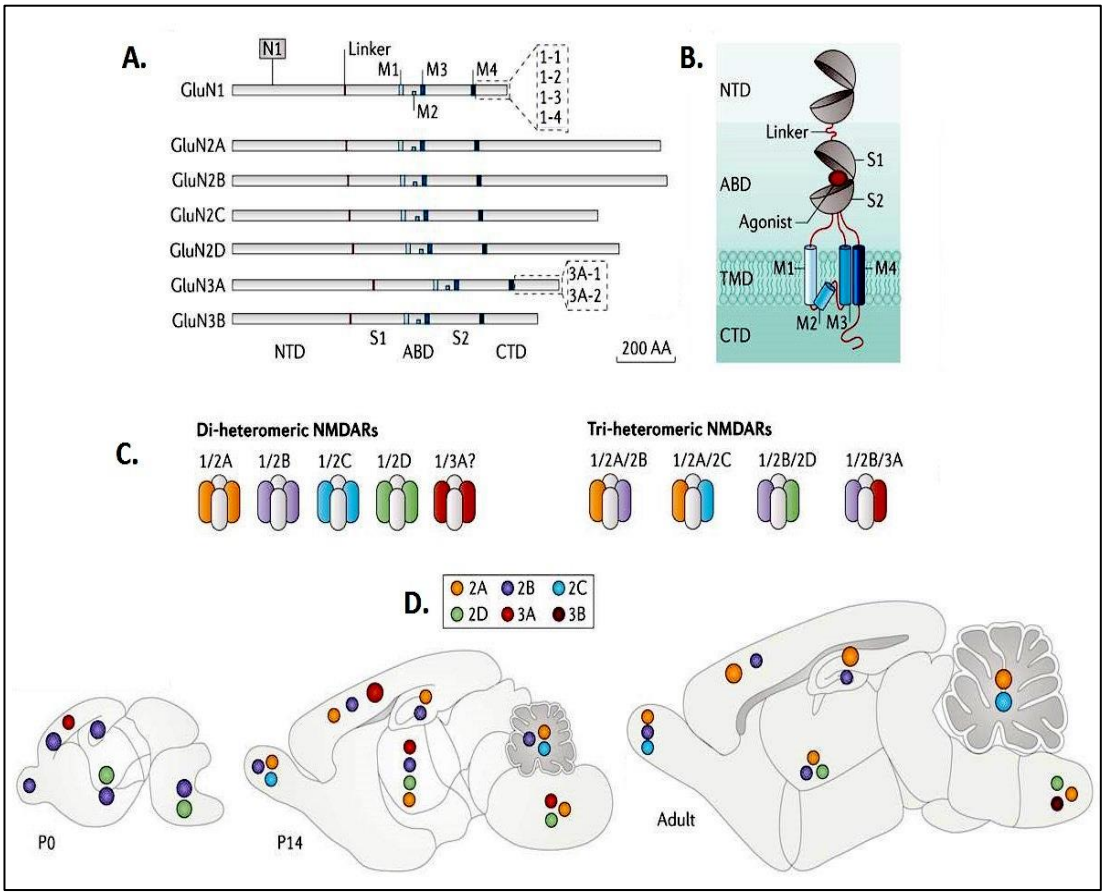


Figure 5: NMDAR subunit diversity, structure and expression.

(A) The seven NMDAR subunits that have been identified: GluN1, GluN2A-D and GluN3A-B. GluN1 and GluN3A subunits undergo further alternative splicing. M1-M4 represent membrane segments. (B) Modular architecture shared by all GluN subunits consisting of the N-terminal domain (NTD), the agonist-binding domain (ABD), the transmembrane domain (TMD) containing the channel pore, and the intracellular C-terminal domain (CTD). (C) Example of possible combinations of NMDAR subunit assemblies. (D) GluN subunit expression in the mouse brain at day of birth (postnatal day 0 (P0)), 14 days after birth (P14) and at the adult stage. Adapted from Paoletti et al. (2013).

1.2.4 The Q/R/N Site and mRNA Editing

The narrow selectivity filter region of NMDARs is formed at the M2 loop domain and constitutes an important amino acid that controls single channel conductance, Ca^{2+} influx and voltage-dependent block by Mg^{2+} as well as polyamines (Burnashev, 1998; Burnashev et al., 1992; Traynelis et al., 2010). In GluN1 and GluN2A-D, this site is occupied by asparagine (N), while in AMPAR (except GluA2) and KAR (except some GluK1 and GluK2), the site is occupied by glutamine (Q). These sites promote Ca^{2+} permeability. In GluA2 and some GluK1 and GluK2, mRNA editing replaces Q by the positively charged arginine (R) that abolishes Ca^{2+} permeability and prevents the block by intracellular polyamines that causes inward rectification in GluA2-lacking AMPARs. The site has thus been termed the 'Q/R/N site' (Burnashev, 1998; Wollmuth et al., 1996; Wollmuth and Sakmann, 1998) and has been widely studied in terms of its effect on permeation and channel conductance. An alignment of amino acid sequences for NMDAR subunits in both rat and human in contrast to GluA1 and GluA2 at the homologous position in relation to the Q/R/N site is presented in figure 6.

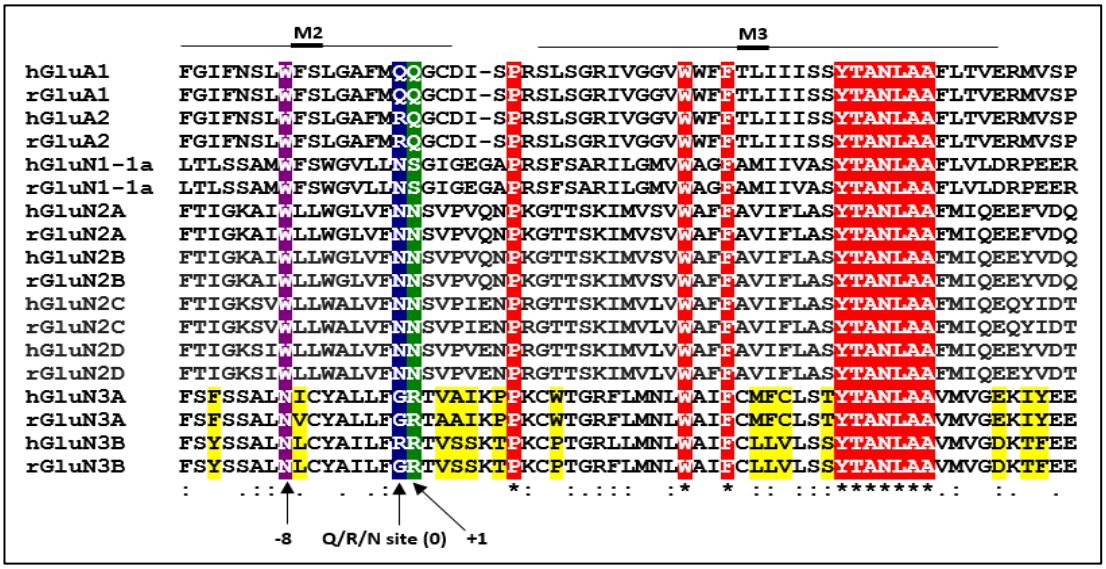


Figure 6: Amino acid sequences of NMDAR subunits aligned with AMPAR subunits, GluA1 and GluA2 at the major pore lining regions (M2-M3) in rat and human.

In relation to the Q/R/N amino acid, this site is considered as position 0 and highlighted in blue. The adjacent amino acid to the right considered as position +1 (highlighted in green) and amino acid at position -8 (highlighted in purple) are also of interest in this study. Differences between GluN3A and GluN3B are highlighted in yellow. Fully conserved residues are highlighted in red, also indicated with asterisks. Double dots represent groups of strongly similar residues and single dots represent groups of weakly similar residues. r = rat, h = human. Sequence alignment was generated via http://www.ebi.ac.uk/Tools/msa/clustalo/

In the conventional heteromeric NMDAR composition, N occupying the Q/R/N site in GluN1/GluN2 subunits confers the receptor's property of high Ca^{2+} permeability. Analogous to the situation, GluA2 in AMPARs with R at the Q/R/N site when co-expressed with other AMPAR subunits, cause a reduction in Ca^{2+} permeability and blocking potency by AMPAR open channel blockers including polyamines, polyamine-containing toxins and dicationic derivatives of adamantine (Bolshakov et al., 2005; Cavara and Hollmann, 2008; Mellor and Usherwood, 2004; Strømgaard and Mellor, 2004). One study has shown that in GluN1, amino acid replacement at the Q/R/N position was found to strongly affect Ca^{2+}permeability but not block by Mg^{2+}. In GluN2, however, the same study revealed an almost opposite effect; i.e. a mutation at this site was demonstrated to heavily influence Mg^{2+} block activity although having only weak effects on Ca^{2+} ion permeation (Burnashev et al., 1992).

In the less well characterised members, GluN3A-B, this site is occupied in most cases by glycine (G) which might explain why NMDARs containing either of these subunits are less permeable to Ca^{2+} (Ciabarra et al., 1995; Sucher et al., 1995). Also of significance to the role of GluN3 subunits is the next residue downstream which is R at the +1 site as opposed to Q, S, or N in other members of iGluR subunits. This R is also very likely involved in ion permeation as previous studies have shown that it has an impact on open channel block. Mg^{2+}, memantine and MK-801 have been demonstrated to have binding sites at N of the Q/R/N site in both GluN1 and GluN2 subunits and the +1 residue adjacent to this in GluN2 (Burnashev et al., 1992; Kashiwagi et al., 2002; Mori et al., 1992; Sakurada et al., 1993). Interestingly, DNA sequencing has revealed that human GluN3B contains R, both at the Q/R/N and +1 sites in contrast to all other known GluN3 subunits which may confer even stronger resistance to open channel block and Ca^{2+} permeability (Andersson et al., 2001; Nishi et al., 2001). Another important residue is Tryptophan (W) at the -8 site; when mutated to N in GluN2, blocking potencies of memantine and MK-801 are reduced (Kashiwagi et al., 2002). The equivalent position in GluN3A and GluN3B is occupied by N while all other subunits contain a W. These sites were further investigated in the present study.

1.3 NMDA RECEPTOR CHANNEL BLOCK

NMDA receptor antagonists can be classified into four categories as depicted in figure 7: (i) competitive antagonists which bind and block the NMDAR agonist binding site; (ii) glycine antagonists which bind and block the binding site of glycine as the co-agonist; (iii) non-competitive antagonists which bind other sites on the NMDAR, for example the allosteric sites, thus inhibiting the NMDAR; and (iv) uncompetitive antagonists which bind to a site within the pore thus blocking the receptor channel (Kim et al., 2002).

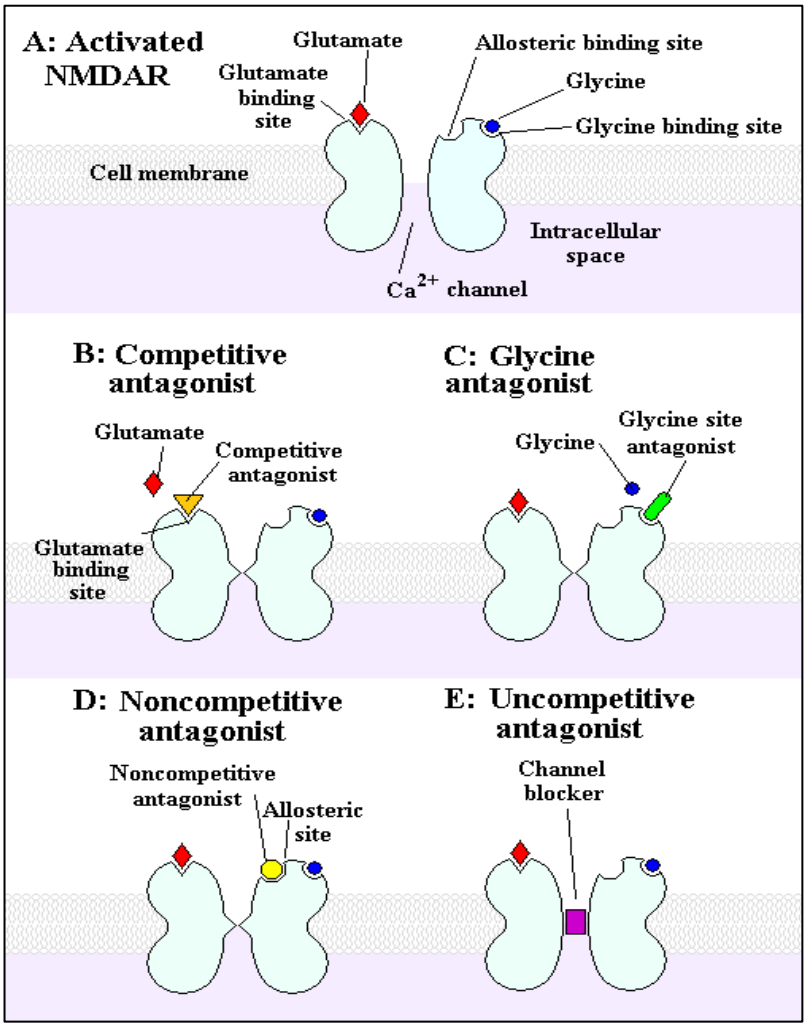


Figure 7: A simplified schematic showing activated NMDAR and the mechanism of NMDAR block by various types of antagonists. Adapted from Kim et al. (2002) and Delldot (2007).

NMDA receptors can be antagonised by Zn^{2+}, Mg^{2+} and polyamines in a voltage-dependent manner, a characteristic which is important for the regulation of neuronal physiological function (Traynelis et al., 2010). While Mg^{2+} was postulated to bind in the channel pore (Nikolaev et al., 2012), Zn^{2+} and polyamines may also bind at the ATD site in both GluN1 and GluN2 subunits (Blanke and VanDongen, 2009).

This present study assessed several known NMDA antagonists such as Mg^{2+}, memantine, MK-801, philanthotoxin-343 (PhTX-343) and a variety of new compounds derived from memantine, spermine and spermidine as discussed further in this section.

1.3.1 Mg^{2+}

Numerous studies in the 1980s and 1990s have established that Mg^{2+} blocks NMDARs in a voltage-dependent manner (Ault et al., 1980; Mayer et al., 1984; Nowak et al., 1984; Paoletti et al., 1995). Regulation of NMDAR by extracellular Mg^{2+} block plays a pivotal role in synaptic plasticity which mediates higher cognitive function such as learning and memory (Traynelis et al., 2010). A mutagenesis study by Mori et al. (1992) suggested that the N residue at the Q/R/N site of the M2 domain constitutes the binding site for Mg^{2+}. It was found that Mg^{2+} block was void when the N was substituted with Q at the Q/R/N site of either GluN1 or GluN2, or indeed both. Consistent with previous studies, McClymont et al. (2012) demonstrated the voltage-dependent block by Mg^{2+} and substantiated the evidence that GluN3 caused reduction of Mg^{2+} block when incorporated with GluN1-1a/GluN2A subunits. Even more interesting is that GluN3B resulted in an even higher IC_{50} value for Mg^{2+} compared to GluN3A and observed at all three membrane potentials tested.

1.3.2 Memantine

Memantine (chemical name: 1-amino-3,5-dimethyladamantane hydrochloride, molecular formula: $C_{12}H_{21}N$ HCl) is an un-competitive NMDAR blocker currently used as a clinical drug to treat the symptoms of moderate to severe Alzheimer's disease (Atri et al., 2013). Memantine was first marketed in Germany in 1982 which was originally intended for use in the treatment of organic brain syndrome – a term representing any mental disorder associated with changes in brain tissue (Diamond, 2011; Forest Laboratories, 2003). The structure of memantine is presented in figure 8.

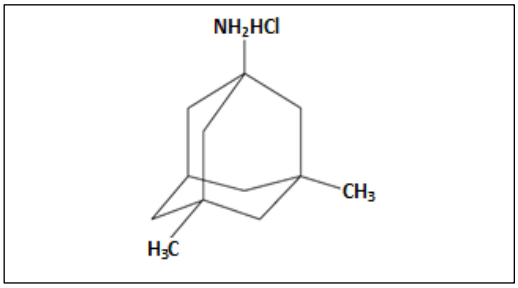


Figure 8: Chemical structure of memantine.
Adapted from Molinuevo (2005).

As an open channel blocker, memantine requires pre-activation of the receptor channel by an agonist before inhibition can take place (Frolund et al., 2010). It works by preventing excitotoxicity without interfering with physiological activation of the receptor essential for normal brain function. This may be the reason for its success in treating Alzheimer's disease compared to other inhibitors. Patients generally tolerate memantine well due to its moderate blocking potency resulting in minimal side effects often seen in treatments with other strong antagonists (Robinson, 2008).

Antagonism by memantine is reported to be highly voltage-dependent and shows little selectivity on three combinations of NMDAR (GluN1/GluN2A, GluN1/GluN2B, GluN1/GluN2D) expressed in HEK-293 cells (Bresink et al., 1996). However, McClymont et al. (2012) reported that incorporation of GluN3 subunits in a GluN1/GluN2A receptor assembly does affect memantine block where IC_{50} of

memantine was increased at all membrane potentials tested. Similar to Mg^{2+} block, GluN3B greatly reduces memantine inhibition compared to GluN3A.

1.3.3 MK-801

MK-801 (chemical name: (+)-5-methyl-10, 1 1-dihydro-5*H*-dibenzo[*a,d*]cyclohepten-5,10-imine maleate, molecular formula: $C_{16}H_{15}N$) also known as dizocilpine was first discovered by Merck in 1982. It is a potent and selective un-competitive antagonist of the NMDA receptor (Foster and Wong, 1987; Wong et al., 1986). The chemical structure of MK-801 is presented in figure 9.

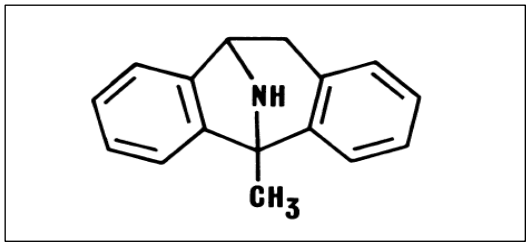


Figure 9: Chemical structure of MK-801.
Adapted from and Wong et al. (1986).

MK-801 possesses secondary amine and benzenoid functions and displays a wide array of biological properties including anticonvulsant and anaesthetic (Kovacic and Somanathan, 2010). MK-801 is also known to affect the processing underlying sensory (Al-Amin and Schwarzkopf, 1996) and locomotor activity (Liljequist et al., 1991).

Wong et al. (1986) reported that MK-801 possesses high-affinity binding properties to NMDA receptors in rat brain membranes especially in the hippocampus. Other regions displaying high affinity were cerebral cortex, corpus striatum, and medulla-pons, while no binding was detected in the cerebellum. In contrast to memantine, it has a very slow onset with slow block recovery. *In vitro* neurophysiological studies using a preparation of rat cortical-slice show a potent, selective, and un-competitive blocking by MK-801 of depolarizing responses to NMDA, but not to other agonists such as kainate or quisqualate. The compound however has been demonstrated to

selectively bind to GluN1/GluN2A and GluN1/GluN2B subunit combinations compared to receptor assemblies containing GluN2C and GluN2D in both HEK-293 cells as well as *Xenopus* oocytes (Laurie and Seeburg, 1994; Yamakura et al., 1993). However, more recent findings have demonstrated that MK-801 has the ability to also block NMDAR containing GluN2C or GluN2D but is dependent on the pH as well as stereo-selectivity of the compound (Dravid et al., 2007).

Electrophysiology experiments have demonstrated that the potency of MK-801 to inhibit NMDA responses is found to be use-dependent, where the extent of blockade is accelerated by addition of NMDA agonists instead of the duration which the receptor is exposed to MK-801 (Foster and Wong, 1987). Mutagenesis studies have demonstrated that the binding site for MK-801 may overlap with or be the same as, Mg^{2+} and memantine at the Q/R/N, +1 and other sites of the channel pore (Kashiwagi et al., 2002; Mori et al., 1992). This may explain the similarity of blocking pattern by MK-801 with Mg^{2+} and memantine, and that GluN3 generally results in a reduction of channel block by these compounds although less significantly by MK-801 (McClymont et al., 2012).

MK-801, however, was shown to possess certain characteristics which compromised its use in clinical settings. Unlike memantine, it is not well tolerated in human and is more potent on receptor combinations containing subunits abundantly found in the cortex. Early studies also showed that MK-801 exerts negative side-effects including stereotypy, catalepsy, motor incoordination and psychomimetic-like side effects (Bresink et al., 1996; Koek et al., 1988), acute cytopathological changes in neurons (Olney et al., 1989), memory and learning impairments as well as cardiovascular changes (Bischoff and Tiedtke, 1992; Danysz et al., 1995).

1.3.4 Polyamines: Spermine and Spermidine

Spermine is a natural polyamine formed from spermidine and found in almost all prokaryotic and eukaryotic cells (Seiler, 2005). Both spermine and spermidine are involved in various metabolic functions necessary for cell growth and proliferation (Zini et al., 2009). The chemical structures of spermine and spermidine are shown in figure 10.

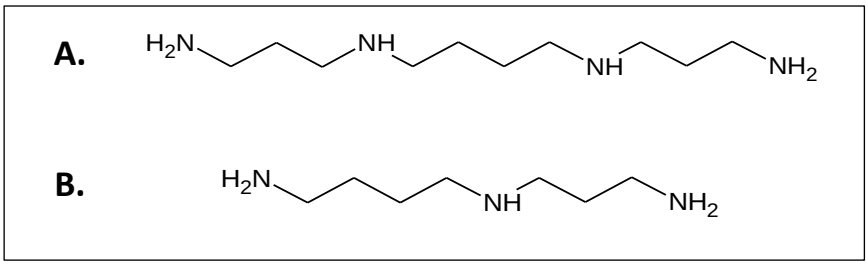


Figure 10: Chemical structures of (A) spermine and (B) spermidine.
Adapted from Williams (1997a).

The original discovery that NMDAR may be regulated by polyamines was shown by Ransom and Stec (1988) who demonstrated that spermine and spermidine at higher concentrations enhanced the binding of MK-801 to NMDAR. Both spermine and spermidine were also shown to directly block NMDAR, with the latter somewhat less potent than the former (Williams, 1997b). The current study employed several polyamines known to block NMDAR such as philanthotoxin-343 as well as novel spermine-derived compounds.

1.3.5 Philanthotoxin Analogues

The philanthotoxin isolated from solitary digger wasp, *Philanthus triangulum* venom was first discovered by T. Piek and colleagues noting that it exerted glutamate receptor blocking properties (Piek et al., 1971; Piek et al., 1980; Piek and Njio, 1975). The natural pure toxin, containing a butyryl/tyrosyl/polyamine structure was eventually purified and termed PhTX-433. Subsequently two closely related analogues, PhTX-334 and PhTX-343 (numerals denote the number of methylenes between the amino group of the spermine moiety from left to right) were synthesized

but still retaining the pharmacologically active properties (Eldefrawi et al., 1988). Philanthotoxin compounds are typically 2.0 to 4.0 nm long, and contain a polyamine chain with an amide-linked aromatic amino acid at the headgroup. Due to its length, it was postulated that the molecule would interact with multiple amino acids within the channel pore (Bähring and Mayer, 1998).

Shown in figure 11 are the chemical structures of PhTX-433 which consists of a tyrosyl headgroup and a butyryl side chain attached to a thermospermine moiety and PhTX-343 with thermospermine exchanged for symmetrical spermine.

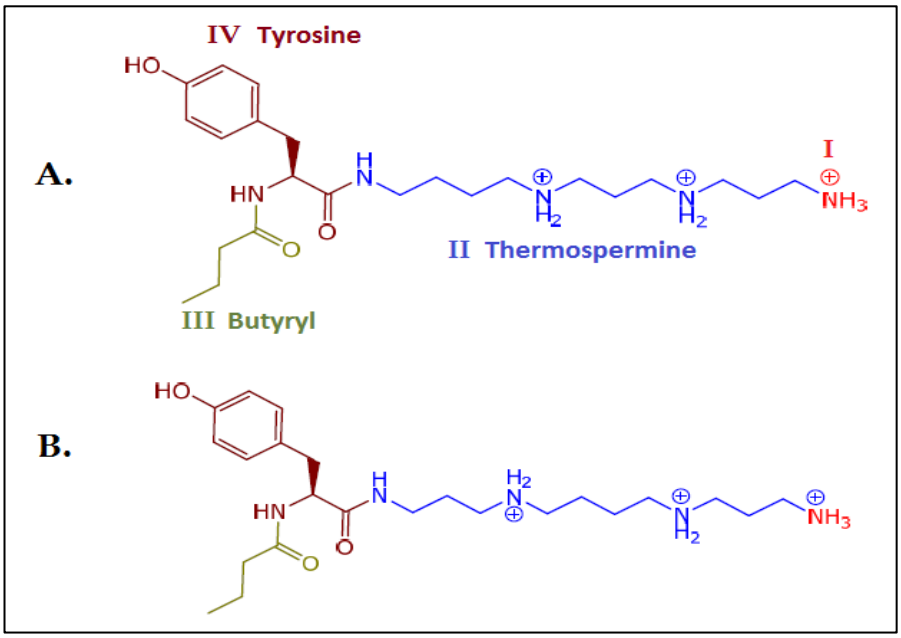


Figure 11: Chemical structures of (A) PhTX-433 and (B) PhTX-343.
The structures of philanthotoxin compounds are composed of (i) an ammonium group, (ii) a long polyamine (thermospermine) chain, (iii) an aliphatic butyryl group and (iv) an aromatic tyrosyl group. Adapted from Frolund et al. (2010) and Kachel (2014).

PhTX-343 is an un-competitive antagonist for all three classes of glutamate receptors including NMDAR (Bähring and Mayer, 1998; Brackley et al., 1993; Huang et al., 1997). Antagonism by PhTX-343 is reported to be use- and voltage-dependent suggesting the interaction of this compound with open channel conformations of the receptor and exhibit slow dissociation from the binding site (Brackley et al., 1993).

A previous study showed that at concentrations of 0.1 and 10 µM, PhTX-343 blocked the glutamate response by 9% and 61% in *Xenopus* oocytes expressing GluN1/GluN2A subunits at -60 mV (Frolund et al., 2010). In the study by McClymont et al. (2012), PhTX-343 block was shown to be strongly dependent on membrane potential which suggests a deep pore binding site for this compound. In relation to GluN3, blocking by this compound was only affected at a less negative membrane potentials. The IC_{50} of PhTX-343 was significantly higher in NMDAR co-expressed with GluN3 subunits compared to GluN1/GluN2A assembly without GluN3A or GluN3B.

A variety of synthetic philanthotoxin analogues have been developed as structural modifications have been shown to improve potency and selectivity of the compound (Strømgaard et al., 2005). The current study evaluated two novel philanthotoxin analogues which were synthesized in collaboration with Dr. Henrik Franzyk and Prof. Kristian Strømgaard from the University of Copenhagen, Denmark. These compounds were incorporated with a cyclohexyl- or benzyl-group. A previous study by Mellor et al. (2003) showed enhanced blocking potencies on ionotropic glutamate receptors for philanthotoxin analogues containing these two moieties. For one of the analogues, the tyrosine group was replaced with a cyclohexylalanine and termed as cyclohexylalanine-philanthotoxin-343 (Cha-PhTX-343). For the other analogue, two modifications were introduced, the tyrosyl group was substituted with cyclohexylalanine and a benzene was introduced at the butyryl group. The compound was hence termed as benzyl-cyclohexylalanine-philanthotoxin-343 (Bn-Cha-PhTX-343). Structures of the compounds are displayed in figure 12.

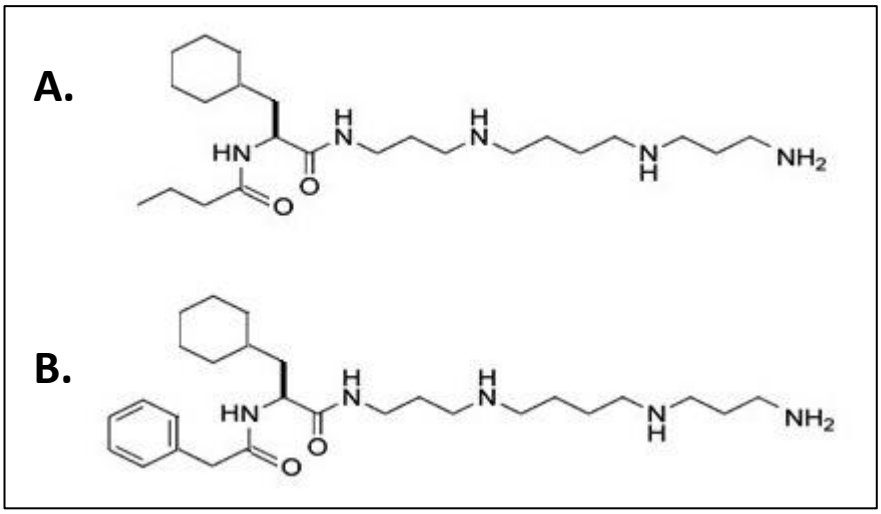


Figure 12: Structure of philanthotoxin analogues. (A) Cyclohexylalanine-philanthotoxin-343 (Cha-PhTX-343), (B) Benzyl-cyclohexylalanine-philanthotoxin-343 (Bz-Cha-PhTX-343).

1.4 ALZHEIMER'S DISEASE (AD) AND NMDA RECEPTORS

1.4.1 Epidemiology of Dementia and AD

Dementia is a global health problem which affects not only individuals suffering from the disease and their society but it also has a profound effect on global productivity and world economics (Murphy et al., 2014). Alzheimer's Disease (AD) is the most prevalent type of dementia which accounts for about 60-80% of all dementia cases (Imtiaz et al., 2014). According to a comprehensive systematic review and meta-analysis conducted by Prince et al. (2013), it was estimated that 35.6 million of the world population suffered from dementia in 2010. Western Europe had the highest number of population suffering from dementia with 7 million, followed by East Asia (5.5 million), South Asia (4.5 million) and North America (4.4 million). Ranking the countries with the highest number of people living with dementia, China came in first with 5.4 million, followed by USA (3.9 million), India (3.7 million), Japan (2.5 million), Germany (1.5 million), Russia (1.2 million), France (1.1 million), Italy (1.1 million) and Brazil (1.0 million). It was estimated that there were 9.9 million new cases in 2015 bringing the total to 46 million people suffering from dementia today. This is larger than the entire population of Spain (Prince et al., 2015).

With the increase of worldwide population longevity, the prevalence was expected to increase over the years and will almost quadruple in the next 30 years (Prince et al., 2015; Reitz and Mayeux, 2014). 2010 to 2050 projections by Prince et al. (2013) estimated a moderate increase for developed regions: 87% rise in Europe, 148% in the developed Asia-Pacific countries, 151% in North America and 200% in South Latin America (starting from a high point of the present incidence at the time the report was produced). Starting from a low base, other parts of Latin America and North Africa/Middle East were predicted to experience tremendous increases of more than 400% to 500%. Starting from a high base, other parts of Asia would also experience rapid growth with 282% increase in South Asia and 311% in East Asia. Modest increases were expected in Sub-Saharan Africa (100% to 300%) due to high occurrence of child mortality and AIDS. Figure 13 depicts the global incidence of worldwide population suffering from dementia and the projection for the next 35 years.

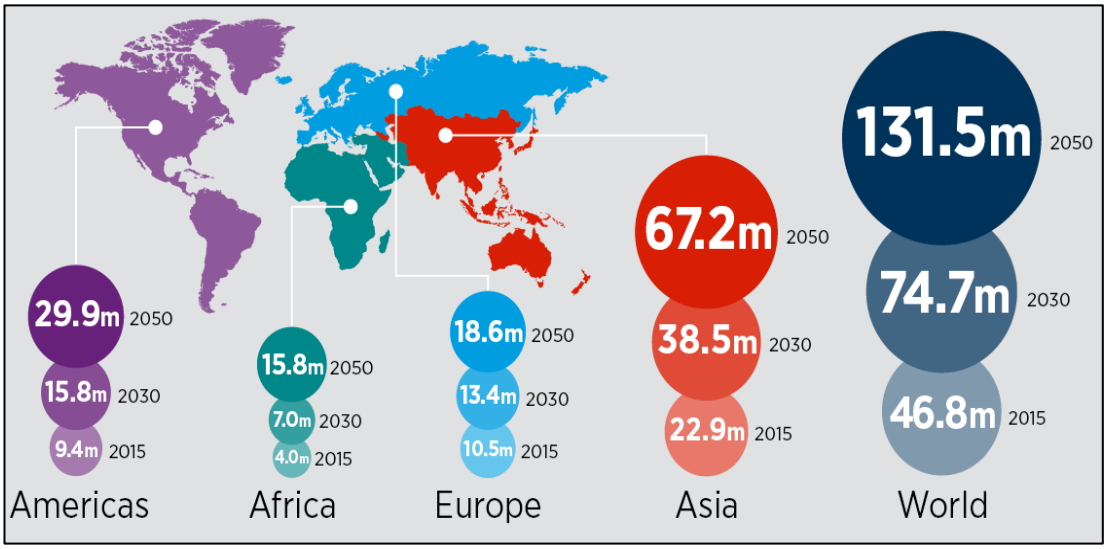


Figure 13: Global incidence of people living with dementia.
Source: Prince et al. (2015)

Dementia has put an extreme burden on the world economy. According to the World Alzheimer Report 2015, global costs for medical, social and informal care of dementia patients have risen from US$ 604 billion in 2010 to US$ 818 billion in 2015. The cost is estimated to increase to a trillion dollars by the year 2018. These alarming facts

and figures emphasize the importance of research into the neuropathogenesis of dementias and AD, the development of therapeutic strategies, as well as prevention mechanism for this debilitating disease.

1.4.2 Pathogenesis of AD

Dementia is manifested by progressive deterioration of cognitive functions especially memory impairments and inability to execute normal daily activities (O'Brien and Wong, 2011; Riedel, 2014). AD was first described by a German psychiatrist, Dr. Alois Alzheimer more than a century ago when he was presented with a female patient (Auguste Deter, 51 years old) whom over the years, experienced memory loss, paranoia, hallucinations and general cognitive decline before she died (Qiu et al., 2009). Post-mortem histopathology investigations of her brain revealed abundant cortical plaques and neurofibrillary tangles that were later confirmed to be the primary features of the disease (Goedert and Ghetti, 2007; Miklossy, 2015). Since then, extensive research has been conducted concerning the pathophysiology of AD and until now definite answers remain ambiguous due to the multifactorial nature of the disease. Unfortunately, a cure is still a long way off. The general consensus, however, acknowledges the notion that progressive accumulation of β-amyloid (Aβ) protein underlies the pathogenesis of AD (Crews and Masliah, 2010) and that such plaques are normally surrounded by neurofibrillary tangles and accompanied by intense microgliosis as well as loss of neurons, white matter and synapses (Reitz and Mayeux, 2014). 20% to 30% of AD cases, however, also presented with cerebrovascular pathologies mainly atherosclerosis (Dolan et al., 2010) and aggregation of Lewy bodies (Schneider et al., 2007) mixed with neuritic plaques and neurofibrillary tangles composed of hyperphosphorylated tau protein (O'Brien and Wong, 2011). An example of a brain biopsy from an AD patient revealing senile plaques and neurofibrillary tangles is presented in figure 14.

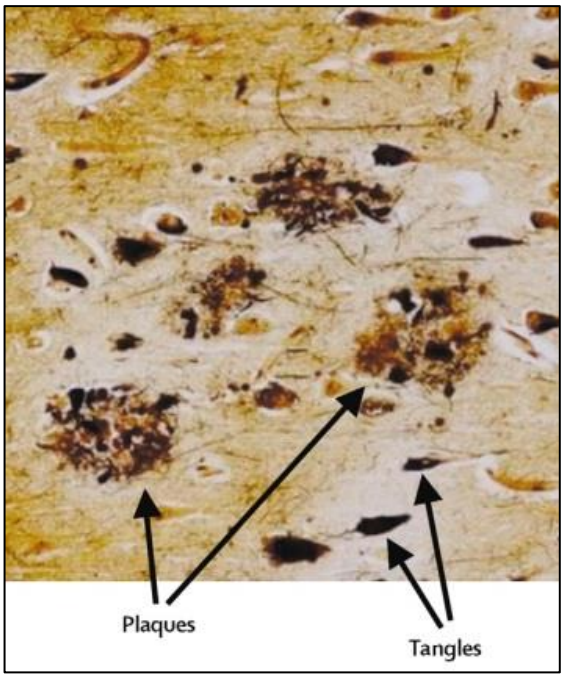


Figure 14: Senile plaques and neurofibrillary tangles observed in the cortex of an Alzheimer's disease patient. Source: Blennow et al. (2006)

It is widely postulated that the neuropathological changes in AD are the results of both environmental and genetic factors. Although the majority of AD cases remain causally unknown, one to five percent of the cases are attributed to genetic hereditary factor which result in presentation of an early onset type of AD (EOAD) (Reitz and Mayeux, 2014).

Four major genetic predisposing factors underlying the pathogenesis of predominantly early AD in relation to the Aβ phenotype are summarized in table 4.

Table 4: Genetic predisposition to Alzheimer's disease in relation to Aβ expression.

Chromosome	Gene Defect	Aβ Phenotype	Onset
21	*APP* mutation	Increased total Aβ or $A\beta_{42}$	Early
14	*PSEN1* mutation	Increased $A\beta_{42}$	Early
1	*PSEN2* mutation	Increased $A\beta_{42}$	Early
19	*APOε4* variant	Increased Aβ plaques and vascular deposits	Late and early

Adapted from Selkoe (2004).

EOAD, also termed as familial Alzheimer's disease (FAD) is a rare autosomal dominant form of AD commonly associated with mutations in three main genes: *APP* gene on chromosome 21 which encodes the amyloid precursor protein; *PSEN1* gene on chromosome 14 encoding presenilin-1 (PS-1); and *PSEN2* gene located on chromosome 1 which codes for presenilin-2 (PS-2) (Crews and Masliah, 2010). Mutations in all three genes involved in EOAD are thought to contribute towards Aβ and tau pathologies (Iqbal et al., 2014). APP is the precursor molecule which undergoes proteolysis giving rise to the neurotoxic Aβ plaques, the key hallmark of AD (O'Brien and Wong, 2011). PS-1 and PS-2 selectively elevate $A\beta_{42}$, the most toxic amyloidogenic form of the protein plaque (Younkin, 2006). Studies have also shown that PS-1 and PS-2 have roles in the activity of γ-secretase, an enzyme that cleaves APP forming Aβ peptide (De Strooper et al., 1998; Vassar, 1999). Approximately half of all FAD patients are reported to possess damaging loss-of-function mutations in the *PSEN* genes (Bi, 2010).

The majority of late onset Alzheimer's disease (LOAD) cases are sporadic and idiopathic (Iqbal et al., 2014). Whereas EOAD is linked to the build-up of Aβ plaques in the brain, sporadic Alzheimer's disease (SAD) or LOAD has been associated with the failure to remove excess Aβ in the brain resulting in imbalance of production and clearance (Dong et al., 2012; Selkoe, 2004). LOAD is characteristically heterogeneous and is attributed to the interaction of both genetic and environmental factors (Crews and Masliah, 2010). Indeed more recently, it has been postulated that the interaction between genetic and environment factors in neurological and neurodegenerative diseases may occur through epigenetic mechanisms (Landgrave-Gomez et al., 2015).

APOε4 allele of the *APOE* gene located on chromosome 19q13 is one of the few known large effect genetic risk factors for LOAD. Apolipoprotein E4 (ApoE4) encoded by the *APOE* gene is thought to interact via two different pathways; one is amyloid-dependent and the other is not. Spinney (2014) described the first pathway as involving ApoE possibly acting as a molecular pathological chaperone in promoting the deposition of Aβ protein in the brain whereas the second pathway involves the

metabolism of ApoE into toxic fragments that have harmful effects on mitochondria and the cell skeleton (Spinney, 2014).

Numerous studies have been conducted to elucidate the pathological role of Aβ in EOAD and LOAD. Research findings have demonstrated that Aβ oligomer interferes with calcium signalling, instigates oxidative damage and induces mitochondrial dysfunction (Dong et al., 2012). Aβ dimers were shown to inhibit hippocampal synaptic plasticity *in vivo* (Klyubin et al., 2008) whereas neurons exposed to $A\beta_{42}$ results in rapid loss of tau-dependent microtubule assembly. Walsh and Selkoe (2004) provided evidence of a damaged synaptic morphology and decline in postsynaptic receptor function caused by soluble Aβ oligomers. This synaptic deficits and disruption of neuronal networks potentially caused by Aβ are postulated as contributing to the etiopathogenesis of cognitive dysfunction in AD (Dong et al., 2012).

In LOAD, the failure to degrade and remove Aβ have also been linked to many enzymes such as neprilysin (NEP) and insulin-degrading enzyme (IDE). Studies have shown that these enzymes are reduced in AD resulting in the failure of Aβ clearance (Dong et al., 2012; Miners et al., 2008).

A schematic diagram representing potential mechanisms underlying AD development in relation to Aβ formation (often termed the amyloid cascade hypothesis) is outlined in figure 15.

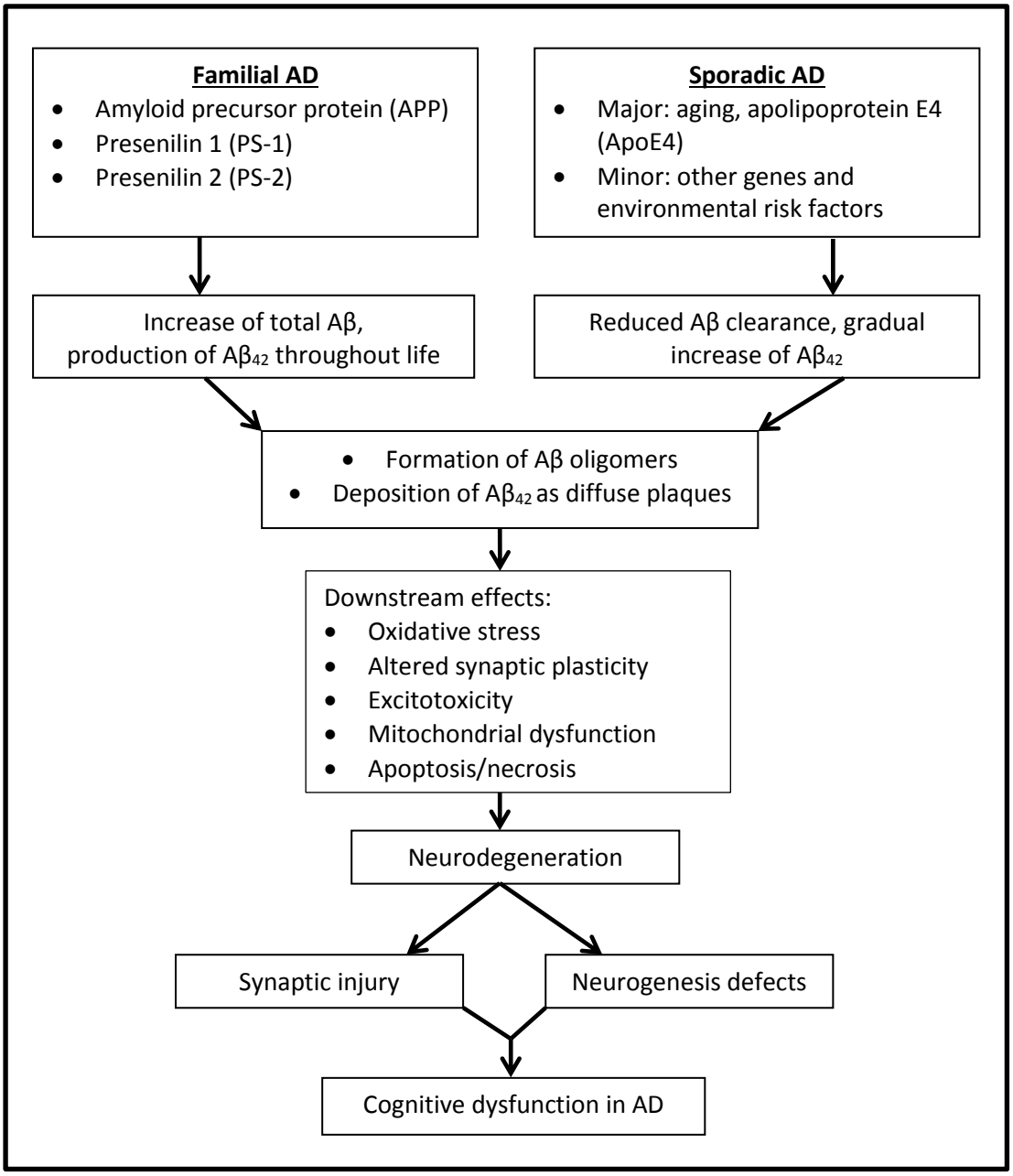


Figure 15: Schematic diagram of the amyloid cascade hypothesis underlying AD pathogenesis.

Cellular dysfunction will lead to the formation of Aβ plaques which in turn contribute to neurogenesis defects and synaptic damage ultimately causing impairments of the cognitive function seen in Alzheimer's disease. It is, however, important to note that although the direct association between Aβ and neuropathology is unquestioned, the exact mechanism by which Aβ pathology impairs neuronal function and memory remains unclear. Adapted from Blennow et al. (2015), Crews and Masliah (2010), Dong et al. (2012) and Selkoe (2004).

Aside from the amyloid cascade, the cholinergic pathway is another model for AD pathology and it is what most currently available AD therapeutics were based on (Craig et al., 2011; Francis et al., 1999). Investigations undertaken in the late 60s to mid-70s revealed marked decline of an enzyme involved in acetylcholine (ACh) production - choline acetyltransferase (ChAT), decreased uptake of choline as well as reduced ACh release in AD patients. These findings support the notion of a 'cholinergic deficiency' (Francis et al., 1999). The fact that ACh neurotransmission is implicated in the role of learning and memory (Fibiger, 1991), cholinergic deficits were suggested to significantly contribute to cognitive impairment observed in AD patients (Araujo et al., 2005; Francis et al., 1999).

Another pathological characteristic strongly associated with AD is oxidative stress (Moreira et al., 2005). *In vitro* models have demonstrated that cells exposed to Aβ induce excess flux of Ca^{2+} and oxidative damage contributing towards neurotoxicity (Mattson, 2004; Tabner et al., 2005). Aβ was hypothesized to be involved in the production of peptidyl radicals (Hensley et al., 1994) and the direct generation of H_2O_2 (Tabner et al., 2005). It is, however, unclear when exactly oxidative stress starts to play a role in the AD pathogenesis. Drake et al. (2003) and Moreira et al. (2005) suggested that oxidative stress precedes the event by which formation of senile plaques and tangles took place, as well as prefibrillar deposition of Aβ demonstrated by *in vivo* model. Tamagno et al. (2002) noted that oxidative stress stimulates activation of β-secretase activity, an enzyme essential for the processing of APP to Aβ-protein.

A model of the neurochemical changes observed in Alzheimer's disease is illustrated by Meltzer and Francis (2001) and as shown in figure 16.

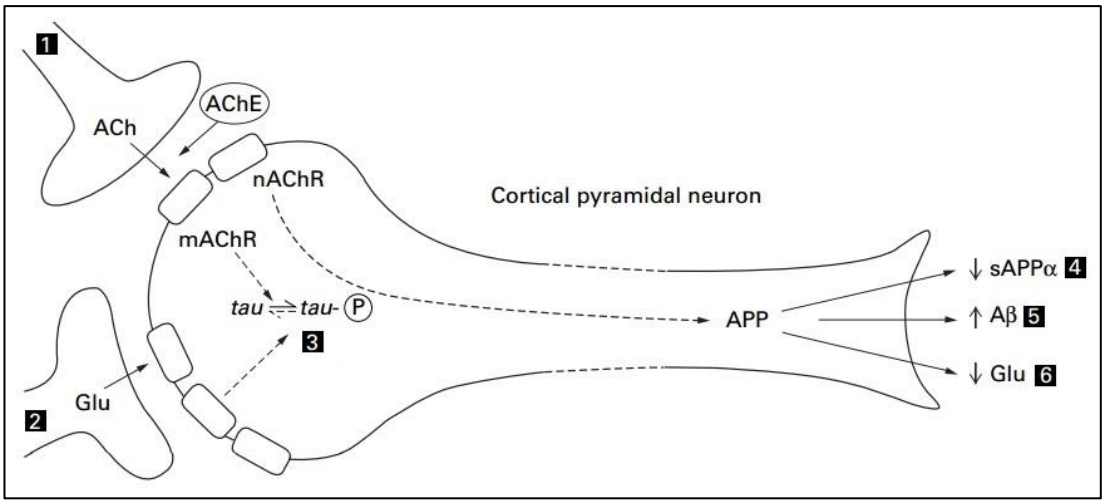


Figure 16: Proposed neurochemical alterations in AD cortical synaptic transmission.

(1) Decreased cholinergic activation; (2) Decreased glutamatergic neurotransmission due to neuron or synapse loss; (3) tau hyperphosphorylation leading to formation of neurofibrillary tangles; (4) decreased excretion of soluble APP; (5) elevation of Aβ production; (6) decreased glutamate production. It is hypothesised that these alterations result in the development of AD clinical symptoms and contribute to the spread of pathology. Adapted from Meltzer and Francis (2001).

1.4.3 NMDAR-Implicated Pathogenesis

As it has long been established that NMDARs are involved in synaptic plasticity, learning and memory (Takatsuki et al., 2001), they are thought to have important roles in the underlying pathophysiology of AD (Malinow, 2012). Much evidence exists linking the pathogenesis of AD with NMDARs and Aβ proteins particularly the oligomeric soluble form. For example, increased levels of Aβ proteins have been shown to interfere with synaptic excitatory glutamatergic neurotransmission in the brain especially NMDAR (Hu et al., 2009; Lacor et al., 2007; Roselli et al., 2005) thus disrupting synaptic plasticity (Crouch et al., 2008; Klyubin et al., 2008; Walsh et al., 2002). A study by Snyder et al. (2005) discovered that exposure to Aβ promoted endocytosis of NMDAR and prolonged depression of NMDA-evoked currents in cortical neuronal cells. In addition, reduced expression of NMDARs have been observed in neuron cells of AD mouse models (Snyder et al., 2005).

Using hippocampal cell cultures, Lacor et al. (2007) demonstrated that the ability of Aβ oligomers to specifically attach to excitatory pyramidal neurons cause reduction of NMDAR expression, decrease in dendritic spine density and damage synaptic morphology. These findings have been supported by a study conducted by Shankar et al. (2007) who observed that Aβ oligomers stimulate hippocampal synaptic loss via an NMDAR-dependent signalling pathway. Oligomeric Aβ was also shown to stimulate Fyn kinase leading to GluN2B phosphorylation of the NMDARs, which result in dendritic spine loss and synaptic impairment (Um et al., 2012). Fyn is a tyrosine kinase important in the normal physiological function of synaptic transmission, and hence has an implicated role in Aβ signalling as well as tau phosphorylation (Nygaard et al., 2014). Moreover, Tackenberg et al. (2013) provided evidence that dendritic spine loss as a result of Aβ stimulation was mediated by GluN2A-containing NMDA receptors whereas GluN2B was shown to be involved in Tau-dependent neurodegeneration.

The distinct property of NMDAR being highly permeable to Ca^{2+} is also key in linking the receptor channel to the pathological state of AD. NMDAR-dependent synaptic plasticity mechanisms correspond to Ca^{2+} flow resulting in potentiation or depression. High influx of Ca^{2+} triggers the amplification of synaptic strength resulting in long-term potentiation (LTP) (Sanz-Clemente et al., 2013). In contrast, defective NMDAR resulting in low permeability of Ca^{2+} for a long duration may induce long-term depression (LTD) leading to reduced efficacy of the synaptic neurotransmission (Holtmaat and Svoboda, 2009). Texido et al. (2011) demonstrated that Aβ oligomers cause excess Ca^{2+} influx leading to neuronal cell death. Electrophysiological analysis on *Xenopus laevis* oocytes have shown that Aβ oligomers directly activate both NMDAR subunit combinations - GluN1/2A and GluN1/2B with the former displaying a larger response.

In an experiment where hippocampal slice cultures were applied with Aβ oligomers for 20 minutes, Tamburri et al. (2013) noted that the Aβ oligomers induced synaptic depression and that this was independent of NMDAR ion-flux. Instead it appeared to be mediated by NMDAR in a metabotropic manner. Findings by Kessels et al. (2013) supported this model, and further suggested that NMDAR activation occurs via the GluN2B subunit. Aβ oligomers eventually result in the loss of synaptic responses mediated by GluN2B leading to a switch of subunit composition from GluN2B to GluN2A. It was therefore proposed that ion-flux is not required for Aβ-induced synaptic depression but rather was mediated by conformational changes of the NMDAR subunits.

Soluble oligomeric Aβ have been shown to impair LTP in hippocampal neurons (Klyubin et al., 2004; Walsh et al., 2002) and the disruption of synaptic transmission is suggested to be the result of LDP (Cheng et al., 2009; Kim et al., 2001). Rowan et al. (2003) have described that oligomer Aβ in the sub-nanomolar range were able to rapidly block prolonged LTP both in hippocampal slices as well as intact hippocampus of *in vivo* models. Due to the role of LTP in hippocampus function, Rowan et al. proposed that this disruption of LTP and synaptic plasticity which is highly dependent on NMDAR-activity may cause cognitive impairments observed early in AD patients. This model is depicted in the schematic diagram in figure 17.

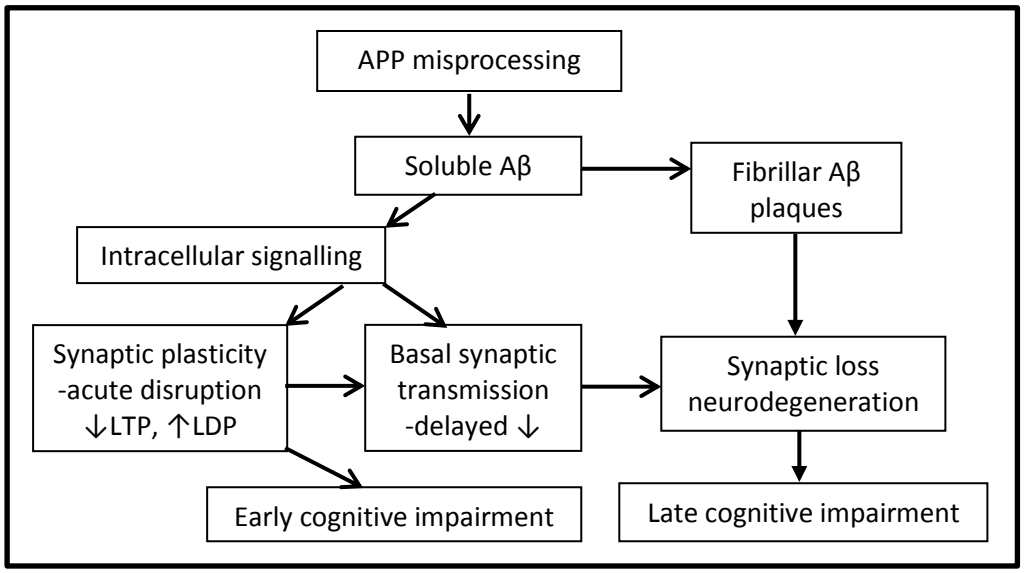


Figure 17: Proposed action of Aβ oligomers on hippocampal synaptic plasticity and neurotransmission leading to the development of cognitive decline seen in dementia.

Soluble Aβ oligomers may interfere with intracellular signalling, NMDAR-mediated transmission and cholinergic transmission leading to LTP inhibition and LTD stimulation of the excitatory neurotransmission. A delayed reduction in basal AMPA -mediated transmission might be caused by a shift from LTP-like to LTD-like synaptic plasticity and increased vulnerability to excitotoxicity. The imbalance between rapid deterioration of synaptic plasticity versus delayed reduction in basal transmission would contribute to the mild cognitive dysfunction seen in preclinical AD (Rowan et al., 2003).

De Felice et al. (2007) has linked the disruption of LTP and synaptic plasticity to Aβ oligomer-induced oxidative stress. This study observed elevated reactive oxygen species (ROS) production, neuronal damage and mitochondrial dysfunction in hippocampal neuronal cultures exposed with Aβ oligomers via NMDAR-dependent calcium flux. Interestingly, memantine was found to completely protect the cells against Aβ oligomer-induced oxidative damage and reduced intraneuronal calcium which is necessary for ROS formation. Due to the fact that a small amounts of ROS are essential for the normal physiological process of synaptic plasticity, the study proposed that impairment of NMDAR activity coupled with oxidative stress are implicated in the pathogenesis of AD.

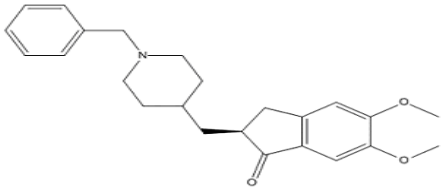
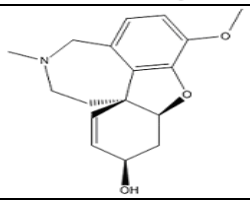
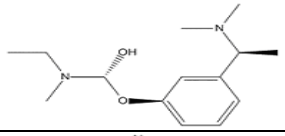
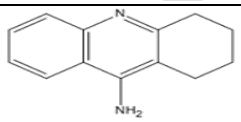
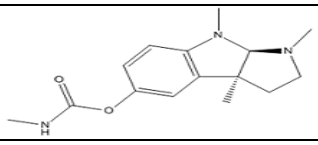
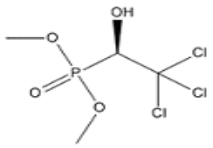
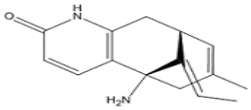
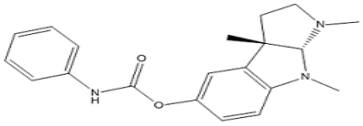
The implication of NMDARs in the pathogenesis of AD is complex. Based on numerous findings that Aβ has a direct effect on NMDAR, and the fact that memantine is well-tolerated in AD patients, this forms the basis of the present study looking into NMDAR inhibition. $A\beta_{1-40}$ has been shown to induce inward current, cause increased intracellular Ca^{2+} levels and cause cell death by activating NMDAR (Alberdi et al., 2010).

1.4.4 AD Treatments

There are two categories of drugs currently approved by the US Food and Drug Administration (FDA) for the treatment of AD; (i) acetylcholinesterase inhibitors (AChEI) and (ii) NMDAR antagonists. These drugs were designed not to 'cure' but to suppress the symptoms associated with AD and their treatment effects are clinically modest at best (Bi, 2010).

AChEIs are the main treatment presently used in clinical settings for AD patients. The action of this drug is to inhibit acetylcholinesterase which in turn will maintain and/or increase acetylcholine (ACh) availability in the central nervous system without being broken down by the enzyme (Nowotny et al., 2001). Cholinergic depletion has long been associated with AD whereby ACh neurotransmitter, essential for learning and memory, is markedly decreased in AD patients (Francis, 2005). The three currently available AChEIs approved by the FDA are donepezil (Aricept), rivastigmine (Exelon) and galantamine (Riminyl). These drugs are prescribed for mild-to-moderate symptoms of AD patients. Evidence from more than 30 randomised control trials have shown improved cognitive function in individuals with mild-to-moderate AD prescribed with these drugs although the effects were considered modest at best (Birks and Harvey, 2006; Birks et al., 2015; Loy and Schneider, 2006). Tacrine (Cognex) was actually the first clinically approved AChEI in 1993. However, it was poorly tolerated by AD patients and was eventually discontinued by the FDA due to incidence of associated liver toxicity (Mehta et al., 2012). Table 5 lists AChEIs currently used in AD treatment as well as several other compounds still under clinical trial or pre-clinical investigation.

Table 5: List of acetylcholinesterase inhibitors (AChEI).

Drug	Chemical Structure
Donepezil (Aricept)	
Galantamine (Riminyl)	
Rivastigmine (Exelon)	
Tacrine (Cognex)	
Physostigmine (Antilirium)	
Metrifonate	
Huperzine A	
Phenserine	

Donepezil, rivastigmine and galantamine are presently used clinically to treat AD symptoms (Nascimento and Martins, 2012). Tacrine was the first approved AChEI but was eventually discontinued by FDA due to adverse effects (Mehta et al., 2012). Physostigmine also exerts detrimental effects on hepatic and cardiovascular function which limit its use in clinical settings (Francis et al., 1999). Metrifonate is a long acting irreversible AChEI but was withdrawn from further development due to incidences of neuromuscular dysfunction and respiratory paralysis in AD participants (Lopez-Arrieta and Schneider, 2006). Huperzine A is a Chinese herb extract exhibiting potent, selective, and well tolerated AChEI properties. Early studies have shown it improves cognitive function, daily living activity, and global clinical assessment in AD patients (Yang et al., 2013). Phenserine is also being clinically studied as a non-competitive AChEI drug that has independent modulatory effects on Aβ generation as well as improving cognitive activity (Winblad et al., 2010).

The second class of drug treatment for AD are NMDAR antagonists with memantine being the only glutamatergic-targeting drug currently approved in clinical use. Memantine is prescribed for individuals with moderate-to-severe symptoms of AD (Ballard et al., 2011). Treatment with memantine is well-tolerated and beneficial to improve cognitive function and neuropsychiatric symptoms (McShane et al., 2006). A number of characteristics are thought to contribute towards memantine's well-tolerated nature in patients, namely that memantine is non-competitive, possesses moderate affinity, displays strong voltage-dependency and rapidly unblocks. These factors together contribute to allowing normal physiological transmission whilst only blocking pathological Ca^{2+} influx as well as oxidative stress (Danysz and Parsons, 2012).

At present, most current research in drug developments has been leaning towards the suppression and clearance of Aβ plaques. This is due to the popularity of the amyloid cascade hypothesis to explain the cause of AD (Iqbal et al., 2014). Inhibitors for α- and γ-secretase have been studied as potential therapeutics due to their involvement in APP processing to generate Aβ protein (Blennow et al., 2006). Immunotherapy has also been researched by which attachment of antibodies onto Aβ plaques and oligomers might be able to induce clearance from the central nervous system (Bard et al., 2000; Schenk et al., 2004).

Tau phosphorylation and aggregation have also been studied as potential targets which lead to the development of several glycogen synthase kinase-3β (GSK3β) inhibitors such as lithium and valproate. GSK3β has been described as the molecular link connecting Aβ and tau protein as it is involved in APP processing and other signalling pathways of Aβ formation (Llorens-Martin et al., 2014). Cumulative data suggest a promising future for GSK3 inhibitors. The challenge faced by drug developers is to produce a compound within the therapeutic level since there have been reports of potential toxicity ranging from hypoglycemia to tumorigenesis and neuron deregulation. GSK3 is essential for life, therefore complete inhibition would prevent cells from operating normally (Eldar-Finkelman and Martinez, 2011).

With mounting evidence that oxidative damage is a major player in AD (Nunomura et al., 2006; Smith et al., 2000), numerous studies have conducted investigations on antioxidants as potential therapeutic compounds. Antioxidants act to remove, scavenge and inhibit ROS and their precursors. Exogenous antioxidants such as vitamin C (ascorbic acid) and E (tocopherol/tocotrienol) are potent radical scavengers and chain-breaking molecules which have been used in clinical trials for AD patients (Mecocci and Polidori, 2012). Although antioxidant therapy does improve cognitive function in some of these trials, there is no definite proof that antioxidants are neuroprotective against AD. To address this issue, researchers have shown that antioxidants in combination with other therapeutic drugs have demonstrated positive synergistic effect (Gilgun-Sherki et al., 2003). One major issue that affects their efficacy, however, is their limited permeability through the blood-brain barrier (Gilgun-Sherki et al., 2001).

Another therapeutic strategy currently being investigated is the combination of drugs to enhance treatment of AD. A comprehensive systematic review and meta-analysis conducted by Matsunaga et al. (2015) concluded that combination therapy of cholinesterase inhibitors and memantine provided benefits in terms of cognition, behavioural disturbances, daily activities and overall impression in moderate-to-severe AD patients. A second meta-analysis, however, showed combination therapy has small but a significant impact on the improvement of cognitive and behavioural measures but not on daily living activities (Farrimond et al., 2012). The combination of two clinically approved AD drugs into a single dosage has also been tried and tested. Namzaric - a new formulation containing memantine extended release (28 mg) and donepezil (10 mg) was synthesized and recently approved by the FDA in the hope to enhance AD treatment. Clinical trials revealed that their bioavailability was equivalent with the consumption of memantine and donepezil given separately supporting their pharmacokinetic efficacy (Boinpally et al., 2015).

1.4.5 Multi-Target-Directed Ligands (MTDL)

Despite the benefits, combination therapy does, however, present some drawbacks. Increased side effects and possible drug-drug interaction might be expected due to multiple drug use. A possible approach to overcome this problem is by designing a single chemical entity with multiple targets and biological properties termed as multi-target-directed ligands (MTDLs) (Bolognesi et al., 2009b). Several benefits have been discussed regarding the use of MTDLs, such as their low affinity to bind to target sites. Drugs with low affinity but possess selective binding are expected to have lower prevalence and reduced side-effects compared to high affinity single-targeting drugs (Korcsmaros et al., 2007). The MTDL strategy has led to the development of a drug termed as memoquin, a combinatorial form of polyamineamide caproctamine, an AChEI and idebenone, a potent antioxidant (Bolognesi et al., 2009b). Idebenone, synthetically derived from co-enzyme Q was shown to alleviate cognitive dysfunction in mild-to-moderate AD (Gutzmann and Hadler, 1998) and has a neuroprotective effect against $A\beta_{40}$-induced neurotoxicity in hippocampal neurons (Hirai et al., 1998). In their experimental analysis, the *in vitro* profile showed that memoquin demonstrated the ability to bind and inhibit AChE, as well as suppress ROS formation, Aβ aggregation and β-secretase activity. The *in vivo* profile in an AD mouse model showed that memoquin was able to prevent cholinergic loss, decrease Aβ formation and tau hyperphosphorylation as well as restoring memory in object recognition tests. Hence it shows promise as a potential AD treatment (Bolognesi et al., 2009b).

In light of this initial pre-clinical success, several other multi-target drugs have been synthesized. They display a degree of potential where a few have undergone clinical trials. Ladostigil (TV-3326), which is currently in a phase II clinical trial (Bolognesi et al., 2009c) was synthesized by combining rivastigmine with a monoamine oxidase (MAO) antagonist, rasagiline which also possess antioxidant properties and is involved in APP processing (Youdim, 2006). Ladostigil was found to be able to enhance ACh stimulation, reduce Aβ level and protect neuronal cells from neurotoxicity in an AD model. The ability of this compound to inhibit MAO, reduce H_2O_2 and subsequently oxidative stress are favourable characteristics for AD therapy

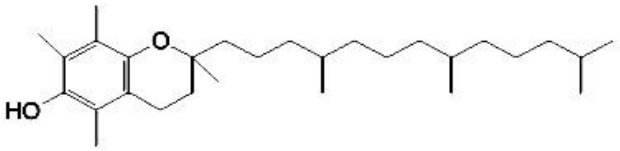
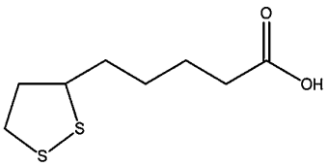
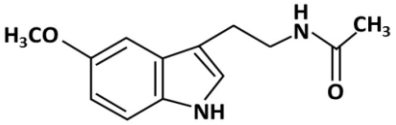
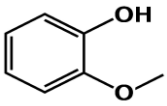
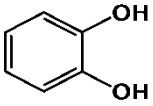
(Weinreb et al., 2009). Also derived from rasagiline, another series of MTDLs, M30 HL-20 were similarly developed but they have the ability to chelate iron. This property along with rasagiline's capacity as an MAO inhibitor, are beneficial to address the elevated levels of MAO and iron seen in AD, Parkinson's disease and ageing (Youdim, 2006).

In this present study, several novel MTDLs were developed in collaboration with Dr. Michela Rosini (University of Bologna) combining several functional moieties as well as established drugs with known medical benefits to address pathological issues in AD. 21 MTDL compounds were evaluated in this study; thirteen novel MTDLs were derived from the combination of memantine and antioxidants, three were synthesized by incorporating antioxidants with polyamine spermine, while five others were donepezil-derived compounds combined with carvedilol.

Memantine was used in the MTDL design due to its well-tolerated effect in AD patients and its versatility to address several issues related to Aβ pathology as discussed in the previous section. Polyamine was also chosen to be incorporated with antioxidants since it represent a universal template to be modified as a potential NMDAR blocker. Incorporation of different pharmacophores into the polyamine backbone can tune both affinity and selectivity for any given receptor (Melchiorre et al., 2003). Polyamines such as spermine and spermidine are low affinity blockers of the receptor, thus combining the polyamine chain to aromatic substituents such as antioxidant moieties may enhance their blocking potency (Berger et al., 2006).

Since oxidative stress is a strong contributing factor to AD pathology, the incorporation of antioxidant functional groups with a well-established NMDAR blocker was hypothesized to improve the treatments of AD. The antioxidants used in this study were α-tocopherol, lipoic acid, melatonin, methoxyphenol and catechol as listed in table 6.

Table 6: Antioxidants used in the multi-target-directed ligands study.

Antioxidant compound	Chemical Structure
α-tocopherol	
Lipoic acid	
Melatonin	
Methoxyphenol	
Catechol	

Adapted from Fukuzawa et al. (2004), Huang et al. (2014), Raghava Raju et al. (2013), Shen et al. (2016) and Shi et al. (2008).

On their own, some of these antioxidants have also shown to be beneficial in AD both in pre-clinical experiments as well as in patients. α-tocopherol, which is a chemical compound found in Vitamin E, is a lipid-soluble chain-breaking antioxidant found in lipid membranes, circulating lipoproteins and low-density lipoprotein (LDL) particles (Foy et al., 1999). *In vivo* studies have shown that vitamin E inhibited CNS lipid peroxidation and protein aggregation of Aβ plaques in rats and improved cognitive function in rodents. In a controlled trial by Sano et al. (1997), mild-to-moderate AD patients under vitamin E (α-tocopherol, 2000 IU/day) regimen presented slower deteriorative progression compared to those not taking the antioxidant. This was reproduced by another clinical trial which observed delayed deterioration and

progression of AD in patients receiving 2000 IU of vitamin E daily (Feng and Wang, 2012).

Lipoic acid is an essential cofactor for mitochondrial enzyme complexes which has the potential to suppress the development of AD by enhancing the production of acetylcholine. It is also able to supress oxidative stress by scavenging and inhibiting generation of free radicals, increasing reduced glutathione as well as modulating redox-sensitive inflammatory processes (Fava et al., 2013; Holmquist et al., 2007; Maczurek et al., 2008). Clinically, lipoic acid has been shown beneficial in AD whereby 600 mg/day of alpha-lipoic acid (ALA) improved cognitive functions in patients (Fava et al., 2013).

Melatonin is a naturally occurring hormone produced primarily in the pineal gland (Dragicevic et al., 2011), and has been reported to be deficient in AD patients. Besides being a powerful radical scavenger itself, melatonin also enhances the activity and expression of other endogenous antioxidants such as superoxide dismutase, glutathione peroxidase, catalase and nitric oxide synthase (Nishida, 2005). A double-blind controlled trial with 3 mg/day of melatonin in AD patients improved their night time sleep and cognitive performances (Asayama et al., 2003). The fact that reduction of melatonin levels was previously associated with AD (Liu et al., 1999) made this compound a potentially good therapeutic candidate.

The methoxyphenol which can be found naturally in curcumin (Masuda et al., 1999) is a potent radical scavenger and has been shown to possess strong radical scavenging activities and to protect neuronal cells against oxidative stress-induced neurotoxicity in animal models (Fujisawa et al., 2004; Kadoma et al., 2007). It has also been demonstrated to suppress Aβ plaque formation via a multiple cascade reaction (Cole et al., 2005). At present, curcumin is in a Phase II clinical trial to investigate its effect on cognitive function and Aβ quantity in AD patients (Small, 2011).

As for catechol, *in vitro* analysis has suggested that abietic acid-derived catechol possess antioxidant properties and is able to interact with hypochlorous acid (HOCl),

a powerful proinflammatory oxidant and has a protective effect against oxidation (Justino et al., 2006). *In vivo* experiments have also demonstrated that catechol derived from virgin olive oil exerts antioxidant effect in rat brain tissue induced with lipid peroxidation (De La Cruz et al., 2015).

The current study also made use of currently available drugs for the design of MTDL compounds where the functional moiety of donepezil was incorporated with carvedilol. Donepezil, as described earlier is one of three available AChEI/ChEIs in clinical use aside from rivastigmine and galantamine (Molino et al., 2013). In contrast, carvedilol is a beta-blocker used in the treatment of congestive heart failure (CHF) and high blood pressure. However, researchers have shown that carvedilol has the ability to form a complex with Aβ thus suppressing aggregation of Aβ into oligomeric fibrils (Howlett et al., 1999). The structure of carvedilol is displayed figure 18.

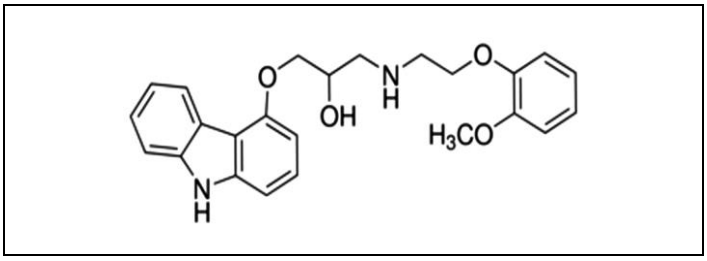


Figure 18: Structure of carvedilol.
Source: Chen and Hong (2016).

In addition to its antihypertensive property, carvedilol has also been shown to act as a non-competitive NMDAR blocker, possess antioxidant capacity, protect against neuronal excitotoxicity induced by glutamate and restores Na^+/glutamate transporter activity (Lysko et al., 1998; Lysko et al., 1994). These properties make this drug a beneficial component for the MTDL drug design. An *in vivo* experiment presented a positive outcome with AD mouse models administered orally with carvedilol. The β-blocker was shown to disrupt biochemical and neuropathological changes underlying cognitive decline in AD; Aβ oligomers were reduced and cognitive performance was elevated (Wang et al., 2011). A phase 4 clinical trial is currently underway to investigate the effectiveness and safety of carvedilol treatment in Alzheimer's disease patients (Rosenberg, 2011).

1.5 *XENOPUS LAEVIS* OOCYTE EXPRESSION SYSTEM FOR STUDYING ION CHANNELS

The unfertilised oocytes of the *Xenopus laevis* South African clawed frog, have long been used as a model for expressing protein receptors, transporters and ion channels to study drug response (Buckingham et al., 2006; Miledi, 1982; Sigel, 2001). First described more than 40 years ago, Gurdon and colleagues successfully expressed functional proteins in *Xenopus* oocytes injected with genetic materials. DNA injected into the nuclei or RNA into the cytoplasm of the cell will be processed into functional proteins expressed on the cell surface (Gurdon et al., 1971; Mertz and Gurdon, 1977). The processing of genetic materials in *Xenopus* oocytes is presented in figure 19.

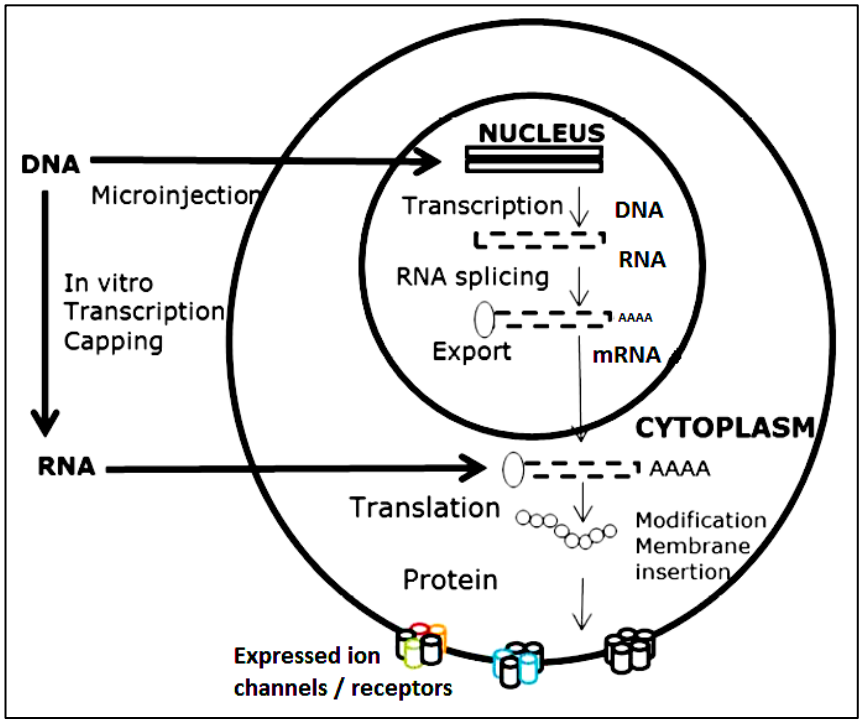


Figure 19: Genetic processing of injected DNA/RNA in *Xenopus laevis* oocytes into ion channels/receptors. Adapted from Kachel (2014).

The relatively large size of oocytes (1 to 1.2 mm in diameter) makes it conveniently feasible to inject up to 50 nl of cRNA or cDNA into the cell to express the encoded proteins and subsequently used for electrophysiology recordings (Buckingham et al., 2006; Moeller and Fenton, 2010; Sigel, 2001). Changes in membrane currents as a result of drug-receptor interaction may be easily measured and controlled by two-

electrode voltage clamp (TEVC) electrophysiology (Sigel, 2001). When a compound solution is applied to the oocyte, ion channels will open up affecting the flow of ions through the membrane. By taking a reading of the changes in ion currents using TEVC, it allow investigators to determine how cells are affected by specific compounds or molecules (Bierwitz and Schwarz, 2014).

The oocyte expression system has been demonstrated to faithfully translate neurotransmitter receptors (Parker et al., 1985; Sakai et al., 1986; Schofield et al., 1987; Sumikawa et al., 1981) as well as ion channel and receptor proteins (Barnard et al., 1982; Gundersen et al., 1984). NMDA receptors have been shown to express in *Xenopus* oocytes when injected with genetic materials since the late 80s. In fact, NMDARs were first cloned using expression cloning in *Xenopus* oocytes (Moriyoshi et al., 1991).

Key characteristics of NMDA receptors were successfully reproduced with *Xenopus* oocytes with responses potentiated by co-application of NMDA and glycine as its co-agonist and blocked by Mg^{2+} in a voltage-dependent manner (Kushner et al., 1988; Lerma et al., 1989; Planells-Cases et al., 1993; Verdoorn et al., 1987; Yamazaki et al., 1992). The lack of other excitatory protein receptors on *Xenopus* oocytes makes it a versatile system to express and study NMDAR without interference from other responses evoked by other receptors (Lerma et al., 1989).

In general, ion channels and receptors can interact with a number of molecules resulting in reduced or altered permeation of ions. Such action is the basic principle of drug development targeting ion channels and receptors applied in the pharmaceutical industry. Using electrophysiology analysis, block of ion or receptor channels expressed in *Xenopus* oocytes by an inhibitor molecule can be measured by the changes of membrane current as a result of ion permeations. The movements of ions between cytoplasm and extracellular space create electrical potential difference which can be detected by electrodes (Bierwirtz and Schwarz, 2014). Two-electrode voltage clamp (TEVC) electrophysiology employs two electrodes, one sensing the voltage, and the second electrode injects current to maintain the voltage at the

desired membrane potential. When a solution or compound is perfused onto the oocyte, receptor channels will open resulting in flux of ions across the membrane. This will then be detected by the voltage electrode and counteracted by current injection via the current electrode. The latter is transferred to a recording software in a computer. Figure 20 shows an oocyte impaled by two electrodes in the TEVC electrophysiology setup while figure 21 displays a schematic diagram of the oocyte expression system.

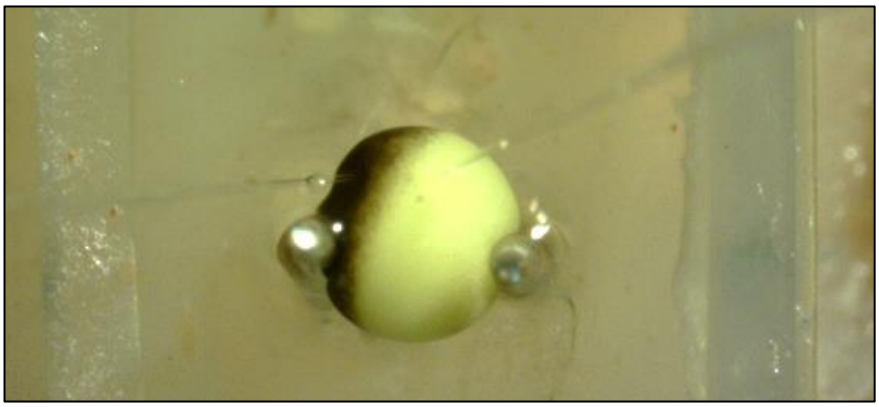


Figure 20: A microscopic visual of *Xenopus* oocyte in the bath chamber with two glass electrodes impaling the cell.

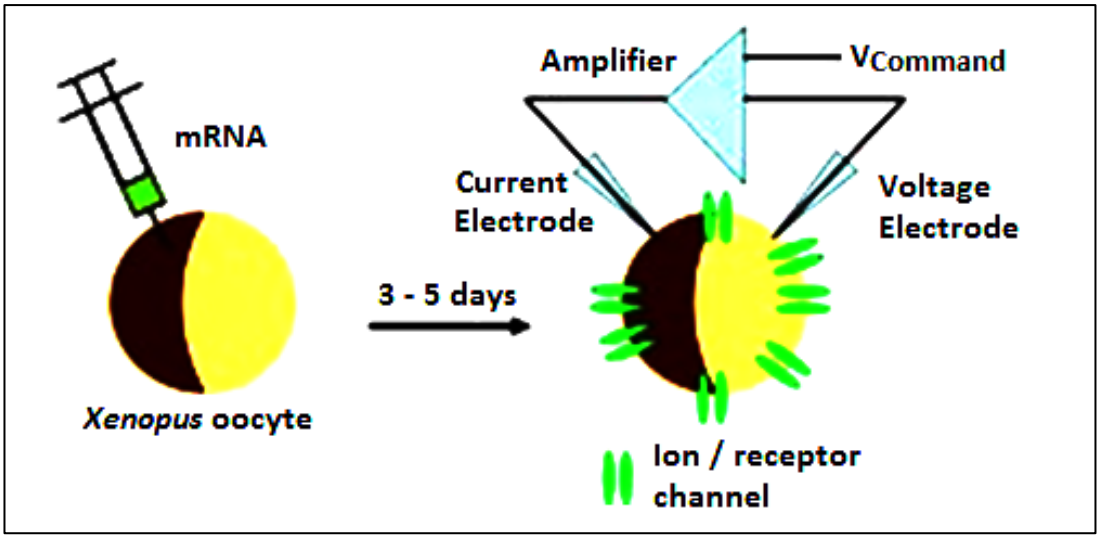


Figure 21: Schematic diagram of the oocyte expression system and utilisation of two-electrode voltage clamp (TEVC). Adapted from Jansen (2016).

Using the data obtained from the TEVC protocol, receptor channel block is quantified by the Hill equation (first described by Archibald Hill, 1910) which measures the ratio

of current evoked in the presence of an antagonist to the current without it. Data from a range of concentration is used to produce a ligand-dose response curve from which the IC_{50} of antagonists are estimated (Bierwirtz and Schwarz, 2014; Pusch, 2006; Weiss, 1997). This will be further explained in Chapter 2, Methodology.

1.6 THESIS PROJECT OBJECTIVES

The first objective of this study was to characterize wild type GluN1-1a and GluN2A NMDAR subunits electrophysiologically using well-known open channel blockers; Mg^{2+}, memantine, MK-801 and philanthotoxin-343 as well as evaluating two novel PhTX-343 derivatives; Cha-PhTX-343 and Bz-Cha-PhTX343.

The second objective was to determine the effects of Q/R/N, +1 and -8 sites modification in the pore region (M2) of NMDAR on blocking potencies of the antagonists. NN at the Q/R/N and +1 sites in GluN2A subunits were double-mutated to GR and RR, while W at -8 position relative to the Q/R/N site was mutated to N. These mutated GluN2A subunits were co-expressed with GluN1-1a and characterised with open channel blockers using TEVC electrophysiology.

The third objective was to evaluate novel compounds as part of the multi-target-directed ligands (MTDL) therapeutic strategy for Alzheimer's disease. Thirteen novel compounds composed of memantine-derivatives incorporated with antioxidant headgroups, three spermine-derived polyamines also incorporated with antioxidants and five combinatorial forms of donepezil and carvedilol were tested on GluN1-1a and GluN2A subunits as NMDAR antagonists. IC_{50}s of these compounds were compared to that of memantine as the established therapeutic and also to the endogenous NMDAR blocker, Mg^{2+}. The donepezil-derived compounds were also tested on α4β2 and α7 nicotinic acetylcholine receptors (nAChR) to see whether they would exert agonistic or antagonistic properties on nAChRs, as donepezil was originally designed to target the cholinergic pathway.

CHAPTER 2

METHODOLOGY

2.1 DNA CLONING AND mRNA PREPARATION

2.1.1 Preparation of Chemically Competent Cells

Prior to DNA cloning, competent cells were prepared using the standard calcium chloride ($CaCl_2$) method. JM109 *E. coli* were seeded in 5 ml of lysogeny/luria broth (LB) (1% tryptone, 0.5% yeast extract, 1% NaCl, adjusted to pH 7.5) and grown overnight in a 50 ml falcon tube under vigorous shaking at 37 °C. 50 ml of LB were then added to 5 ml of the overnight culture and incubated at 37 °C with shaking for two hours until the optical density (OD) of the cell suspension reached approximately 0.60 in order for the cells to divide at an exponential rate. The suspension was put on ice for 15 minutes then spun at 10,000 *g* for ten minutes at 20 °C. The supernatant was removed and the cells resuspended in 10 ml of chilled and filtered 0.1 M $CaCl_2$, placed on ice for ten minutes and spun again at 10,000 *g* for ten minutes at 20 °C. The supernatant was removed and the cells were resuspended in 2 ml chilled and filtered 0.1 M $CaCl_2$, ready for use in bacterial transformation.

2.1.2 Plasmid DNA

Rat DNA sequences for GluN1-1a and GluN2A were inserted into pRK7 plasmids, while GluN3A and GluN3B DNA sequences were inserted into pcDNA3.1(+) plasmids. GluN1-1a was inserted between HindIII and BamHI sites, GluN2A between EcoR1 and XbaI sites, GluN3A between BamHI and NotI sites, and GluN3B was inserted between EcoRI and XbaI sites as shown in figures 22 and 23.

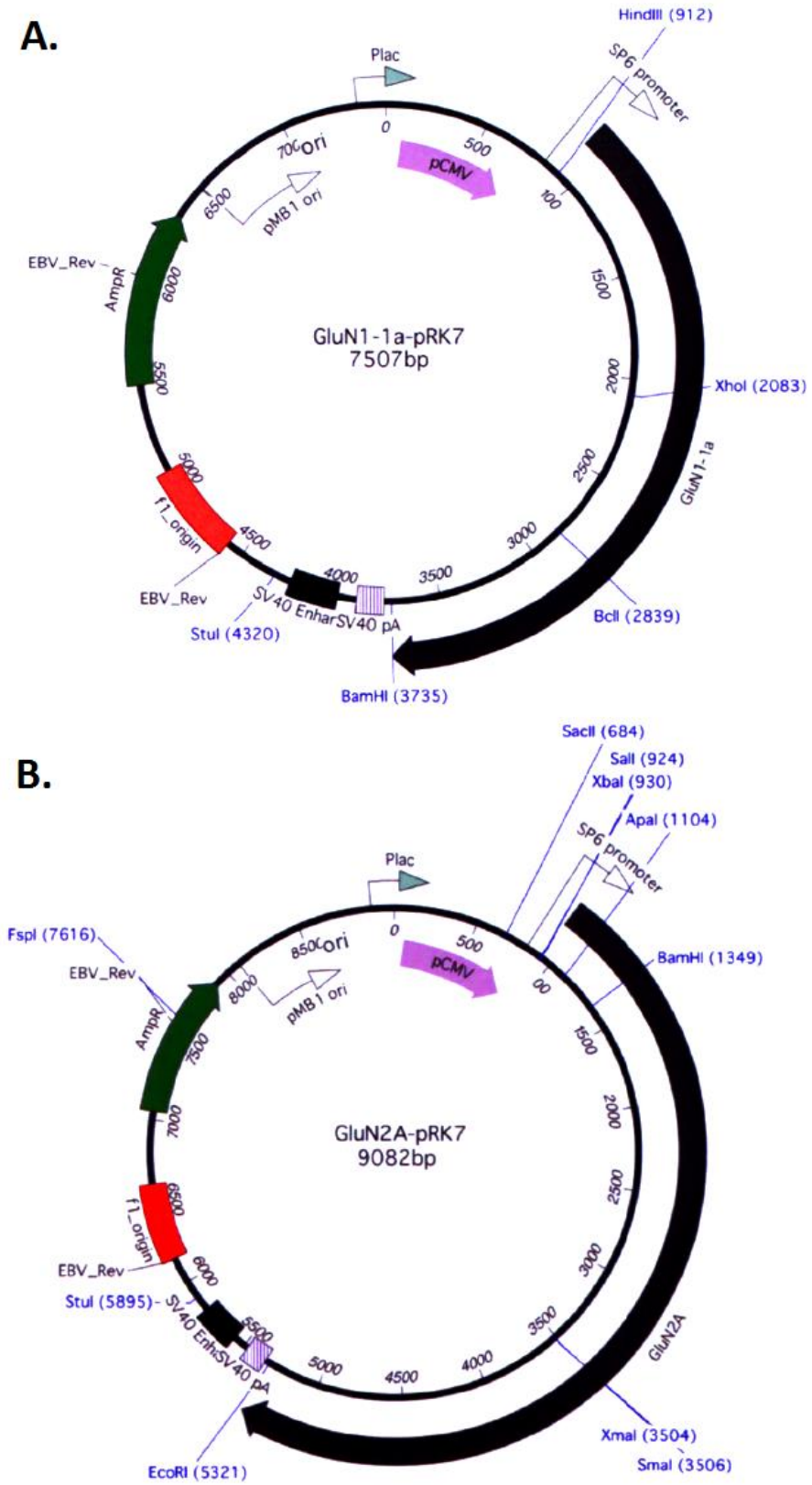


Figure 22: Vector maps for (A) GluN1-1a and (B) GluN2A in pRK7.

The pRK7 plasmid was Sanger sequenced with SP6 primer confirming the presence of inserts. Single cutter restriction enzyme sites (BamHI in GluN1-1a, EcoRI in GluN2A) for linearization are also shown.

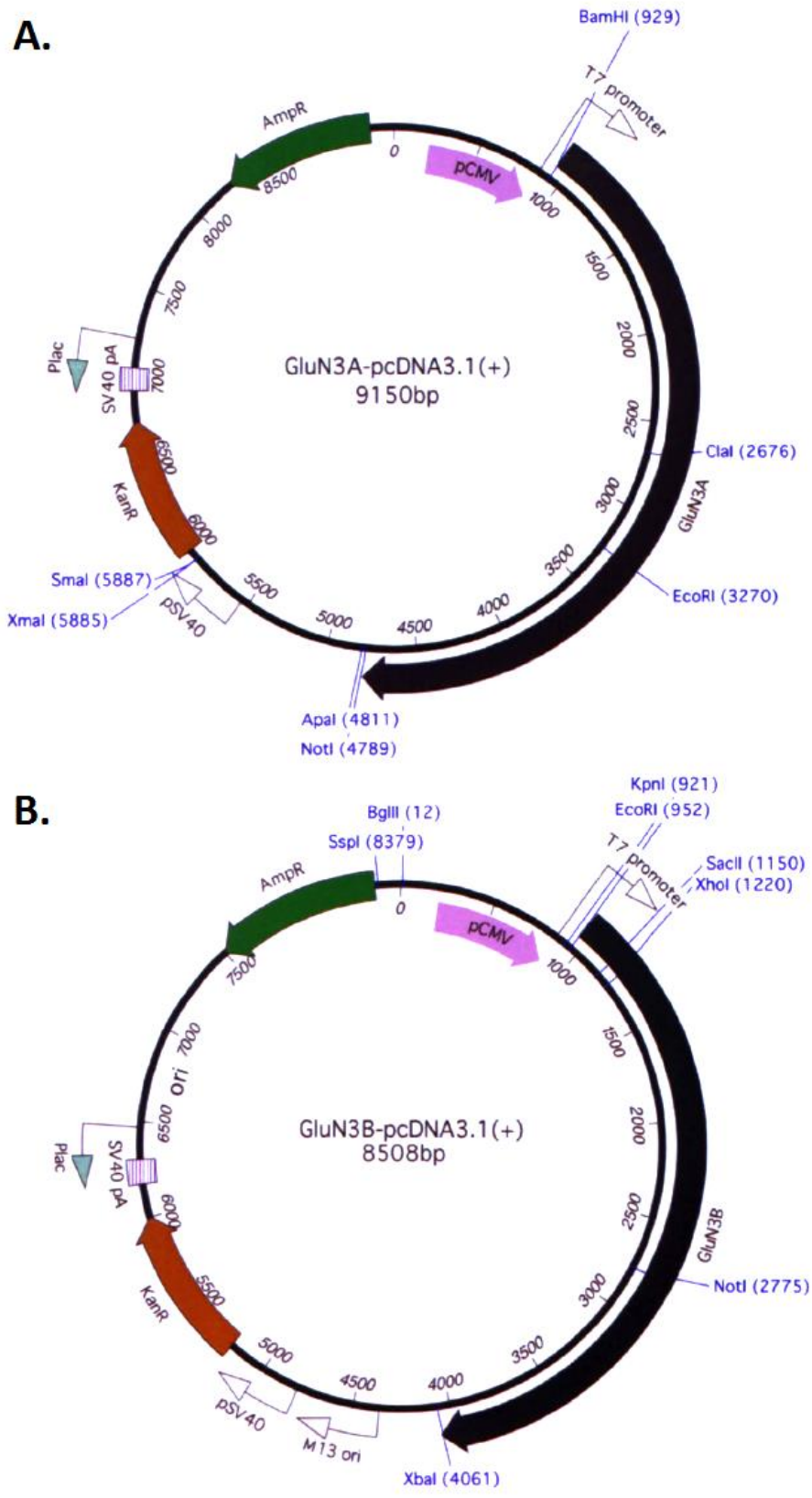


Figure 23: Vector maps for (A) GluN3A and (B) GluN3B in pcDNA3.1(+).

The pcDNA3.1(+) plasmid was Sanger sequenced with T7 primer confirming the presence of inserts. Single cutter restriction enzyme sites (NotI in GluN3A, XbaI in GluN3B) for linearization are also shown.

2.1.3 Bacterial Transformation

1 µl of the plasmid DNA (300–1500 ng) was added to 200 µl of the freshly prepared chemically competent cell suspension in a sterile eppendorf tube, mixed and placed on ice for 20 minutes. The mixture was heat-shocked in a 42 °C water bath for one minute and subsequently put on ice for two minutes. 1 ml of super optimal broth with catabolite repression (SOC) medium (1% tryptone, 0.5% yeast extract, 1% NaCl, 10 mM glucose, adjusted to pH 7.5) was then added to the tube and left in a 37 °C water bath for another 30 minutes. Under sterile conditions, 250 µl of the plasmid-containing bacteria were plated onto LB agar (1% tryptone, 0.5% yeast extract, 1% NaCl, 1.5% agarose, adjusted to pH 7.5) containing 50 µg/ml ampicillin and grown overnight in a 37 °C incubator. The following day, a single colony was picked and inoculated in 5 ml of LB broth with 50 µg/ml ampicillin and left overnight at 37 °C under vigorous shaking.

2.1.4 Plasmid Purification

The plasmid DNA (pDNA) was then purified using the QIAprep Spin Miniprep Kit (Qiagen). 1.5 ml of the cell culture was transferred into a sterile eppendorf tube and spun at 17,000 *g* in a microcentrifuge for three minutes at room temperature (15-25 °C) to harvest the bacterial cells. The supernatant was discarded and the process above was repeated by adding another 1.5 ml of the overnight cell culture into the eppendorf tube and centrifuged for another three minutes. The supernatant was removed and the pellet of bacterial cells was resuspended in 250 µl Buffer P1 containing RNase A until it was completely dissolved. 250 µl of Buffer P2 was added and mixed thoroughly by gently inverting the tube four to six times. 350 µl of Buffer P3 was then added and immediately mixed thoroughly again by inverting the tube four to six times. The mixture was centrifuged at 17,000 *g* for ten minutes at 15-25 °C. The supernatant was applied to the QIAprep spin column by decanting or pipetting, and subsequently centrifuged at 17,000 *g* for one minute at 15-25 °C. 0.5 ml Buffer PB was added to wash the QIAprep spin column and spun again at 17,000 *g* for one minute. The QIAprep spin column was then washed again by adding 0.75

ml Buffer PE and spun at 17,000 *g* for another one minute. The flow-through was discarded and it was centrifuged for an additional one minute to remove residual wash buffer. The QIAprep column was placed in a sterile 1.5 ml microcentrifuge eppendorf tube and 50 µl Buffer EB (10 mM Tris-Cl, pH 8.5) or double distilled water (ddH_2O) was added to the centre of the QIAprep column. To elute the DNA, the column was left to stand for one minute and then spun for a further one minute at 17,000 *g*. Finally, the concentration of the pDNA was measured using the Nanodrop spectrophotometer (Thermo Scientific).

2.1.5 DNA Restriction Digest

Restriction digests were carried out to linearize the plasmid for mRNA preparation using suitable restriction enzymes (BamHI for GluN1-1a; EcoRI for GluN2A; NotI for GluN3A, and XbaI for GluN3B). The digestion procedure was carried out by mixing the following in a microcentrifuge tube: 5 µg pDNA, 5 µl restriction enzyme, 5 µl suitable buffer based on the enzymes used, 5 µl Bovine Serum Albumin (BSA) (0.1 mg/ml) and made up to a total volume of 50 µl with ddH_2O. The mixtures were incubated for one hour in a 37 °C bath to allow linearization of the DNA to take place. Termination of the restriction enzyme digestion was carried out by adding 2.5 µl of 100 mM EDTA solution, 5 µl of 3 M ammonium acetate and 100 µl of 100% ethanol to the mixture and kept frozen at -20 °C for one hour to completely end the reaction. Afterwards, the mixture was spun at 17,000 *g* at 4 °C for 15 minutes in a microcentrifuge. Most of the supernatant was then removed, and spun again at 17,000 *g* at 4 °C for five minutes. The rest of the supernatant was removed and the DNA pellet was left open to air-dry for five minutes in a sterile laminar flow cabinet. The DNA was resuspended in 5 µl of ddH_2O and its concentration was determined using the Nanodrop spectrophotometer (Thermo Scientific).

2.1.6 Agarose Gel Electrophoresis

Enzyme restriction digest was confirmed by visualising the DNA using agarose gel electrophoresis to ensure the enzymes only cut once and linearization had taken place. Stock solution of 50 X Tris-acetate-EDTA (TAE) was prepared with 24.2 g Tris Base, 5.71 ml glacial acetic acid, 10 ml 0.5 M EDTA and made up to 100 ml. The stock solution was diluted to 1 X for preparation of agarose gel. 50 ml of the diluted TAE solution was added to 0.75 g agarose powder and dissolved by heating the mixture in a microwave for one minute. 1 µl of 1% ethidium bromide was added into the mixture, gently swirled and poured into a gel tray with a suitable comb to produce wells for DNA samples. Once the gel had solidified, it was placed into a gel electrophoresis kit (Bio-Rad) and 1 X TAE was filled into the tank until the gel was fully covered. 1 µl of DNA samples and 1 kb plus DNA ladder (Invitrogen) were mixed with loading dye before loading into the wells. The gel was allowed to run at 70 V for one hour and subsequently the DNA bands were visualised using Chemidoc XRS and Quantity One image capture software (Bio-Rad). Examples of gel pictures of the uncut and linearized pDNA are displayed in figure 24.

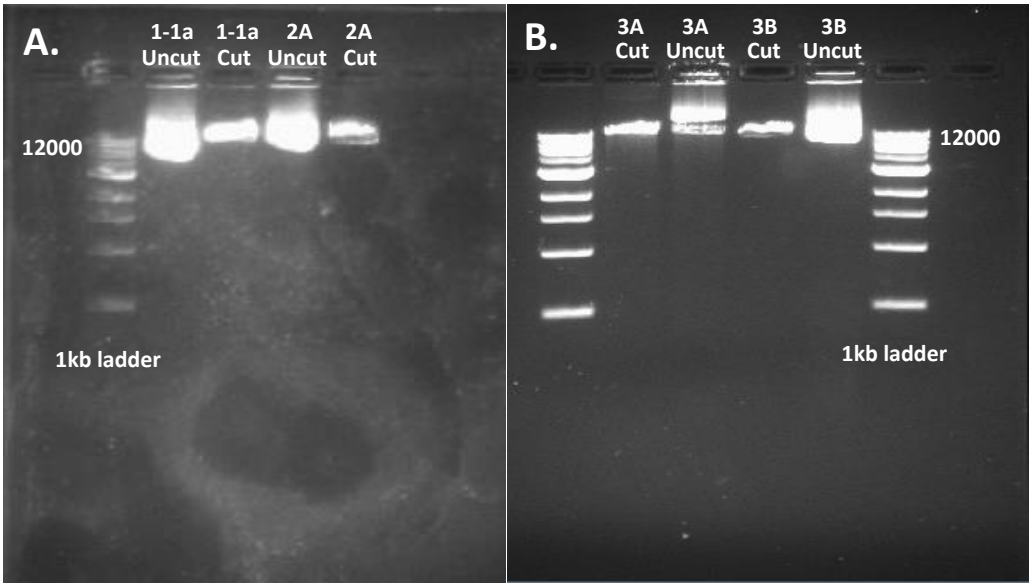


Figure 24: Agarose gel electrophoresis of uncut and linearized pDNA of GluN1-1a, GluN2A, GluN3A and GluN3B NMDA receptor subunits.

(A) GluN1-1a and GluN2A DNA single digest. Lanes show 1kb plus DNA ladder, Uncut GluN1-1a, GluN1-1a cut with BamHI, Uncut GluN2A, and GluN2A cut with EcoRI, (B) GluN3A and GluN3B DNA single digest. Lanes show 1kb plus DNA ladder, GluN3A cut with NotI, Uncut Glu3A, GluN3B cut with XbaI, Uncut GluN3B and 1 kb plus DNA ladder.

2.1.7 mRNA Transcription

Once the DNA was confirmed to be linearized, mRNA was transcribed using the SP6 (for GluN1-1a and GluN2A) or T7 (for GluN3A and GluN3B) mMESSAGE mMACHINE kit (Invitrogen). 0.1-1 µg of DNA was added to a reaction assembly containing reagents provided with the kit: 10 µl of 2 X NTP/CAP, 2 µl of 10 X reaction buffer, 2 µl of enzyme mix, and made up to 20 µl with nuclease free water. The reaction mixture was incubated at 37 °C in a water bath for two hours. After incubation, the RNA was recovered by ending the reaction with 30 µl of lithium chloride precipitation solution and 30 µl nuclease-free water and frozen at -20 °C for a minimum of one hour to ensure complete termination. The RNA was centrifuged at 17,000 *g* for 15 minutes at 4 °C and the supernatant was then removed. The pelleted RNA was washed with 1 ml of 70% ethanol and spun again for 15 minutes. The supernatant was discarded and the resulting pellet was resuspended in 15 µl nuclease-free ddH_2O water. The RNA concentration was measured using a Nanodrop spectrophotometer and diluted to the desired concentration for injection. The samples were stored at -80 ˚C before use.

2.2 SITE-DIRECTED MUTAGENESIS

To analyse the impact of the Q/R/N, +1 and -8 sites in the M2 region of the NMDA receptor subunits, site-specific mutations to replace the desired amino acids were created by employing the QuickChange II XL Site-Directed Mutagenesis Kit (Stratagene).

2.2.1 Primer Design

The oligonucleotide primers for Polymerase Chain Reaction (PCR) for use in site-directed mutagenesis experiments were designed using an online software, PrimerX (www.bioinformatics.org/primerx). The primer sequences were as displayed in table 7.

Table 7: Primers used to produce mutations in NMDA receptor subunits using site-directed mutagenesis protocol.

Mutation	Primer Sequence
GluN3A$_{(G729N/R730N)}$	FW: 5' CTGCTATGCCCTTCTGTTTAACAACACAGCAGCCATCAAACCCCC 3' RV: 5' GGGGGTTTGATGGCTGCTGTGTTGTTAAACAGAAGGGCATAGCAG 3'
GluN3A$_{(N721W)}$	FW: 5' CCTTCTCCTCAGCTTTGTGGGTCTGCTATGCCCTTCTG 3' RV: 5' CAGAAGGGCATAGCAGACCCACAAAGCTGAGGAGAAGG 3'
GluN3B$_{(G629N/R630N)}$	FW: 5' GCTATGCCATTCTCTTTAACAACACTGTCTCCAGTAAGACGCCC 3' RV: 5' GGGCGTCTTACTGGAGACAGTGTTGTTAAAGAGAATGGCATAGC 3'
GluN3B$_{(N621W)}$	FW: 5' CTTACTCCTCCGCGCTCTGGCTGTGCTATGCCATTC 3' RV: 5' GAATGGCATAGCACAGCCAGAGCGCGGAGGAGTAAG 3'
GluN2A$_{(N614G/N615R)}$	FW: 5' CCTCTGGGGCCTGGTCTTCGGCAGATCTGTGCCTGTCCAGAATC 3' RV: 5' GATTCTGGACAGGCACAGATCTGCCGAAGACCAGGCCCCAGAGG 3'
GluN2A$_{(N614R/N615R)}$	FW: 5' CTCTGGGGCCTGGTCTTCAGACGCTCTGTGCCTGTCCAGAATC 3' RV: 5' GATTCTGGACAGGCACAGAGCGTCTGAAGACCAGGCCCCAGAG 3'
GluN2A$_{(W606N)}$	FW: 5' CTATTGGAAAAGCTATAAACCTCCTCTGGGGCCTGGTC 3' RV: 5' GACCAGGCCCCAGAGGAGGTTTATAGCTTTTCCAATAG 3'

2.2.2 PCR Reaction

50 ng of double stranded DNA (dsDNA) template and 125 ng of purified forward and reverse oligonucleotide primers (Eurofins Genomics) were added to a mixture containing 5 µl of 10 X reaction buffer and 1 µl of dNTP mix provided with the kit. Nuclease-free ddH_2O was added to the mixture to a final volume of 50 µl and subsequently mixed with 1 µl of *PfuUltra* high-fidelity (HF) DNA polymerase. Control reactions were also assembled containing 2 µl (10 ng) of pWhitescript 4.5-kb control template, 1.25 µl (125 ng) of forward and reverse oligonucleotide control primers, 5 µl of 10 X reaction buffer, 1 µl of dNTP mix, 3 µl of QuickSolution reagent and 35.5 µl nuclease-fee ddH_2O making a final volume of 50 µl. All the reaction assemblies were then placed in a thermal cycler and allowed to run according to the PCR cycling parameters outlined in table 8.

Table 8: PCR cycling parameters for site-directed mutagenesis experiments.

Segment	Cycles	Temperature	Time
1	1	95 °C	30 seconds
2	18	95 °C (*)	30 seconds
		55 °C (§)	1 minute
		68 °C (†)	1 minute / kb plasmid (9 minutes for GluN3A 8.5 minutes for GluN3B 9 minutes for GluN2A)
3	1	68 °C	7 minutes

The thermal cycling procedure involves denaturation of the dsDNA template (*), annealing of the mutagenic primers which contains the desired mutations to the plasmid DNA template (§), and extension of the primers by *PfuUltra* HF DNA polymerase to generate a mutated plasmid (†).

Once the temperature cycling had completed, the PCR products were subjected to treatment with enzyme *Dpn* I. The endonuclease enzyme functions to digest parental DNA template and to select for mutation-containing synthesized DNA. The nicked vector DNAs containing the desired mutations were then transformed into XL10–Gold Ultracompetent cells and subsequently purified using QIAprep Spin Miniprep Kit as previously described in 2.1.4. The DNAs were then Sanger sequenced using a 3130xl ABI PRISM Genetic Analyser (Life Technologies) to examine whether the mutation had been produced via the experiment. Primers for DNA sequencing were designed using Pimer3 online software (Rozen and Skaletsky, 2000) to anneal around 200 bp upstream from the desired mutation and are displayed in table 9.

Table 9: Primers designed for DNA sequencing of NMDA receptor subunits containing the mutations produced via site-directed mutagenesis.

Primer	Sequence
GluN3A_seq	5’ TCAATACCGCACGAAGCCAG 3’
GluN3B_seq	5' TATGGTGCGCACGAGAGAC 3'
GluN2A_seq(i)	5’ GGTGAAGTGGTCTATCAACGAGCA 3’
GluN2A_seq(ii)	5’ GTCTCCCCTTCTGCTTTCCT 3’

2.3 *XENOPUS* OOCYTE EXPRESSION SYSTEM

2.3.1 Oocyte Preparation

Xenopus laevis oocytes used in this study were obtained from the European *Xenopus* Resource Centre (EXRC), Portsmouth, United Kingdom. The oocytes were treated with 1 mg/ml type 1A collagenase enzyme (Sigma-Aldrich) in Ca^{2+}-free Barth's gentamicin theophylline pyruvate (GTP) solution which contains 96 mM NaCl, 2 mM KCl, 1 mM $MgCl_2$, 5 mM HEPES, 2.5 mM pyruvic acid, 0.5 mM theophylline and 0.05 mg gentamicin, adjusted to pH 7.5 with NaOH. The tube containing the oocytes was placed on a Luckham RS500 recipro-shake major to facilitate separation for approximately 40-60 minutes in an 18 °C incubator to remove connective tissues and follicular cells. Treated oocytes were then rinsed with Ca^{2+}-free GTP solution for three to four times until a clear solution was obtained and kept incubated in normal Barth's GTP solution (with inclusion of 1.8 mM $CaCl_2$) at 18 °C prior to microinjection. Figure 25 shows the *Xenopus* oocytes pre- and post-treatment with collagenase enzyme.

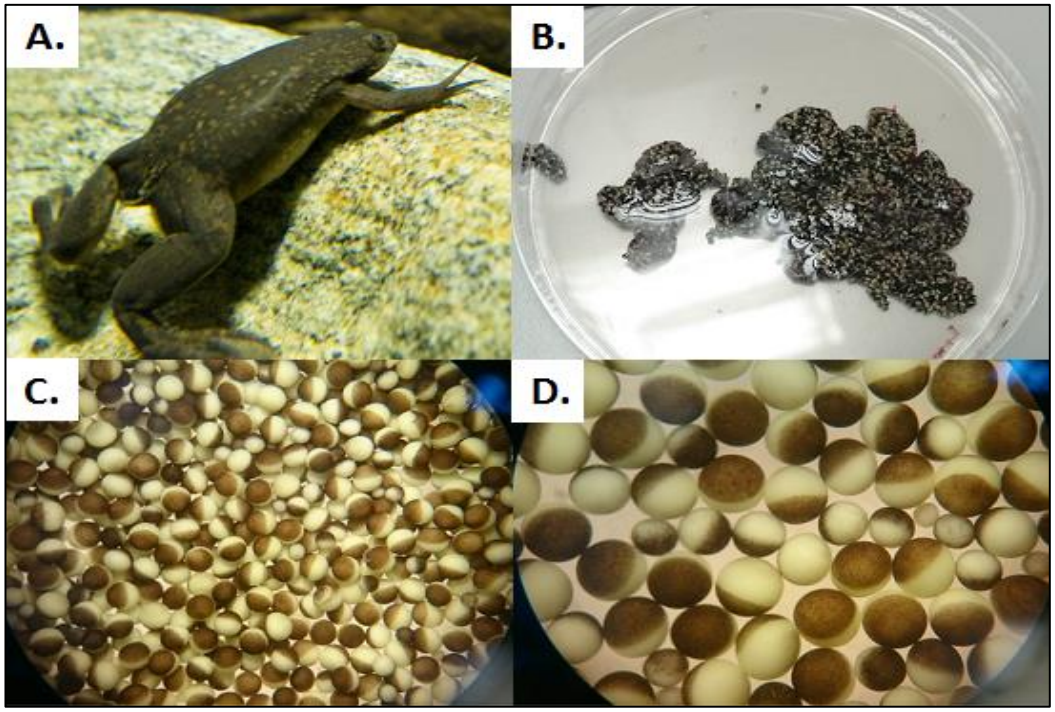


Figure 25: The *Xenopus laevis* frog and oocytes.

(A) The South African clawed frog, *Xenopus laevis* (Moine, 2008), (B) Undigested *Xenopus* oocytes, (B) and (C) *Xenopus* oocytes digested with collagenase type 1A (1 mg/ml) in 1 X GTP observed under the microscope at 16 X and 32 X magnification respectively.

The healthiest and undamaged oocytes were selected by observing the size, shape, colour and resilience of the oocytes. Those selected were expected to be at stage IV or V of their developmental phase (figure 26). At this stage, the oocytes are thought to be optimal for cRNA expression (Allen et al., 2007; Mertz and Gurdon, 1977). Developmental stages of *Xenopus* oocytes are shown in figure 26.

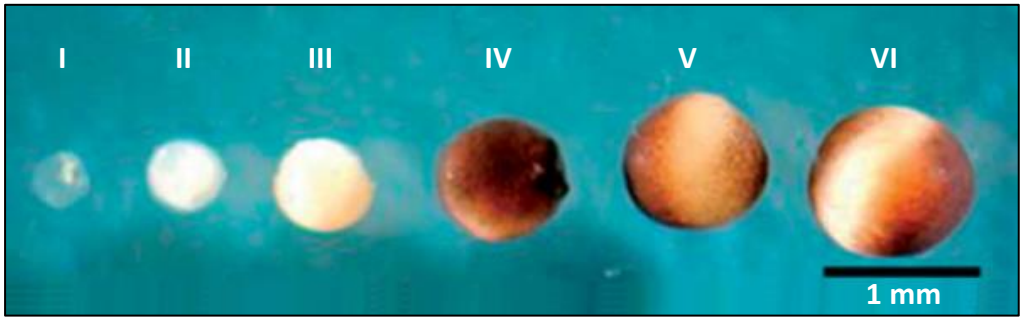


Figure 26: Developmental stages (I – VI) of *Xenopus laevis* oocytes.
Oocytes at stage IV and V were selected for cRNA injection as they are found to be optimal for processing of genetic materials into functional proteins (Allen et al., 2007; Mertz and Gurdon, 1977).

2.3.2 Oocyte Microinjection

A minimum of 250 ng cRNA encoding the NMDA receptor subunits were injected using a nanolitre injector (World Precision Instruments) which injects 50.6 nl of solution into each oocyte (as shown figure 27).

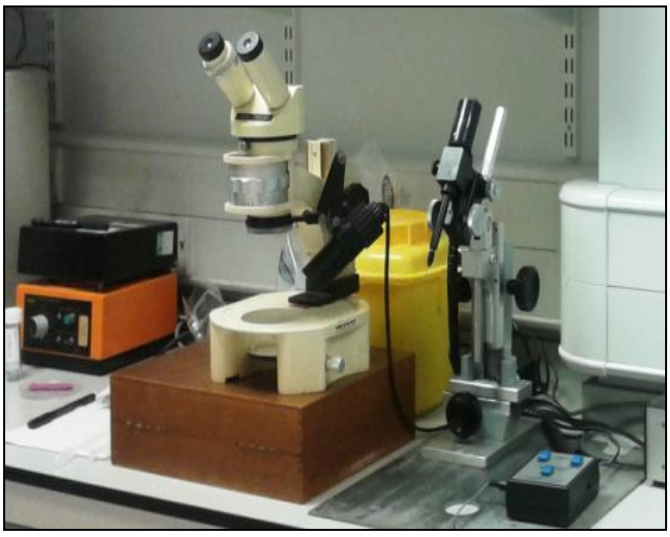


Figure 27: Nanoinjector used for injection of cRNAs into *Xenopus laevis* oocytes.

Fine glass pipettes were pulled from 3.5 nanolitre glass bores (World Precision Instruments) using the 700c vertical pipette puller (David Kopf Instruments). The end tip of the glass pipettes were carefully broken with a pair of forceps and filled with sterile paraffin oil before clamping on to the nanolitre injector needle. cRNA was gently drawn into the pipette avoiding any accumulation of air bubbles. The cRNA was then injected into healthy oocytes that had been selected and incubated at 18 °C in normal Barth's GTP solution. The medium containing the oocytes was replaced with fresh sterile solution after 24 hours and incubated for a further 48 hours to allow expression of NMDA receptor subunits before assaying.

2.4 ELECTROPHYSIOLOGICAL MEASUREMENT

2.4.1 Two-Electrode Voltage-Clamp (TEVC)

Intracellular electrodes were prepared from borosilicate glass capillaries (TW150F-4, World Precision Instruments) using a P-97 Flaming Brown micropipette puller (Sutter Instrument Company). Pulled glass capillaries were filled with 3 M KCl which works as a good conductor to minimize the resistance which should be in the range between 0.5 and 3 MΩ; if otherwise, the electrodes were replaced. Injected oocytes expressing the desired receptors were placed in a perfusion chamber and continuously perfused with a Mg^{2+}-free *Xenopus* ringer containing 96 mM NaCl, 2 mM KCl, 1.8 mM $CaCl_2$ and 10 mM HEPES, adjusted to pH 7.5 with NaOH. Two glass electrodes filled with 3 M KCl (one to measure membrane potential and the other to inject current) were then impaled through the cell membrane as depicted in figure 28.

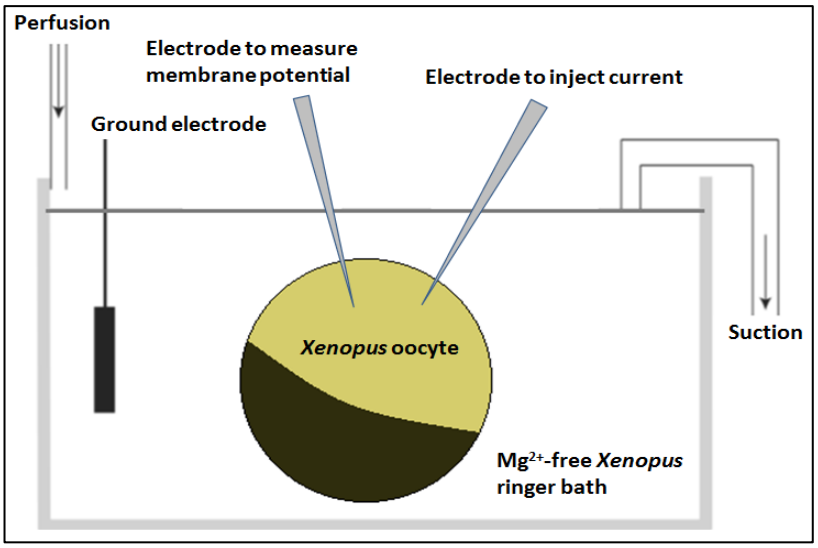


Figure 28: Diagram representation of two-electrode voltage clamp.

The figure shows an oocyte being placed in a chamber perfused with Mg^{2+}-free *Xenopus* ringer and two electrodes were impaled through the membrane. One electrode measures the membrane potential while the other electrode passes current to clamp the oocyte at the desired potential. Adapted from Goldin (2006).

The resting membrane potential was observed; both electrodes should be in agreement between -20 and -50 mV for the cells to be accepted for electrophysiology recordings. Voltage was clamped at the desired holding potentials using a voltage clamp amplifier, Axoclamp-2A (Axon Instruments) and responses were elicited by manually perfusing the drugs/test compounds using a Valvelink 8 gravity perfusion system (Automatic Scientific). The output current responses were transferred by an analog-to-digital (A/D) converter to a computer and recorded via the WinEDR software (John Dempster, Strathclyde Electrophysiology Software). The output from the Axoclamp was filtered at 100 Hz while the digitization rate was set at 100 samples for every seconds. The data were transferred to GraphPad Prism software to yield the respective EC_{50} or IC_{50} values. The TEVC setup used in this study is displayed in figure 29.



Figure 29: Electrophysiology set-up to record drug/test compound responses on receptor channels expressed on *Xenopus laevis* oocytes.

2.4.2 Determination of NMDA and Glycine EC_{50}

NMDA (Ascent Scientific) was prepared as a stock solution of $1x10^{-2}$ M, diluted in Mg^{2+}-free ringer and stored at -20 °C. To determine its half maximal effective concentration (EC_{50}), the stock solution was subsequently subjected to serial dilutions in Mg^{2+}-free ringer containing 10 µM glycine (Sigma) ranging from 0.1 to 1000 µM. NMDA co-applied with glycine was tested on GluN1-1a/GluN2A NMDAR at -75 mV holding potential. For optimization purposes, NMDA/glycine solution was applied onto the oocytes and the duration for it to achieve steady-state was determined by multiple trial and errors. One minute of application time was found to be sufficient for NMDA in the presence of glycine to reach its steady-state. Mean activation measurements (peak and steady-state) were determined at each concentration of NMDA as the percentage of maximum response. The data were then plotted and fitted by a four-parameter logistic equation (Hill equation) in GraphPad Prism software to yield the EC_{50} value of NMDA (refer to section 2.7, Data Analysis). Based on the EC_{50} obtained, the suitable concentration of NMDA was used in subsequent recordings to assay antagonists. A similar protocol was used to determine the EC_{50} for glycine whereby increasing concentration of glycine (0.01 to 100 µM) were co-

applied with 100 µM NMDA and electrophysiologically tested at -75 mV. Glycine was prepared freshly on the day of testing as it was found that the compound does not remain active when stored over a long period of time.

2.4.3 Determination of Antagonists IC_{50}

NMDAR antagonists used in this study were Mg^{2+}, memantine (Sigma), MK-801 (Merck) and philanthotoxin analogues (Dr. Henrik Franzyk and Prof. Dr. Kristian Strømgaard, University of Copenhagen). The antagonist compounds were diluted in Mg^{2+}-free *Xenopus* ringer containing NMDA (100 µM) and glycine (10 µM) in tenfold serial dilutions ranging from 0.001 to 100 µM. The compounds were subsequently tested electrophysiologically on NMDAR-expressing oocytes at -50, -75 and -100 mV.

Perfusion of NMDA/glycine onto the oocytes was applied for one minute allowing it to reach steady-state, followed by 30 seconds of subsequent antagonist applications in increasing concentration. Mg^{2+}-free ringer solution was then applied for two minutes to allow recovery to baseline current before the next applications of NMDA/glycine and test compounds at a different holding potential.

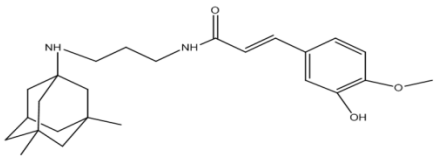
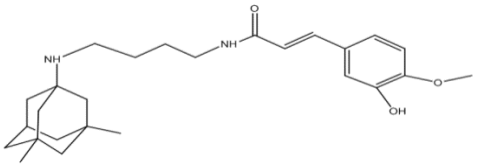
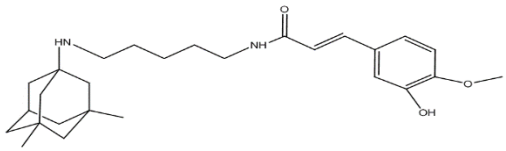
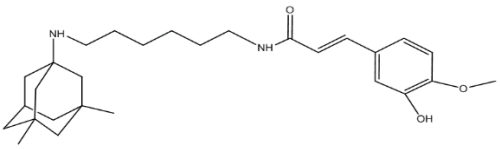
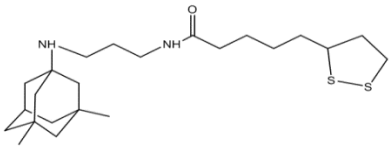
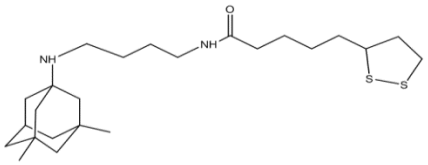
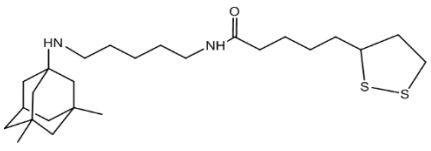
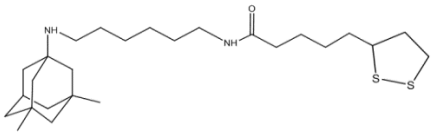
Current changes when applied with antagonists were normalized to the control current without antagonists. The concentration-inhibition curves were then plotted and fitted with the Hill equation using GraphPad Prism software to calculate the half maximal inhibitory concentration (IC_{50}) of antagonists (refer to section 2.7, Data Analysis). Recordings were obtained from separate oocytes (at least two and typically five) across at least two different batches of oocytes.

2.5 MULTI-TARGET-DIRECTED LIGANDS

Novel multi-target-directed ligands (MTDL) were tested to evaluate their inhibitory potency on GluN1-1a and GluN2A NMDA receptor subunits. These compounds were synthesized in collaboration with Dr. Michela Rosini from the University of Bologna, Italy. Solid compounds were dissolved in 100% DMSO to obtain a stock solution of $1x10^{-2}$ M and kept stored in -20 °C. For electrophysiology assay, the stock solutions were diluted in Mg^{2+}-free ringer solution containing 100 µM NMDA and 10 µM glycine in tenfold serial dilutions ranging from 0.01 µM to 100 µM. The maximum final DMSO concentration in the solution preparation was 1%; a previous study has shown that it produced no inhibitory effect when applied to NMDAR expressing oocytes at that concentration (Crofts, 2011).

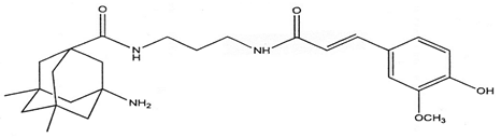
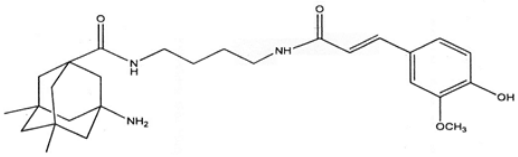
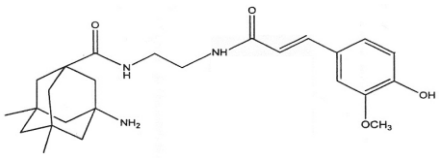
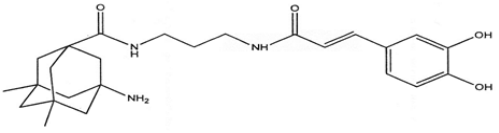
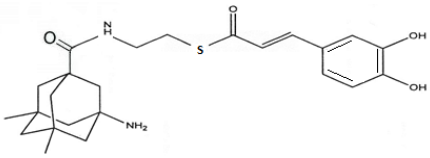
Four series of novel compounds were evaluated in this study with memantine-derivatives being the first and named as MAB compounds. Four of the compounds (MAB23(2), MAB14, MAB22, MAB30) were attached with an antioxidant headgroup, methoxyphenol by a polymethylene/amide backbone with different chain lengths. The other four compounds (MAB7, MAB15, MAB21, MAB32) were incorporated with a lipoic acid functional group which are light- and thermosensitive. Structures of the compounds are displayed in table 10.

Table 10: Novel memantine-derivative (MAB) MTDL compounds incorporated with a methoxyphenol or lipoic acid moiety assessed in this study.

Compound	Chemical Structure	Molecular weight
MAB23(2)		412.57
MAB14		426.60
MAB22		440.63
MAB30		454.66
MAB7		424.71
MAB15		438.73
MAB21		452.76
MAB32		466.79

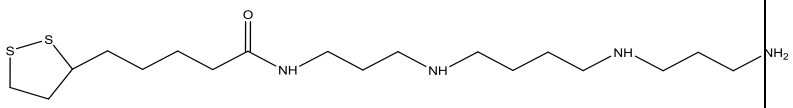
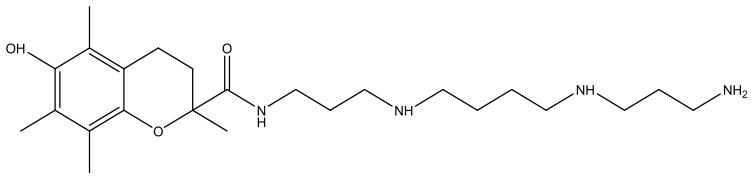
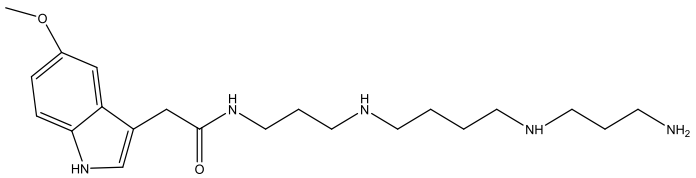
The second series of MTDLs were also derived from memantine. However instead of attachment to the amine group of memantine, an additional amide group was introduced to attach the antioxidant moiety to the memantine carbon skeleton. The first three compounds named FC7, FC12 and FC17 were incorporated with methoxyphenol while FC20 was attached with catechol. Finally, the GB compound is similar to FC20 but with an amine replaced with a sulphide in the linker chain. Structures of the second series of the memantine-derivative MTDLs are displayed in table 11.

Table 11: Novel memantine-derivative (FC/GB) MTDL compounds incorporated with methoxyphenol or catechol moiety assessed in this study.

Compound	Chemical Structure	Molecular Weight
FC7		455.59
FC12		469.62
FC17		441.56
FC20		441.56
GB13		444.59

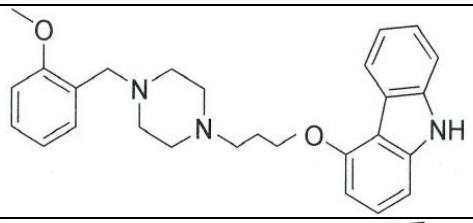
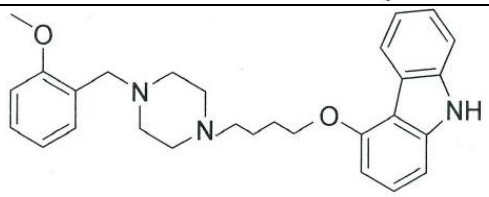
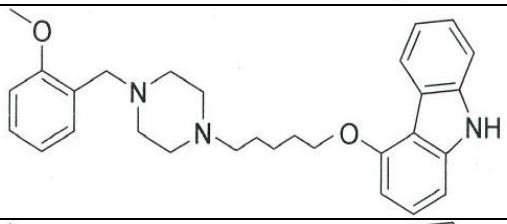
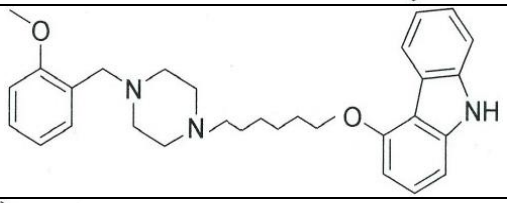
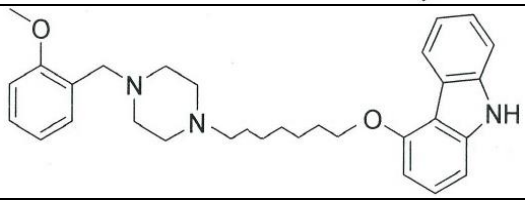
The third series of MTDLs termed as CR compounds were composed of a spermine polyamine backbone, each of them attached to a different antioxidant headgroup. CR8 was incorporated with lipoic acid, CR18 attached with α-tocopherol while CR24 was attached with melatonin. Structures of the compounds are displayed in table 12.

Table 12: Novel spermine-derived polyamine MTDLs (CR) assessed in this study.

Compound	Chemical Structure	Molecular weight
CR8		733
CR18		545
CR24		535

The fourth and final series of MTDLs termed as MGM compounds evaluated in this study were composed of 1-(2-methoxybenzyl)-piperazine linked via different lengths of spacers (n=3-7) to a carbazole moiety. The former chemical structure was derived from donepezil while the latter was derived from carvedilol. Combining the pharmacophores of these two drugs was postulated to yield a compound with non-competitive NMDAR-blocking property, exert anti-amyloidogenic effect, possess antioxidant property and able to interact with the AChE gorge (Rosini et al., 2008). Structures of the compounds are displayed in table 13.

Table 13: Donepezil-derived MTDL compounds assessed in this study.

Compound	Chemical Structure	Molecular weight
MGM10		429.56
MGM12		443.59
MGM3		457.62
MGM2		471.64
MGM11		485.67

2.5.1 Electrophysiology of MTDL Compounds

Different approaches were used to evaluate the inhibitory potencies of MTDLs to maintain continuity with previous studies. For the first three series of MTDLs (MAB, FC/GB and CR), a single holding potential (-60 mV) was used to clamp the oocytes. NMDA/glycine solution was applied for one minute followed by 30 seconds co-application of a test compound at the lowest concentration. This step was repeated with the subsequent higher concentrations of test compounds with two minutes of Mg^{2+}-free ringer application in between to allow recovery to baseline. This protocol

generated five different traces for a range of five different concentrations of test compounds. The percentage of current inhibited was calculated for each concentration and used to determine the IC_{50} value via Graphpad Prism.

To assess voltage-dependent block, dilutions of the MTDL compounds were prepared based on their respective IC_{50} concentrations made up in NMDA (100 µM) and glycine (10 µM) solution. Each compound was tested against oocytes expressing GluN1-1a/GluN2A subunits clamped at -40 mV, -60 mV, -80 mV and -100 mV. Using the same protocol as above, NMDA/glycine solution was applied for one minute followed by co-application of test compounds for 30 seconds. Mg^{2+}-free ringer solution was applied for two minutes allowing recovery to baseline current before adjusting to a higher holding potential and subsequent application of NMDA/glycine and test compounds. The blocking percentage at each voltage was calculated and fitted to the Woodhull equation. A replicate of at least three oocytes across two different batches were carried out for each compound.

A different strategy was employed for MGM compounds whereby the IC_{50}s of the compounds were obtained at three different holding potentials; -50, -80 and -100 mV. As the control, NMDA (100 µM) and glycine (10 µM) without test compounds were perfused for 1 minute followed by 2 minutes of recovery interval. This step was repeated with co-application of NMDA/glycine and MGM compounds in tenfold increasing concentration generating a set of five traces. Steady-state responses were measured and normalized as a percentage of the control response. The data were fitted with the Hill equation to generate the IC_{50}s obtained from the concentration-inhibition curve. To assess voltage-dependency, the IC_{50}s obtained for all three holding potentials were then fitted with the Woodhull model to yield the δ values.

Aside from responses on NMDAR, MGM compounds were further tested on α4β2 and α7 subunits of nicotinic acetylcholine receptors (nAChR). Previous binding studies have shown that donepezil-derived compounds were able to bind with nAChRs, but whether they act as agonists or antagonists had not yet been determined. Therefore, these compounds were first diluted in *Xenopus* ringer to 10

and 100 µM concentrations and tested alone with α4β2 and α7 nAChRs at -80 mV. The percentage of the evoked inward currents by MGM compounds against the control response (10 and 100 µM ACh respectively) were calculated to measure their agonistic properties. To measure antagonistic properties, the compounds were diluted in constant concentration of 10 µM ACh for α4β2 assay and 100 µM ACh for testing on α7. This was based on the sensitivity of ACh to the respective subunits (Kachel, 2014). The oocytes were clamped at three holding potentials (-50, -80 and -100 mV) and the recording protocol was conducted similarly to the NMDAR assay but with ten minute intervals (instead of two minutes) between each application to allow complete recovery. The IC_{50} values for antagonism of peak responses were calculated from concentration-response curves (Hill equation) and also fitted with the Woodhull equation to assess voltage dependency. Peak responses were measured rather than steady-state level due to their fast recovery rate particularly α7 nAChRs (Kachel, 2014).

2.6 DATA ANALYSIS

EC_{50} and IC_{50} values for test compounds were obtained by using nonlinear regression by fitting a four-parametric logistic equation (Hill equation) to a concentration-response and concentration-inhibition plots respectively in GraphPad Prism 6 (GraphPad Software Inc). The Hill equations used to determine the EC_{50} (Eq. 1) and IC_{50} (Eq. 2) are presented below.

$$\%\ maximum\ response = \frac{100}{1 + 10^{((\log_{10} EC_{50} - X) \times HillSlope)}} \qquad \text{(Eq. 1)}$$

$$\%\ control\ response = \frac{100}{1 + 10^{((\log_{10} IC_{50} - X) \times HillSlope)}} \qquad \text{(Eq. 2)}$$

Where X is $\log_{10}$[agonist] (Eq. 1) or $\log_{10}$[antagonist] (Eq. 2).

To determine if the EC_{50} or IC_{50} values of the compounds were significantly different to each other, they were compared pairwise using the extra sum-of-squares F-test to a null hypothesis of EC_{50}/IC_{50} being the same for each pair (GraphPad Software Inc). The p value to determine statistical significance was set at 0.05.

To determine voltage-dependence, the δ values were calculated using IC_{50}s of the test compounds. The δ value represents the fraction of the membrane potential acting at the site, where 0 represents the electric field at the external entrance to the channel and 1 represents the internal entrance to the channel. This value is useful to predict binding sites of the channel blockers.

For this purpose, the Woodhull model was used to calculate the parameter δ from the following equation (Woodhull, 1973).

$$IC_{50}(V_h) = IC_{50}(0\ mV)\ \times \exp\left(\frac{z\delta V_m F}{RT}\right) \qquad \text{(Eq. 3)}$$

z is the valence of the blockers, V_h is the membrane potential (mV), *R* is the gas constant, *T* is absolute temperature (K) and *F* is Faraday's constant (C/mol).

Voltage-dependence can also be measured by the blocking percentage, taking activation before the channel blocker application as 0% and the baseline current as 100%. The data was fitted to the following Woodhull equation (Ferrer-Montiel et al., 1998; Woodhull, 1973).

$$Y = \frac{Y_{max} - Y_{min}}{\left(1 + {}^{[B]}/_{K_D}\right) e^{z\delta({}^{FE}/_{RT})}} \qquad \text{(Eq. 4)}$$

Y is the percentage of control response, [*B*] is the blocker concentration, K_D is the dissociation constant at 0 mV, *z* is the charge (valence) of the molecule, *F* is Faraday's constant (C/mol), *E* is the membrane potential, *R* is the gas constant and *T* is the absolute temperature (K).

CHAPTER 3

NMDA RECEPTOR CHARACTERIZATION

3.1 SUMMARY

This chapter describes the characterization of GluN1-1a/GluN2A subunit combinations expressed in *Xenopus laevis* oocytes. Concentration response curves were produced via electrophysiology recordings to generate the EC_{50}s for NMDA and glycine as the agonist and co-agonist, as well as the IC_{50}s for well-known NMDAR inhibitors namely Mg^{2+}, memantine, MK-801, PhTX-343 and some derivatives. Woodhull analysis were also performed to determine voltage-dependency and estimate binding sites. This study has established a working oocyte expression system for drug evaluation which retains the pharmacological characteristics of the conventional NMDAR subunits. Largely, the results obtained for NMDA and glycine EC_{50}s as well as Mg^{2+}, memantine, MK-801 and PhTX-343 IC_{50}s were in agreement with many other published literatures employing *Xenopus* oocytes expressing GluN1-1a/GluN2A NMDAR subunits. All of the antagonist compounds tested also blocked NMDA/glycine responses in a voltage-dependent manner.

3.2 NMDA RECEPTOR AGONISM

3.2.1 NMDA and Glycine Activation

Separate applications of NMDA (100 µM) or glycine (10 µM) alone did not trigger any response on GluN1-1a/GluN2A-containing NMDA receptors tested at -75 mV. When NMDA and glycine were co-applied together, a large inward current was evoked as expected and demonstrated in figure 30.

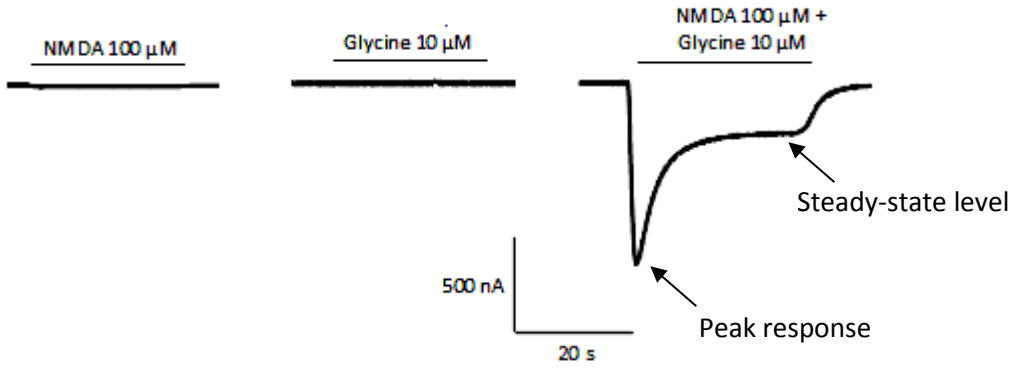
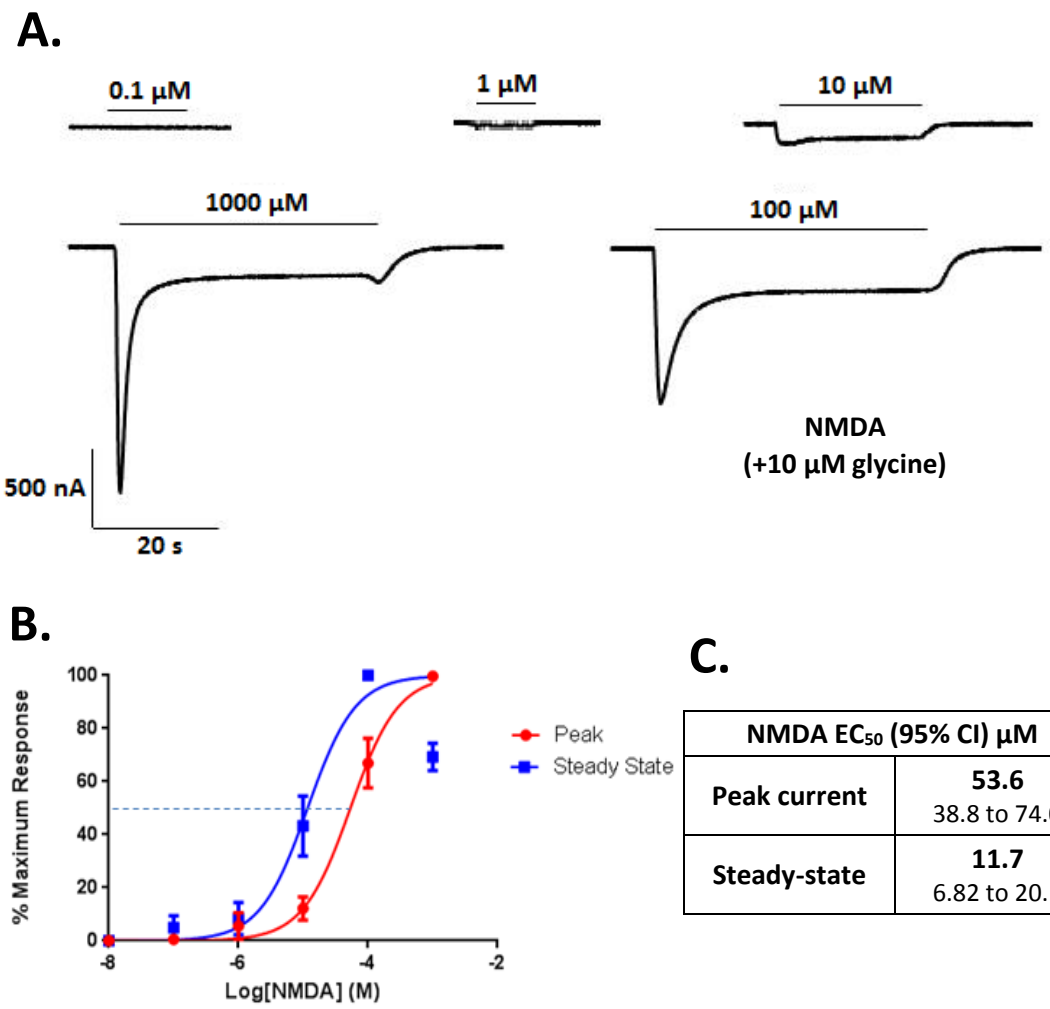


Figure 30: TEVC recordings of NMDA and glycine activation mediated by GluN1-1a/GluN2A-containing NMDA receptors at -75 mV.

NMDA (100 µM) or glycine (10 µM) alone did not elicit any response. A large inward currents were elicited with co-application of NMDA (100 µM) and glycine (10 µM).

3.2.2 EC_{50} of NMDA

Concentration-response data for NMDA (0.1 to 1000 µM) co-applied with glycine (10 µM) were used to determine the EC_{50} value of the NMDAR agonist mediated by GluN1-1a and GluN2A NMDAR subunits at -75 mV (figure 31). The EC_{50} obtained from this study was 53.6 (95% CI 38.8 to 74.0) µM for the peak response and 11.7 (95% CI 6.82 to 20.1) µM for the steady-state level. A concentration of 100 µM NMDA was confirmed efficient to evoke a response on NMDAR and was used in subsequent recordings to assay antagonists with co-application of 10 µM glycine.



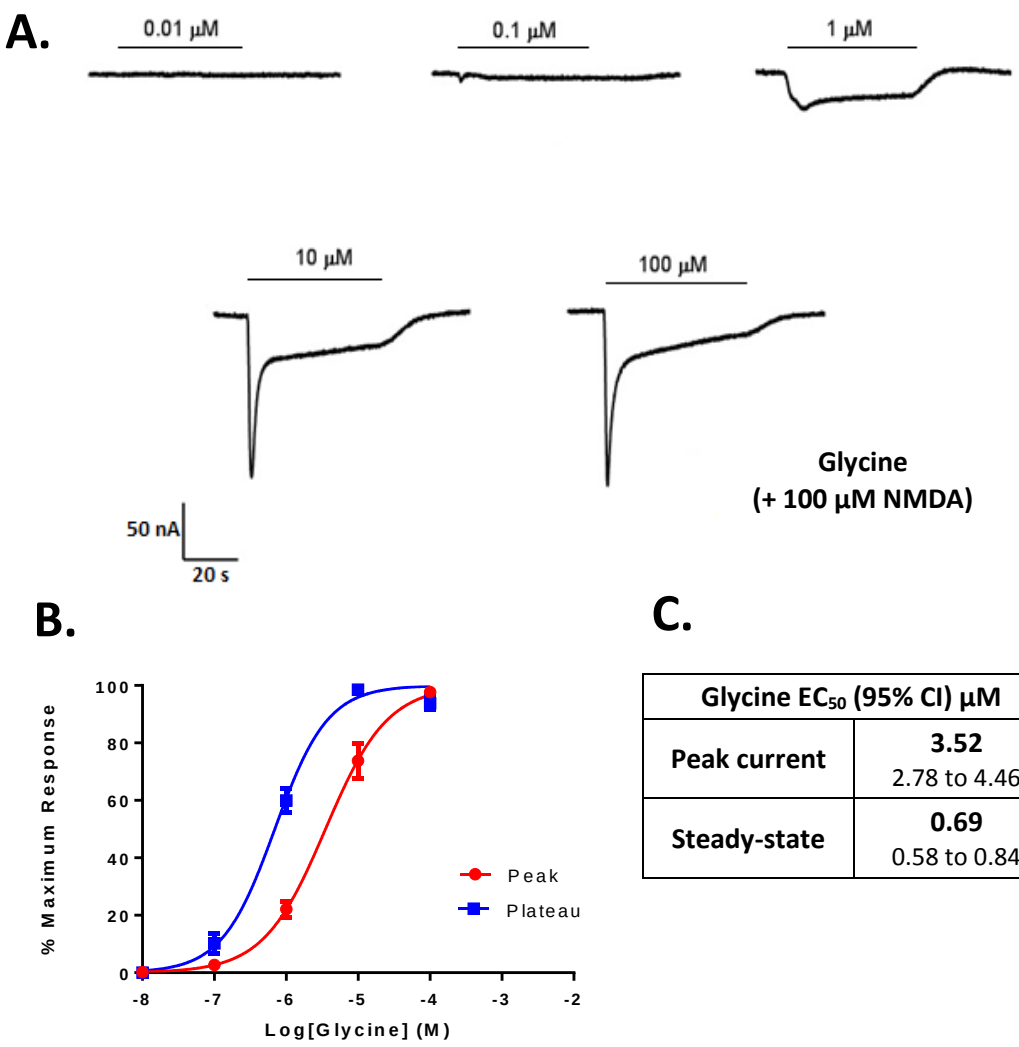
NMDA EC_{50} (95% CI) µM	
Peak current	**53.6** 38.8 to 74.0
Steady-state	**11.7** 6.82 to 20.1

Figure 31: Concentration-response relationship for NMDA co-applied with glycine mediated by GluN1-1a/GluN2A-containing receptors.

(A) TEVC recordings of NMDA-evoked currents at tenfold increasing concentration (0.1–1000 µM) tested at -75 mV, (B) Percentage control response (mean ± SEM, n=5) plotted and fitted with the Hill equation, (C) EC_{50} (95% CI) values for NMDA at peak and steady-state level obtained via the concentration-inhibition curves.

3.2.3 EC_{50} of Glycine

Concentration-response data for glycine (0.01 to 100 µM) co-applied with NMDA (100 µM) were used to determine the EC_{50} value of glycine mediated by GluN1-1a and GluN2A NMDAR subunits at -75 mV (figure 32). The EC_{50} obtained from this study was 3.52 (95% CI 2.78 to 4.46) µM for the peak response and 0.69 (95% CI 0.58 to 0.84) µM for the steady-state level. A concentration of 10 µM glycine was confirmed efficient to evoke a response on NMDAR when co-applied with 100 µM NMDA and was used in subsequent recordings to assay antagonists.



Glycine EC_{50} (95% CI) µM	
Peak current	**3.52** 2.78 to 4.46
Steady-state	**0.69** 0.58 to 0.84

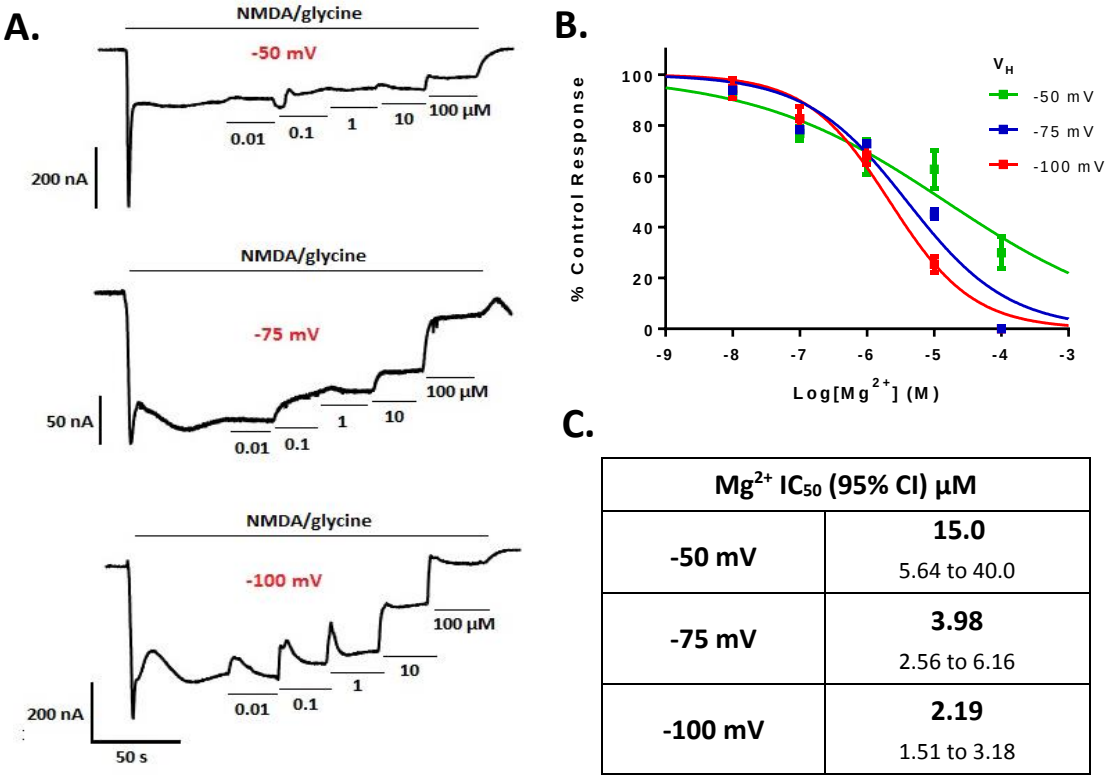
Figure 32: Concentration-response relationship for glycine co-applied with NMDA mediated by GluN1-1a/GluN2A-containing receptors.

(A) TEVC recordings of NMDA/glycine-evoked currents at tenfold increasing concentration (0.01–100 µM) tested at -75 mV, (B) Percentage control response (mean ± SEM, n=11) plotted and fitted with the Hill equation, (C) EC_{50} (95% CI) values for glycine at peak and steady-state level obtained via the concentration-inhibition curves.

3.3 NMDA RECEPTOR ANTAGONISM BY OPEN CHANNEL BLOCKERS

3.3.1 Mg^{2+}

The antagonism of responses to NMDA and glycine by tenfold increment of Mg^{2+} concentration (0.01 to 100 µM) mediated by GluN1-1a/GluN2A were used to determine IC_{50} values at three different holding potentials. The IC_{50}s obtained were 15.0 (95% CI 5.64 to 40.0), 3.98 (95% CI 2.56 to 6.16) and 2.91 (95% CI 1.51 to 3.18) µM at -50, -75 and -100 mV respectively. IC_{50}s of Mg^{2+} increased as holding potentials were also increased suggesting that Mg^{2+} potency is affected by membrane potential. Significant differences ($p<0.05$) were observed between IC_{50}s across all holding potentials confirming the voltage-dependence of block of NMDA/glycine responses by Mg^{2+}. The results are shown in figure 33.



C.

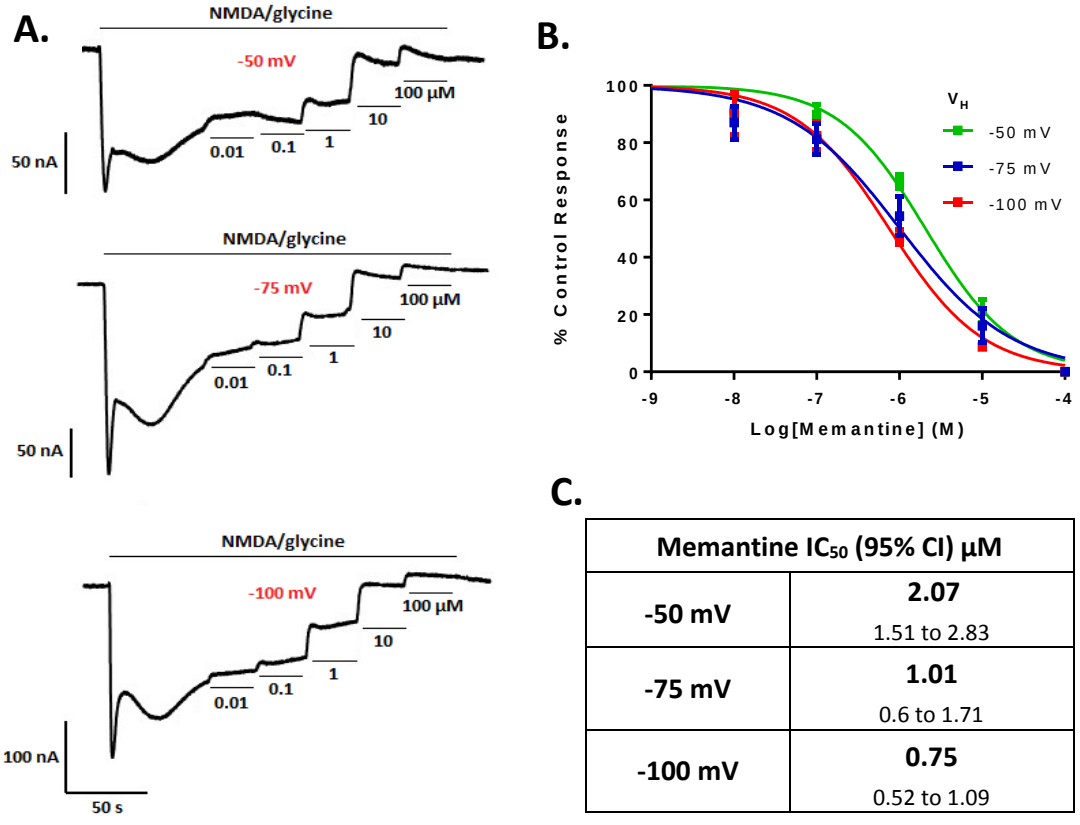
Mg^{2+} IC_{50} (95% CI) µM	
-50 mV	**15.0** 5.64 to 40.0
-75 mV	**3.98** 2.56 to 6.16
-100 mV	**2.19** 1.51 to 3.18

Figure 33: Mg^{2+} block of NMDA/glycine responses in GluN1-1a/GluN2A-containing NMDA receptors.

(A) TEVC recordings for Mg^{2+} (0.01–100 µM) block at three holding potentials, -50, -75 and -100 mV, (B) Concentration-inhibition curves for Mg^{2+} block. Percentage control response (mean ± SEM, n=5-6) values were plotted and fitted with the Hill equation, (C) IC_{50} (95% CI) values for Mg^{2+} generated from the concentration-inhibition curves. Significant differences were observed between IC_{50}s across all voltages ($p<0.05$).

3.3.2 Memantine

Block of NMDA/glycine responses by a range of memantine concentrations (0.01 to 100 µM) on GluN1-1a/GluN2A were measured electrophysiologically and used to determine IC_{50} values at three different holding potentials. The IC_{50}s obtained were 2.07 (95% CI 1.51 to 2.83), 1.01 (95% CI 0.6 to 1.71) and 0.75 (95% CI 0.52 to 1.09) µM recorded at -50, -75 and -100 mV respectively. IC_{50}s of memantine were increased as holding potentials were also increased. Significant differences were observed between IC_{50}s at -50 mV compared to both at -75 mV ($p=0.018$) and at -100 mV ($p<0.0001$) suggesting the voltage-dependence of block of NMDA/glycine responses by memantine. The results are shown in figure 34.



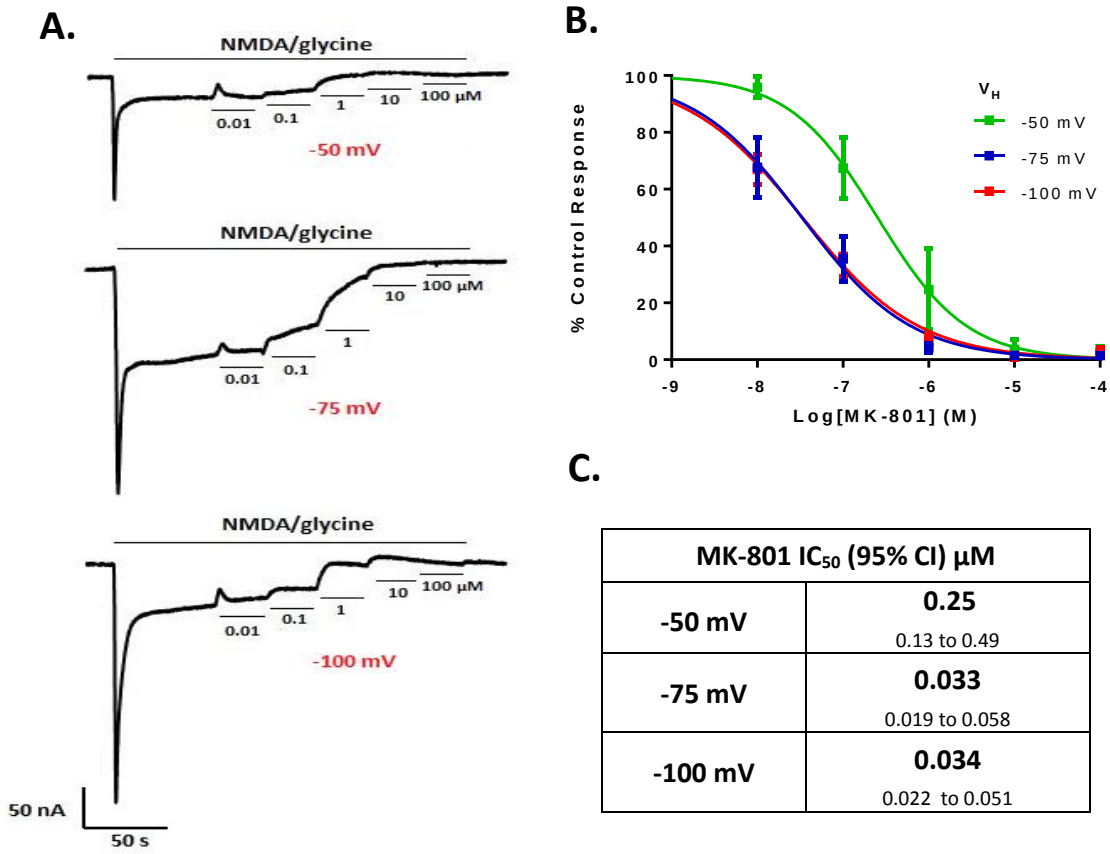
C.

Memantine IC_{50} (95% CI) µM	
-50 mV	**2.07** 1.51 to 2.83
-75 mV	**1.01** 0.6 to 1.71
-100 mV	**0.75** 0.52 to 1.09

Figure 34: Memantine block of NMDA/glycine responses in GluN1-1a/GluN2A-containing NMDA receptors.
(A) TEVC recordings for memantine (0.01–100 µM) block at three holding potentials, -50, -75 and -100 mV, (B) Concentration-inhibition curves for memantine block. Percentage control response (mean ± SEM, n=5) values were plotted and fitted with the Hill equation, (C) IC_{50} (95% CI) values for memantine generated via the concentration-inhibition curves. Significant differences were observed between IC_{50}s at -50 mV compared to both at -75 mV ($p=0.018$) and at -100 mV ($p<0.0001$).

3.3.3 MK-801

Antagonism of NMDA/glycine responses by MK-801 was determined by using tenfold increment of compound concentrations (0.01 to 100 µM) and tested electrophysiologically on GluN1-1a/GluN2A NMDA receptors at three different holding potentials. IC_{50} values obtained from the concentration-inhibition curves were 0.25 (95% CI 0.13 to 0.49), 0.033 (95% CI 0.019 to 0.058) and 0.034 (95% CI 0.022 to 0.051) µM recorded at -50, -75 and -100 mV respectively. Significant differences were observed between IC_{50}s at -50 mV compared to both at -75 and -100 mV ($p<0.0001$) suggesting that MK-801 blocks NMDA in a voltage-dependent manner. The results are presented in figure 35.



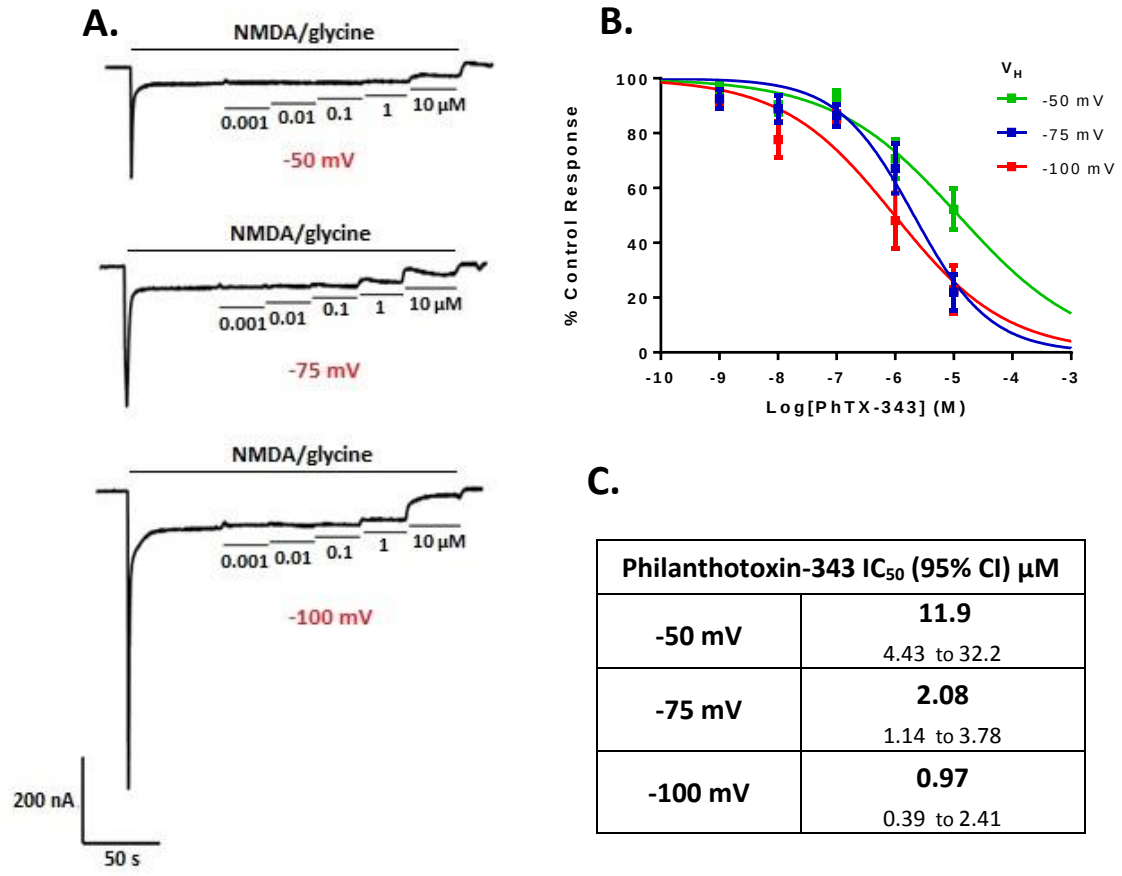
C.

MK-801 IC_{50} (95% CI) µM	
-50 mV	**0.25** 0.13 to 0.49
-75 mV	**0.033** 0.019 to 0.058
-100 mV	**0.034** 0.022 to 0.051

Figure 35: MK-801 block of NMDA/glycine responses in GluN1-1a/GluN2A-containing NMDA receptors.
(A) TEVC recordings for MK-801 (0.01–100 µM) block at three holding potentials, -50, -75 and -100 mV, (B) Concentration-inhibition curves for MK-801 block. Percentage control response (mean ± SEM, n=5) values were plotted and fitted with the Hill equation, (C) IC_{50} (95% CI) values for MK-801 generated via the concentration-inhibition curves. Significant differences were observed between IC_{50}s at -50 mV compared to both at -75 and -100 mV ($p<0.0001$).

3.3.4 Philanthotoxin-343

Inhibition of NMDA/glycine responses by tenfold increment of PhTX-343 concentrations (0.001 to 10 µM) mediated by GluN1-1a/GluN2A were measured to generate the concentration-inhibition curve fitted with the Hill equation. The IC_{50}s obtained were 11.9 (95% CI 4.43 to 32.2), 2.08 (95% CI 1.14 to 3.78) and 0.97 (95% CI 0.39 to 2.41) µM recorded at -50, -75 and -100 mV respectively. IC_{50}s of PhTX-343 increased as holding potentials were adjusted up. Significant differences were observed between IC_{50}s at -50 mV compared to both at -75 mV (p=0.0007) and at -100 mV (p=0.0003) suggesting the voltage-dependence of block of NMDA/glycine responses by PhTX-343. The results are presented in figure 36.



C.

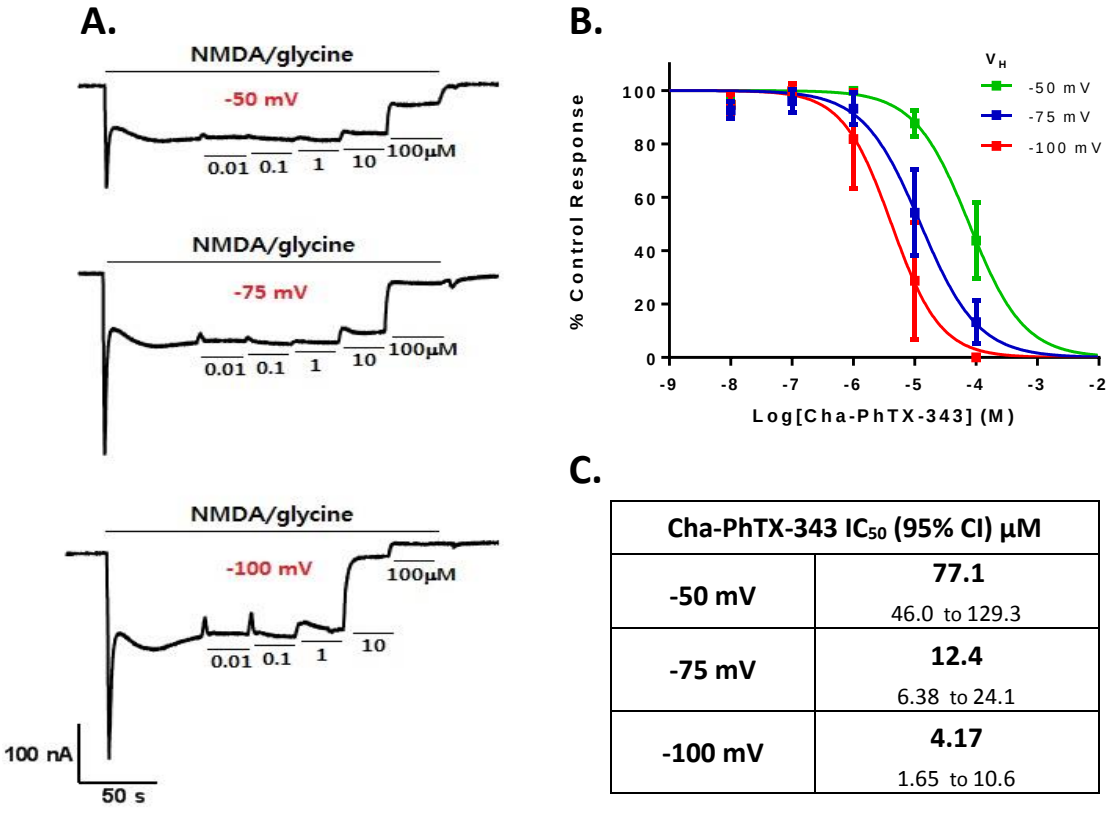
Philanthotoxin-343 IC_{50} (95% CI) µM	
-50 mV	**11.9** 4.43 to 32.2
-75 mV	**2.08** 1.14 to 3.78
-100 mV	**0.97** 0.39 to 2.41

Figure 36: PhTX-343 block of NMDA/glycine responses in GluN1-1a/GluN2A-containing NMDA receptors.

(A) TEVC recordings for PhTX-343 (0.001–10 µM) block at three holding potentials, -50, -75 and -100 mV, (B) Concentration-inhibition curves for PhTX-343 block. Percentage control response (mean ± SEM, n=4-7) values were plotted and fitted with the Hill equation, (C) IC_{50} (95% CI) values for PhTX-343 generated via the concentration-inhibition curves. Significant differences were observed between IC_{50}s at -50 mV compared to both at -75 mV (p=0.0007) and at -100 mV (p=0.0003).

3.3.5 Cha-PhTX-343

Cha-PhTX-343, a philanthotoxin analogue, was investigated to assess its inhibitory effect on GluN1-1a/GluN2A NMDA receptors. Block of NMDA and glycine responses by tenfold increment of compound concentrations (0.01 to 100 µM) yielded IC_{50}s of 77.1 (95% CI 46.0 to 129.3), 12.4 (95% CI 6.38 to 24.1) and 4.17 (95% CI 1.65 to 10.6) µM at -50, -75 and -100 mV respectively. IC_{50}s of this compound increased as holding potentials were also increased. Significant differences ($p<0.05$) were observed between IC_{50}s across all holding potentials suggesting the voltage-dependence block of NMDA/glycine by Cha-PhTX-343. The results are shown in figure 37.



C.

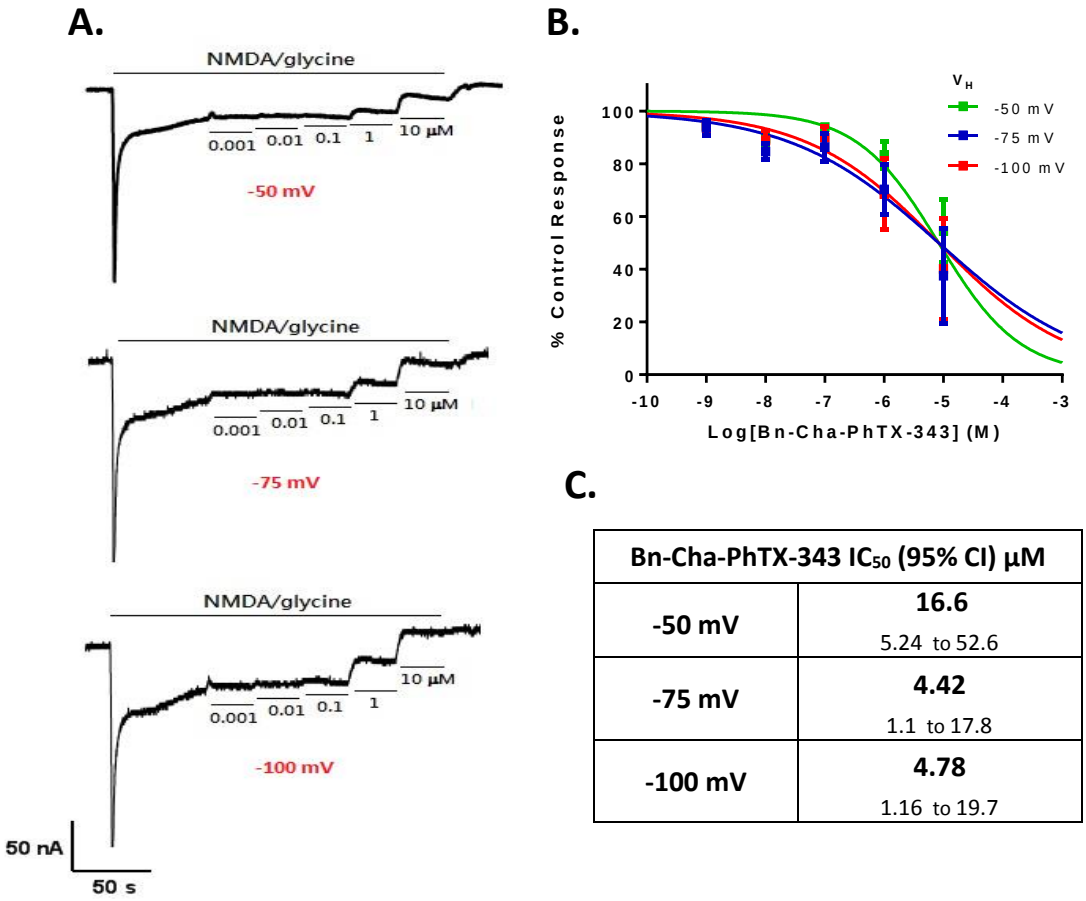
Cha-PhTX-343 IC_{50} (95% CI) µM	
-50 mV	**77.1** 46.0 to 129.3
-75 mV	**12.4** 6.38 to 24.1
-100 mV	**4.17** 1.65 to 10.6

Figure 37: Cha-PhTX-343 block of NMDA/glycine responses in GluN1-1a/GluN2A-containing NMDA receptors.

(A) TEVC recordings for Cha-PhTX-343 (0.001–10 µM) block at three holding potentials, -50, -75 and -100 mV, (B) Concentration-inhibition curves for Cha-PhTX-343. Percentage control response (mean ± SEM, n=4-5) values were plotted and fitted with the Hill equation, (C) IC_{50} (95% CI) values for Cha-PhTX-343 generated via the concentration-inhibition curves. Significant differences were observed between IC_{50}s across all holding potentials ($p<0.05$).

3.3.6 Bn-Cha-PhTX-343

Another philanthotoxin analogue, Bn-Cha-PhTX-343, was also investigated to examine its antagonism potency on GluN1-1a/GluN2A NMDA receptors. Block of NMDA and glycine responses by this compound in tenfold increasing concentration (0.01 to 100 µM) yielded IC_{50}s of 16.6 (95% CI 5.24 to 52.6), 4.42 (95% CI 1.1 to 17.8) and 4.78 (95% CI 1.16 to 19.7) µM at -50, -75 and -100 mV respectively. The compound was more potent at more negative holding potentials as IC_{50}s at -75 and -100 mV were similar and much lower than that at -50 mV although the differences were not statistically significant (p>0.05). The results are shown in figure 38.



C.

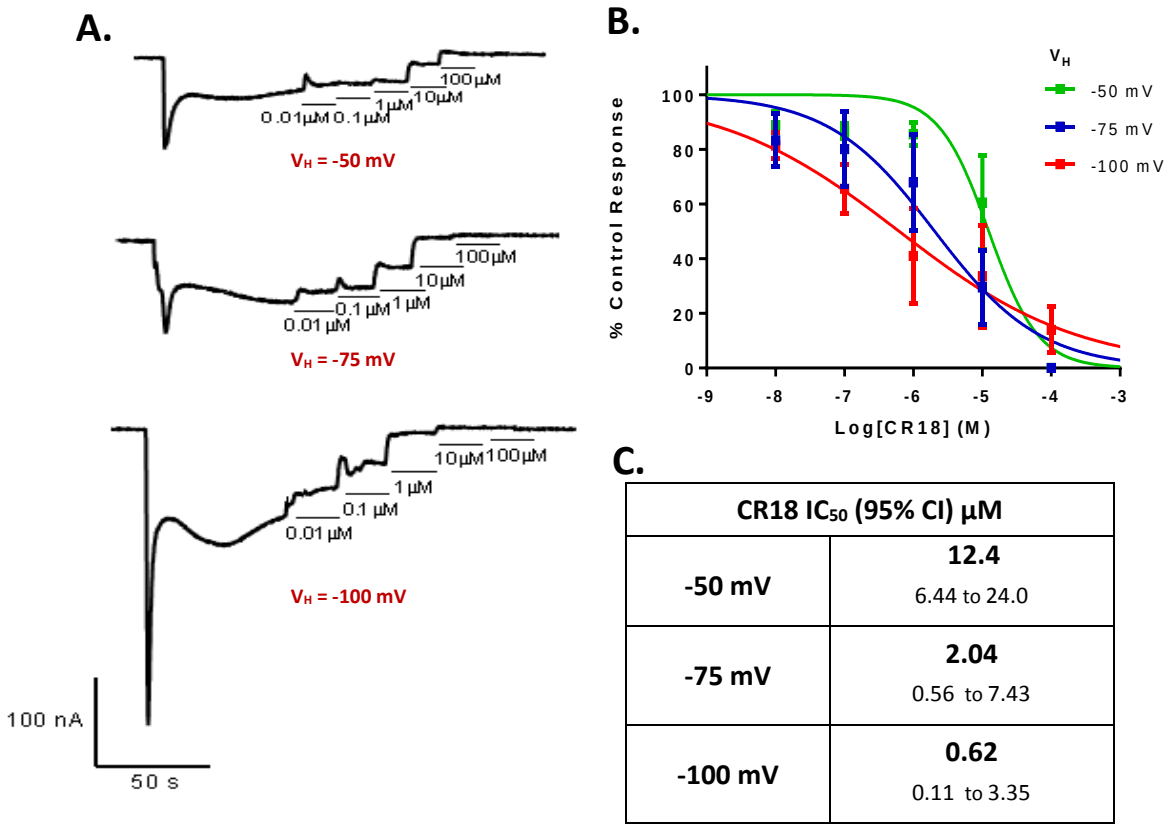
Bn-Cha-PhTX-343 IC_{50} (95% CI) µM	
-50 mV	**16.6** 5.24 to 52.6
-75 mV	**4.42** 1.1 to 17.8
-100 mV	**4.78** 1.16 to 19.7

Figure 38: Bn-Cha-PhTX-343 block of NMDA/glycine responses in GluN1-1a/GluN2A-containing NMDA receptors.

(A) TEVC recordings for Bn-Cha-PhTX-343 (0.001–10 µM) block at three holding potentials, -50, -75 and -100 mV, (B) Concentration-inhibition curves for Bn-Cha-PhTX-343. Percentage control response (mean ± SEM, n=6) values were plotted and fitted with the Hill equation, (C) IC_{50} (95% CI) values for Bn-Cha-PhTX-343 generated via the concentration-inhibition curves. No significant differences were observed across all voltages.

3.3.7 CR18

CR18 was the most potent MTDL compound (results presented in chapter 3.3) and therefore was characterized with wild type and mutated NMDAR subunits. Inhibition of NMDA/glycine responses by increasing concentrations of CR18 (0.01 to 100 µM) mediated by GluN1-1a/GluN2A were measured to determine its IC_{50} value at three holding potentials. The IC_{50}s obtained were 12.4 (95% CI 6.44 to 24.0), 2.04 (95% CI 0.56 to 7.43) and 0.62 (95% CI 0.12 to 3.35) µM at -50, -75 and -100 mV respectively. IC_{50}s of CR18 increased as holding potentials were also increased suggesting a voltage-dependent block. Significant differences were observed between IC_{50s} at -50 mV compared to both at -75 mV (p=0.0183) and at -100 mV (p=0.0031). The results are presented in figure 39.



C.

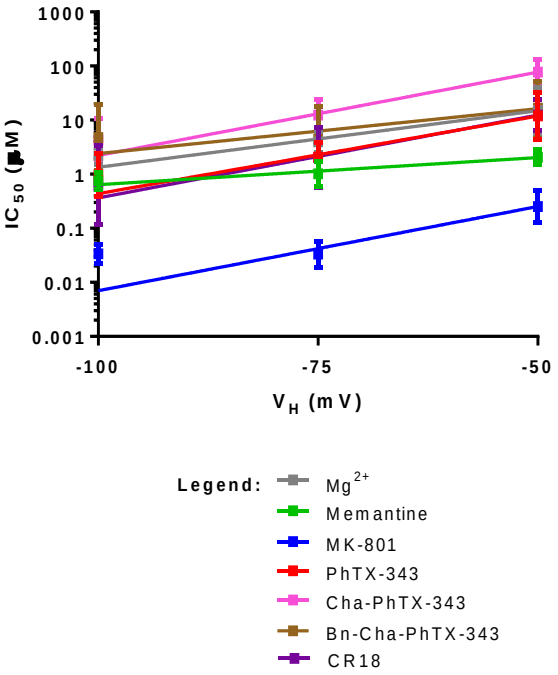
CR18 IC_{50} (95% CI) µM	
-50 mV	**12.4** 6.44 to 24.0
-75 mV	**2.04** 0.56 to 7.43
-100 mV	**0.62** 0.11 to 3.35

Figure 39: CR18 block of NMDA/glycine responses in GluN1-1a/GluN2A-containing NMDA receptors.
(A) TEVC recordings for CR18 (0.01–100 µM) block at three holding potentials, -50, -75 and -100 mV, (B) Concentration-inhibition curves for CR18 block. Percentage control response (mean ± SEM, n=3-4) values were plotted and fitted with the Hill equation, (C) IC_{50} (95% CI) values for CR18 generated via the concentration-inhibition curves. Significant differences were observed between IC_{50s} at -50 mV compared to both at -75 mV (p=0.0183) and at -100 mV (p=0.0031).

3.3.8 δ Value

IC_{50} values for each compound at all holding potentials were fitted to the Woodhull model to obtain the δ value which is useful to predict binding sites of the channel blockers. All of the compounds (except MK-801 and Bn-Cha-PhTX-343) yielded very similar δ values which may suggest that they bind at the same binding site or close to each other. The δ values obtained from the voltage-dependence curves were 0.62, 0.59, 0.56, 0.61 and 0.60 for Mg^{2+}, memantine, philanthotoxin-343, Cha-PhTX-343 and CR18 respectively. MK-801 had the highest δ value with 1.84 which may suggest a deeper binding block for the compound while Bn-Cha-PhTX-343 had the lowest (0.33) suggesting a shallower binding site. The voltage-dependent curves and δ values are presented in figure 40.

A.



B.

Compounds	δ (95% CI)
Mg^{2+}	**0.62** -0.67 to 1.9
Memantine	**0.59** -0.95 to 2.13
MK-801	**1.84** -6.53 to 10.21
PhTX-343	**0.56** -0.47 to 1.6
Cha-PhTX-343	**0.61** -0.05 to 1.26
Bn-Cha-PhTX-343	**0.33** -1.46 to 2.11
CR18	**0.60** 0.07 – 1.13

Figure 40: Voltage-dependence of inhibition for all compounds mediated by GluN1-1a/GluN2A-containing NMDA receptors.

(A) Voltage-dependence curves, IC_{50} (95% CI) μM for all compounds fitted with the Woodhull equation, (B) δ values for all compounds obtained from the voltage-dependence curves.

3.4 DISCUSSION

In the first part of this study, characterization of NMDA receptors using well-established agonists and antagonists as well as several new compounds were conducted electrophysiologically in *Xenopus laevis* oocytes expressing GluN1-1a/GluN2A NMDAR subunits. GluN1-1a was chosen as it is the most predominant GluN1 isoform in the brain (Bresink et al., 1996) while GluN2A is the most abundantly expressed GluN2 subunit (along with GluN2B) in adult forebrain (Wyllie et al., 2013).

3.4.1 NMDA Receptor Agonism

The present study showed that NMDA or glycine alone does not evoke any (or very minute) response on NMDAR expressed in *Xenopus* oocytes. When the two compounds were co-applied together, as expected the receptors elicited inward currents. It is widely established that glycine is fundamentally required as a co-agonist for the induction of NMDA receptors in oocytes either by NMDA or glutamate. This corresponds with an early voltage-clamp analysis on RNA-injected oocytes by Kleckner and Dingledine (1988) whereby no response was elicited when NMDA was applied without glycine. A large inward current was evoked when NMDA was then co-applied with glycine. In a study on Ca^{2+} entry into locust muscle, it was demonstrated that glycine enhanced the response of glutamate and NMDA but not that of quisqualate (Khan, 1994). Other amino acids can, however, replace glycine as the co-agonist for glutamate or NMDA, with D-serine and D-alanine being the most potent (Kleckner and Dingledine, 1988).

The EC_{50}s for NMDA obtained from this study were 53.6 µM for the peak response and 11.7 µM at the steady-state level. These values were comparable with previous studies which obtained EC_{50} of NMDA mediated by GluN1/GluN2A NMDAR ranging between 1 to 100 µM; 8.42 µM by McClymont (2010), 57 µM by Ishii et al. (1993) and 75 µM by Risgaard et al. (2010). As for glycine, the EC_{50}s obtained were 3.52 µM for the peak response and 0.69 µM for the steady-state level. Previous studies have demonstrated similar findings, e.g. an EC_{50} value of 0.67 µM was obtained by Kleckner

and Dingledine (1988), 1.27 µM by McClymont (2010) and 1.31 µM by Chen et al. (2008).

Based on these EC_{50} values, a concentration of 100 µM NMDA co-applied with 10 µM glycine was used in subsequent antagonist assays. These concentrations were considered optimal and sufficient to saturate all NMDA receptor assemblies (Li, 1999). Previous studies have exhibited reduced responses when the glycine concentration used was higher than this but the same was not reported with NMDA (de Carvalho et al., 1996; Mirshahi and Woodward, 1995).

3.4.2 NMDA Receptor Antagonism

3.4.2.1 Mg^{2+}

NMDAR block by Mg^{2+} is an important characteristic of the receptor to regulate Ca^{2+} permeability. Mg^{2+} block reduces Ca^{2+} influx at resting potential but dissociates from the receptor during depolarization (Dingledine et al., 1999). The findings that Mg^{2+} selectively antagonizes responses to NMDA but not other iGluR agonists like kainate or quisqualate was discovered more than 30 years ago (Davies and Watkins, 1977; Evans et al., 1977). The critical site by which Mg^{2+} blocks the NMDAR is at the N (of the Q/R/N site) in GluN1 and GluN2 and +1 (GluN2) sites within the pore of the M2 region (Burnashev et al., 1992; Sakurada et al., 1993; Wollmuth et al., 1998a; b).

IC_{50}s for Mg^{2+} block of NMDA/glycine responses in GluN1-1a/GluN2A obtained from this study were 15.0 µM (-50 mV), 3.98 µM (-75 mV) and 2.19 µM (-100 mV). These findings were consistent with previous studies employing GluN1/GluN2A NMDAR with slight variations depending on the membrane potential tested and the concentration of agonists used. For example, Kuner and Schoepfer (1996) reported an IC_{50} value of approximately 20 µM tested at -60 to -70 mV, Qian et al. (2005) obtained an IC_{50} of 11.8 µM at -85 mV, Gilling et al. (2009) reported an IC_{50} of 19.5 µM tested at -70 mV, while McClymont et al. (2012) obtained IC_{50} values of 16.0, 4.23 and 1.74 µM recorded at -50, -75 and -100 mV respectively. Liu et al. (2001) reported

IC_{50}s of 15.0 µM when Mg^{2+} was applied with 500 µM NMDA and 100 µM glycine, 7.6 µM with 10 µM NMDA and 100 µM glycine and 8.8 µM with 500 µM NMDA and 3 µM glycine, all tested at -80 mV.

Early studies showed that the activation by excitatory amino acids of NMDARs is highly sensitive to the membrane potential and it has been suggested that the NMDAR is coupled to a voltage-sensitive conductance (Mayer et al., 1984). Voltage-dependent ion channels conduct ions at high rates and regulated by the voltage across the membrane (Bezanilla, 2005). This study demonstrated that Mg^{2+} block increased as the holding potentials were more negative. Significant differences were observed between IC_{50}s across all voltages which clearly suggest that Mg^{2+} block followed a voltage-dependent manner. Patch-clamp experiments have also exhibited voltage-dependent block of current flow through ion channels by Mg^{2+} activated by L-glutamate (Mayer et al., 1984). The block of Mg^{2+} in a voltage-dependent manner is said to be paramount for changing synaptic efficacy involved in the glutamate-mediated neuronal plasticity (Collingridge and Bliss, 1987). The δ value obtained via the voltage-dependent curve fitted with the Woodhull model confirmed that the Mg^{2+} binding site is located approximately 0.62 through the electric field from the extracellular surface. This value was similar to that reported by Zhua and Auerbacha (2001) - 0.6 and McClymont (2010) - 0.65, where the location corresponds with the proposed location of the Q/R/N site.

3.4.2.2 Memantine

Antagonism of NMDAR channels by memantine occurs in a use-dependent manner where it can only bind in the channel pore in the presence of agonist. Clinical findings have shown that memantine is well-tolerated and largely credited to its moderate affinity, fast blocking and dissociation rate and strong voltage dependency (Rammes et al., 2008). Several of these characteristics were assessed in this study using two-electrode voltage-clamp electrophysiology. The present data demonstrated that the block of NMDA/glycine responses by memantine in GluN1-1a/GluN2A expressed in *Xenopus* oocytes displayed a similar inhibition trend to Mg^{2+} albeit with much more

potency. This is expected due to their overlapping binding site in the M2 region of the NMDAR channel pore. This was evident by the kinetics of unblock in the presence of both (Chen et al., 1992; Sobolevsky et al., 1998).

IC_{50}s for memantine obtained in this study were 2.07, 1.01 and 0.75 µM recorded at -50, -75 and -100 mV respectively. The values obtained in this research were well within the range reported by previous studies. In patch-clamp experiments using HEK-293 cells, Bresink et al. (1996) recorded a memantine IC_{50} of 0.93 µM on L-glutamate-evoked responses in GluN1/GluN2A NMDAR at -70 mV while Kotermanski et al. (2009) reported an IC_{50} of 1.25 µM at -66 mV. Gilling et al. (2009) and Parsons and Gilling (2007) obtained IC_{50}s of 0.79 and 1.87 µM respectively both recorded at -70 mV also using HEK-293 cells. Studies employing *Xenopus* oocytes expressing GluN1/GluN2A NMDAR reported IC_{50}s in the micromolar range. For instance, McClymont et al. (2012) reported IC_{50}s of 3.94, 2.48 and 0.80 µM at -50, -75 and -100 mV respectively while Ferrer-Montiel et al. (1998) reported an IC_{50} of 0.3 µM at -80 mV. Wrighton et al. (2008) obtained memantine IC_{50}s of 3.2, 1.7 and 0.86 µM recorded at -40, -60 and -80 mV respectively in GluN1/GluN2A NMDAR induced by glutamate while Dravid et al. (2007) recorded IC_{50}s of 4.36 and 2.25 µM at pH 7.6 and 6.9 respectively . This range of memantine concentration is at a therapeutically relevant level used in the treatment of AD (Gilling et al., 2009).

This study confirmed that memantine blocks NMDA/glycine responses in a voltage-dependent manner with the δ value of 0.59. The δ value describes the fraction of the transmembrane field the drug experiences when blocking the NMDA receptor channel. Close or similar δ values were reported by previous studies which showed strong voltage-dependent inhibition by memantine; i.e. 0.9 (Gilling et al., 2009), 0.83 (Parsons and Gilling, 2007), 0.8 (Parsons et al., 1995) and 0.77 (Ferrer-Montiel et al., 1998). More importantly, the δ value obtained in this study corresponds with the structural predictions of the Q/R/N and +1 binding sites. It confirmed that the binding site of memantine overlaps or close to that of Mg^{2+} (Cull-Candy, 2007), as the value obtained for both compounds were nearly identical.

Within memantine's therapeutic window, its fast kinetic property to block and unblock NMDAR, which contrasts to high-affinity channel blockers such as MK-801 and phencyclidine (PCP), allows suppression of excitotoxicity whilst maintaining physiological transmission of the receptor (Kornhuber and Quack, 1995). The fast kinetic property also reduces memantine's proneness to be trapped inside the NMDAR compared to MK-801 and PCP (Gilling et al., 2009).

3.4.2.3 MK-801

MK-801 is a selective, un-competitive NMDAR inhibitor which blocks NMDA/glycine responses in a use-dependent manner. The magnitude of block by MK-801 is greatly enhanced as agonist concentration is increased (Foster and Wong, 1987). Huettner and Bean (1988) early on concluded that MK-801 cannot block or unblock the channel unless it has been opened by the agonist and that the drug binds within the channel pore itself.

This study evaluated concentration-inhibition and voltage-dependency of MK-801 in GluN1-1a/GluN2A NMDA receptors using two-electrode voltage clamp. The IC_{50}s for MK-801 block of NMDA/glycine responses obtained in this study were 34 nM (-100 mV), 33 nM (-75 mV) and 254 nM (-50 mV). Other studies have also shown that MK-801 is a potent NMDAR inhibitor with IC_{50}s in the nanomolar range. Mediated by GluN1/GluN2A NMDAR subunits, Frankiewicz et al. (1996) obtained an IC_{50} of 140 nM tested at -70 mV, McClymont et al. (2012) reported IC_{50}s of 190, 210 and 500 nM recorded at -100, -75 and -50 mV respectively, while at -40 mV, Dravid et al. (2007) reported IC_{50}s of 15 and 6 nM at pH7.6 and 6.9 respectively.

Huettner and Bean (1988) suggested that the binding sites for MK-801 and Mg^{2+} are close to one another (or overlapped) due to the ability of Mg^{2+} to inhibit MK-801 block of the NMDAR channel in a voltage-dependent manner. It was, however, reported that block of L-glutamate induced-responses by MK-801 in GluN1/GluN2A was less voltage-dependent compared to memantine (Bresink et al., 1996). The

present study supported this finding where IC_{50}s at -75 and -100 mV were identical. A significant difference was only observed when IC_{50}s at those two holding potentials were compared to that recorded at -50 mV.

The high potency of MK-801 coupled with its slow dissociation from the NMDAR channel and less pronounced functional voltage-dependency leads to the trapping of the compound in the channel pore. As a result, the compound is unable to leave the channel within the normal excitatory synaptic potential time course, thus not only blocking pathological activation, but also physiological function of NMDA receptors (Rammes et al., 2008) making it unsuitable for clinical use.

Due to the potency and neuroprotective effect of MK-801, analogues of the drug have been developed to attenuate or abolish its unwanted psychomimetic effects. Bachurin and colleagues synthesized three series of novel compounds; monobenzylamino, benzhydrylamino, and dibenzylamino (DBA) analogues of MK-801 with the latter being a potent NMDAR and Ca^{2+} uptake blocker without producing psychomimetic effects within the therapeutic dose interval. The study also elucidated the pivotal role of the hydrogen bond formed between these analogues and amino acid N at the Mg^{2+} binding site within the NMDAR channel pore. It was suggested that the irreversibility of MK-801 binding to NMDAR compared to Mg^{2+} and DBA compounds was due to the strong hydrophobic interaction between MK-801 and the hydrophobic pocket in the NMDAR channel complex contributing to the PCP-like side effects (Bachurin et al., 2001).

3.4.2.4 Philanthotoxin Analogues

In the present study, PhTX-343 alongside two novel analogues were tested on GluN1-1a/GluN2A NMDA receptors. The analogues were modified by introducing cyclohexylalanine and benzene into the compound. The extra headgroups were expected to enhance potency of the compounds by increasing hydrophobicity and size. The modification would allow stronger interactions in the hydrophobic vicinity

of the NMDAR pore due to a larger headgroup. Proposed interaction of PhTX-343 and its analogues with AMPA and NMDA receptors are displayed in figure 41.

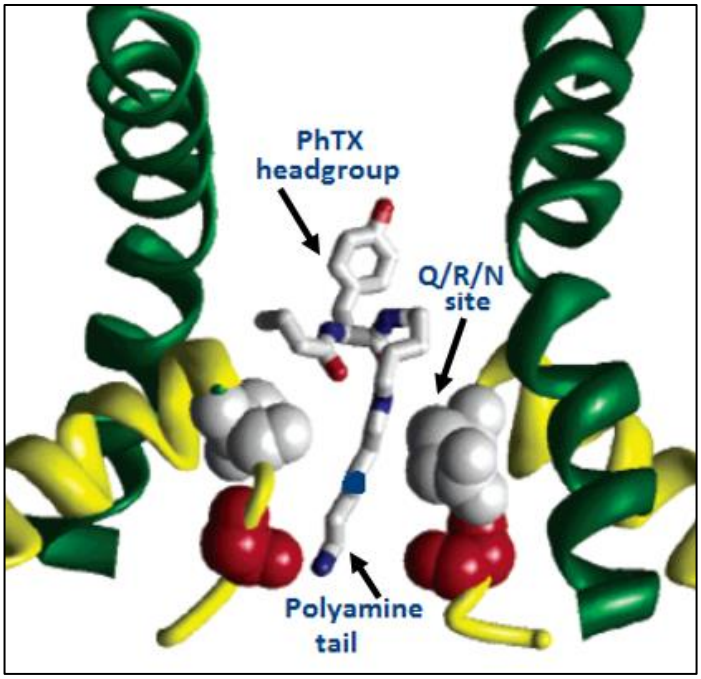


Figure 41: A model of philanthotoxin docking in the GluA1 receptor channel.
The M2 helices are represented by the yellow ribbons, the green ribbons represent M3. The Q/R/N site is also indicated. Adapted from (Andersen et al., 2006).

The philanthotoxin analogues will most likely interact with the NMDAR pore similar to PhTX-343 and other polyamine toxins. The distal aromatic headgroup interacts in the hydrophobic vestibule above the Q/R/N site located just above the narrowest region of the channel pore while the linear polyamine tail will penetrate beyond the Q/R/N site and bind deep in the pore (Bähring and Mayer, 1998). It was previously reported that the narrowest portion within the NMDAR channel pore is only 0.55 nm wide thus making the compound unlikely to permeate through the channel (Villarroel et al., 1995).

IC_{50}s for PhTX-343 block of NMDA/glycine responses in GluN1-1a/GluN2A NMDA receptor recorded in the present study were 11.9 µM (-50 mV), 2.08 µM (-75 mV) and 0.97 (-100 mV). These results are comparable with previous studies; Brackley et al. (1993) reported PhTX-343 IC_{50} of 2.5 µM tested on cells clamped at -80 mV, Mellor et al. (2003) reported IC_{50}s of 13.2, 2.01 and 0.98 µM recorded at -60, -80 and -100

mV respectively, while McClymont et al. (2012) obtained PhTX-343 IC_{50}s of 17.2 µM (-50 mV), 2.95 µM (-75 mV) and 0.30 µM (-100 mV).

This study, however, does not show that the new analogues, Cha-PhTX-343 and Bn-Cha-PhTX-343 are more potent than PhTX-343 in blocking NMDA/glycine responses in GluN1-1a/GluN2A subunits. IC_{50}s for Cha-PhTX-343 were 77.1 µM (-50 mV), 12.4 µM (-75 mV) and 4.17 µM (-100 mV) while Bn-Cha-PhTX-343 generated IC_{50}s of 16.7 µM (-50 mV), 4.42 µM (-75 mV) and 4.78 µM (-100 mV). Blocking potency for Bn-Cha-PhTX-343, an analogue containing a benzyl and cyclohexylalanine moiety, was comparable with PhTX-343 as no significant differences were observed between IC_{50}s of both compounds at all voltages tested. Cha-PhTX-343 was less potent where IC_{50}s at all voltages were higher to that of PhTX-343; significant differences were observed at -50 and -75 mV.

The δ values for the three compounds obtained in the present study were 0.56 (PhTX-343), 0.61 (Cha-PhTX-343) and 0.33 (Bz-Cha-PhTX-343). This study showed that PhTX-343 and both novel analogues demonstrated strong voltage-dependence of inhibition. This is consistent with other findings by McClymont et al. (2012) and Mellor et al. (2003) suggesting the compounds bind deep inside the channel pore. The headgroup of Cha-PhTX-343 is predicted to bind near the Q/R/N site similar to PhTX-343, as well as Mg^{2+} and memantine based on their identical δ values (0.62 for Mg^{2+} and 0.59 for memantine). Bn-Cha-PhTX-343 may have the shallowest binding site due to its larger headgroup size resulting in less penetration of the molecule inside the NMDAR channel pore.

3.4.2.5 CR18

Out of all the multi-target-directed ligands tested in this thesis project, CR18 was found to be the most potent NMDAR antagonist (further discussed in Chapter 5). CR18 was synthesized by incorporating an α-tocopherol moiety into a polyamine spermine backbone. This compound was developed to simultaneously block NMDAR-induced excitotoxicity and suppress oxidative stress occurring in Alzheimer's disease.

IC_{50}s for CR18 block of NMDA/glycine responses mediated by GluN1-1a and GluN2A subunits obtained in this study were 12.42 µM (-50 mV), 2.041 µM (-75 mV) and 0.622 µM (-100 mV). At -75 and -100 mV, IC_{50}s for CR18 were comparable to that of memantine ($p>0.05$) indicating their high potency to block NMDA/glycine responses. Only at -50 mV was the IC_{50} significantly higher than memantine. This is, however, possibly due to the limited availability of the compound, where only three sets of recordings were conducted at -50 mV. Increasing the number of replicates might provide a more reliable IC_{50} value as the confidence interval was quite large. CR18 was also found to act in a voltage-dependent manner. Characterization of CR18 is further discussed in Chapter 5, Multi-Target-Directed Ligands study.

CHAPTER 4

PORE REGION (M2) MUTATION STUDY

4.1 SUMMARY

The initial aim of this chapter was to investigate the effects of the Q/R/N, +1 and -8 sites in the M2 region of GluN3 subunits on channel block of NMDARs when compared to GluN1-1a/GluN2A alone. It was hypothesized that the variations at these sites in GluN3 contributed to the reason as to why when these subunits are incorporated into the GluN1-1a/GluN2A, channel properties of NMDARs were altered. The project was also set out to determine whether R at the Q/R/N site in human GluN3B provides a higher level of resistance to channel block and Ca^{2+} permeability than its rat counterpart. Unfortunately, this study could not find evidence of GluN3 expression. A change of strategy was employed to introduce mutations in the GluN2A subunit to resemble GluN3 at three residues – the N, N+1 and N-8 sites in the M2 region. The double mutations N614G/N615R and N614R/N615R did result in significant changes in potency of the blockers, with the latter (RR mutation) resulted in greater reduction of channel block compared to the former (GR mutation). The point mutation W606N, had no significant effects on the blocking properties of the channel blockers studied.

4.2 GLUN3 SITE-DIRECTED MUTAGENESIS

Site-directed mutagenesis was employed to study the impact of the Q/R/N, +1 and -8 sites in the M2 region of GluN3 subunits on channel block. A previous study reported that there is a reduction in blocking potency by GluN3A inclusion in an NMDAR which can be reversed by mutations of either G729 (Q/R/N site) or R730 (+1 site) to N but that this reversal is frequently incomplete (McClymont et al., 2012). Thus, the first part of this section attempted to analyse the combined impact of the

G and R residues at these sites by constructing a double mutation in GluN3 subunits; G729N/R730N in GluN3A and G629N/R630N in GluN3B. Their susceptibility to block by Mg^{2+} and other channel blockers were then be observed to see if this is restored to, or close to, that seen in GluN3-lacking NMDARs. The -8 position (N721 in GluN3A, N621 in GluN3B) were also investigated by mutating N to W as found in all other NMDAR subunits.

First, to determine the effectiveness of the Site-Directed QuickChange II XL kit to produce mutations in NMDAR subunits, control experiments were conducted alongside the mutation samples. pWhitescript 4.5-kb control plasmid (Agilent Technologies) provided in the mutagenesis kit was used to demonstrate the mutation efficiency of plasmids. The control plasmid contains a stop codon (TAA) at the site where a glutamine codon (CAA) would normally exist in the β-galactosidase gene of the pBluescript II SK(-) phagemid. XL-10 Gold ultracompetant cells transformed with this control plasmid would appear white on LB-ampicillin agar plates containing isopropyl β-D-1-thiogalactopyranoside (IPTG) and 5-bromo-4-chloro-3-indolyl-β-D-galactopyranoside (X-gal) because β-galactosidase activity has been suppressed. The oligonucleotide control primers created a point mutation that reverted the T base of the stop codon (TAA) in the β-galactosidase gene encoded on the pWhitescript 4.5kb control template to a C base to produce a glutamine codon (CAA). Following transformation, colonies appeared as blue colony phenotype suggesting the production of β-galactosidase (β-gal+) confirming the success of the mutagenesis experiment (figure 42B).

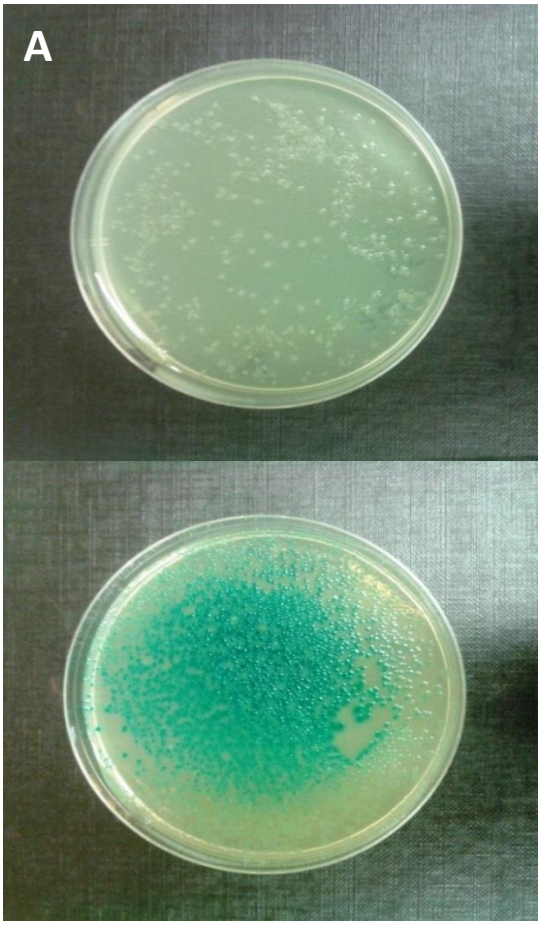


Figure 42: Site-Directed QuickChange II XL Mutagenesis control and sample plates.
(A) Sample mutagenesis plate, (B) Mutagenesis control plate.

PCR products which were successfully generated via the site-directed mutagenesis protocol were then Sanger sequenced to confirm that the mutations were correct. The resulting Sanger sequencing chromatographs are displayed in figure 43 (GluN3A mutations) and 44 (GluN3B mutations).

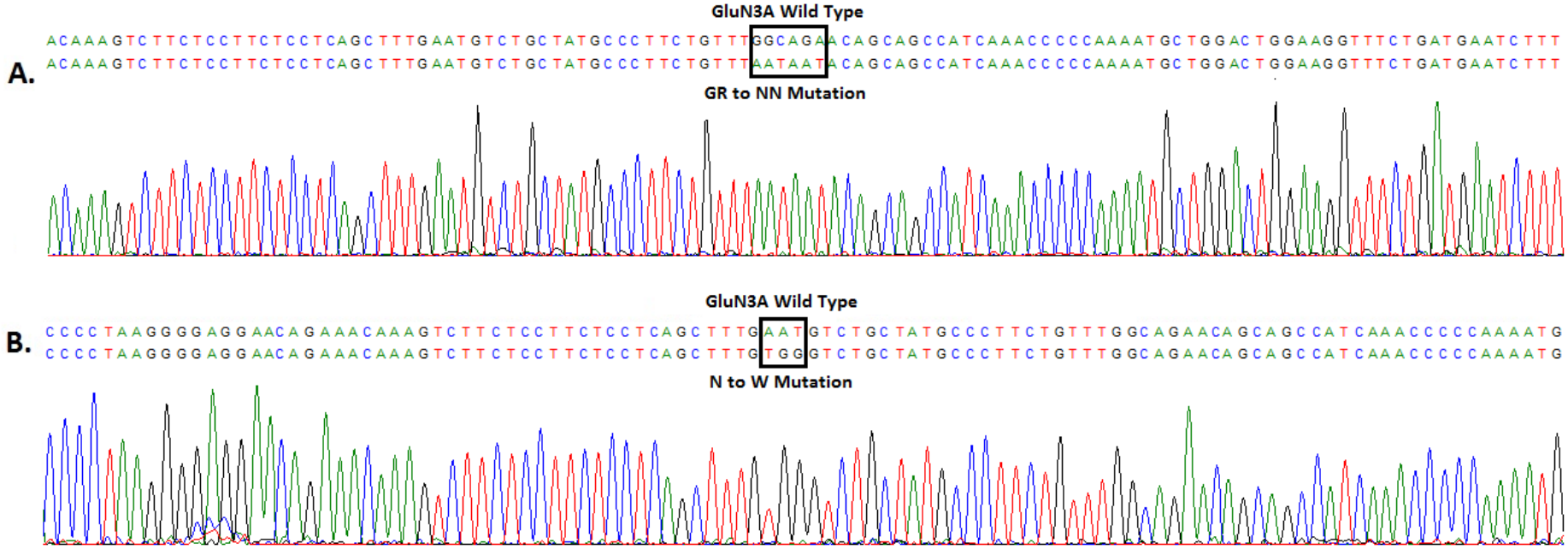


Figure 43: Chromatograms of nucleotide sequence from the site-directed mutagenesis PCR products showing the mutations generated in GluN3A subunits. (A) GluN3A$_{(G729N/R730N)}$ mutation; GR [GGCAGA] at the Q/R/N and +1 positions in GluN3A wild type was double-mutated to NN [AATAAT] to resemble the GluN2A subunit. (B) GluN3A$_{(N721W)}$ mutation; N [AAT] at -8 position with regards to the Q/R/N site in GluN3A wild type was mutated to W [TGG] as found in GluN1-1a and GluN2A subunits.

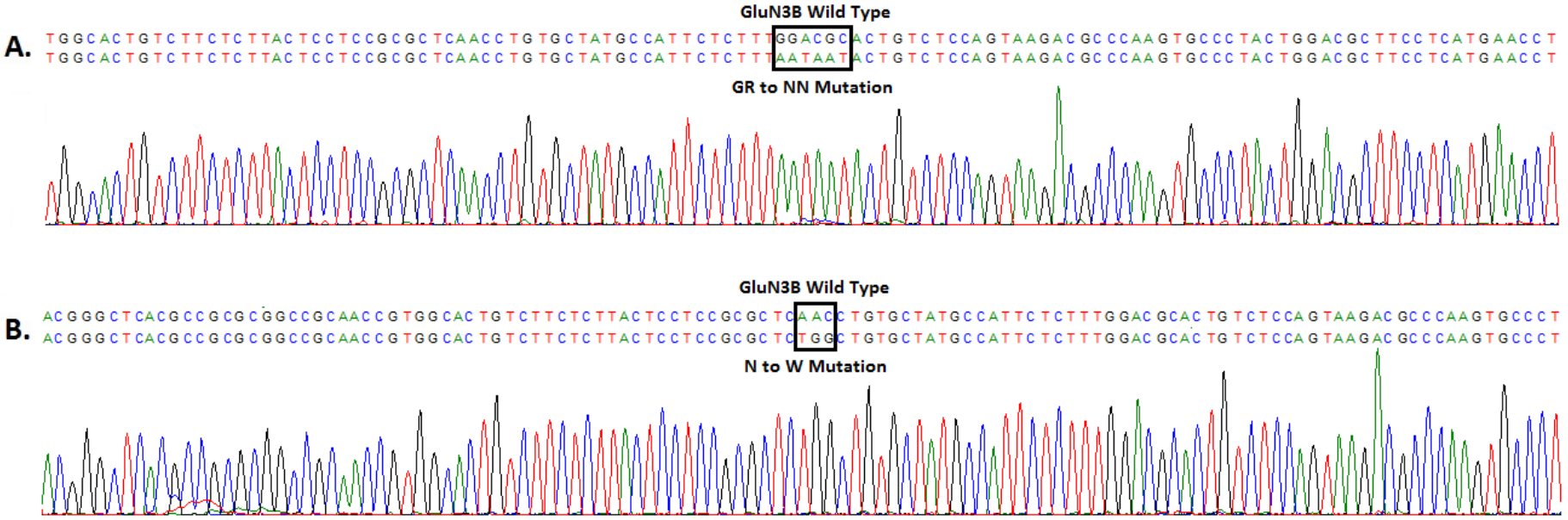


Figure 44: Chromatograms of nucleotide sequence from the site-directed mutagenesis PCR products showing the mutations generated in GluN3B subunits. (A) GluN3B$_{(G629N/R630N)}$ mutation; GR [GGACGC] at the Q/R/N and +1 positions in GluN3B wild type was double-mutated to NN [AATAAT] to resemble GluN2A subunit. (B) GluN3B$_{(N621W)}$ mutation; N [AAC] at -8 position with regards to the Q/R/N site in GluN3B wild type was mutated to W [TGG] as found in GluN1-1a and GluN2A subunits.

4.2.1 Validation of GluN3 Expression by Glycine Sensitivity Testing

Before GluN3 mutations were co-expressed with GluN1-1a/2A and tested electrophysiologically with open channel blockers, it was important that the wild type GluN3A and GluN3B subunits were tested for expression in oocytes for comparisons to be made. Expression of GluN3 subunits were validated by glycine sensitivity testing based on prior information that GluN3 provides stronger affinity to glycine compared to GluN1 subunits (McClymont, 2010; McClymont et al., 2012; Nilsson et al., 2007). Therefore, the existence of GluN3 when co-expressed with GluN1-1a/2A subunits would be expected to evoke smaller inward currents but more sensitive to glycine thus generating lower EC_{50} compared to GluN1-1a/2A when tested with NMDA and glycine. The findings of this study however revealed similar patterns of responses towards tenfold increment of glycine concentrations (0.1 to 100 µM co-applied with 100 µM NMDA) with all combination of NMDAR subunits tested as shown by trace recordings in figure 45.

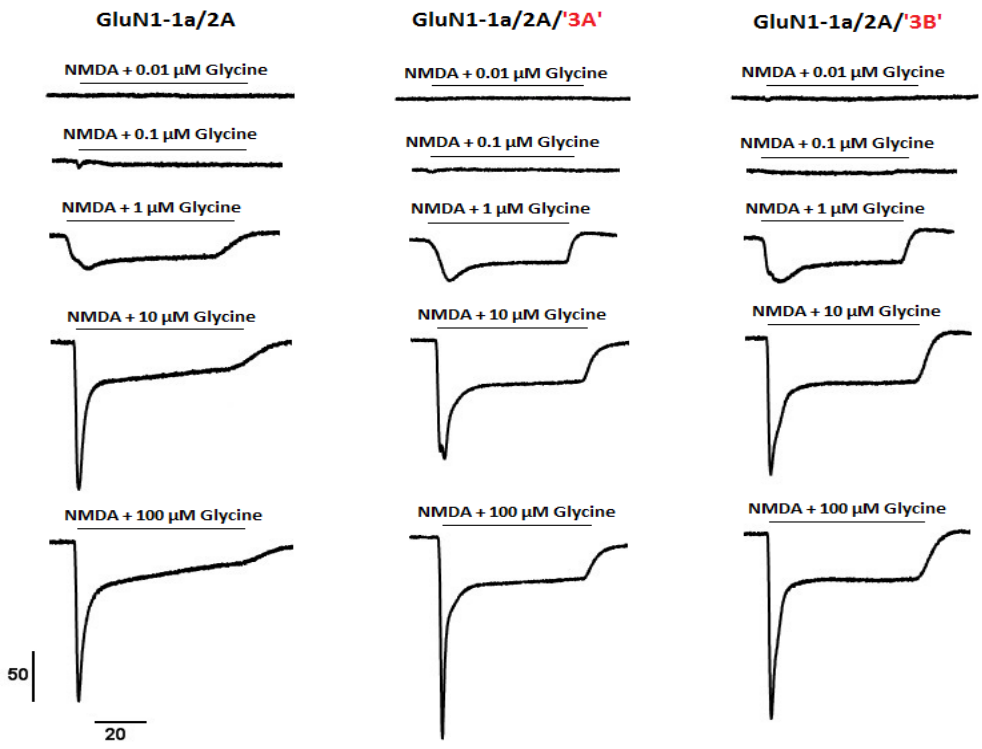
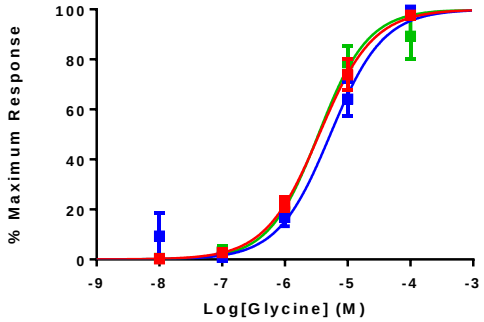
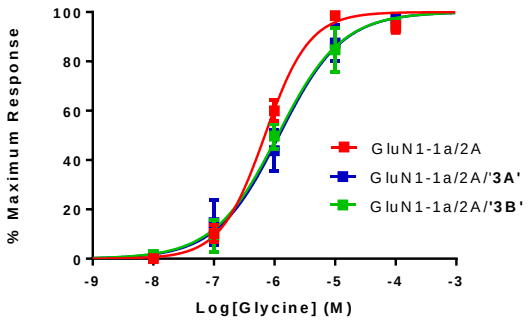


Figure 45: TEVC recordings of 100 µM NMDA-evoked currents co-applied with tenfold increasing concentration of glycine (0.1–100 µM) tested at -75 mV on GluN1-1a/2A, GluN1-1a/2A/'3A' and GluN1-1a/2A/'3B'.

Percentage control response (mean ± SEM, n=10-14) values obtained from the traces were plotted and fitted with the Hill equation to generate concentration-response curves. EC_{50}s (95% CI) generated from the curves did not reveal any significant differences (p>0.05) between all combination of subunits tested which suggested that both GluN3 subunits were not expressed (figure 46).

A.





B.

NMDAR Subunit Combination	Peak Response EC_{50} (µM, 95% CI)
GluN1-1a/2A	**0.69** 0.58 to 0.84
GluN1-1a /2A/'3A'	**1.2** 0.73 to 1.98
GluN1-1a /2A/'3B'	**1.12** 0.71 to 1.77

NMDAR Subunit Combination	Steady-State EC_{50} (µM, 95% CI)
GluN1-1a /2A	**3.52** 2.78 to 4.46
GluN1-1a /2A/'3A'	**5.3** 3.65 to 7.7
GluN1-1a /2A/'3B'	**3.43** 2.27 to 5.18

Figure 46: Concentration-response relationship for glycine co-applied with NMDA tested against GluN1-1a/2A, GluN1-1a/2A/'3A' and GluN1-1a/2A/'3B'.
(A) Percentage control response (mean ± SEM, n=10-14) plotted and fitted with the Hill equation, (B) EC_{50} (95% CI) values for glycine at peak and steady-state level. No significant differences were observed between all subunit combinations.

4.3 GLUN2A SITE-DIRECTED MUTAGENESIS

Due to the uncertainty of expressing and incorporating GluN3 subunits into functional NMDARs, a different strategy was implemented to study the Q/R/N and adjacent sites. Instead of mutating GluN3, the GluN2A subunit was instead reverse mutated to resemble the former. Mutated GluN2A subunits were then co-expressed with GluN1-1a and assessed whether blocking potency of antagonists were suppressed when compared to wild type. NN at the Q/R/N and +1 sites in GluN2A were double-mutated to GR (N614**G**/N615**R**) to resemble rat GluN3A and GluN3B. The same sites were also mutated to RR (N614**R**/N615**R**) to resemble human GluN3B subunits. Finally, W at the -8 position with regards to the Q/R/N site in GluN2A was mutated to N (W606N) as found in both rat and human GluN3 subunits. PCR products generated via site-directed mutagenesis method were Sanger sequenced to confirm that the mutations were successful. The following figure 47 indicated that the mutations were correct as shown by the Sanger sequencing chromatograms.

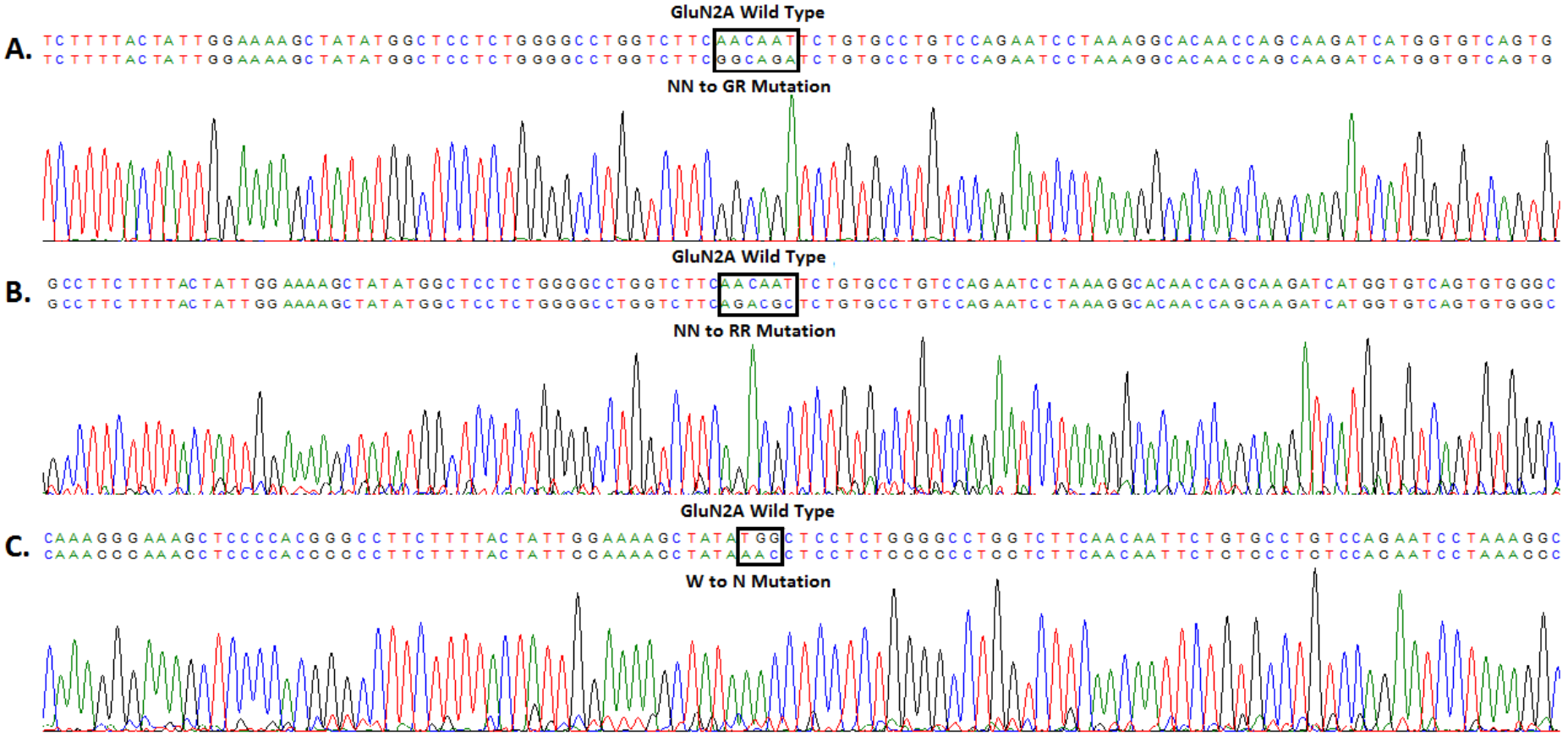


Figure 47: Chromatograms of nucleotide sequence from the site-directed mutagenesis PCR products showing the mutations generated in GluN2A subunits. (A) GluN2A$_{(N614G/N615R)}$ mutation; NN [AACAAT] at 614/615 positions in GluN2A were mutated to GR [GGCAGA] to resemble the Q/R/N and +1 sites in rat GluN3 subunits. (B) GluN2A$_{(N614R/N615R)}$ mutation; NN [AACAAT] at 614/615 positions in GluN2A were mutated to RR [AGACGC] to resemble the Q/R/N and +1 sites in human GluN3B subunits. (C) GluN2A$_{(W606N)}$ mutation; W [TGG] occupying the 606 position in GluN2A was mutated to N [AAC] to resemble the -8 position in relative to the Q/R/N site in both rat and human GluN3 subunits.

4.4 NMDAR ANTAGONISM ON MUTATED GLUN2A

4.4.1 Mg^{2+}

Electrophysiological recordings of NMDA/glycine inhibition by increasing concentrations of Mg^{2+} (0.01 to 100 µM) on NMDAR containing GluN2A mutations were used to determine their IC_{50} values at three holding potentials. The data were then compared to responses on wild type GluN1-1a/2A subunits. At all voltages, block by Mg^{2+} on NMDAR containing the RR mutation in GluN2A ($2A_{N614\mathbf{R}/N615\mathbf{R}}$) resulted in the highest IC_{50}, and were all significantly higher than 1-1a/2A (44-, 27- and 43-fold higher at -50, -75 and -100 respectively) and 1-1A/$2A_{W606N}$. In contrast, GR mutation in GluN2A ($2A_{N614\mathbf{G}/N615\mathbf{R}}$) only resulted in a significant increase at -50 mV compared to wild type (16-fold) and 1-1A/$2A_{W606N}$. GluN$2A_{W606N}$ mutation did not appear to significantly affect NMDA antagonism by Mg^{2+} as no significant differences were observed between inhibition at 1-1a/$2A_{W606N}$ and wild type at all holding potentials. The results are presented in table 14 and figure 48.

Table 14: IC_{50} values for Mg^{2+} on NMDARs containing GluN2A mutations and compared with IC_{50} on wild type GluN1-1a/GluN2A.

	Mg^{2+} IC_{50} (95% CI) µM			
Voltage (mV)	**1-1a/2A**	**1-1a/$2A_{W606N}$**	**1-1a/$2A_{N614G/N615R}$**	**1-1a/$2A_{N614R/N615R}$**
-50	**15.0 (n=6)** 5.64 to 40.0	**22.2 (n=7)** 13.9 to 35.5	**236.8 (n=3)** 42.9 to 1308 * p=0.0019 § p<0.0001	**658.4 (n=6)** 77.6 to 5587 * p=0.0001 § p<0.0001
-75	**3.97 (n=5)** 2.56 to 6.16	**4.39 (n=7)** 2.71 to 7.11	**3.22 (n=5)** 2.24 to 4.64	**108.7 (n=5)** 43.4 to 272 * p<0.0001 § p<0.0001 † p<0.0001
-100	**2.19 (n=5)** 1.51 to 3.18	**2.36 (n=8)** 1.62 to 3.44	**1.42 (n=4)** 0.59 to 3.43	**94.0 (n=4)** 47.8 to 185 * p<0.0001 § p<0.0001 † p<0.0001

* denotes statistical significance against 1-1a/2A
§ denotes statistical significance against 1-1a/$2A_{W606N}$
† denotes statistical significance against 1-1a/$2A_{N614G/N615R}$

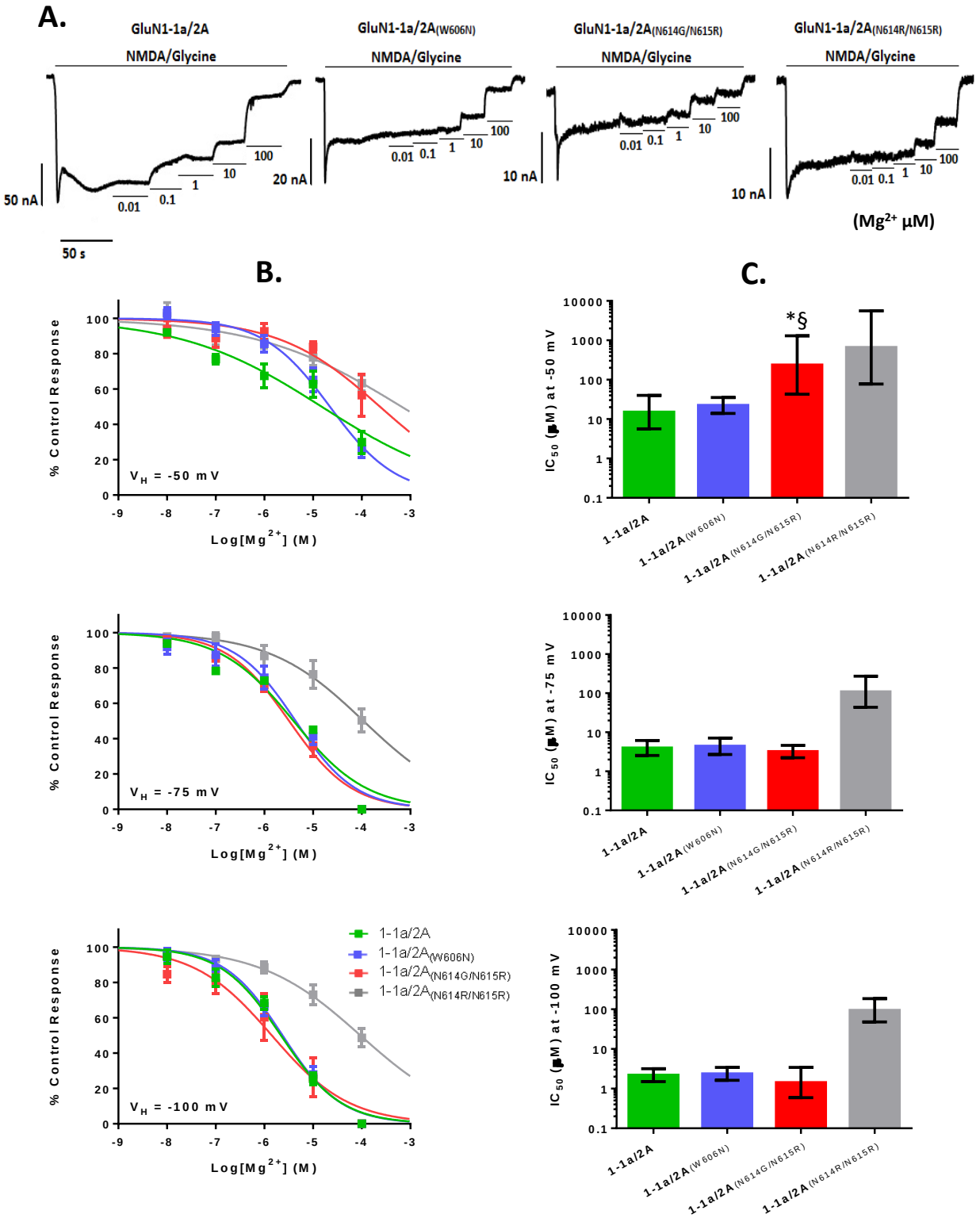


Figure 48: Concentration-inhibition relationship for Mg^{2+} block of NMDA/glycine on NMDARs containing GluN2A mutations compared with block on wild type GluN1-1a/GluN2A subunits.

(A) TEVC recordings of Mg^{2+} (0.01 -100 µM) block at -75 mV, (B) Concentration-inhibition curves for Mg^{2+} block. Percentage control response (mean ± SEM, n=3-8) values plotted and fitted with the Hill equation to estimate IC_{50} values, (C) Bars represent IC_{50} (95% CI) µM. (*) denotes statistical significance against 1-1a/2A, (§) against 1-1a/$2A_{W606N}$ and (†) against 1-1a/$2A_{N614G/N615R}$.

4.4.2 Memantine

GluN2A mutations resulted in an obvious trend of NMDAR inhibition when tested with memantine at all holding potentials. The RR mutation in GluN2A ($2A_{N614\mathbf{R}/N615\mathbf{R}}$) caused the most reduced antagonistic property of memantine resulting in the highest IC_{50} values, followed by 1-1a/$2A_{N614\mathbf{G}/N615\mathbf{R}}$ and 1-1a/$2A_{W606N}$ respectively. Significant increase of IC_{50}s were observed at 1-1a/$2A_{N614\mathbf{R}/N615\mathbf{R}}$ compared to both wild type (126-, 42- and 22-fold at -50, -75 and -100 mV respectively) and 1-1a/$2A_{W606N}$ (also at all voltages). GR mutation in GluN2A also resulted in significant increase of IC_{50}s compared to wild type (96-, 5-, and 9-fold at -50, -75 and -100 mV respectively) and 1-1a/$2A_{W606N}$ although less significant at -75 and -100 mV for the latter mutation. $GluN2A_{W606N}$ reduced inhibition slightly but only yielded a significant difference in IC_{50} (2-fold higher) compared to wild type at -50 mV. In general, these data gave memantine IC_{50} subunit order as 1-1a/2A < 1-1a/$2A_{W606N}$ < 1-1a/$2A_{N614\mathbf{G}/N615\mathbf{R}}$ < 1-1a/$2A_{N614\mathbf{R}/N615\mathbf{R}}$ at all voltages. The results are presented in table 15 and figure 49.

Table 15: IC_{50} values for memantine on NMDARs containing GluN2A mutations and compared with IC_{50} on wild type GluN1-1a/GluN2A.

	Memantine IC_{50} (95% CI) µM			
Voltage (mV)	**1-1a/2A**	**1-1a/$2A_{W606N}$**	**1-1a/$2A_{N614G/N615R}$**	**1-1a/$2A_{N614R/N615R}$**
-50	**2.07 (n=5)** 1.51 to 2.83	**4.09 (n=7)** 2.79 to 5.8 * p=0.0112	**198.8 (n=4)** 11.0 to 3594 * p<0.0001 § p<0.0001	**259.9 (n=4)** 49.6 to 1363 * p<0.0001 § p<0.0001
-75	**1.01 (n=5)** 0.6 to 1.71	**2.13 (n=8)** 1.21 to 3.75	**4.64 (n=4)** 1.53 to 14.1 * p=0.0075	**42.2 (n=5)** 13.2 to 135 * p<0.0001 § p<0.0001 † p=0.0101
-100	**0.76 (n=5)** 0.52 to 1.09	**1.65 (n=7)** 0.79 to 3.46	**6.51 (n=4)** 1.48 to 28.7 * p=0.0008	**16.2 (n=5)** 4.65 to 56.5 * p<0.0001 § p=0.0013

* denotes statistical significance against 1-1a/2A
§ denotes statistical significance against 1-1a/$2A_{W606N}$
† denotes statistical significance against 1-1a/$2A_{N614G/N615R}$

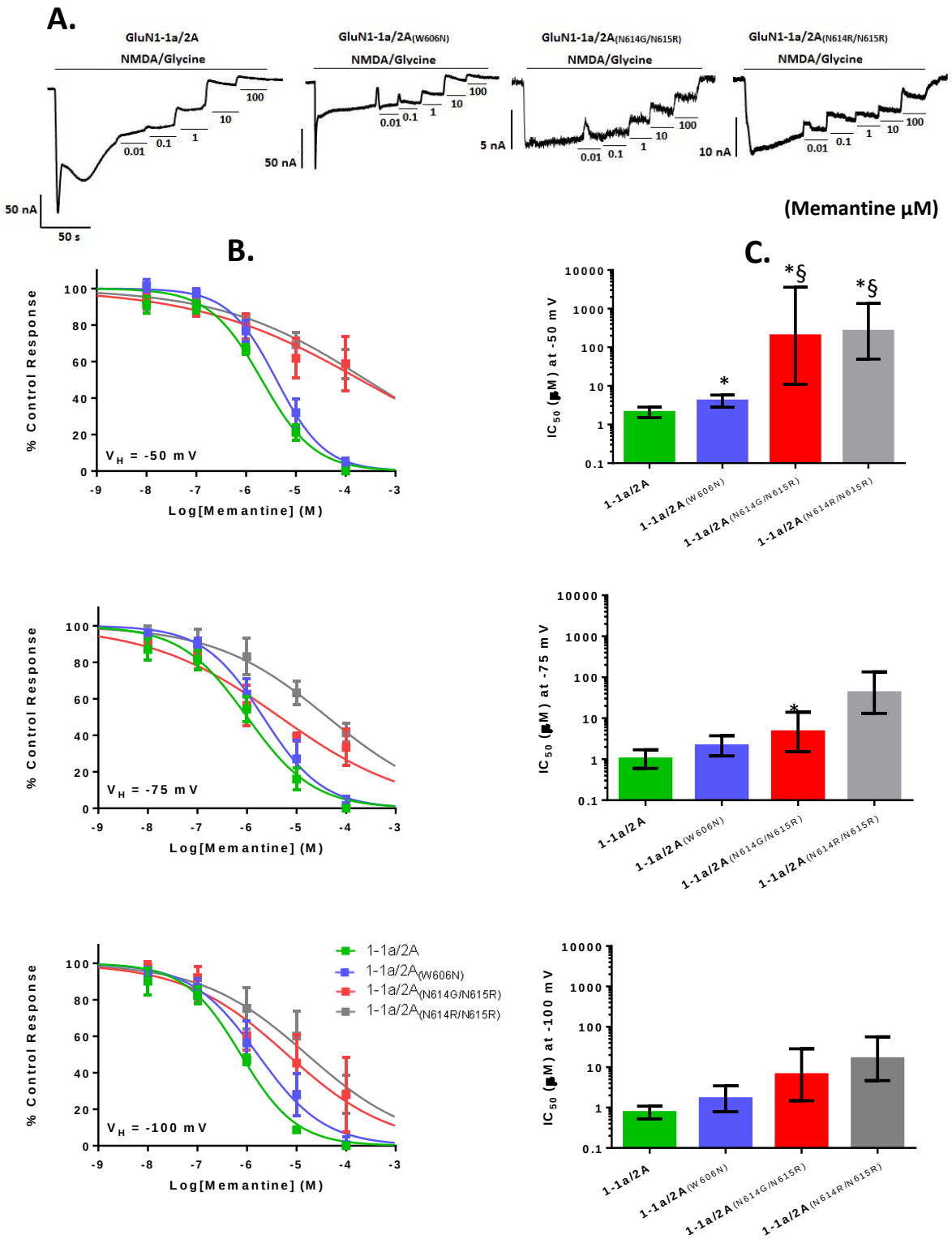


Figure 49: Concentration-inhibition relationship for memantine block of NMDA/glycine on NMDARs containing GluN2A mutations compared with block on wild type GluN1-1a/GluN2A subunits.

(A) TEVC recordings of memantine (0.01-100 µM) block at -75 mV, (B) Concentration-inhibition curves for memantine block. Percentage control response (mean ± SEM, n=4-8) values plotted and fitted with the Hill equation to estimate IC_{50} values, (C) Bars represent IC_{50} (95% CI) µM; (*) denotes statistical significance against 1-1a/2A, (§) against 1-1a/2A$_{W606N}$ and (†) against 1-1a/2A$_{N614G/N615R}$.

4.4.3 MK-801

IC_{50}s for MK-801 were significantly altered when tested in NMDAR containing both double mutations at all holding potentials. IC_{50}s for GluN2A$_{N614R/N615R}$ increased 67-, 325- and 181-fold at -50, -75 and -100 mV respectively, while GluN2A$_{N614G/N615R}$ resulted in increased IC_{50}s of 33-, 132- and 64-fold at -50, -75 and -100 mV respectively compared to wild type. The RR mutation also resulted in even higher IC_{50}s when compared to the GR mutation with a significant difference observed at -50 mV (2-fold difference). The W606N mutation in GluN2A did not appear to alter the IC_{50} of MK-801 as no significant differences were observed at all voltages. The results are presented in table 16 and figure 50.

Table 16: IC_{50} values for MK-801 on NMDARs containing GluN2A mutations and compared with IC_{50} on wild type GluN1-1a/GluN2A.

	MK-801 IC_{50} (95% CI) µM			
Voltage (mV)	**1-1a/2A**	**1-1a/2A$_{W606N}$**	**1-1a/2A$_{N614G/N615R}$**	**1-1a/2A$_{N614R/N615R}$**
-50	**0.25 (n=5)** 0.13 to 0.49	**0.2 (n=4)** 0.02 to 1.71	**8.21 (n=5)** 0.95 to 71.2 * p=0.0005 § p=0.0108	**17.4 (n=2)** $2.48x10^{-6}$ to $1.21x10^{8}$ * p<0.0001 § p<0.05 † p<0.05
-75	**0.033 (n=5)** 0.019 to 0.058	**0.038 (n=5)** 0.022 to 0.066	**4.34 (n=5)** 1.06 to 17.7 * p<0.0001 § p<0.0001	**10.8 (n=5)** 1.03 to 112 * p<0.0001 § p<0.0001
-100	**0.034 (n=5)** 0.022 to 0.051	**0.029 (n=5)** 0.018 to 0.048	**2.17 (n=6)** 0.15 to 30.8 * p=0.0030 § p=0.0029	**6.18 (n=3)** 0.59 to 64.2 * p<0.0001 § p<0.0001

* denotes statistical significance against 1-1a/2A
§ denotes statistical significance against 1-1a/2A$_{W606N}$
† denotes statistical significance against 1-1a/2A$_{N614G/N615R}$

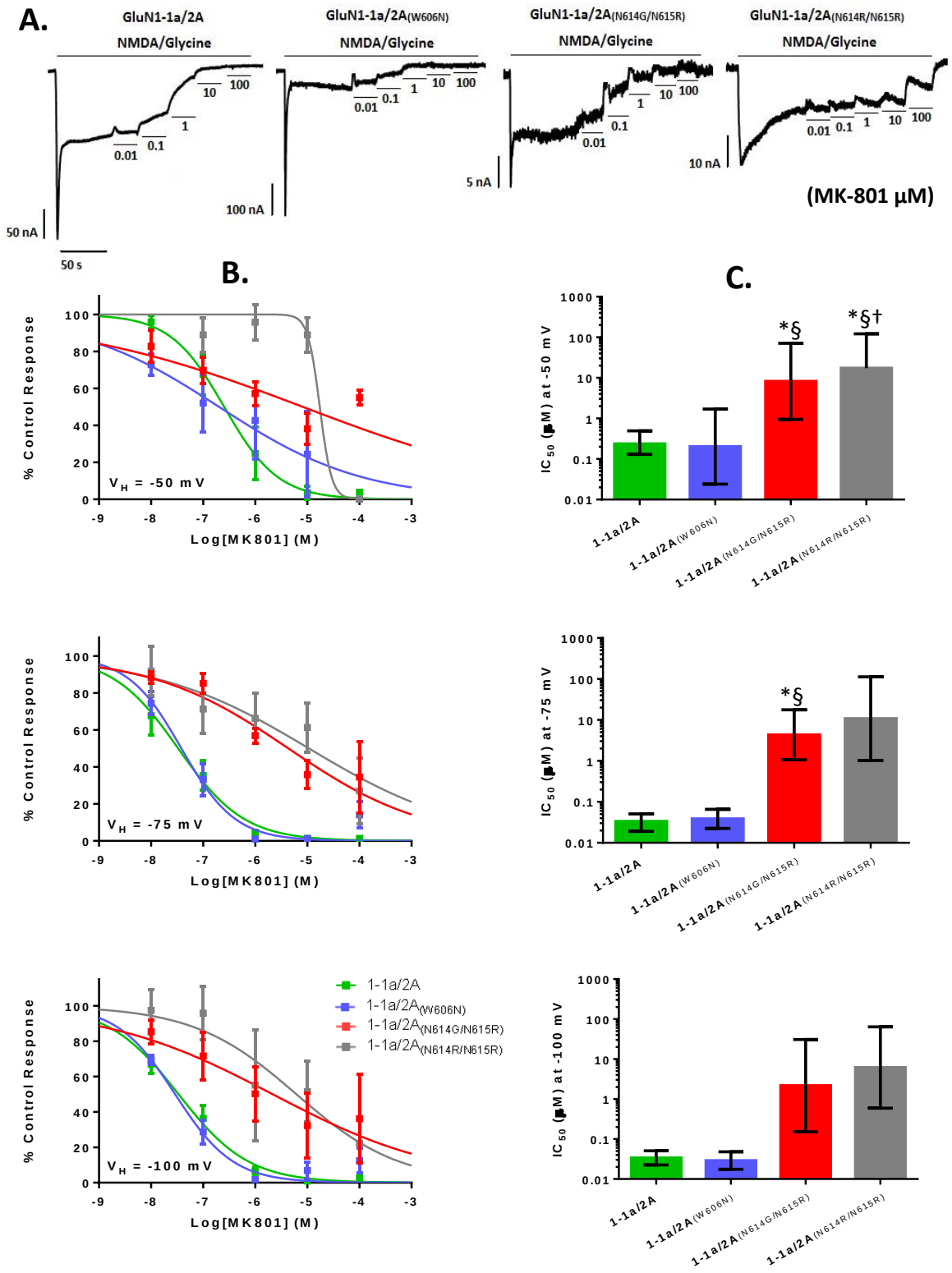


Figure 50: Concentration-inhibition relationship for MK-801 block of NMDA/glycine on NMDARs containing GluN2A mutations compared with block on wild type GluN1-1a/GluN2A subunits.

(A) TEVC recordings of MK-801 (0.01 -100 µM) block at -75 mV, (B) Concentration-inhibition curves for MK-801 block. Percentage control response (mean ± SEM, n=2-6) values plotted and fitted with the Hill equation to estimate IC_{50} values, (C) Bars represent IC_{50} (95% CI) µM; (*) denotes statistical significance against 1-1a/2A, (§) against 1-1a/2A$_{W606N}$ and (†) against 1-1a/2A$_{N614G/N615R}$.

4.4.4 Philanthotoxin-343

Philanthotoxin-343 IC_{50}s generated for all receptor combinations did not reveal any significant differences at all three holding potentials. Results are presented in table 17 and figure 51.

Table 17: IC_{50} values for philanthotoxin-343 on NMDARs containing GluN2A mutations and compared with IC_{50} on wild type GluN1-1a/GluN2A.

	Philanthotoxin-343 IC_{50} (95% CI) µM			
Voltage (mV)	**1-1a/2A**	**1-1a/2A$_{W606N}$**	**1-1a/2A$_{N614G/N615R}$**	**1-1a/2A$_{N614R/N615R}$**
-50	**11.9 (n=7)** 4.43 to 32.2	**14.2 (n=5)** 2.82 to 71.4	**15.2 (n=5)** 5.95 to 38.9	**12.0 (n=4)** 3.98 to 36.3
-75	**2.08 (n=5)** 1.14 to 3.78	**1.96 (n=4)** 1.07 to 3.6	**2.9 (n=4)** 1.83 to 4.62	**1.81 (n=4)** 0.23 to 14.0
-100	**0.97 (n=4)** 0.39 to 2.41	**0.56 (n=4)** 0.31 to 1.01	**0.80 (n=5)** 0.26 to 2.48	**1.39 (n=5)** 0.52 to 3.71

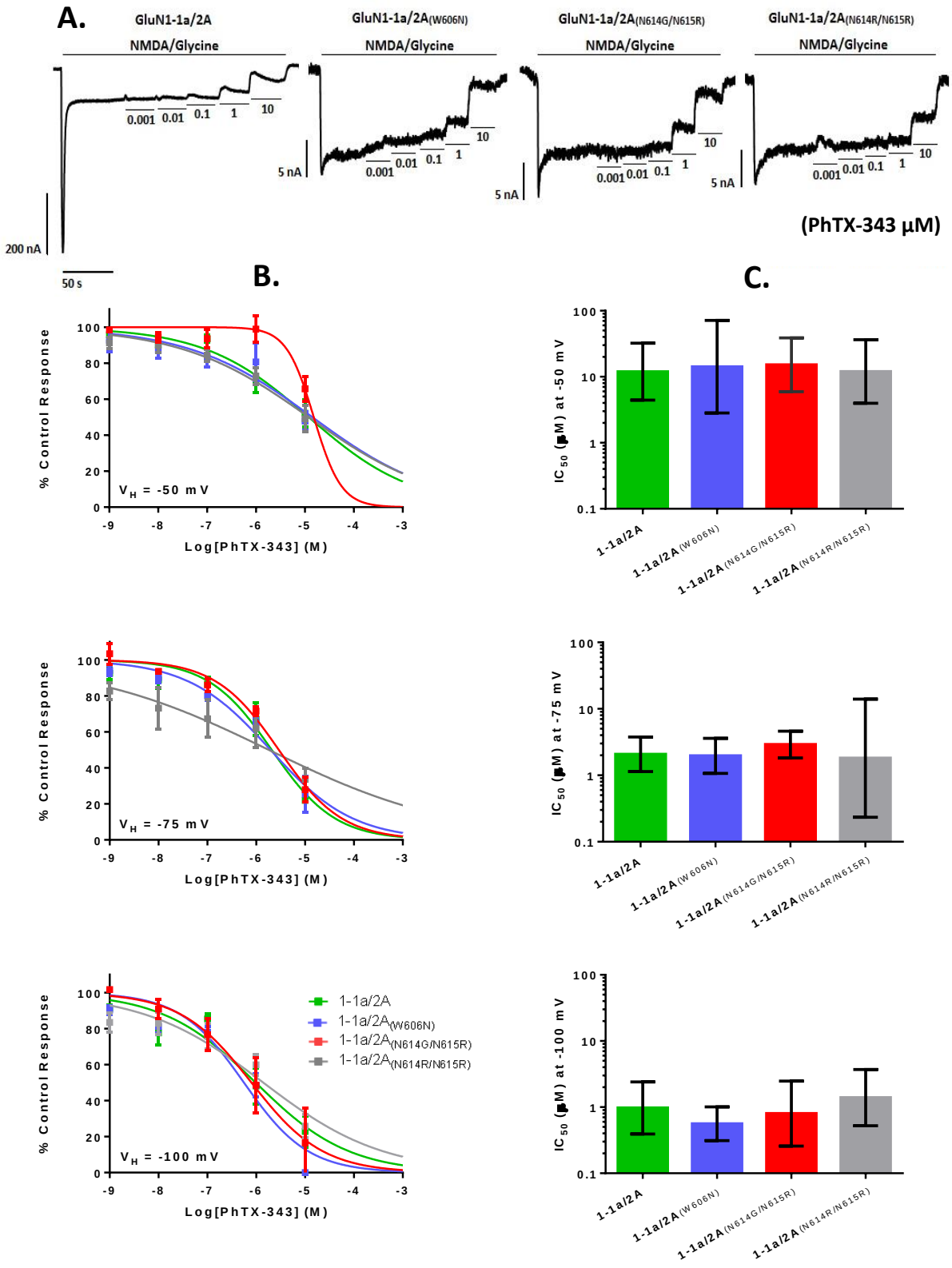


Figure 51: Concentration-inhibition relationship for Philanthotoxin-343 block of NMDA/glycine on NMDARs containing GluN2A mutations compared with block on wild type GluN1-1a/GluN2A subunits.

(A) TEVC recordings of PhTX-343 (0.01-100 µM) block at -75 mV, (B) Concentration-inhibition curves for PhTX-343 block. Percentage control response (mean ± SEM, n=4-7) values plotted and fitted with the Hill equation to estimate IC_{50} values, (C) Bars represent IC_{50} (95% CI) µM; no significant difference was observed between all subunit combinations.

4.4.5 CR18

Due to limited availability, it was not possible to test CR18 in all subunit combinations at all the desired holding potentials (refer to table 10, NA denotes not tested). The GluN2A$_{N614R/N615R}$ mutation did appear to affect blocking potencies of CR18 as IC_{50}s were higher (2-, 7- and 15-fold at -50, -75 and -100 mV respectively) compared to wild type. The GluN2A$_{N614G/N615R}$ mutation only resulted in a significant increase of IC_{50} (24-fold) at -100 mV but not at -75 mV. IC_{50} of CR18 at GluN2A$_{W606N}$ increased 2-fold compared to wild type tested at -100 mV although the differences were not significant. No differences were observed between IC_{50}s tested on 1-1a/2A$_{N614R/N615R}$ and 1-1a/2A$_{N614G/N615R}$ subunits recorded at -75 and -100 mV. The results are presented in table 18 and figure 52.

Table 18: IC_{50} values for CR18 compound on NMDARs containing GluN2A mutations and compared with IC_{50} on wild type GluN1-1a/GluN2A.

	CR18 IC_{50} (95% CI) µM			
Voltage (mV)	**1-1a/2A**	**1-1a/2A$_{W606N}$**	**1-1a/2A$_{N614G/N615R}$**	**1-1a/2A$_{N614R/N615R}$**
-50	**12.4 (n=3)** 6.44 to 23.0	**NA**	**NA**	**22.3 (n=4)** 10.6 to 47.0
-75	**2.04 (n=3)** 0.56 to 7.43	**NA**	**3.88 (n=3)** 1.52 to 9.94	**13.4 (n=4)** 6.28 to 28.5 * p=0.0081
-100	**0.62 (n=4)** 0.12 to 3.35	**1.29 (n=2)** 0.22 to 7.55	**14.6 (n=3)** 4.41 to 48.1 * p=0.0041 § p=0.0196	**9.4 (n=4)** 4.97 to 17.8 * p=0.0023 § p=0.0196

* denotes statistical significance against 1-1a/2A
§ denotes statistical significance against 1-1a/2A$_{W606N}$
† denotes statistical significance against 1-1a/2A$_{N614G/N615R}$

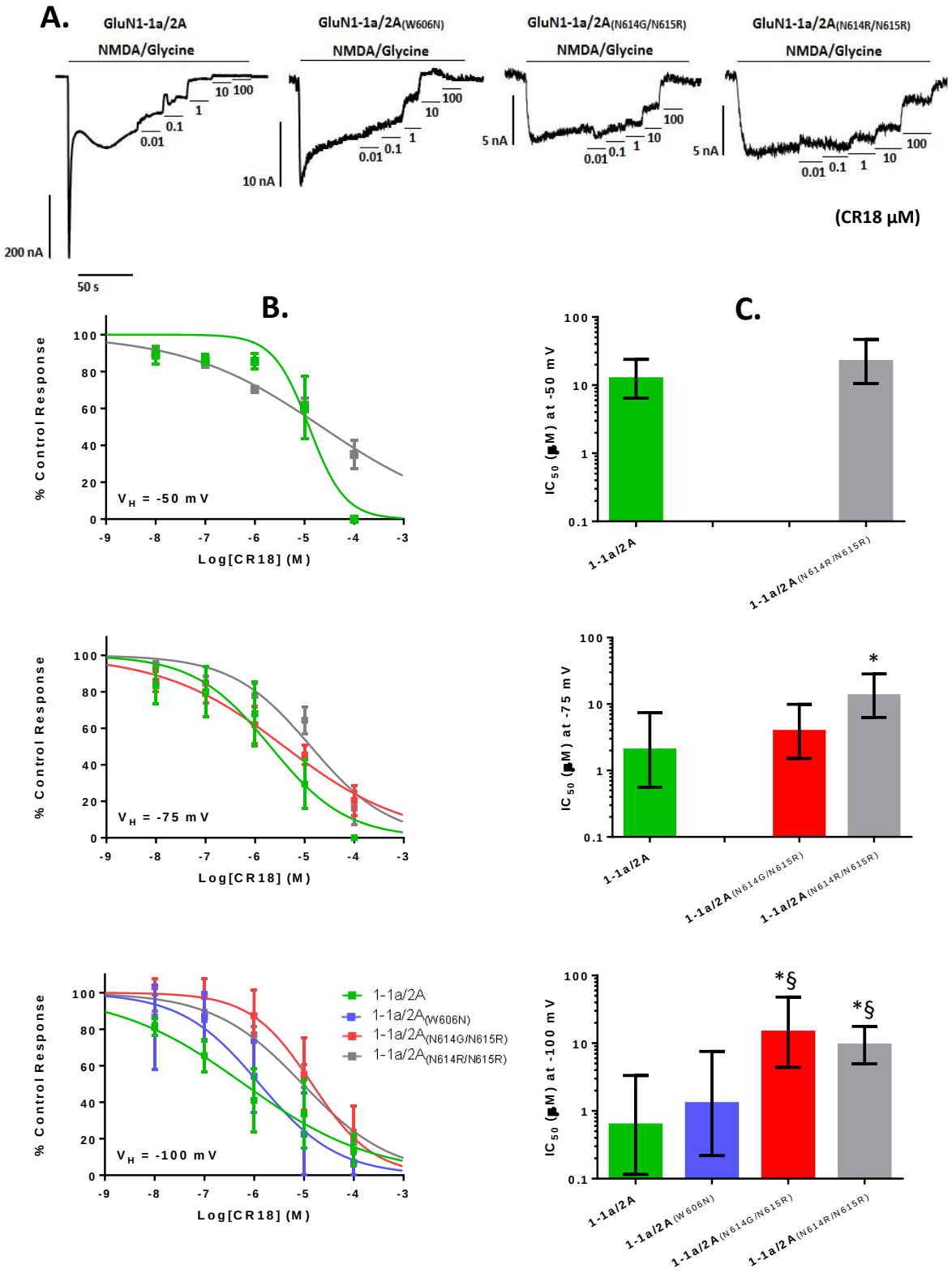


Figure 52: Concentration-inhibition relationship for CR18 block of NMDA/glycine on NMDARs containing GluN2A mutations compared with block on wild type GluN1-1a/GluN2A subunits.

(A) TEVC recordings of CR18 (0.01-100 µM) block at -75 mV, (B) Concentration-inhibition curves for CR18 block. Percentage control response (mean ± SEM, n=2-4) values plotted and fitted with the Hill equation to estimate IC_{50} values, (C) Bars represent IC_{50} (95% CI) µM; (*) denotes statistical significance against 1-1a/2A, (§) against 1-1a/2A$_{W606N}$ and (†) against 1-1a/2A$_{N614G/N615R}$.

4.5 VOLTAGE-DEPENDENCE OF INHIBITION

Concentration-inhibition values fitted with the Hill equation were compared between each holding potential and assessed whether the GluN2A mutations resulted in altered behaviour compared to wild type. The IC_{50}s were then fitted with the Woodhull equation to generate their δ values.

4.5.1 GluN2A$_{(W606N)}$ Mutation

Voltage-dependence of block of channel blockers in NMDAR containing the GluN2A$_{(W606N)}$ mutation demonstrated similar patterns as compared to responses in wild type NMDAR. In general, IC_{50}s were reduced as membrane voltages became more negative. Block at -100 mV was significantly higher than that at -50 mV for all channel blockers. Block by Mg^{2+} and philanthotoxin-343 were particularly affected by membrane potentials where IC_{50}s generated were significantly different across all voltages. Results are presented in table 19 and figure 53.

Table 19: Comparison of IC_{50} values for channel blockers on NMDARs containing GluN2A$_{W606N}$ mutation across three different holding potentials.

	IC_{50} (95% CI) µM on GluN1-1a/2A$_{W606N}$		
Voltage (mV) / Compounds	**-50 mV**	**-75 mV**	**-100 mV**
Mg^{2+}	**22.2 (n=7)** 13.9 to 35.5	**4.39 (n=7)** 2.71 to 7.11 * p<0.0001	**2.36 (n=8)** 1.62 to 3.44 * p<0.0001 † p=0.0462
Memantine	**4.09 (n=7)** 2.79 to 5.8	**2.13 (n=8)** 1.21 to 3.75	**1.65 (n=7)** 0.79 to 3.46 * p=0.0262
MK-801	**0.2 (n=4)** 0.02 to 1.71	**0.038 (n=5)** 0.022 to 0.066	**0.029 (n=5)** 0.018 to 0.048 * p=0.0288
PhTX-343	**14.2 (n=5)** 2.82 to 71.4	**1.96 (n=4)** 1.07 to 3.6 * p=0.0044	**0.56 (n=4)** 0.31 to 1.01 * p<0.0001 † p=0.0037

* denotes statistical significance against -50 mV
† denotes statistical significance against -75 mV

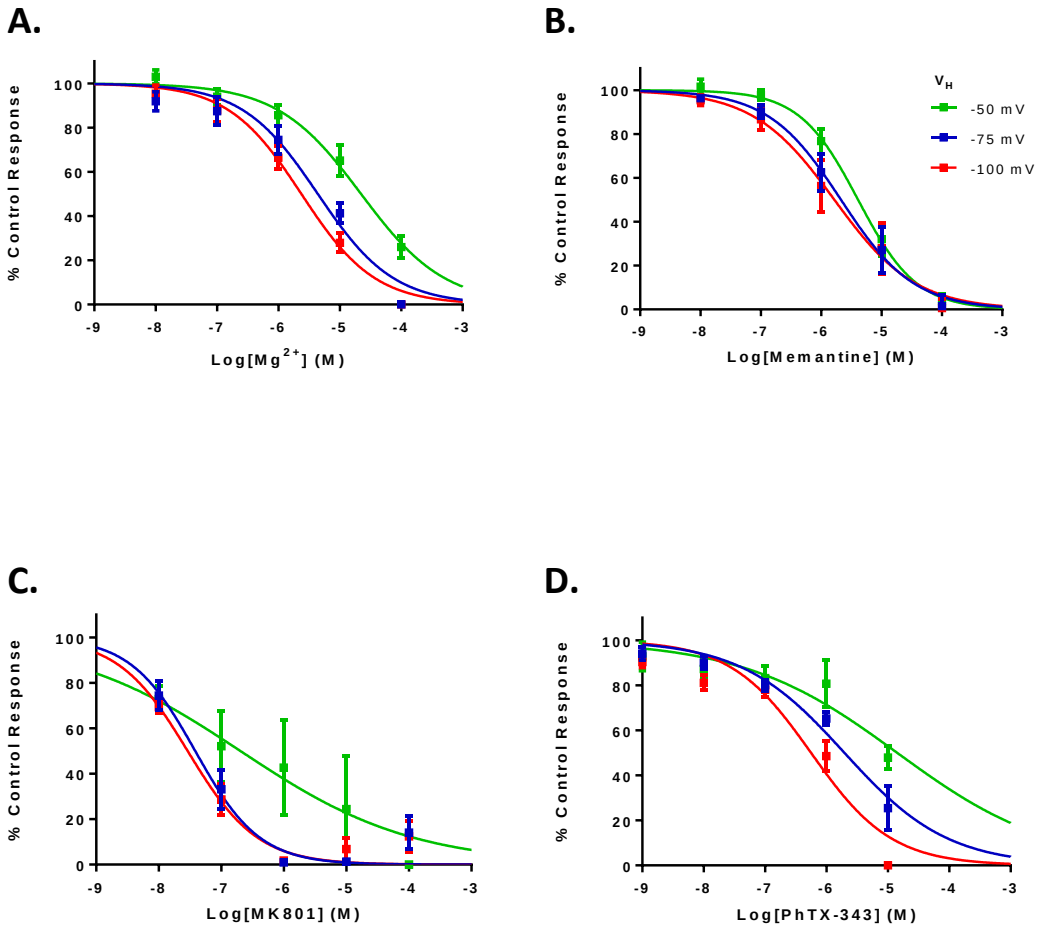


Figure 53: Concentration-inhibition curves showing voltage-dependent block of NMDA/glycine responses by open channel blockers mediated by GluN1-1a/GluN2A$_{(W606N)}$ receptor combination at -50, -75 and -100 mV.

Percentage control response (mean ± SEM) values were plotted and fitted with the Hill equation to generate the IC_{50}s for (A) Mg^{2+}, (B) memantine, (C) MK-801 and (D) PhTX-343.

4.5.2 GluN2A$_{(N614G/N615R)}$ Mutation

Mg^{2+}, memantine and philanthotoxin-343 demonstrated similar patterns of voltage-dependence of block on NMDAR containing GluN2A$_{(N614\mathbf{G}/N615\mathbf{R})}$ mutation as compared to responses in wild type NMDAR as well as NMDAR containing the GluN2A$_{(W606N)}$ mutation. IC_{50}s for these channel blockers were reduced as membrane voltages became more negative; block at -100 mV was significantly higher compared to that at -50 mV. Block for philanthotoxin-343 was particularly affected by membrane potentials where IC_{50}s generated were significantly different across all voltages. MK-801 exhibited a similar trend of reduced IC_{50} as membrane potential is more negative although this was found statistically not significant. Results are presented in table 20 and figure 54.

Table 20: Comparison of IC_{50} values for channel blockers on NMDARs containing GluN2A$_{N614G/N615R}$ mutation across three different holding potentials.

	IC_{50} (95% CI) µM on GluN1-1a/2A$_{N614G/N615R}$		
Voltage (mV) / Compounds	**-50 mV**	**-75 mV**	**-100 mV**
Mg^{2+}	**236.8 (n=3)** 42.9 to 1308	**3.22 (n=5)** 2.24 to 4.64 * p<0.0001	**1.42 (n=4)** 0.59 to 3.43 * p<0.0001
Memantine	**198.8 (n=4)** 11.0 to 3594	**4.64 (n=4)** 1.53 to 14.1 * p<0.005	**6.51 (n=4)** 1.48 to 28.7 * p<0.05
MK-801	**8.21 (n=5)** 0.95 to 71.2	**4.34 (n=5)** 1.06 to 17.7	**2.16 (n=6)** 0.15 to 30.8
PhTX-343	**15.2 (n=5)** 5.95 to 38.9	**2.9 (n=4)** 1.83 to 4.62 * p<0.05	**0.8 (n=5)** 0.26 to 2.48 * p<0.05 † p<0.05
CR18	**NA**	**3.88 (n=3)** 1.52 to 9.94	**14.6 (n=3)** 4.41 to 48.1

* denotes statistical significance against -50 mV
† denotes statistical significance against -75 mV

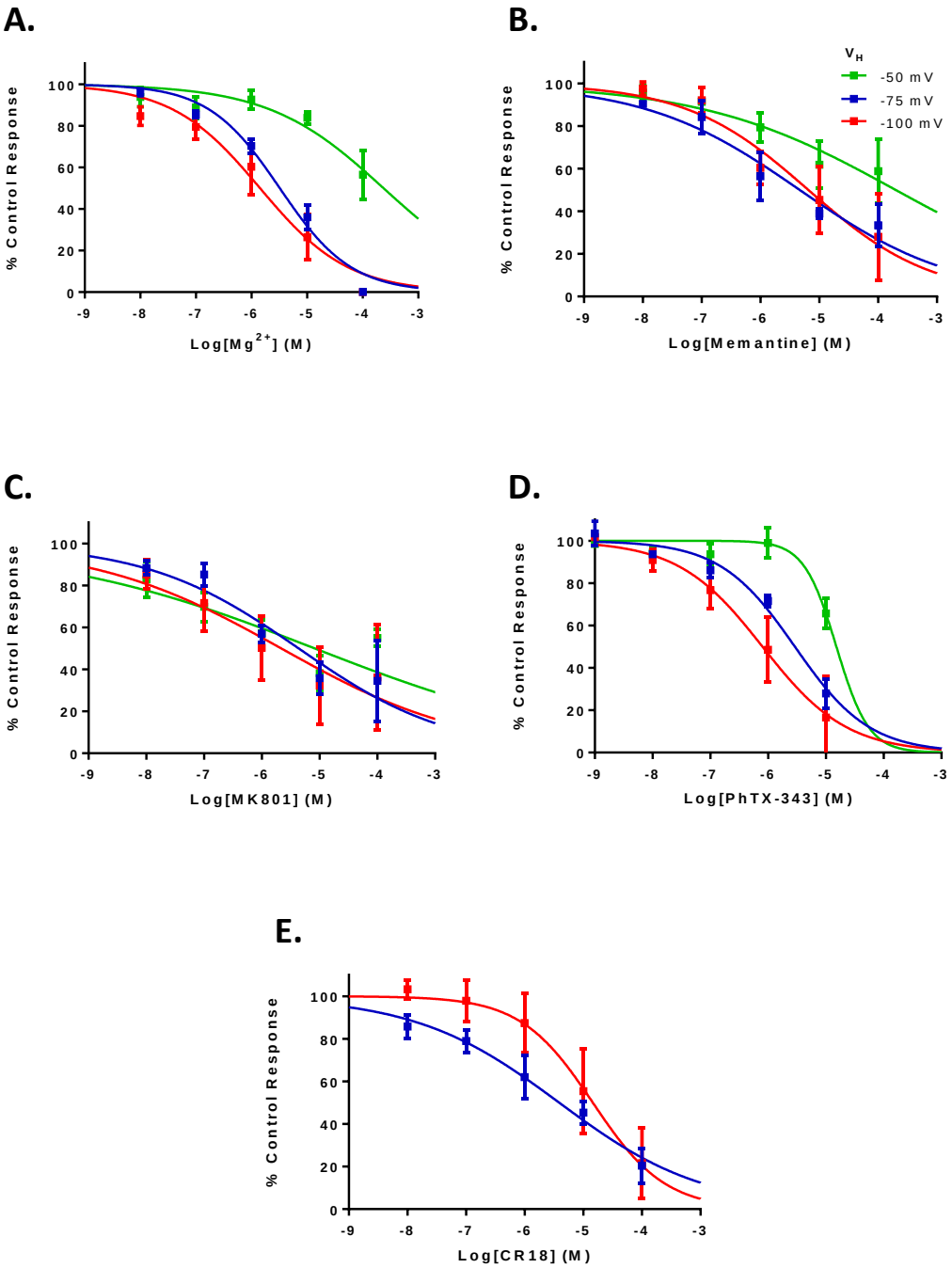


Figure 54: Concentration-inhibition curves showing voltage-dependent block of NMDA/glycine responses by open channel blockers mediated by GluN1-1a/GluN2A$_{(N614G/N615R)}$ receptor combination at -50, -75 and -100 mV.

Percentage control response (mean ± SEM) values were plotted and fitted with the Hill equation to generate the IC_{50}s for (A) Mg^{2+}, (B) memantine, (C) MK-801, (D) PhTX-343 and (E) CR18.

4.5.3 GluN2A$_{(N614R/N615R)}$ Mutation

Similar to the other two mutations, GluN2A$_{(N614\mathbf{R}/N615\mathbf{R})}$ did not seem to affect voltage-dependence of inhibition for the channel blockers. IC_{50} rank order were the same for all compounds where IC_{50}s generated at -100 mV were the lowest followed by -75 mV and -50 mV. Significant differences were observed between IC_{50}s at -100 mV and -50 mV for all compounds (except CR18) although less significance was observed between IC_{50}s at -75 mV and -100 mV. The results are presented in table 21 and figure 55.

Table 21: Comparison of IC_{50} values for channel blockers on NMDARs containing GluN2A$_{N614R/N615R}$ mutation across three different holding potentials.

	IC_{50} (95% CI) µM on GluN1-1a/2A$_{N614R/N615R}$		
Voltage (mV) / Compounds	**-50 mV**	**-75 mV**	**-100 mV**
Mg^{2+}	**658.4 (n=6)** 77.6 to 5587	**108.7 (n=5)** 43.4 to 272	**94.0 (n=4)** 47.8 to 184.8 * p<0.05
Memantine	**259.9 (n=4)** 49.6 to 1363	**42.2 (n=5)** 13.2 to 135.1	**16.2 (n=5)** 4.65 to 56.5 * p<0.05
MK-801	**17.4 (n=2)** (very wide)	**10.8 (n=5)** 1.03 to 112	**6.18 (n=3)** 0.59 to 64.2 * p<0.05
PhTX-343	**12.0 (n=4)** 3.98 to 36.3	**1.81 (n=4)** 0.23 to 14.0	**1.39 (n=5)** 0.52 to 3.71 * p<0.005
CR18	**22.3 (n=4)** 10.6 to 47	**13.4 (n=4)** 6.28 to 28.5	**9.4 (n=4)** 4.97 to 17.8

* denotes statistical significance against -50 mV
† denotes statistical significance against -75 mV

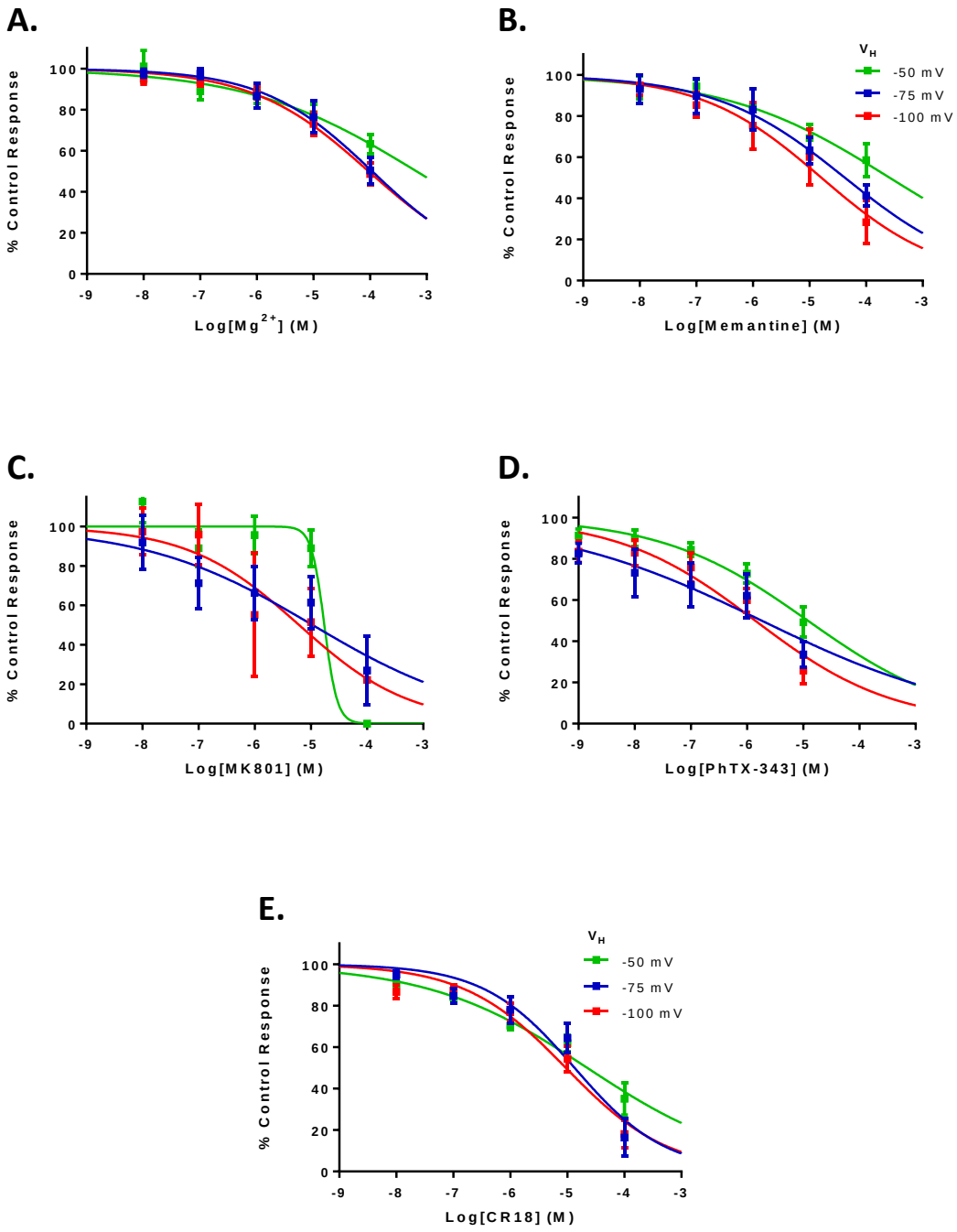


Figure 55: Concentration-inhibition curves showing voltage-dependent block of NMDA/glycine responses by open channel blockers mediated by GluN1-1a/GluN2A$_{(N614R/N615R)}$ receptor combination at -50, -75 and -100 mV.

Percentage control response (mean ± SEM) values were plotted and fitted with the Hill equation to generate the IC_{50}s for (A) Mg^{2+}, (B) memantine, (C) MK-801, (D) PhTX-343 and (E) CR18.

IC_{50}s for channel blockers tested on all subunit combinations were fitted with the Woodhull model equation to determine the δ value which estimates the position of binding sites within the electric field. The GluN2A$_{W606N}$ mutation does not appear to impact the δ values for all compounds as the numbers were relatively similar to wild type with only slight alterations found. Interestingly, both double mutations show the same effect, δ values were increased for Mg^{2+} and memantine and reduced for MK-801 and CR18, suggesting that binding sites were altered by the double mutations. All mutations however, did not appear to alter the δ value of philanthotoxin-343, as the numbers were similar with all subunit combinations. Calculated δ values are presented in table 22 and the corresponding Woodhull-fitted graphs are shown in figure 56. The δ value for Mg^{2+} on 1-1a/2A$_{N614G/N615R}$ was considered ambiguous due to the poorly fitted Woodhull curve and wide confidence interval.

Table 22: Calculated δ values from the Woodhull equation for channel blockers tested on GluN1-1a/2A, GluN1-1a/2A$_{(W606N)}$, GluN1-1a/2A$_{(N614G/N615R)}$ and GluN1-1a/2A$_{(N614R/N615R)}$ subunit combinations.

	δ (95% CI)			
Compound	**1-1a/2A**	**1-1a/2A$_{W606N}$**	**1-1a/2A$_{N614G/N615R}$**	**1-1a/2A$_{N614R/N615R}$**
Mg^{2+}	**0.62** -0.67 to 1.9	**0.77** -0.93 to 2.46	**~ 2.19** (Very wide)	**0.81** -2.41 to 4.02
Memantine	**0.59** -0.95 to 2.13	**0.53** -0.95 to 2.0	**3.78** -12.0 to 20.5	**1.79** -0.67 to 4.25
MK-801	**1.84** -6.54 to 10.2	**1.5** -3.69 to 6.68	**0.67** 0.46 to 0.88	**0.52** 0.24 to 0.79
PhTX-343	**0.56** -0.47 to 1.6	**0.66** 0.09 to 1.24	**0.56** 0.24 to 0.87	**0.58** -1.44 to 2.61
CR18	**0.6** 0.07 to 1.13	**NA**	**NA**	**0.16** -0.04 to 0.35

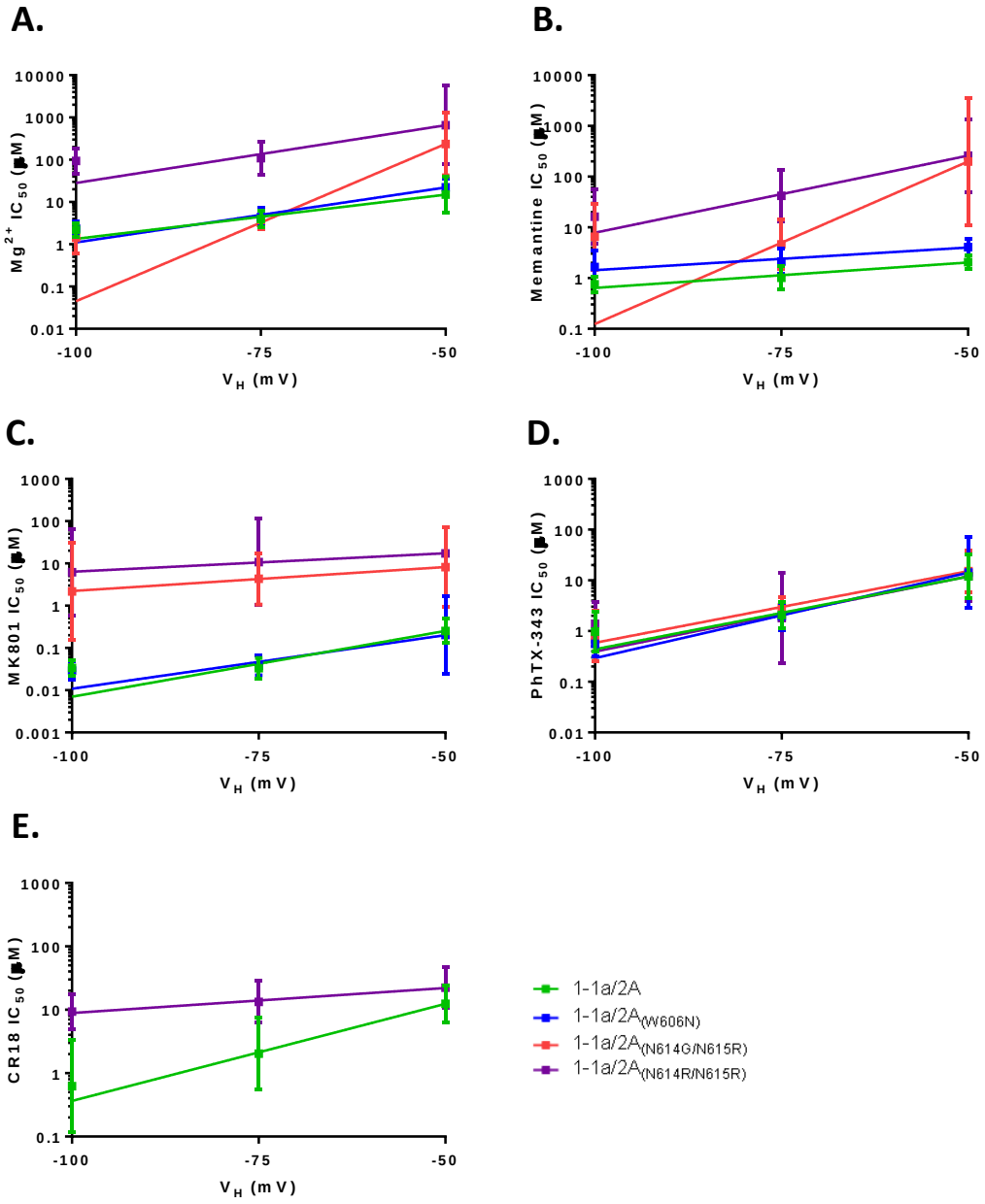


Figure 56: Voltage-dependence of IC_{50} for channel block of NMDA/glycine responses on all NMDA receptor combinations fitted with the Woodhull equation.

IC_{50} (95% CI) μM for (A) Mg^{2+}, (B) memantine, (C) MK-801, (D) philanthotoxin-343 and (E) CR18 tested on GluN1-1a/2A, GluN1-1a/2A$_{(W606N)}$, GluN1-1a/2A$_{(N614\mathbf{G}/N615\mathbf{R})}$ and GluN1-1a/2A$_{(N614\mathbf{R}/N615\mathbf{R})}$ subunit combinations (note altered y-axis).

4.6 DISCUSSION

Despite being discovered and cloned some 20 years ago, the physiological role of GluN3 subunits remains unclear. Although GluN2 subunit variability has been shown to confer the sensitivity of NMDAR block by Mg^{2+} and other channel blockers, more recent studies have implicated the role of GluN3 subunits in reduced NMDAR channel block (McClymont et al., 2012; Paoletti and Neyton, 2007; Petrenko et al., 2003; Tong et al., 2008). Reports have shown that the incorporation of GluN3 into the conventional subunit combination of GluN1 and GluN2 dramatically changes pharmacological properties. Among the alterations associated with GluN3 are the reduction of single channel conductance leading to a downregulating effect on channel current (Das et al., 1998; Sasaki et al., 2002), resistance of Mg^{2+} block (McClymont et al., 2012), and decreased permeability of Ca^{2+} (Matsuda et al., 2002; Sasaki et al., 2002). One important question relating to GluN3's ability to reduce Ca^{2+} permeability is whether this is a favourable property, or if this is negated by the fact that Mg^{2+} block allows activity at more hyperpolarized membrane potentials. This issue is important to address for two main reasons: (i) NMDAR antagonists are being investigated extensively as potential therapeutics for neurodegenerative disorders and the GluN3 subunits could be promising new targets in neuropathological conditions including excitotoxicity and cognitive dysfunction (Kvist et al., 2013; Stys and Lipton, 2007), and (ii) GluN3 subunits have been proposed to possess *in vivo* neuroprotective effects (Káradóttir et al., 2005; Martinez-Turrillas et al., 2012; Nakanishi et al., 2009).

Here, we attempted to further investigate the impact of the Q/R/N and adjacent sites in the M2 pore region of the GluN3 subunits on the reduced inhibitory potency of Mg^{2+} and other open channel blockers. Previous findings have shown that the reduced potency of channel blockers in GluN3A can only be partially restored by reverse mutation of G at the Q/R/N site or R at the +1 site to N (McClymont et al., 2012). Thus, the initial aim of this study was to investigate whether a double reverse mutation at the Q/R/N and +1 sites (GR mutated to NS and NN resembling GluN1 and GluN2A respectively) can completely or still partially restore blocking potency. cRNAs

of mutated GluN3 subunits were co-injected with GluN1-1a and GluN2A into *Xenopus* oocytes and their susceptibility to block by Mg^{2+} and memantine were assessed through voltage-clamp recording.

The findings of this study however revealed no differences between Mg^{2+} and memantine block of NMDA/glycine responses between NMDAR assemblies containing mutated GluN3A or GluN3B at -75 mV versus wild type (data not shown). We then compared Mg^{2+} and memantine block of NMDA/glycine responses in the conventional assembly of GluN1-1a/GluN2A alone verses GluN1-1a/GluN2A co-injected with GluN3A or GluN3B. Again, no significant differences were observed between the three NMDA receptor assemblies (data not shown). These results suggested that both wild type and mutated GluN3 subunits might not be expressed in our *Xenopus* oocyte expression system. In order to validate GluN3 expression, glycine sensitivity testing was conducted to test GluN1-1a/GluN2A expression alone verses GluN1-1a/GluN2A incorporated with GluN3 subunits. *Xenopus* oocytes injected with NMDAR cRNAs were tested with NMDA co-applied with glycine in tenfold increasing concentration (0.01 to 100 µM) at -50, -75 and -100 mV. EC_{50} values obtained via the concentration-inhibition curves fitted with the Hill equation did not reveal any significant differences between all subunit combinations at all voltages tested. Considering that glycine's affinity at the GluN3 binding site is 650 times higher compared to GluN1, in theory the incorporation of GluN3 into NMDA receptor assembly is expected to yield a lower EC_{50} (Yao and Mayer, 2006). This has been demonstrated by McClymont (2010) where glycine's EC_{50} showed a significant reduction in receptor assemblies containing GluN3 than those containing GluN1-1a and GluN2A only. However, we could not confidently conclude that GluN3 were expressed in our oocyte expression system.

Due to the failed attempt at expressing GluN3 subunit, a different strategy was employed. GluN2A was mutated to resemble rat GluN3A and GluN3B as well as human GluN3B. Via site-directed mutagenesis on GluN2A subunit, double-amino acid substitutions (GR and RR) were introduced in place of the polar residues at 614 and 615 positions (replacing NN) which are expected to interact with cations. The single-

substitution, N was also introduced to replace W (at 606; -8 position relative to the Q/R/N site), an amino acid conserved in all other ionotropic glutamate receptors (Sakurada et al., 1993). Mutated GluN2A subunits co-expressed with GluN1-1a were characterised with Mg^{2+}, memantine, MK-801, PhTX-343 and CR18.

Current data revealed that the presence of double R at the Q/R/N and +1 sites greatly reduced open channel block by Mg^{2+}, memantine, MK-801 and CR18. GR substitution also affected channel block although statistically found not as significant. At all voltages tested, IC_{50}s for Mg^{2+} increased 27- to 44-fold in GluN1-1a/2A$_{(N6145\mathbf{R}/N615\mathbf{R})}$ compared to wild type. GluN1-1a/2A$_{(N6145\mathbf{G}/N615\mathbf{R})}$ only resulted in a significant increase at -50 mV with 14-fold compared to wild type. These findings were consistent with previous reports indicating that GluN3A-containing NMDAR (which has GR at the Q/R/N and +1 sites), although affecting blocking potency, the size of effects were relatively small. In a study on hippocampal neurones of transgenic mice overexpressing Glu3A, Tong et al. (2008) also demonstrated a 14-fold increase of Mg^{2+} IC_{50} compared to wild type. McClymont et al. (2012) also reported only a slight increase of Mg^{2+} IC_{50}, between 2- to 10-fold when GluN3 subunits were incorporated into GluN1-1a/GluN2A subunits.

In wild type GluN2A, the Q/R/N and +1 sites are occupied by NN. The mutated subunits contain a G or R at the Q/R/N site, followed by the positively charged R at the +1 position. Thus it was speculated that the loss of the polar partial negative charge of N, as well as the addition of the positive R, reduced Mg^{2+} affinity resulting in increased IC_{50}s. Interestingly, the RR mutation in GluN2A produced even higher IC_{50}s then the subunit combinations containing GR mutation in GluN2A. The increased positive charge caused by double R must have contributed to this phenomenon.

The memantine block demonstrated a similar inhibition pattern with Mg^{2+} but with more significant increases in the IC_{50}s. This is expected as previous studies have noted the similar/or close binding sites of memantine and Mg^{2+} (Chen and Lipton, 2005; Kashiwagi et al., 2002). The presence of RR mutation in GluN2A resulted in 125-, 40-

and 20-fold increase of IC_{50} at -50, -75 and -100 mV respectively. The GR mutation also significantly reduced memantine block but at a smaller magnitude compared to RR.

MK-801 was the most potent NMDAR blocker tested in all subunit combinations at all voltages in this study. The RR mutation in GluN2A had a profound effect on MK-801 inhibition as the IC_{50}s increased 67- to 325-fold compared to wild type. The presence of GR mutation also significantly increased the IC_{50} of MK-801 but much less so where IC_{50}s rose 33- to 133-fold across the three voltages tested. MK-801 was postulated to bind strongly to the Q/R/N site in such a way that agonist can dissociate and the channel can close while it is still trapped in the channel pore. McClymont et al. (2012) demonstrated that a reverse mutation at the Q/R/N site in GluN3A (G729N) restored activity of channel block in the NMDAR channel thus supporting the claim that binding occurs at this region (Kashiwagi et al., 2002).

In the current study, small but significant increases for CR18 IC_{50}s were observed in subunit combinations containing the RR mutation in GluN2A. IC_{50}s increased 2-, 7- and 15-fold at -50, -75 and -100 mV respectively compared to wild type. GR also affected CR18 block where IC_{50}s increased 2- and 25-fold at -75 and -100 mV respectively. CR18 was not tested at -50 mV due to limited availability.

IC_{50}s were similar for PhTX-343 tested against all subunit combinations across all holding potentials. In a study by Kashiwagi et al. (2007) using anthraquinone toxins containing spermine, a mutation at the Q/R/N site in $GluN1_{(N616Q)}$ reduced blocking potencies (>15%) of AQ343 and AQ444 analogues (the chemical structure of the compounds are presented in figure 57 and show similarity with the PhTX-343 polyamine backbone but with differences in the headgroup) . In contrast, single mutations substituting N with G at the homologous Q/R/N and +1 sites in GluN2B enhanced block by AQ343 (Kashiwagi et al., 2007). It is not surprising, therefore, that all mutations constructed in GluN2A subunits in this study did not alter blocking potencies of PhTX-343. This finding did not correspond with a study of AMPA

receptors where an R at the Q/R/N site in GluA2 results in receptors that are not blocked by polyamines (Isaac et al., 2007).

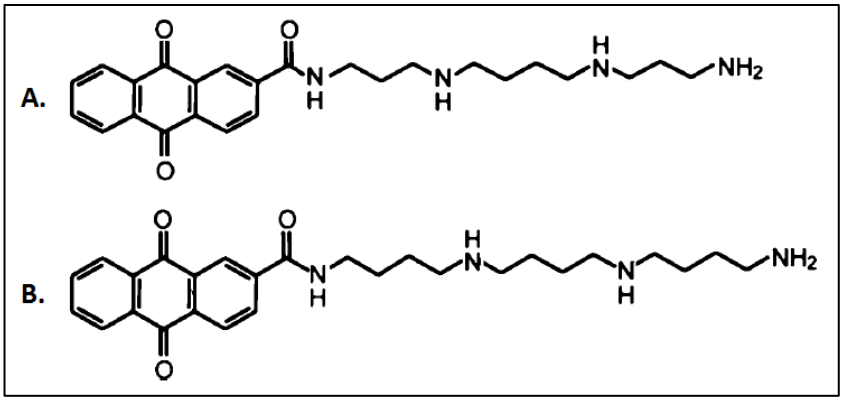


Figure 57: Chemical structures of (A) AQ343 and (B) AQ444.

These anthraquinone analogues were derived from anthraquinone-2-carboxyl chloride. Note that AQ343 consists of similar polyamine backbone to PhTX-343 (Kashiwagi et al., 2004; Kashiwagi et al., 2007).

Numerous studies have demonstrated that the Q/R/N modification altered Ca^{2+} permeability and blocking sensitivity of antagonists. Most early studies, however, were focused on GluN1 subunits and only single substitutions were constructed. Many studies have shown that replacing N with either Q or R at the homologous Q/R/N position in GluN1 resulted in marked decline of Ca^{2+} flux as well as reduced blocking potencies of Mg^{2+}, MK-801 and PCP. In addition to that, blocking by Zn^{2+} and desipramine (an antidepressant) were also found reduced (Burnashev et al., 1992; Mori et al., 1992; Sakurada et al., 1993; Yamakura et al., 1993). More specifically, Sakurada et al. (1993) revealed that N616Q mutation in GluN1 resulted in reduced Ca^{2+} permeability while N616R substitution almost completely diminished ionic currents. Mg^{2+} and MK-801 block were also altered in both mutations, where N616R resulted in more reduced blockade compared to N616Q. Similarly, Ferrer-Montiel et al. (1995) demonstrated that N to Q replacement reduced MK-801 blocking potency by 800-fold as well as PCP by 300-fold. In reverse, replacement of Q to N in the homologous GluA1 AMPA receptor resulted in enhanced sensitivity to MK-801 and PCP block, an increase of 70- and 13-fold respectively (Ferrer-Montiel et al., 1995). The N residue is conserved in GluN1 and all isoforms of GluN2 subunits in the homologous Q/R/N position. It is therefore postulated early on by Sakurada et al.

(1993) that an asparagine ring forms a central part of the receptor channel pore and regulates the constriction and selectivity of ion flux particularly Ca^{2+} as well as channel block by Mg^{2+} and other blockers.

Channel block may also be altered by changes in the size of the channel pore. Modification of the Q/R/N and +1 sites in GluN1 and GluN2 subunits were shown to alter NMDAR channel diameter. As previously noted, the diameter of the NMDAR channel is estimated to be approximately 0.55 nm (Villarroel et al., 1995). Wollmuth et al. (1996) discovered that the GluN1 mutation of N to G at the Q/R/N site (in combination with wild type GluN2A) increased the diameter of the channel pore to 0.75 nm, while GluN2A mutation at the corresponding site does not. In contrast, N to G mutation at the +1 site in GluN2A increased the channel pore to 0.67 nm, while the substitution of S to G at the homologous GluN1 site does not. As expected, double mutations (N to G) at these non-homologues sites had the most pronounced effect as it enlarged the channel pore to approximately 0.87 nm. They concluded that the major determinants of the narrow constriction of the NMDAR channel pore are the N residues at the Q/R/N site of GluN1 and at the +1 site of the GluN2A.

Modification of W to N at -8 position in GluN2A only resulted in small changes in blocking potencies of all NMDAR blockers tested in this study when compared to wild type. For Mg^{2+}, the IC_{50}s in GluN1-1a/GluN2A$_{(W606N)}$ increased slightly at all voltages although these were not statistically significant. Williams et al. (1998) previously reported that the W residue at -8 position in the M2 region of GluN2 subunits controls Mg^{2+} block. In GluN2B, substitution of W_{607} to N, L (leucine) and A (alanine) greatly reduced Mg^{2+} block and permeability of Ba^{2+}. Substitution with Y (tyrosine) or F (phenylalanine), both containing aromatic rings has no or little effect on Mg^{2+} block, suggesting that the loss of activity only occur if there was a loss of the aromatic ring. This also indicates that the W residue may be involved in the binding of divalent cations, in particular Mg^{2+} through a cation-π interaction with the electron-rich aromatic ring of the tryptophan. Based on these findings, they proposed a model in which the M2 loop of GluN2B is folded in such a way that W_{607} is positioned at the narrow constriction, at a level similar to the Q/R/N site in GluN1$_{(N616)}$ and +1 position

in GluN2B$_{(N616)}$. These three residues form the binding site for Mg^{2+}. This amino acid at -8 position located on the supporting alpha helix of the pore loop might also contribute to the constraining of the loop. Therefore, modification at this site is postulated to influence the position of the narrow part of the pore lined by the beta strand part of M2. The study, however, only constructed one mutation in GluN2A where W was substituted with L resulting in abolished Mg^{2+} block. This may indicate that the W residue in GluN2A$_{(W606)}$ may behave in a similar manner with GluN2B.

Similar to Mg^{2+}, GluN2A$_{(W606N)}$ mutation had a slight effect on memantine and CR18 block as IC_{50}s were found to increase 2-fold at all holding potentials with a significant difference observed at -50 mV with memantine. The mutation does not alter inhibition of MK-801 and PhTX-343 as IC_{50}s across all voltages were similar and no significant differences were observed. Although previous studies have shown that the bulky W residue at the -8 position has a profound effect on sensitivity of channel block (Kashiwagi et al., 2002; Williams et al., 1998), the present study only noted a very small effect with Mg^{2+}, memantine and CR18 block of NMDA-induced current. Indeed, substitution of the residue does not alter block of MK-801 and PhTX-343 suggesting that the N residue in GluN3 has only a small or negligible effect on reduced sensitivity of channel block in GluN3-containing NMDARS as demonstrated in several studies.

In order to test voltage-dependency of the compounds, the Woodhull model was utilised. This model was originally developed to measure depth of block by H^+ through the Na^+ channel, but more recently it is thought to represent voltage-dependence or electrical interaction, rather than an actual position in space (Chen and Lipton, 2005; Woodhull, 1973). The electrical field of the NMDA receptor has also been shown to be concentrated around the Q/R/N-site and is weaker in the outer region, meaning depth cannot be accurately described by the model (Antonov et al., 1998). Furthermore, at voltages greater than -60 mV intracellular and extracellular monovalent permeant ions bind to the channel and influence the kinetics of open channel blockers (Antonov et al., 1998; Chen and Lipton, 1997). The findings of this study revealed that all compounds were voltage-dependent in all subunit

combinations tested despite the presence of mutant subunits. The compounds were more potent as the holding potentials became more negative.

Despite reports suggesting that the Woodhull model does not provide reliable predictions for binding sites, our control data in wild type NMDAR provided quite accurate estimation of the blocking site for the channel blockers (except for MK-801). The δ values for Mg^{2+}, memantine, PhTX-343 and CR18 were in the range between 0.56 to 0.62, fitting with the Q/R/N blocking position in the channel pore. Premkumar and Auerbach (1996) have shown that the Mg^{2+} blocks the NMDAR channel pore at the Q/R/N site that is approximately 0.64 through the electric field of the membrane. The present study demonstrated changes of the δ values in NMDAR assembly containing either the GR or RR mutations compared to wild type. The higher δ values calculated for Mg^{2+} and memantine in mutated subunits suggest that smaller NMDAR blockers moved to a deeper site within the channel pore beyond the Q/R/N site. Larger molecules such as PhTX-343 and CR18 might not be able to penetrate the narrow constriction site reflected by their smaller δ values. It is speculated that the double mutations might alter the size of the channel pore particularly at the narrow constriction site in the M2 region.

CHAPTER 5

MULTI-TARGET-DIRECTED LIGANDS STUDY

5.1 SUMMARY

This chapter describes the evaluation of novel compounds as potential therapeutics for AD. All compounds were designed as multi-target-directed ligands possessing multiple targets and biological properties to address the multifactorial nature of the disease. To remain consistent with previous studies, different approaches were employed to assess the MTDL compounds. Block of NMDA/glycine responses by memantine-derivatives and spermine-derived polyamines were tested at -60 mV in GluN1-1a and GluN2A NMDA receptors. Based on the IC_{50} obtained from the concentration-inhibition curves, the concentration was used to determine voltage-dependency recorded at -40, -60, -80 and -100 mV. For donepezil-derived compounds, they were co-applied with NMDA/glycine and recorded at -50, -80 and -100 mV to obtain their concentration-inhibition curves. Since donepezil was designed to target the cholinergic pathway and binding studies have shown that their derivatives possess affinity towards nicotinic receptors, the compounds were also tested on α7 and α4β2 nAChRs to see whether they exhibit any agonistic or antagonistic properties. The IC_{50}s obtained were then fitted with the Woodhull equation to generate their δ values in order to determine voltage-dependency and estimate binding sites in the channel pore. All memantine derivatives were weak NMDAR blockers with the most potent being MAB22 (possessing methoxyphenol moiety) which recorded an IC_{50} of 26.9 μM. The spermine-derived polyamines (CR compounds) were potent NMDAR channel blockers with IC_{50}s (0.69 to 2.35 μM) comparable to memantine (2.28 μM). All compounds were found to act through a voltage-dependent manner as assessed via the Woodhull model. As for the donepezil-derived (MGM) compounds, they were found to be weak NMDAR blockers

but appear to be partially agonistic towards α4β2 nAChRs while selectively antagonize ACh responses in α7 subtypes.

5.2 CONTROL CHANNEL BLOCKERS

To aid comparison with MTDLs, block by Mg^{2+} and memantine was reassessed using the above protocols that differ from those described previously.

5.2.1 Mg^{2+}

The antagonism of responses to NMDA and glycine by tenfold increment concentrations (0.01 to 100 µM) of Mg^{2+} mediated by GluN1-1a/GluN2A were employed to determine its IC_{50} value at -60 mV. The IC_{50} of Mg^{2+} generated via the concentration-inhibition curve obtained from five set of recordings was 10.1 (95% CI 4.74 to 21.4) µM (figure 58).

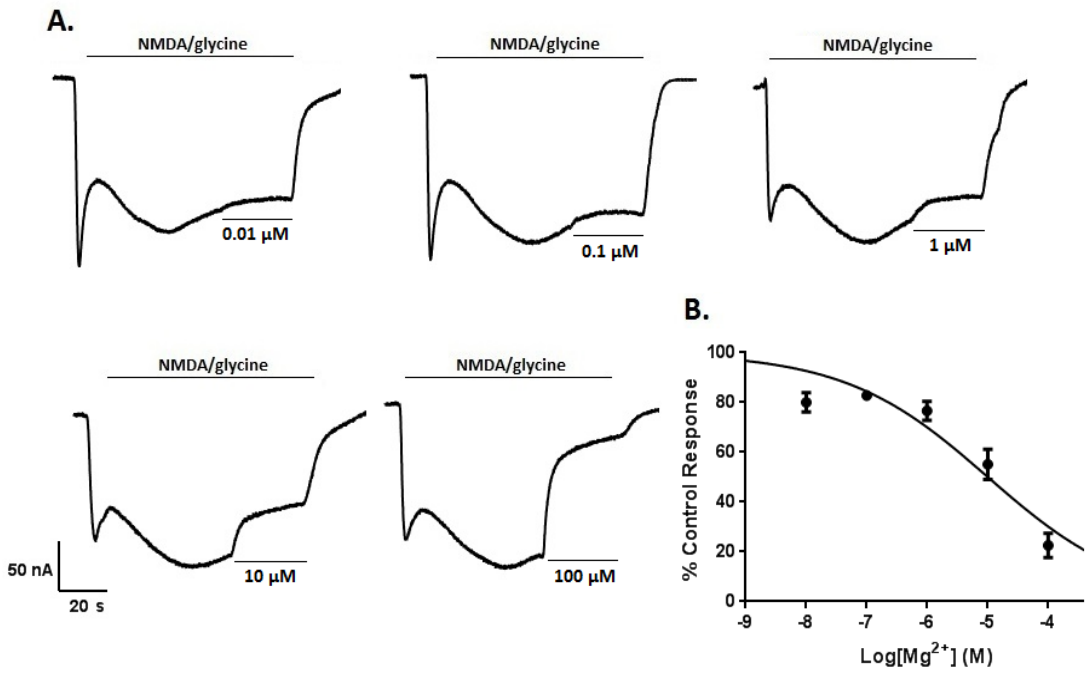


Figure 58: Concentration-dependent Mg^{2+} block of NMDA/glycine responses in GluN1-1a/GluN2A NMDA receptors.

(A) TEVC recordings for Mg^{2+} (0.01–100 µM) block of NMDA/glycine responses at -60 mV on a single oocyte, (B) Concentration-inhibition curve for Mg^{2+} block. Percentage control response (mean ± SEM, n=5) values were plotted and fitted with the Hill equation to yield an IC_{50} of 10.1 (95% CI 4.74 to 21.4) µM.

Based on the IC_{50} obtained, a concentration of 10 µM was used to determine voltage-dependent inhibition of Mg^{2+}. NMDA/glycine responses antagonised by Mg^{2+} on GluN1-1a/GluN2A were assessed at four different holding potentials; -40, -60, -80 and -100 mV. The δ value for Mg^{2+} obtained from the voltage-dependent curve fitted with the Woodhull equation was 1.48 (95% CI -0.48 to 3.44). The results are presented in figure 59.

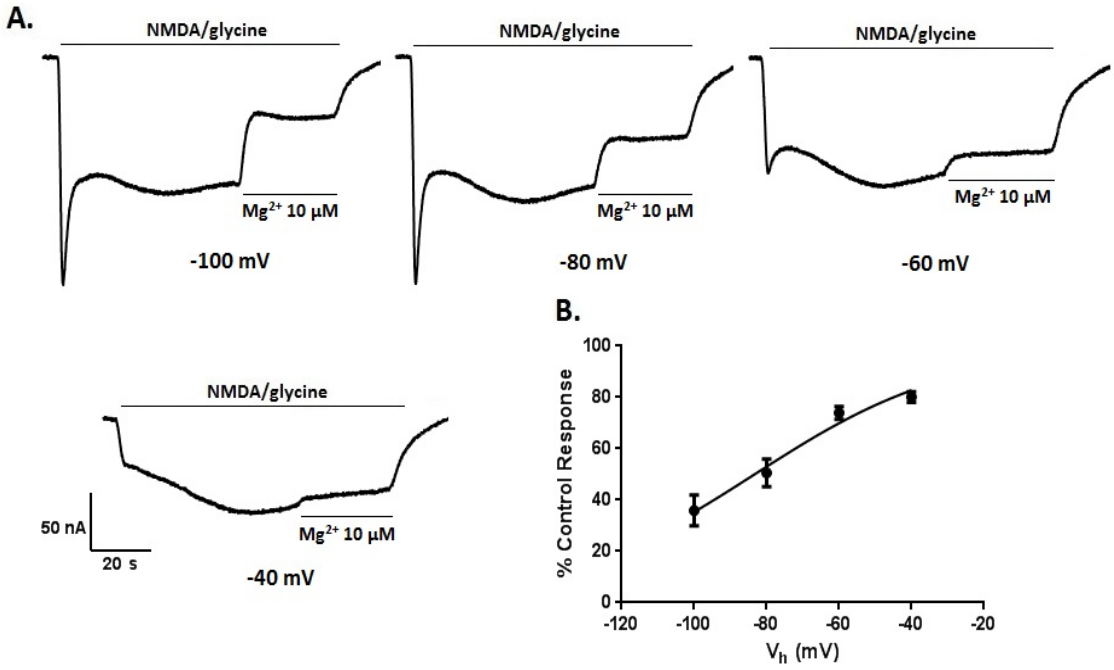


Figure 59: Voltage-dependent Mg^{2+} (10 µM) block of NMDA/glycine in GluN1-1a/GluN2A-containing NMDA receptors.

(A) TEVC recordings of Mg^{2+} block tested at -100, -80, -60 and -40 mV on a single oocyte, (B) Voltage-dependent inhibition curve for Mg^{2+} block. Percentage control response (mean ± SEM, n=3) values were plotted and fitted with the Woodhull equation to yield the δ value.

5.2.2 Memantine

The antagonism of responses to NMDA and glycine by tenfold increment concentrations (0.01 to 100 µM) of memantine mediated by GluN1-1a/GluN2A were employed to determine the IC_{50} value of memantine at -60 mV. The IC_{50} of memantine obtained via the concentration-inhibition curve was 2.28 (95% CI 1.73 to 3.01) µM (n=6) (figure 60).

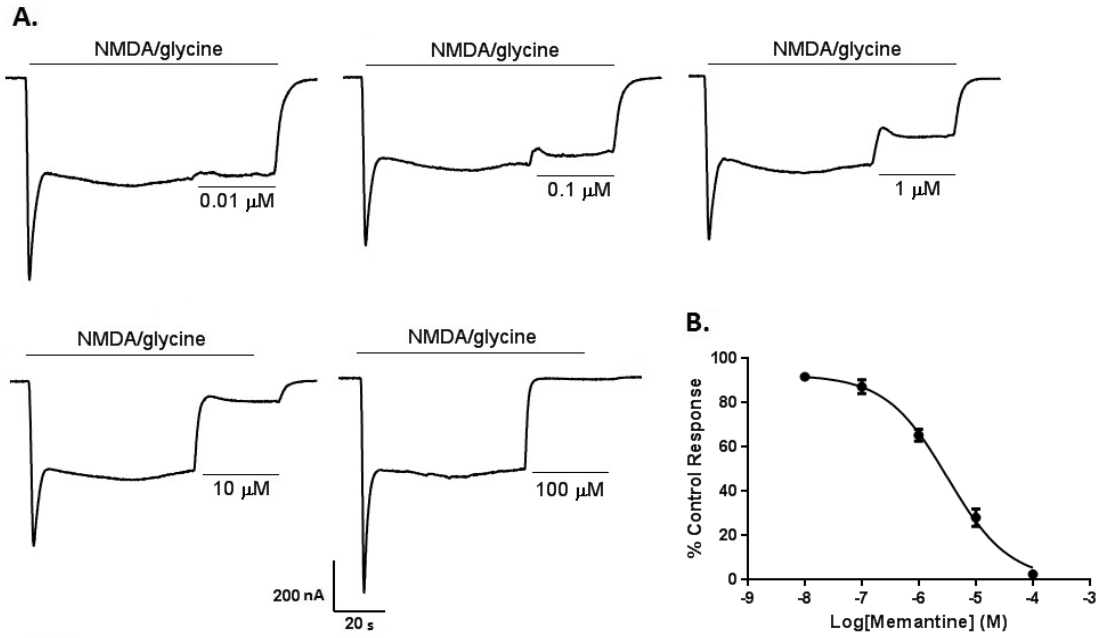


Figure 60: Concentration-dependent memantine block of NMDA/glycine responses in GluN1-1a/GluN2A-containing NMDA receptors.
(A) TEVC recordings for memantine (0.01–100 µM) block of NMDA/glycine responses at -60 mV on a single oocyte, (B) Concentration-inhibition curve for memantine block. Percentage control response (mean ± SEM, n=6) values were plotted and fitted with the Hill equation to yield an IC_{50} of 2.28 (95% CI 1.73 to 3.01) µM.

Based on its IC_{50} value of 2.28 µM, a memantine concentration of 3 µM was used to determine the voltage-dependent inhibition. Responses of NMDA antagonism by memantine on GluN1-1a/GluN2A was assessed at four different holding potentials, -40, -60, -80 and -100 mV. The δ value for memantine obtained from the voltage-dependent curve fitted with the Woodhull equation was 0.4 (95% CI 0.23 to 0.56). The results are presented in figure 61.

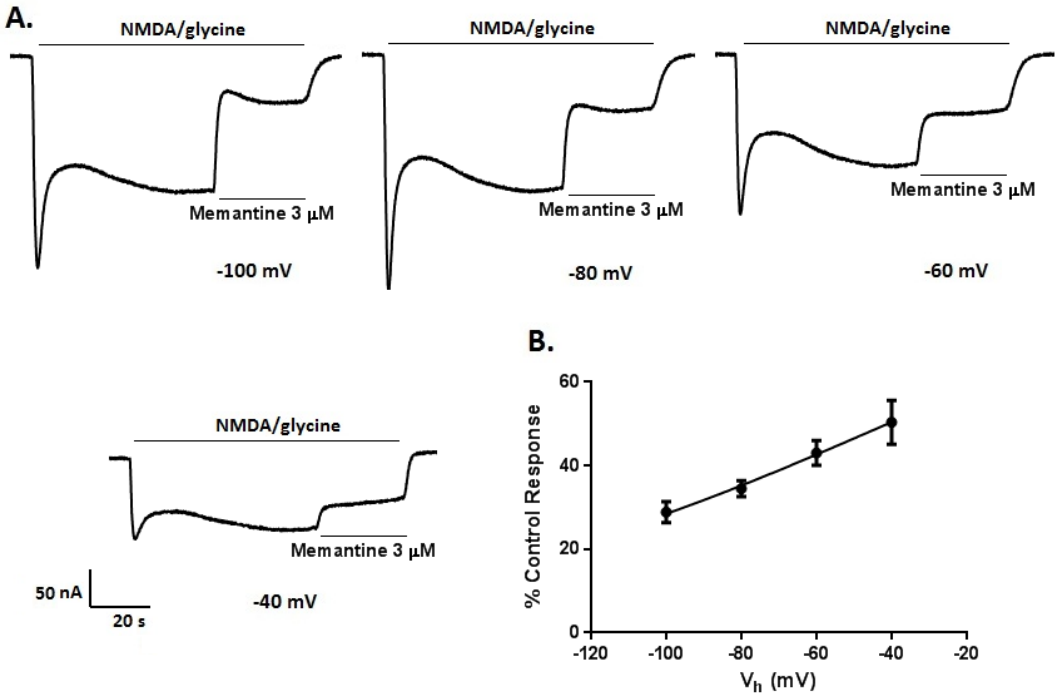


Figure 61: Voltage-dependent memantine (3 µM) block of NMDA/glycine in GluN1-1a/GluN2A-containing NMDA receptors.
(A) TEVC recordings of memantine block tested at -100, -80, -60 and -40 mV on a single oocyte, (B) Voltage-dependent inhibition curve for memantine block. Percentage control response (mean ± SEM, n=5) values were plotted and fitted with the Woodhull equation to yield the δ value.

5.3 MEMANTINE-DERIVATIVE (MAB) COMPOUNDS (i)

5.3.1 Concentration-Inhibition of Methoxyphenol-Containing MAB Compounds

The antagonism of responses to NMDA and glycine by memantine derivatives containing methoxyphenol moiety (MAB23(2), MAB14, MAB22 and MAB30) were examined. The compounds in tenfold increment of compound concentrations (0.01 to 100 µM) were tested on GluN1-1a/GluN2A at -60 mV to determine their IC_{50} values via the Hill equation. Examples of trace recordings of the compounds are presented in figure 62 below. Data were then fitted with the Hill equation to generate their concentration-inhibition curves and estimate the IC_{50}s.

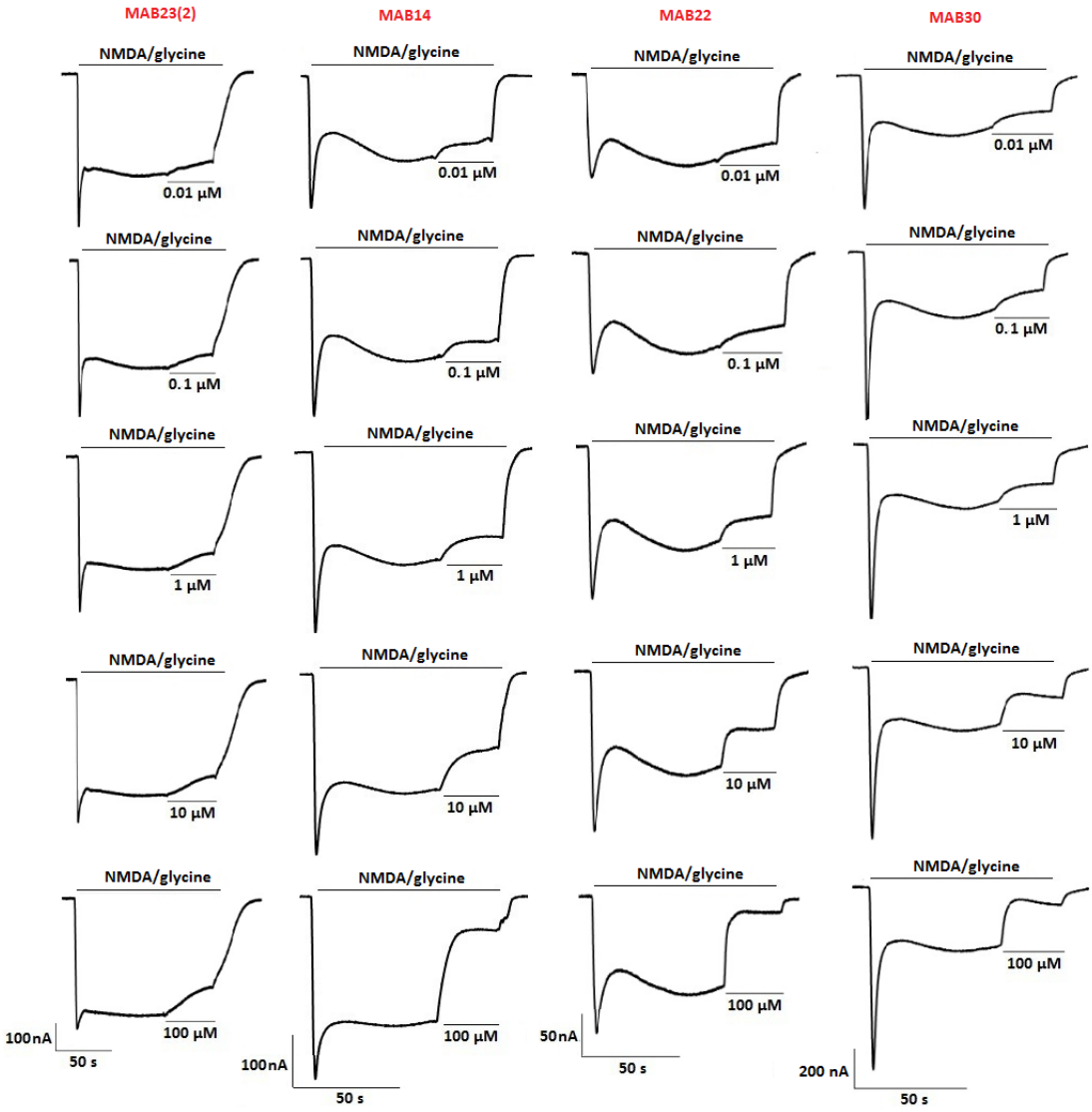
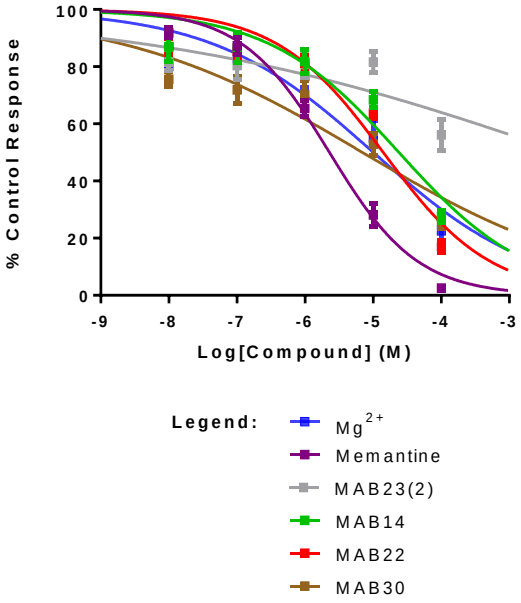


Figure 62: TEVC recordings for MAB23(2), MAB14, MAB22 and MAB30 (0.01–100 µM) block of NMDA/glycine responses at -60 mV on single oocytes.

All memantine-derivatives containing the methoxyphenol moiety exhibited low potency in blocking NMDA/glycine responses in GluN1-1a/GluN2A-containing NMDA receptors at -60 mV. This contrasts with Mg^{2+} and memantine which recorded an IC_{50} of 10.1 and 2.28 µM respectively; significantly lower than all of the compounds. At 26.9 µM, MAB22 recorded the lowest IC_{50}. MAB23(2) yielded a very wide 95% confidence interval and had an IC_{50} of more than 100 µM, thus suggesting its inefficacy. Concentration-inhibition curves for all compounds and their IC_{50}s are presented in figure 63.

A.



B.

Compounds	**IC_{50} (µM)** 95% CI
Mg^{2+}	**10.1** 2.48 to 17.7
Memantine	**2.28** 1.73 to 3.01
MAB14	**43.1** 24.2 to 62.0
MAB22	**26.9** 20.4 - 33.4
MAB30	**38.2** 15.7 to 60.7

Figure 63: Comparison of concentration-inhibition for MAB compounds (containing methoxyphenol moiety), Mg^{2+} and memantine block of NMDA/glycine responses in GluN1-1a/GluN2A NMDA receptors at -60 mV.
(A) Concentration-inhibition curves for the MAB compounds, Mg^{2+} and memantine block. Percentage control response (mean ± SEM) values were plotted and fitted with the Hill equation to estimate their IC_{50}s, (B) IC_{50} values for all compounds (n=6 for memantine, n=5 for all other compounds). 95% confidence intervals are also noted.

5.3.2 Concentration-Inhibition of Lipoic Acid-Containing MAB Compounds

Memantine derivatives containing lipoic acid moiety (MAB7, MAB15, MAB21 and MAB32) were diluted in NMDA/glycine solution in a range between 0.01 µM to 100 µM. Blocking potencies of the compounds at GluN1-1a/GluN2A were measured by electrophysiological recordings at -60 mV. Examples of the TEVC trace recordings are presented in figure 64. Data were then fitted with the Hill equation to generate their concentration-inhibition curves and estimate the IC_{50}s.

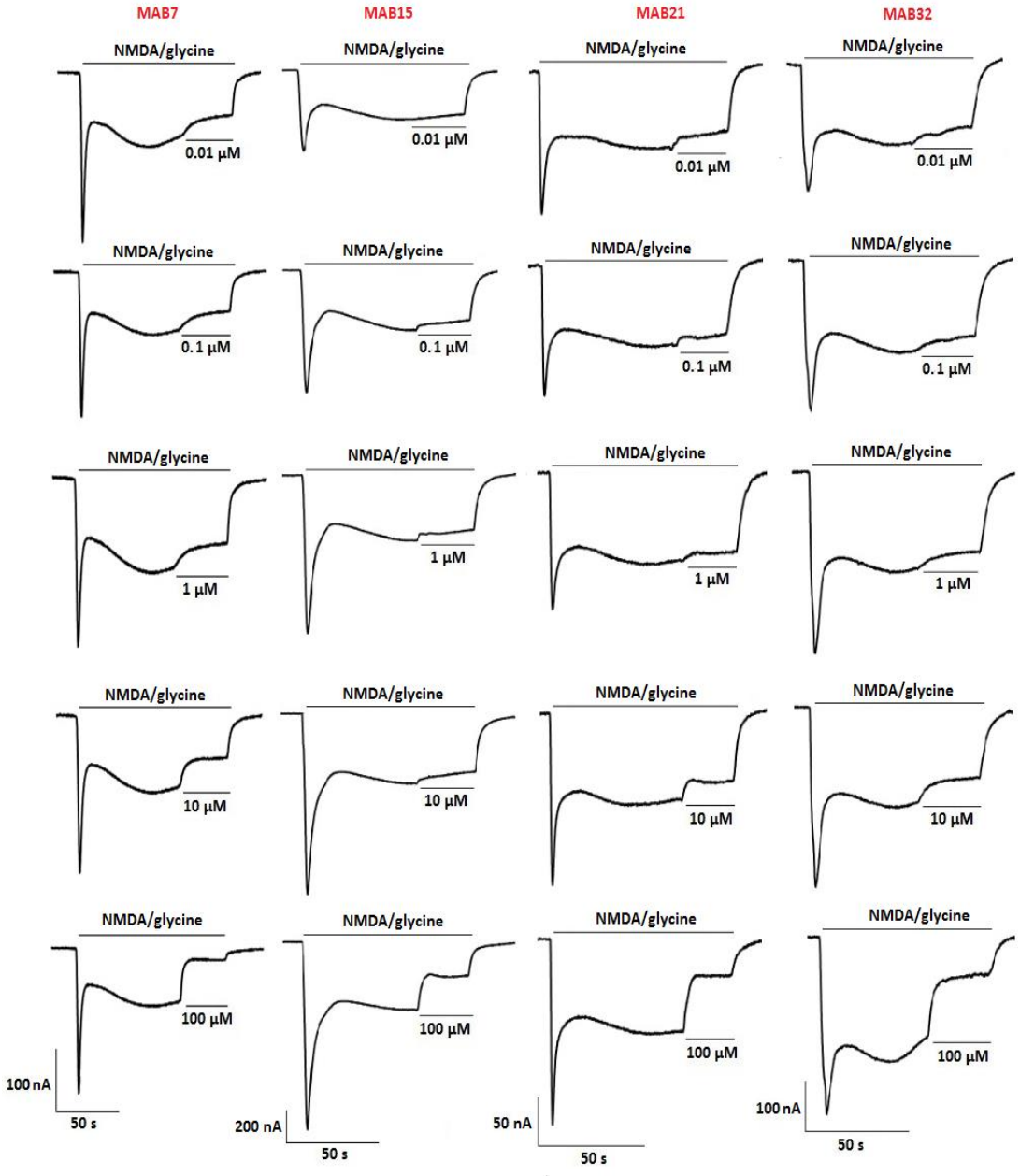


Figure 64: TEVC recordings for MAB7, MAB15, MAB21 and MAB32 (0.01–100 µM) block of NMDA/glycine responses at -60 mV on single oocytes.

Memantine-derivatives containing lipoic acid moiety demonstrated even lower antagonistic property to block NMDA/glycine responses in GluN1-1a/GluN2A-containing NMDA receptors at -60 mV. At 55.9 (95% CI 34.4 to 77.5) µM, MAB7 was the most potent compound, while the others recorded IC_{50}s of more than 100 µM. Concentration-inhibition curves for all compounds are presented in figure 65.

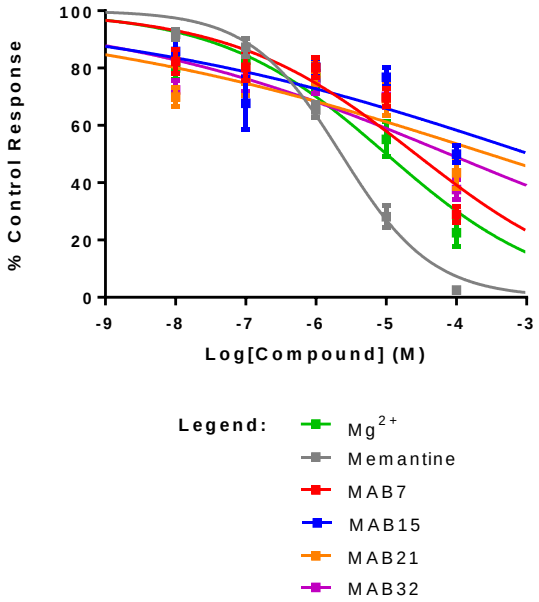


Figure 65: Comparison of concentration-inhibition curves for MAB compounds (containing lipoic acid moiety), Mg^{2+} and memantine block of NMDA/glycine responses in GluN1-1a/GluN2A NMDA receptors at -60 mV.
Percentage control response (mean ± SEM) values were plotted and fitted with the Hill equation (n=6 for memantine, n=5 for all other compounds).

5.3.3 Voltage-Dependence of MAB Compounds

The MAB compounds with considerable blocking properties were assessed for voltage-dependency. The compounds were diluted to their IC_{50} concentrations and block of NMDA/glycine responses mediated by GluN1-1a/GluN2A was measured at four different holding potentials (-40, -60, -80 and -100 mV) across several batches of oocytes. Examples of the TEVC trace recordings are presented in figure 66. Data were fitted with the Woodhull equation to determine their δ values.

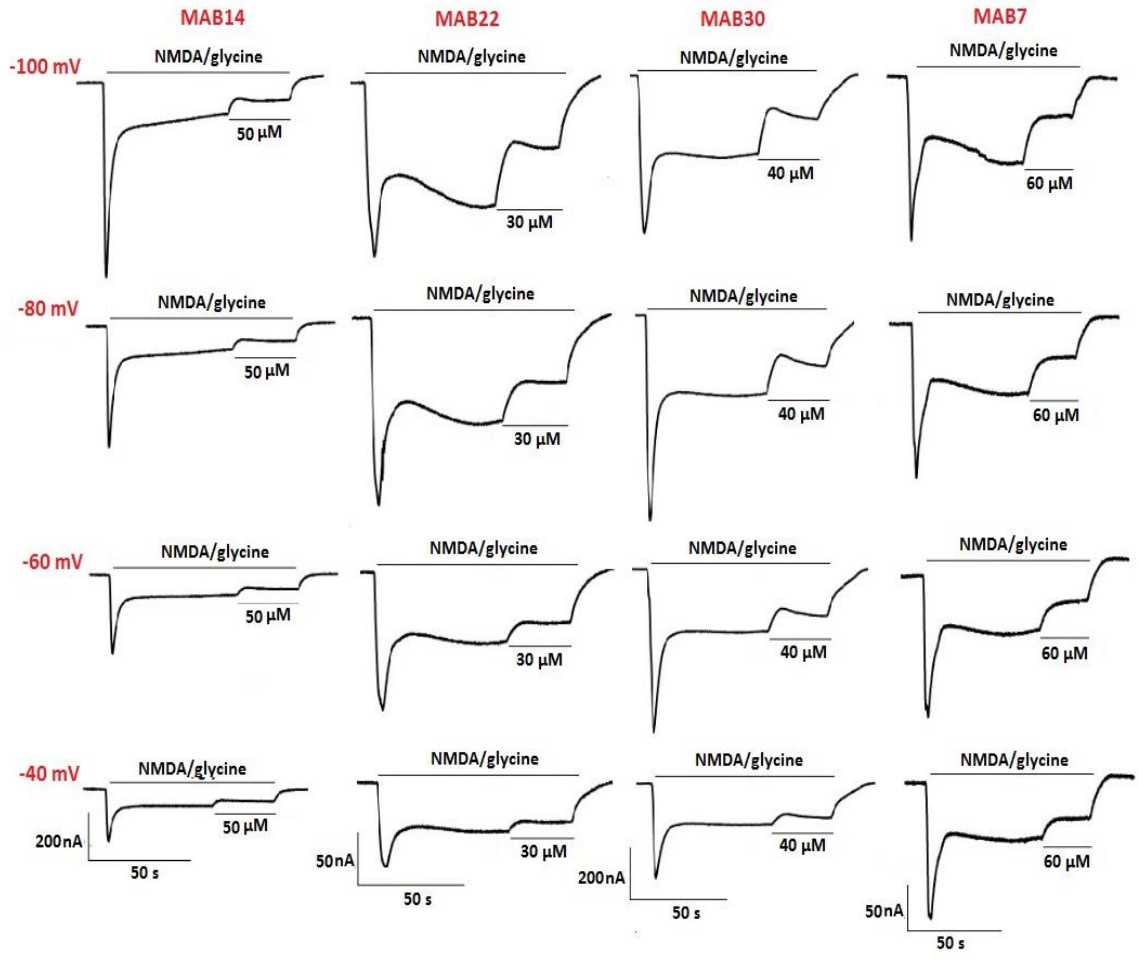
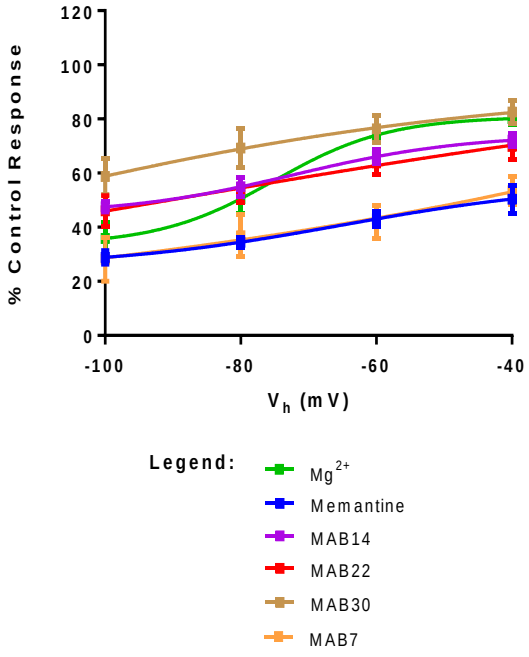


Figure 66: TEVC recordings of MAB compounds (MAB14, MAB22, MAB30 and MAB7) voltage-dependent block of NMDA/glycine responses in GluN1-1a/GluN2 NMDA receptors tested at -100, -80, -60 and -40 mV on single oocytes.

Voltage-dependent block was assessed to calculate an approximate distance across the electric field that the binding site is located. Figure 67 A displays the voltage-dependent inhibition curves fitted according to the Woodhull model. The results of this study showed that three of the memantine-derivative compounds yielded δ values comparable to memantine. MAB14, MAB22, MAB30 and MAB7 each had δ values of 0.46 (95% CI 0.32 to 0.6), 0.43 (95% CI 0.19 to 0.67), 0.51 (95% CI 0.15 to 0.87) and 0.4 (0.09 – 0.78) respectively, which are just slightly higher to that of memantine, 0.4 (95% CI 0.23 to 0.56). These compounds may have a shallow binding block due to their relatively small δ values, but deeper than memantine.

A.



B.

Compounds	δ (95% CI)
Mg^{2+}	**1.48** -0.48 to 3.44
Memantine	**0.4** 0.23 to 0.56
MAB14	**0.46** 0.322 to 0.595
MAB22	**0.43** 0.19 to 0.67
MAB30	**0.51** 0.15 to 0.87
MAB 7	**0.44** 0.09 to 0.78

Figure 67: Comparison of voltage-dependent inhibition of MAB compounds (containing methoxyphenol moiety), Mg^{2+} and memantine block of NMDA/glycine responses in GluN1-1a/GluN2A NMDA receptors.

(A) Voltage-dependent curves for MAB compounds, Mg^{2+} and memantine at four holding potentials, -100, -80, -60 and -40 mV. Percentage control response (mean ± SEM) values were plotted and fitted with the Woodhull model to yield the δ values, (B) δ (95% CI) values of the compounds obtained from the voltage-dependent curves (n=3 for Mg^{2+}, n=5 for memantine, n=6 for MAB14, MAB22 and MAB30, n=5 for MAB7). δ is the estimated position of the binding site within the electric field.

5.4 MEMANTINE-DERIVATIVE (FC/GB) COMPOUNDS (ii)

5.4.1 Concentration-Inhibition of Methoxyphenol-Containing FC Compounds

FC compounds, derived from memantine containing methoxyphenol moiety (FC7, FC12 and FC17) were diluted in NMDA/glycine solution in a range between 0.01 µM to 100 µM. Blocking potency of the compounds at GluN1-1a/GluN2A were measured by electrophysiological recordings at -60 mV. Examples of the TEVC trace recordings are presented in figure 68. Data were then fitted with the Hill equation to generate their concentration-inhibition curves and estimate the IC_{50}s.

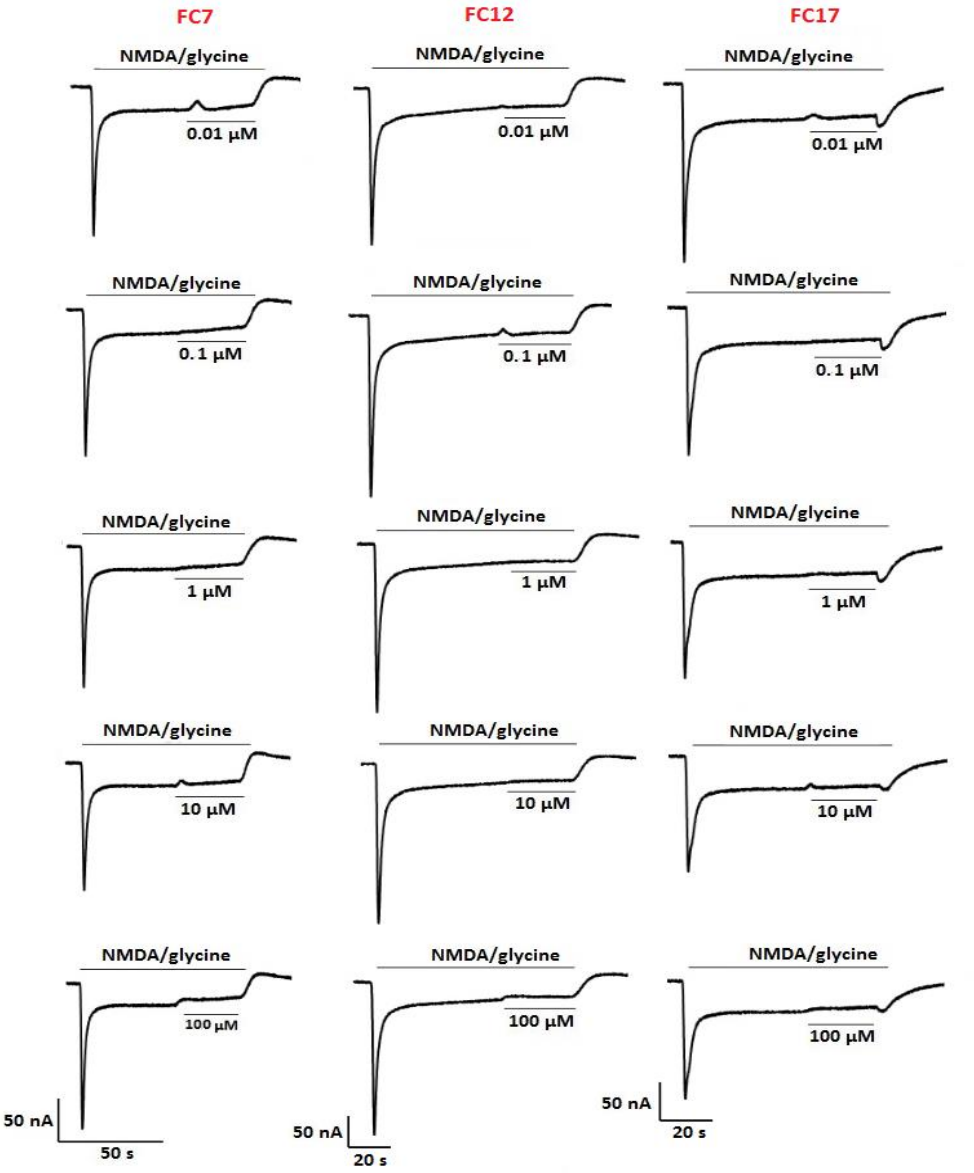


Figure 68: TEVC recordings of FC7, FC12 and FC17 (0.01–100 µM) block of NMDA/glycine responses at -60 mV on single oocytes.

5.4.2 Concentration-Inhibition of Catechol-Containing FC/GB Compounds

The antagonism of responses to NMDA and glycine by memantine derivatives containing a catechol moiety (FC20 and GB13) were examined. The compounds in tenfold increasing concentration (0.01 to 100 µM) were tested on GluN1-1a/GluN2A at -60 mV to determine their IC_{50} values via the Hill equation. Examples of trace recordings of the compounds are presented in figure 69 below. Data were fitted with the Hill equation to generate their concentration-inhibition curves and estimate the IC_{50}s.

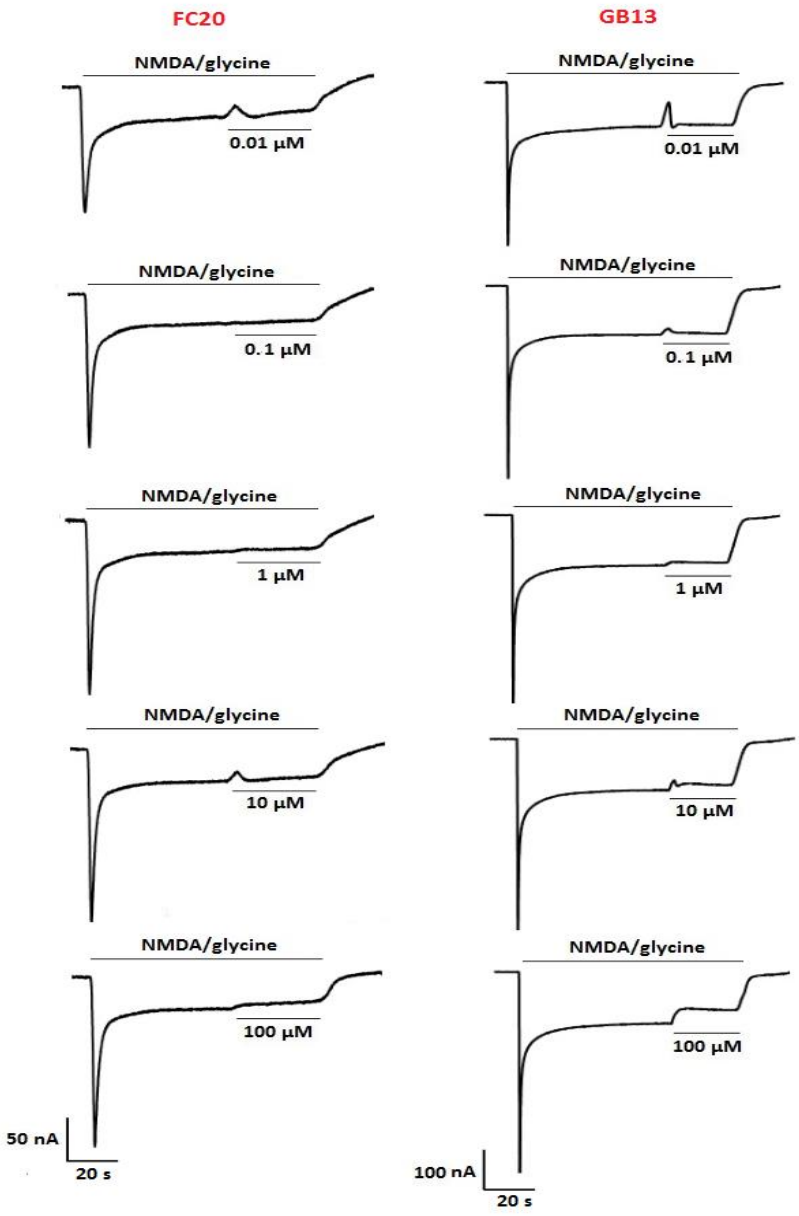


Figure 69: TEVC recordings of FC20 and GB13 (0.01–100 µM) block of NMDA/glycine responses at -60 mV on single oocytes.

All compounds in this series exhibited low potency (or none at all) to block NMDA/glycine responses in GluN1-1a/GluN2-containing NMDA receptors at -60 mV. When extrapolated in the concentration-inhibition curves (figure 70), the FC compounds will yield extremely high IC_{50}s (more than 100 µM). GB13 was the most potent with an IC_{50} of 68.7 (95% CI 37.7 to 99.6) µM. Due to their ineffectiveness in blocking the NMDA receptor channel, voltage-dependent analysis was not further investigated for this series of memantine-derivative compounds. Concentration-inhibition curves for the compounds are presented in figure 70.

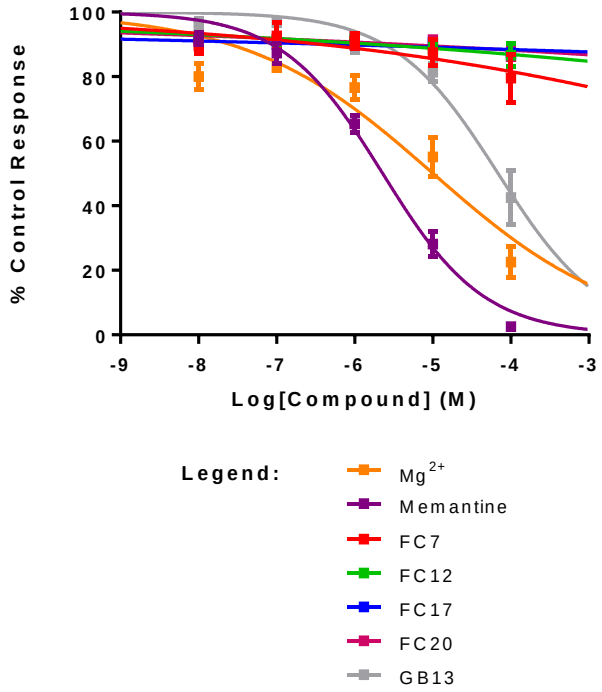


Figure 70: Comparison of concentration-inhibition relationship for FC/GB compounds, Mg^{2+} and memantine block of NMDA/glycine responses in GluN1-1a/GluN2A NMDA receptors at -60 mV.

Percentage control response (mean ± SEM) values were plotted and fitted with the Hill equation to estimate their IC_{50}s (n=5 for Mg^{2+}, n=6 for memantine, FC7 and FC12, n=7 for FC17, n=8 for FC20 and n=10 for GB13).

5.5 SPERMINE-DERIVED POLYAMINE (CR) COMPOUNDS

5.5.1 Concentration-Inhibition of CR Compounds

The antagonism of responses to NMDA and glycine by spermine-derived polyamine compounds (CR8, CR18 and CR24) were examined. The compounds in tenfold increment of compound concentrations (0.01 to 100 µM) were tested on GluN1-1a/GluN2A at -60 mV to determine their IC_{50} values via the Hill equation. Examples of trace recordings of the compounds are presented in figure 71 below. Data were then fitted with the Hill equation to generate their concentration-inhibition curves and estimate the IC_{50}s.

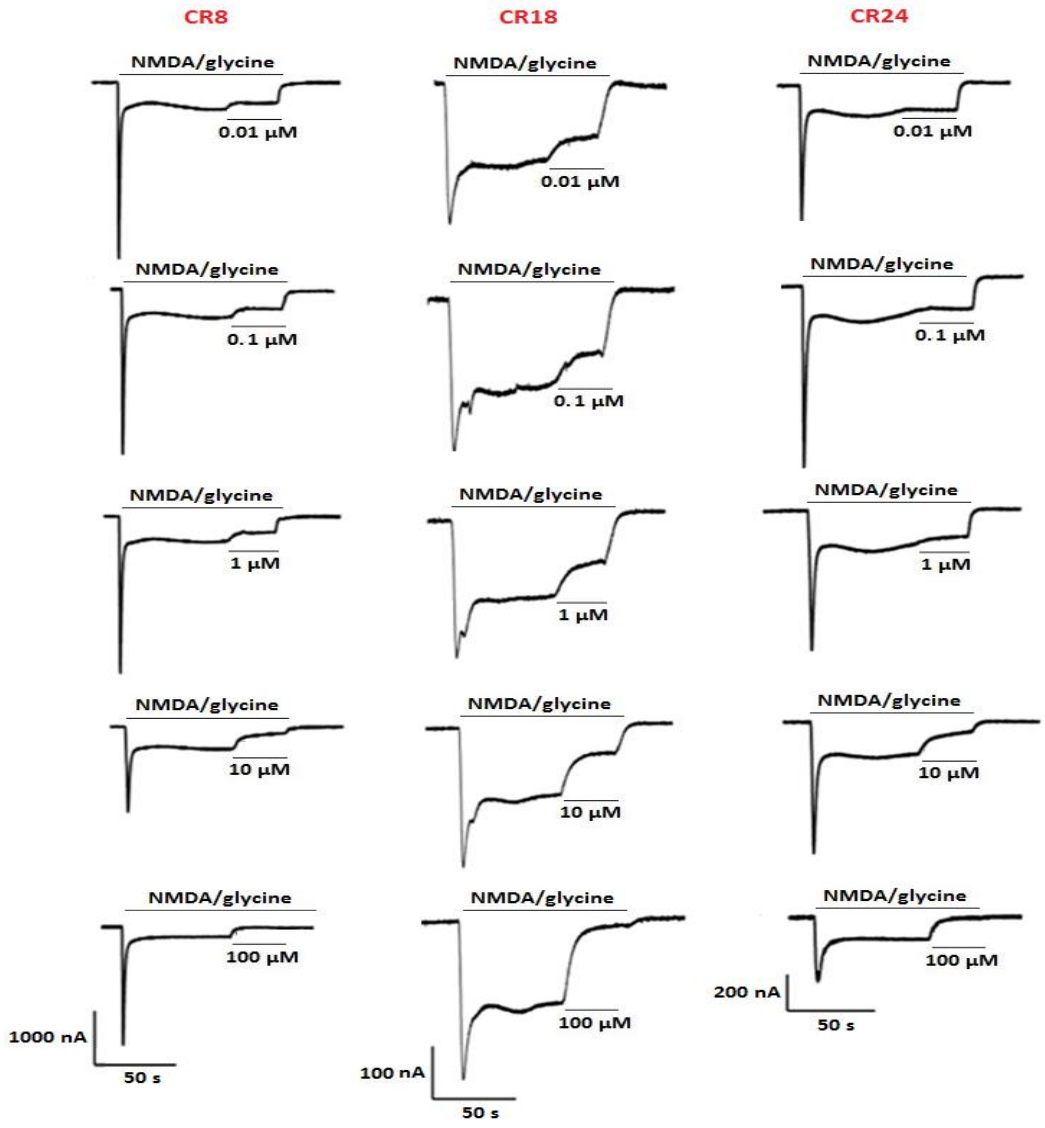
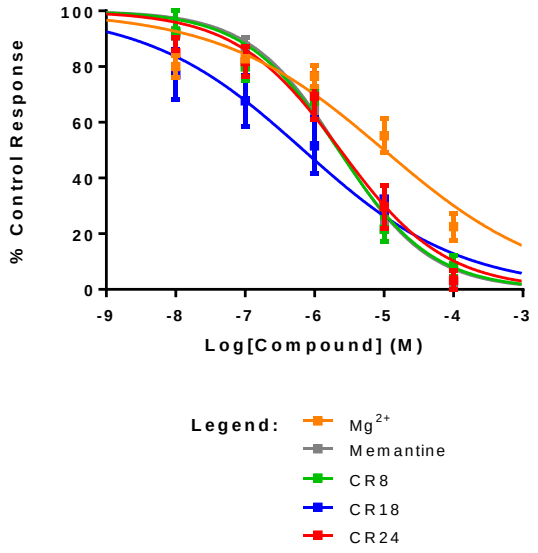


Figure 71: TEVC recordings of CR8, CR18 and CR24 (0.01–100 µM) block of NMDA/glycine responses at -60 mV on single oocytes.

All of the spermine-derived CR compounds were found to be highly effective in blocking NMDA/glycine responses in GluN1/GluN2-containing NMDA receptors at -60 mV. While all CR compounds displayed significantly lower IC_{50}s compared to Mg^{2+}, CR18 was the most potent with IC_{50} of 0.69 (95% CI -0.001 to 1.39) µM. At the highest concentration of 100 µM, CR18 completely blocked NMDA/glycine responses in four out of six oocytes tested, with an average of 100.6% inhibition. At the lowest concentration of 0.01 µM, CR18 averaged 21.0% inhibition. CR8 and CR24 were slightly less potent displaying similar potencies with IC_{50} of 2.21 (95% CI 0.95 to 3.48) and 2.35 (95% CI 0.73 to 3.98) µM respectively. The results are displayed in figure 72 below.

A.



B.

Compound	IC_{50} (95% CI) µM
Mg^{2+}	**10.1** 2.48 to 17.7
Memantine	**2.28** 1.73 to 3.01
CR8	**2.21** 0.95 to 3.48
CR18	**0.69** -0.001 to 1.39
CR24	**2.35** 0.73 to 3.98

Figure 72: Comparison of concentration-inhibition for CR compounds, Mg^{2+} and memantine block of NMDA/glycine responses in GluN1-1a/GluN2A NMDA receptors at -60 mV.

(A) Concentration-inhibition curves for CR compounds, Mg^{2+} and memantine block. Percentage control response (mean ± SEM) values were plotted and fitted with the Hill equation to estimate their IC_{50}s, (B) IC_{50} values for all compounds (n=5 for Mg^{2+}, CR8 and CR24, n=6 for memantine and CR18). 95% confidence intervals are also noted.

5.5.2 Voltage-Dependence of CR Compounds

CR compounds were diluted to their IC_{50} concentrations and used to examine the voltage-dependent inhibition. Antagonism of NMDA/glycine responses by the CR compounds were assessed at four voltages, -40, -60, -80 and -100 mV on *Xenopus* oocytes expressing GluN1-1a/GluN2A NMDAR subunits. Examples of trace recordings of the compounds are presented in figure 73 below. δ values for the compounds were then obtained from voltage-dependent curves fitted with the Woodhull equation.

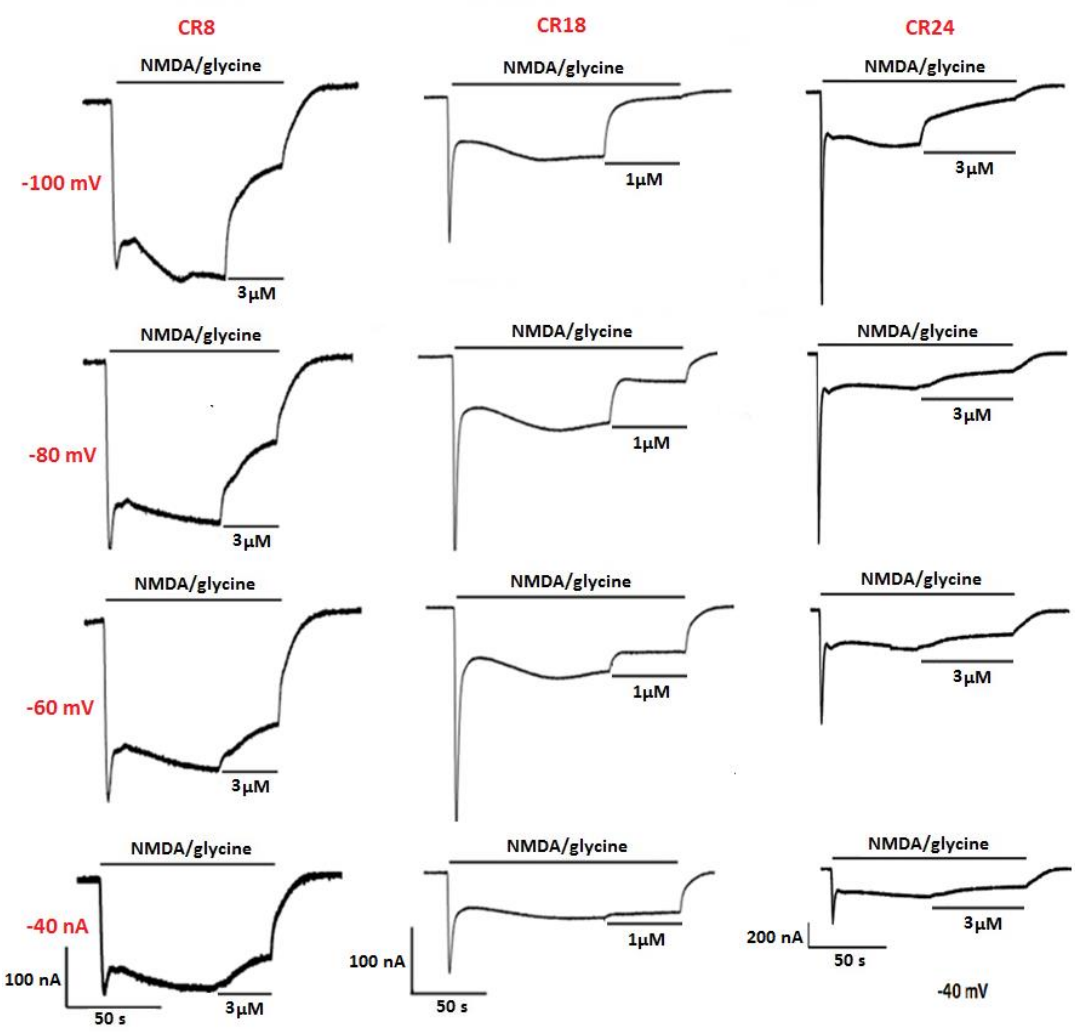
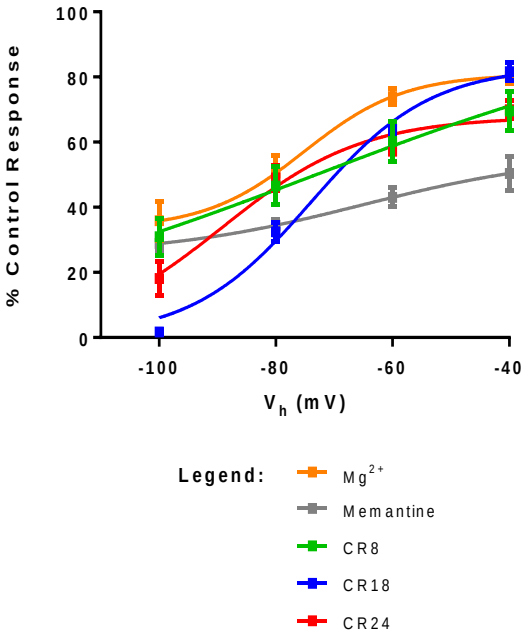


Figure 73: TEVC recordings of CR compounds (CR8, CR18 and CR24) voltage-dependent block of NMDA/glycine responses in GluN1-1a/GluN2 NMDA receptors tested at -100, -80, -60 and -40 mV on single oocytes.

Voltage-dependent block was assessed to calculate an approximate distance across the electric field where the binding site is located. Figure 74 A displays the voltage-dependent inhibition curves fitted according to the Woodhull model. The results of this study revealed that CR8 and CR24 may have a shallower binding block compared to memantine due to their smaller δ values; 0.33 (95% CI -2.37 to 3.04) for CR8 and 0.21 (95% CI -0.18 to 0.6) for CR24. CR18's calculated δ was 0.82 (95% CI 0.43 to 1.21), higher than memantine suggesting a deeper binding site (figure 74 B).

A.



B.

Compound	δ (95% CI)
Mg^{2+}	**1.48** -0.48 to 3.44
Memantine	**0.4** 0.23 to 0.56
CR8	**0.33** -2.37 to 3.04
CR18	**0.82** 0.43 to 1.21
CR24	**0.21** -0.18 to 0.6

Figure 74: Comparison of voltage-dependent inhibition for CR compounds block of NMDA/glycine in GluN1-1a/GluN2A-containing NMDA receptors.

(A) Concentration-inhibition curves for CR compounds at four holding potentials, -100, -80, -60 and -40 mV. Only CR8 and CR18 display a significant difference between them (p=0.0032), (B) δ (95% CI) values of the compounds obtained from the voltage-dependent curves (n=3 for Mg^{2+}, n=5 for all other compounds). δ is the estimated position of the binding site within the electric field.

5.6 DONEPEZIL-DERIVED (MGM) COMPOUNDS

5.6.1 Antagonistic Responses on NMDA Receptor

The antagonism of NMDA and glycine responses by donepezil-derived compounds in tenfold increment of the compound concentrations (0.01 to 100 µM) mediated by GluN1-1a/GluN2A were employed to determine their IC_{50} values at three holding potentials; -50, -80 and -100 mV. MGM2, MGM3 and MGM11 compounds were found to be weak NMDAR blockers. MGM2 and MGM11 were the weakest NMDAR blockers as at all concentrations, only 10% NMDA inhibition at all voltages were found with slight potentiation at higher concentration for MGM11. MGM3 showed a backward concentration-inhibition trend; i.e. the highest NMDA block was at the lowest concentration (0.01 µM) with about 15% inhibition at all voltages tested. Examples of their traces showing their weak antagonistic properties are presented in figures 75-77 where the concentration-inhibition curves were not able to be fitted into the Hill equation and thus unable to calculate their IC_{50}s.

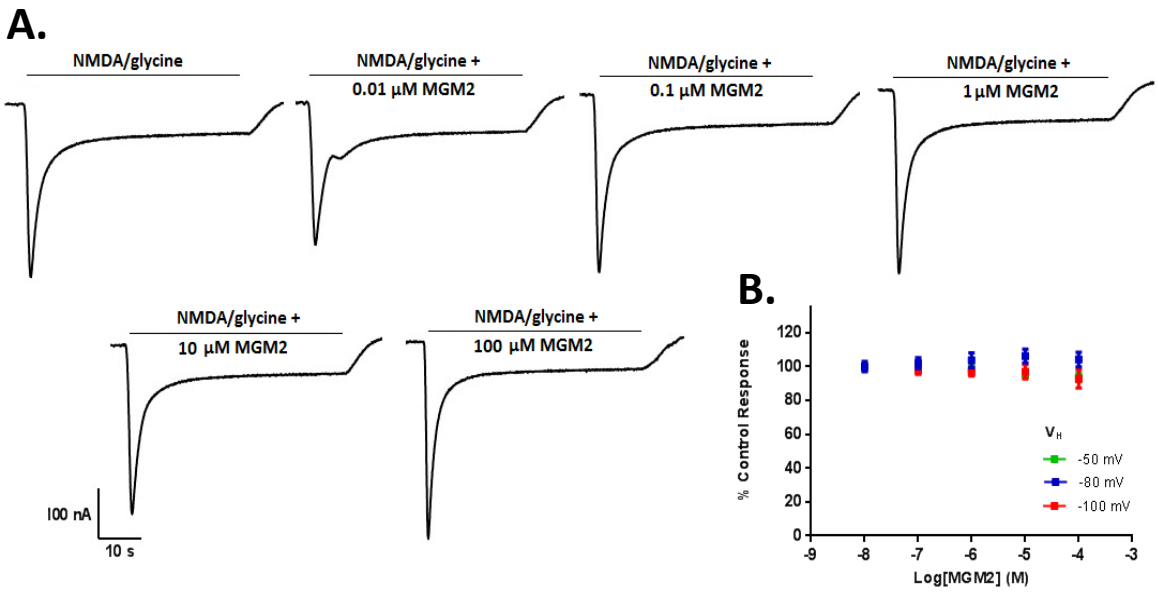


Figure 75: Concentration-inhibition relationship of MGM2 block on GluN1-1a/GluN2A-containing NMDA receptors.

(A) Example of TEVC recordings for MGM2 (0.01–100 µM) block of NMDA/glycine at -50 mV on a single oocyte, (B) Concentration-inhibition relationship for MGM2 block. Percentage control response (mean ± SEM, n=3-4) values were plotted.

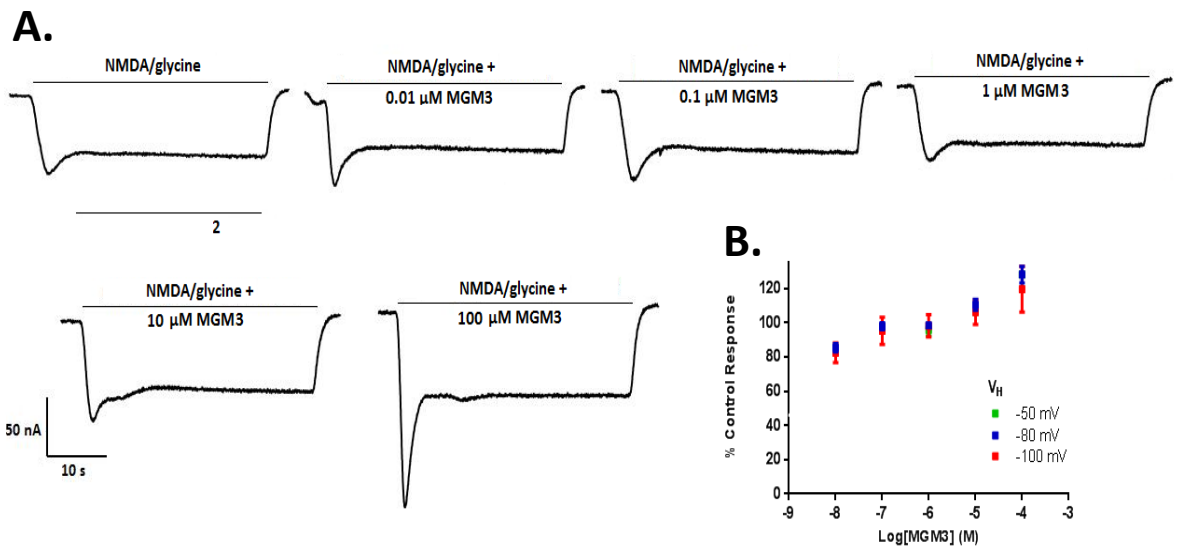


Figure 76: Concentration-inhibition relationship of MGM3 block on GluN1-1a/GluN2A-containing NMDA receptors.

(A) Example of TEVC recordings for MGM3 (0.01–100 µM) block of NMDA/glycine at -80 mV on a single oocyte, (B) Concentration-inhibition relationship for MGM3 block. Percentage control response (mean ± SEM, n=2-3) values were plotted.

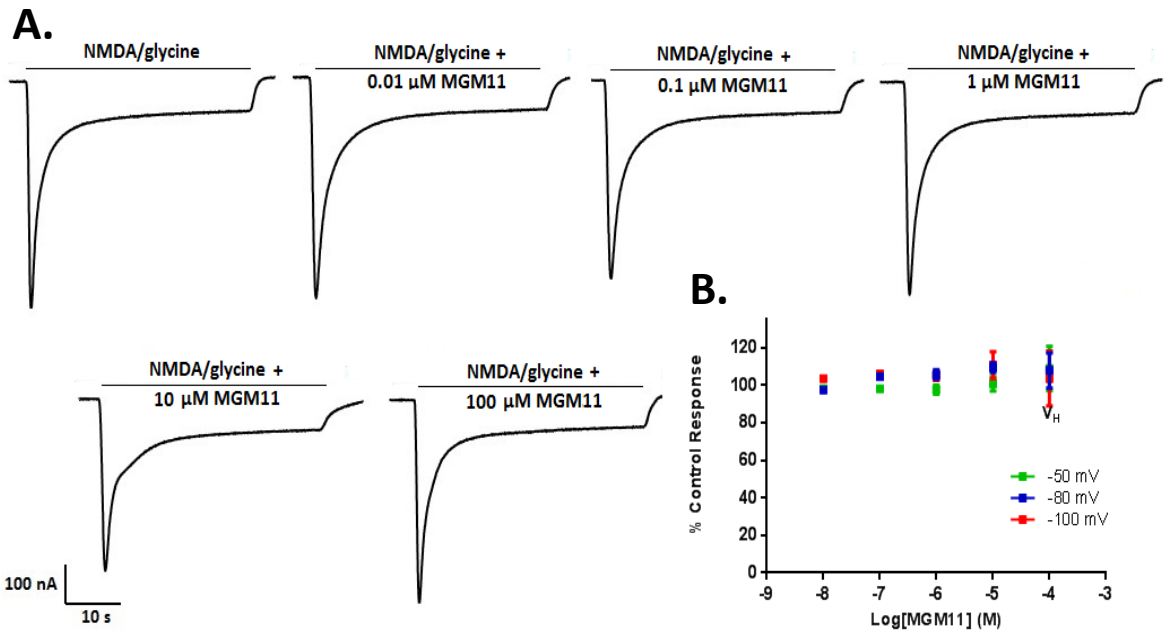


Figure 77: Concentration-inhibition relationship of MGM11 block on GluN1-1a/GluN2A-containing NMDA receptors.

(A) Example of TEVC recordings for MGM11 (0.01–100 µM) block of NMDA/glycine at -100 mV on a single oocyte, (B) Concentration-inhibition relationship for MGM11 block. Percentage control response (mean ± SEM, n=2) values were plotted.

MGM10 exhibited some potency to inhibit NMDA and glycine although very weakly with IC_{50}s obtained from the concentration-inhibition curves were more than 200 µM at all three holding potentials. Blocking potencies tended to reduce with a more negative holding potential. The results were considered ambiguous as the number of oocytes tested were also small. The trace recordings and concentration inhibition curves are presented in figure 78.

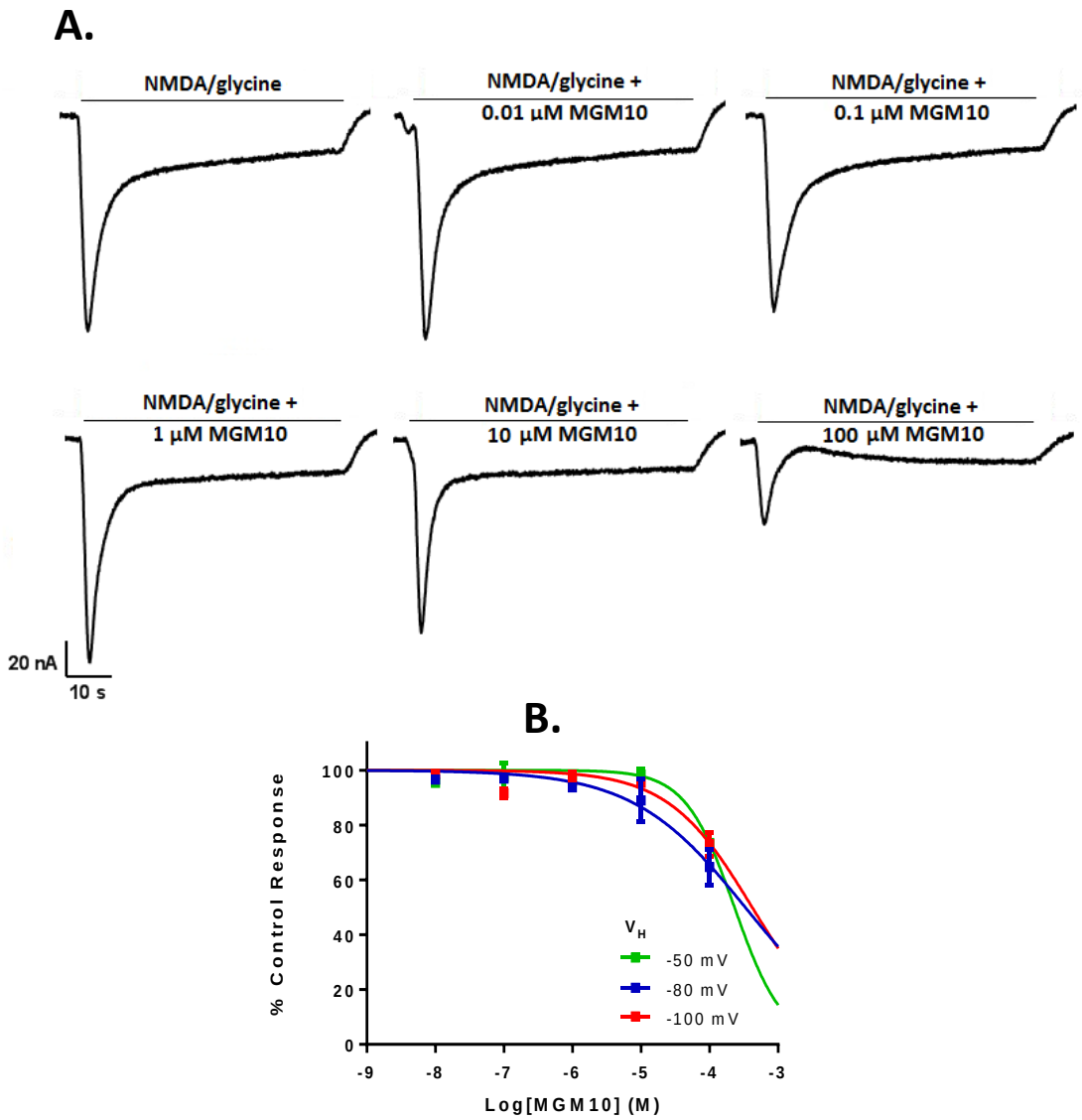
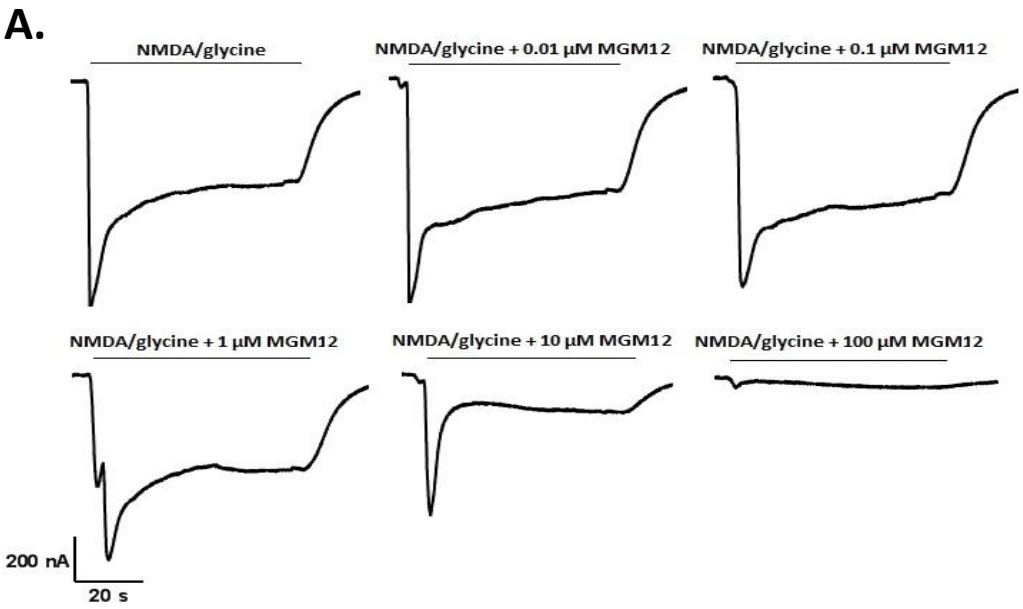


Figure 78: MGM10 block of NMDA/glycine responses in GluN1-1a/GluN2A-containing NMDA receptors.

(A) Example of TEVC recordings for MGM10 (0.01–10 µM) block at -80 mV, (B) Concentration-inhibition curves for MGM10. Percentage control response (mean ± SEM, n=2) values plotted and fitted with Hill equation.

MGM12 was the most potent NMDAR blocker of all donepezil-derived compounds tested. IC_{50}s obtained from the concentration-inhibition curves were 204.9, 12.6 and 7.02 µM recorded at -50, -75 and -100 mV respectively. IC_{50} at -50 mV was significantly lower compared to both at -80 mV (p=0.0291) and at -100 mV (p=0.0012) suggesting the voltage-dependence block of NMDA/glycine by MGM12. δ value obtained from the voltage-dependent curve fitted with Woodhull equation was 2.79 (95% CI -3.2 to 8.8). The results are shown in figure 79.



B.

IC_{50} (95% CI) µM	
-50 mV	**204.9** 13.8 to 3046
-80 mV	**12.6** 3.04 to 52.0
-100 mV	**7.02** 2.61 to 18.9

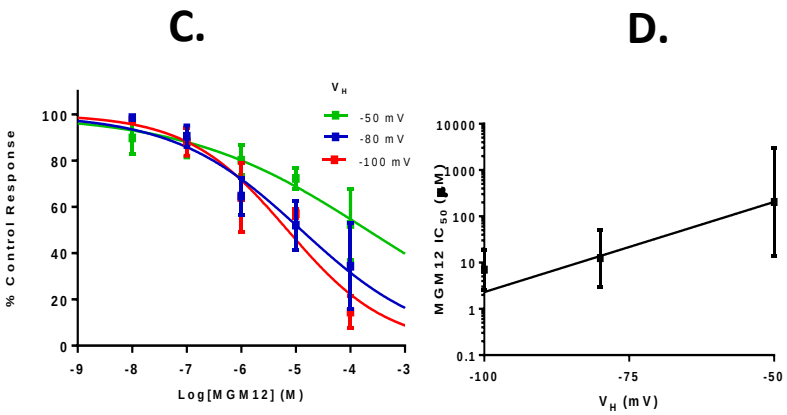


Figure 79: MGM12 block of NMDA/glycine responses in GluN1-1a/GluN2A-containing NMDA receptors.

(A) Example of TEVC recordings for MGM12 (0.01–10 µM) block at -80 mV, (B) IC_{50} (95% CI) values for MGM12, (C) Concentration-inhibition curves for MGM12. Percentage control response (mean ± SEM, n=3) values plotted and fitted with Hill equation, (D) Voltage-dependent inhibition curve for MGM12 block, IC_{50} (95% CI) values plotted and fitted with Woodhull equation to yield the δ value.

5.6.2 Responses on Nicotinic Receptors

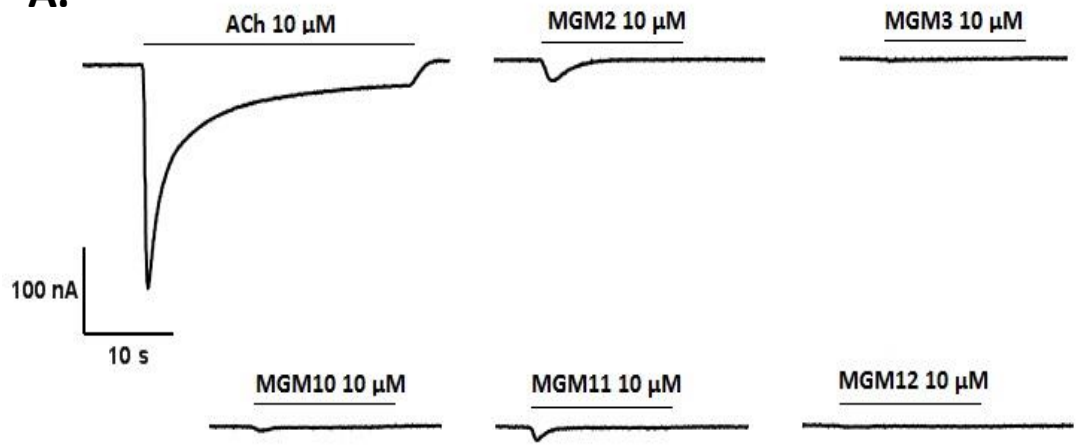
Due to the low blocking potencies on NMDAR, this study subsequently examined what kind of effect the MGM compounds would exert on nicotinic receptors when applied alone and also when co-applied with ACh. Previous ligand-binding studies have shown that donepezil-derived compounds could bind to the ACh binding site thus could be agonists or competitive antagonists. Two functional subunit combinations of nicotinic receptors were tested in this study; α4β2 and α7.

5.6.2.1 Agonistic Responses on Nicotinic Receptors

To assess whether the donepezil-derived MGM compounds would exert any agonistic properties in nicotinic receptors, they were diluted to 10 µM concentration in *Xenopus* ringer and were applied onto α4β2 and α7. Electrophysiology recordings were conducted at -80 mV with TEVC and the percentage of evoked currents in comparison to the control agonist (10 µM ACh) were determined.

The compounds did not elicit any responses with α7 nAChRs. In α4β2, all the compounds evoked small inward currents suggesting weak agonistic behaviour as presented in figure 80.

A.



B.

Compound (10 µM)	Response (%)
ACh	100.0
MGM2	4.758
MGM3	1.424
MGM10	0.442
MGM11	2.666
MGM12	0.340

C.

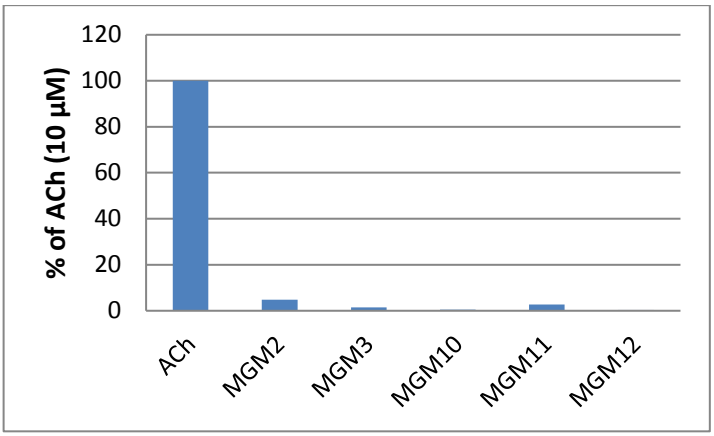
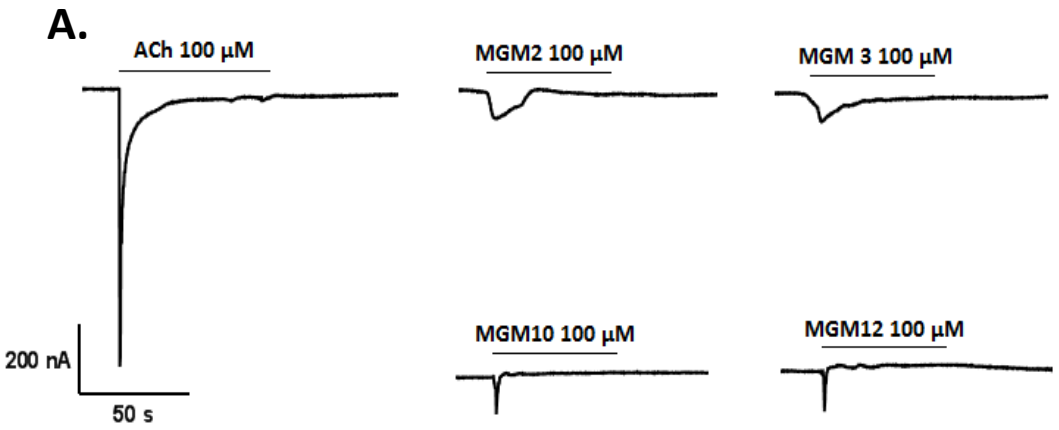


Figure 80: Agonistic responses of MGM compounds (10 µM) on α4β2 nicotinic receptor.
(A) Example of recordings of ACh and MGM compound (10 µM) evoked responses on α4β2 nicotinic receptor on a single oocyte, (B) Mean percentage control response (n=9) of MGM compounds against ACh, and (C) the corresponding bar graph of MGM responses.

The compounds were subsequently dissolved in *Xenopus* ringer to a higher concentration of 100 µM (except MGM11 due to limited availability) and compared with 100 µM ACh to assess whether this would increase agonistic properties. As expected, the evoked inward currents in α4β2 were larger and the percentage control responses were between 15 to 22% as presented in figure 81. No responses were evoked in α7. This data suggest that the MGM compounds may be partial agonists for α4β2 but not α7 nAChRs.



B.

Compound (100 µM)	Response (%)
ACh	100.0
MGM2	19.159
MGM3	14.907
MGM10	21.867
MGM12	17.814

C.

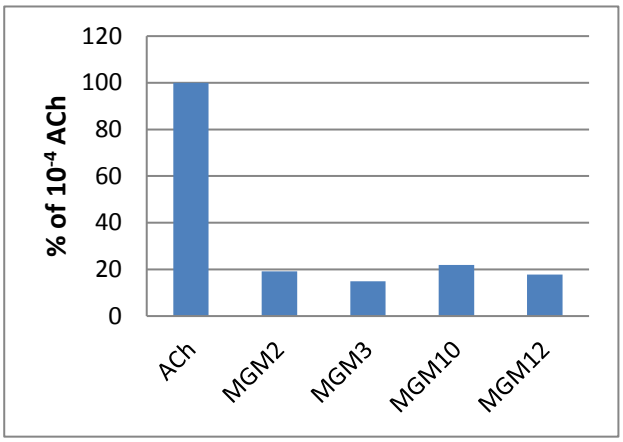


Figure 81: Agonistic responses of MGM compounds (100 µM) on α4β2 nicotinic receptor
(A) Example of recordings of ACh and MGM compound (100 µM) evoked responses on α4β2 nicotinic receptor recorded at -80 mV on a single oocyte, (B) Mean percentage control response (n=6) of MGM compounds against ACh, and (C) the corresponding bar graph of MGM responses.

5.6.2.2 Antagonistic Responses on α4β2 Nicotinic Receptors

All donepezil-derived compounds except MGM12 exhibited low blocking potency of ACh responses on α4β2 nicotinic receptors. Interestingly, MGM2, MGM3 and MGM10 appeared to potentiate responses suggesting they may exhibit, to a certain extent, positive allosteric modulatory property. MGM11 was less consistent with a much weaker inhibitory effect. Traces and concentration-inhibition relationship of these four compounds are displayed in figures 82-85.

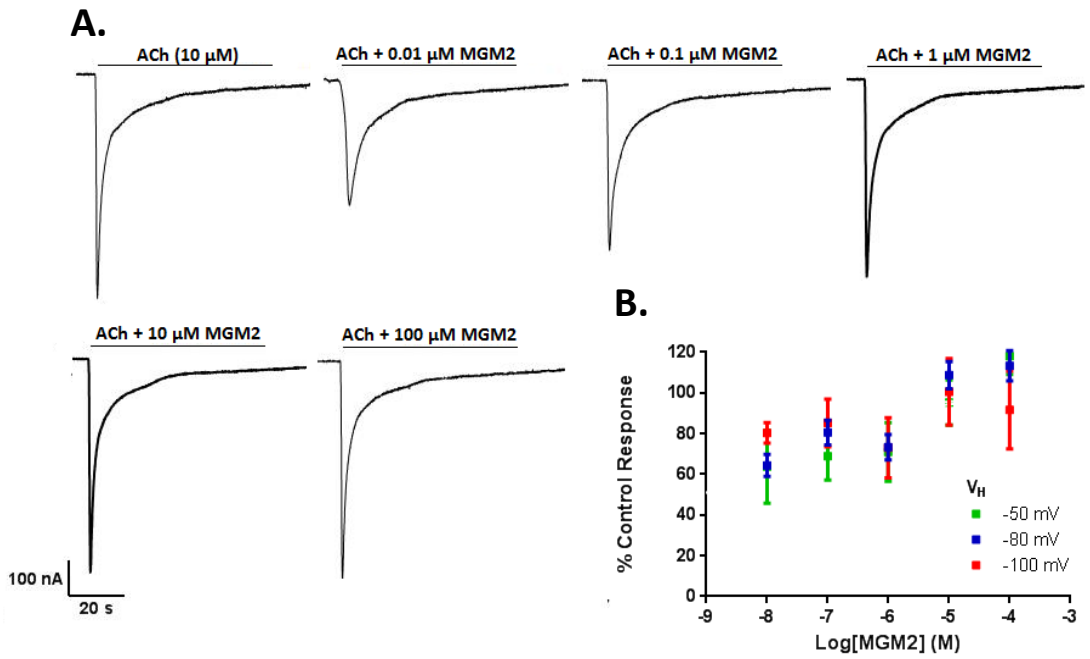


Figure 82: MGM2 block of ACh responses on α4β2 nicotinic receptor.

(A) Example of TEVC recordings for MGM2 (0.01–100 µM) block of ACh responses at -80 mV on a single oocyte, (B) Concentration-inhibition relationship for MGM2 block recorded at three holding potentials (-50, -80 and -100 mV). Percentage control response (mean ± SEM, n=2-5) values were plotted.

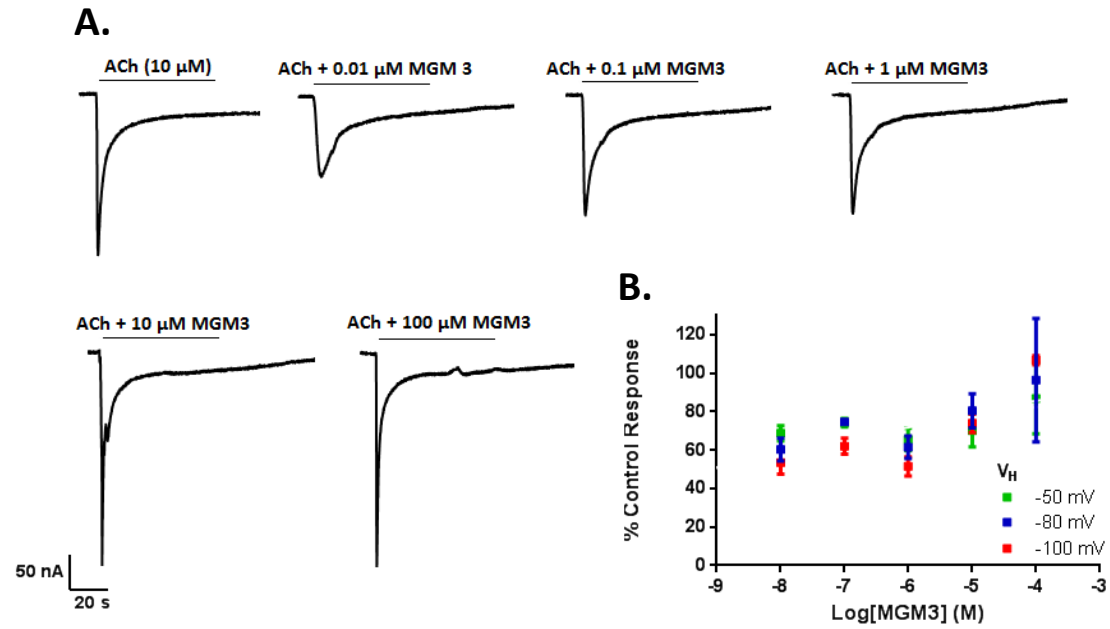


Figure 83: MGM3 block of ACh responses on α4β2 nicotinic receptor.

(A) Example of TEVC recordings for MGM3 (0.01–100 µM) block of ACh responses at -80 mV on a single oocyte, (B) Concentration-inhibition relationship for MGM3 block recorded at three holding potentials (-50, -80 and -100 mV). Percentage control response (mean ± SEM, n=3-4) values were plotted.

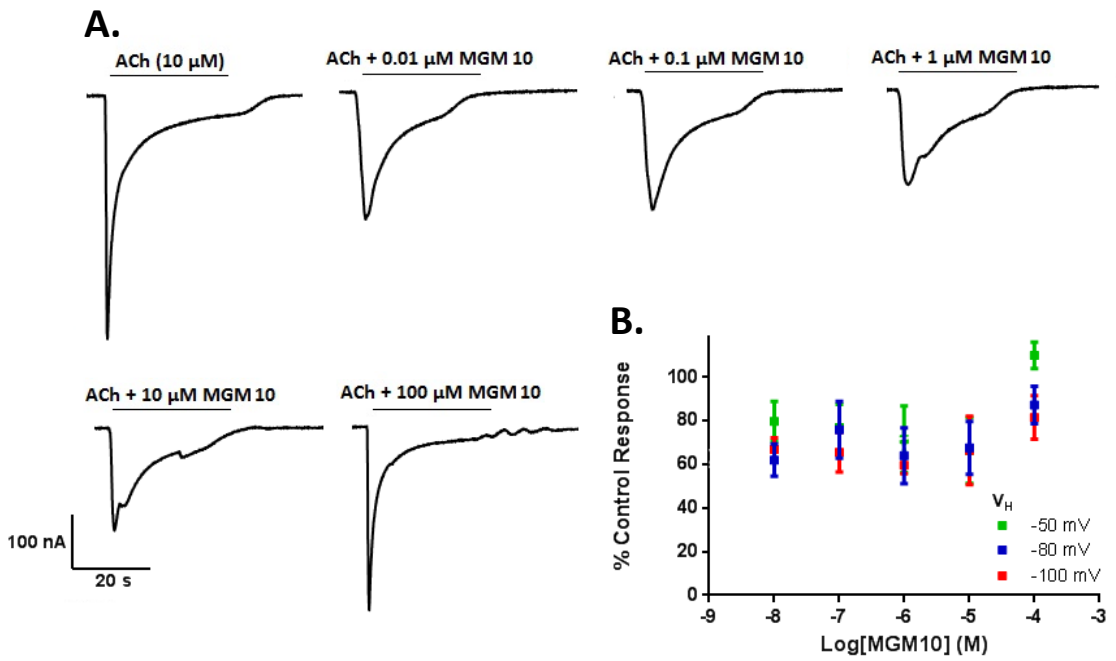


Figure 84: MGM10 block of ACh responses on α4β2 nicotinic receptor.

(A) Example of TEVC recordings for MGM10 (0.01–100 µM) block of ACh responses at -80 mV on a single oocyte, (B) Concentration-inhibition relationship for MGM10 block recorded at three holding potentials (-50, -80 and -100 mV). Percentage control response (mean ± SEM, n=3-4) values were plotted.

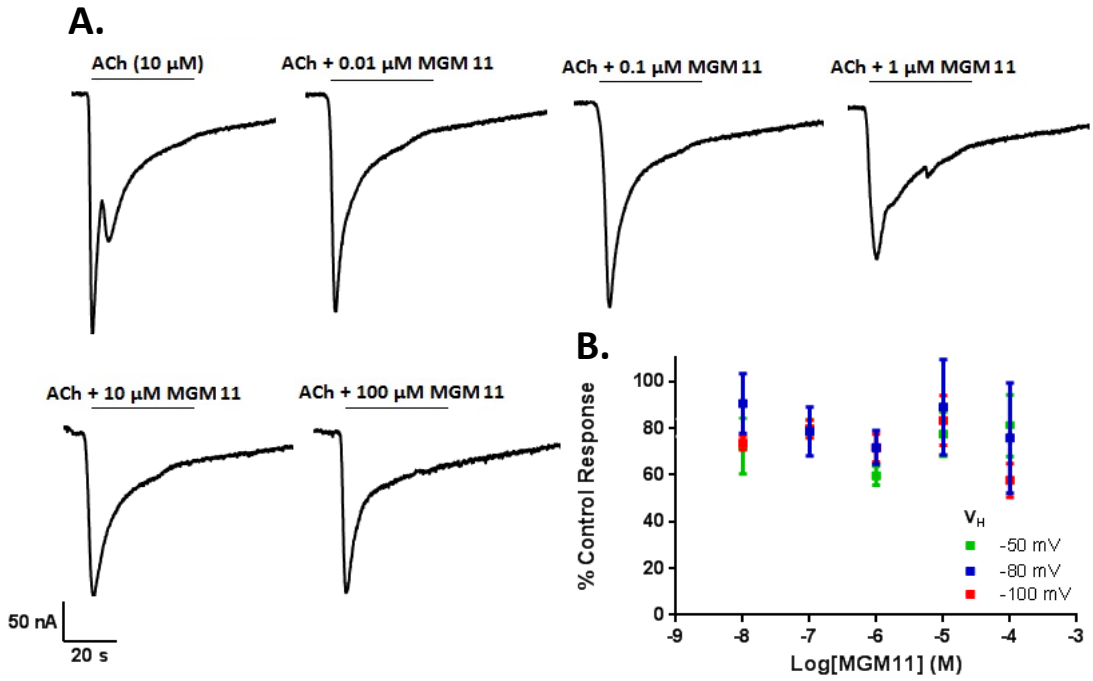
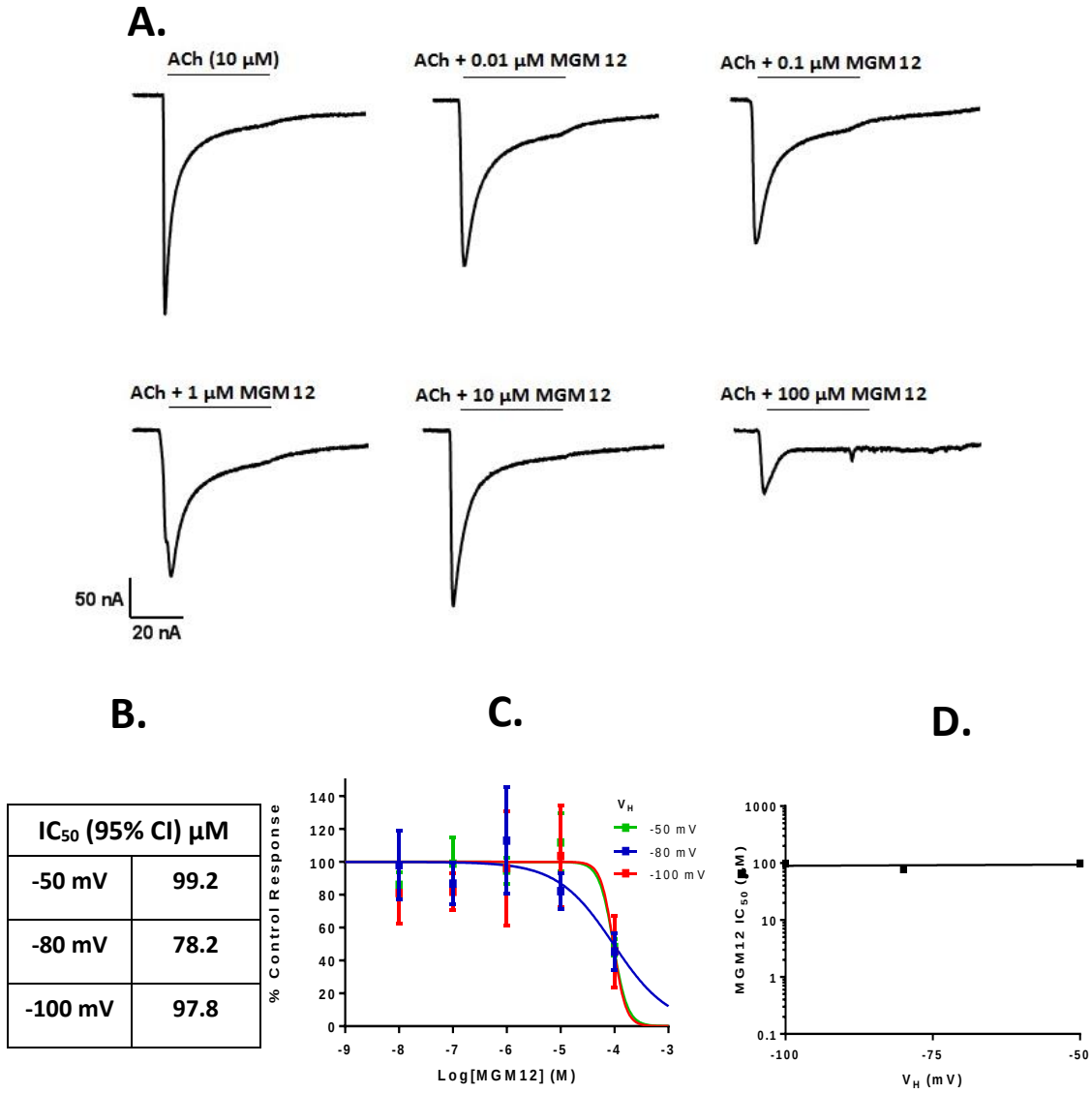


Figure 85: MGM11 block of ACh responses on α4β2 nicotinic receptor.

(A) Example of TEVC recordings for MGM11 (0.01–100 µM) block of ACh responses at -80 mV on a single oocyte, (B) Concentration-inhibition relationship for MGM11 block recorded at three holding potentials (-50, -80 and -100 mV). Percentage control response (mean ± SEM, n=4-5) values were plotted.

MGM12 exhibited some potency to inhibit ACh in α4β2 nicotinic receptors although very weakly. IC_{50}s obtained from the concentration-inhibition curves were 99.2, 78.2 and 97.8 µM recorded at -50, -80 and -100 mV respectively. The IC_{50}s did not show voltage-dependency as differences across all voltages were not significant ($p>0.05$). The δ value obtained from the voltage-dependent curve fitted with the Woodhull equation was 0.024 (95% CI -1.6 to 1.65). The results are presented in figure 86.



IC_{50} (95% CI) µM	
-50 mV	99.2
-80 mV	78.2
-100 mV	97.8

Figure 86: MGM12 block of ACh responses on α4β2 nicotinic receptor.

(A) Example of TEVC recordings for MGM12 (0.01–100 µM) block of ACh responses at -80 mV on a single oocyte, (B) IC_{50} values for MGM12, (C) Concentration-inhibition curves for MGM12 block recorded at three holding potentials (-50, -80 and -100 mV). Percentage control response (mean ± SEM, n=3-4) values were plotted and fitted with Hill equation, (D) Voltage-dependent inhibition curve for MGM12 block. IC_{50} values plotted and fitted with the Woodhull equation to yield the δ value. Note that 95% CI were not stated as they were very wide and unable to be generated via Graphpad Prism.

5.6.2.3 Antagonistic Responses on α7 Nicotinic Receptors

MGM2 was found to be a potent inhibitor of α7 nicotinic receptor at more negative holding potentials. At -100 mV, the IC_{50} obtained from the concentration-inhibition curve was 1.03 µM, while at -50 and -80 mV, the IC_{50}s obtained were both more than 100 µM. These IC_{50} values were considered ambiguous due to the poorly fitted concentration-inhibition curves (figure 87 B). Although the IC_{50}s showed a trend in voltage-dependency, it was statistically insignificant across all holding potentials due to wide confidence intervals, and were not able to fit into the Woodhull model equation to generate a δ value.

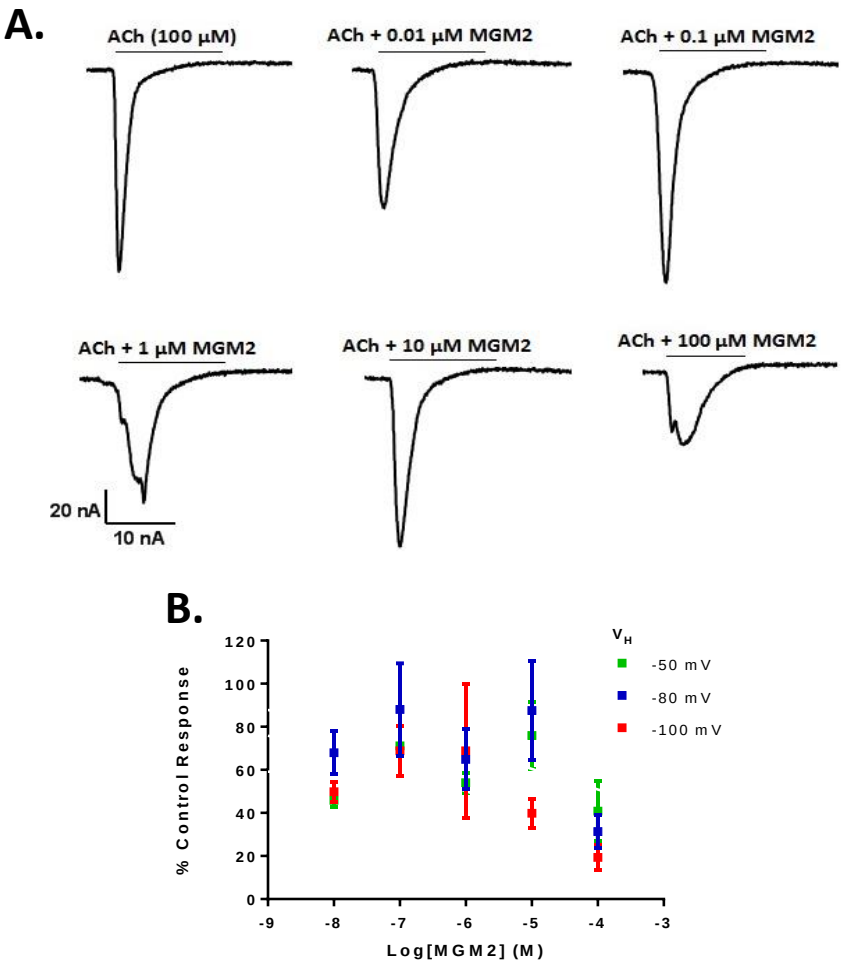
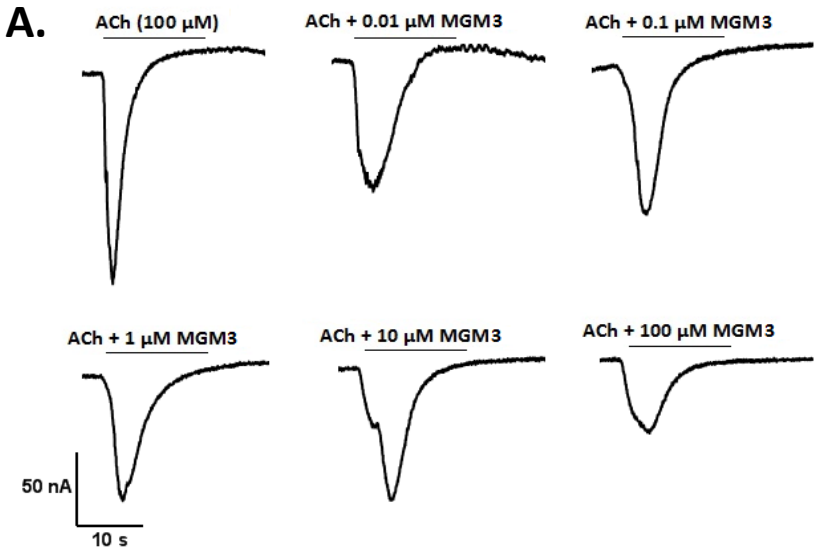


Figure 87: MGM2 block of ACh responses on α7 nicotinic receptor.

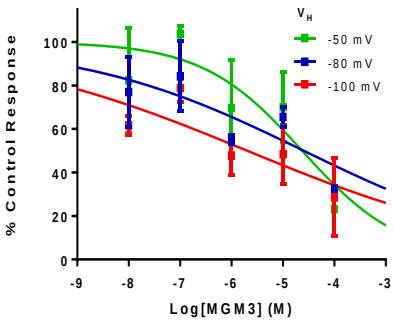
(A) Example of TEVC recordings for MGM2 (0.01–100 µM) block of ACh responses at -80 mV on a single oocyte, (B) Concentration-inhibition curves for MGM2 block of ACh responses. Percentage control response (mean ± SEM, n=2-4) values were plotted.

MGM3 was found to be a somewhat potent ACh inhibitor in α7 nicotinic receptor. IC_{50}s obtained from the concentration-inhibition curves were 23.6 (95% CI 1.13 to 494.2), 25.3 (95% CI 0.33 to 1926) and 2.02 (95% CI 0.13 to 32.6) µM recorded at -50, -80 and -100 mV respectively. The IC_{50}s does not show a trend of voltage-dependency as the differences were statistically insignificant across all holding potentials. The IC_{50}s fitted with the Woodhull model equation yielded a δ value of 0.46. Results are presented in figure 88.



B.

IC_{50} (95% CI) µM	
-50 mV	**23.6** 1.13 to 494.2
-80 mV	**25.3** 0.33 to 1926
-100 mV	**2.02** 0.13 to 32.6



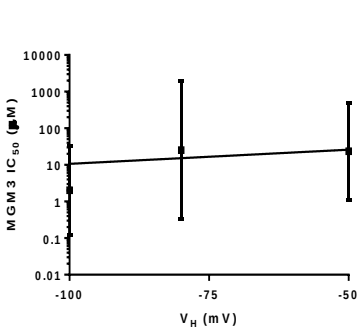
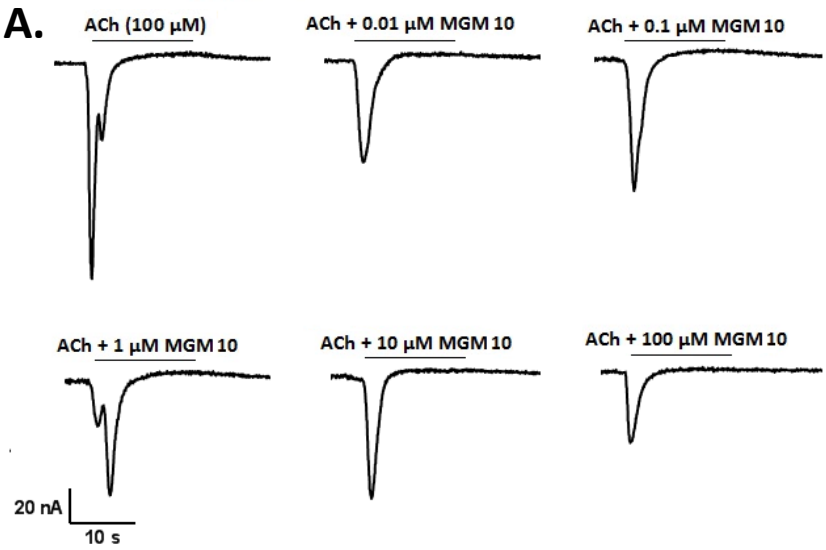


Figure 88: MGM3 block of ACh responses on α7 nicotinic receptor.

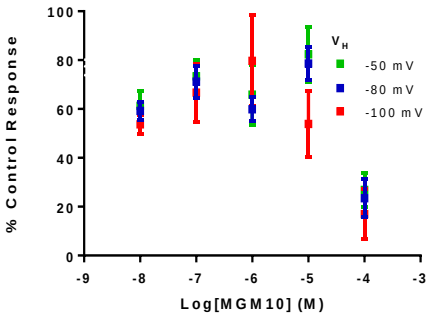
(A) Example of TEVC recordings for MGM3 (0.01–100 µM) block of ACh responses at -80 mV on a single oocyte, (B) IC_{50} (95% CI) values for MGM3 recorded at three holding potentials (-50, -80 and -100 mV), (C) Concentration-inhibition curves for MGM3 block of ACh responses. Percentage control response (mean ± SEM, n=2-4) values were plotted and fitted with the Hill equation. (D) Voltage-dependent inhibition curve for MGM3 block. IC_{50} (95% CI) values were plotted and fitted with the Woodhull equation to yield the δ value.

IC_{50}s obtained from the concentration-inhibition curves for MGM10 were 65.0 (95% CI 0.24 to 17290), 19.8 (95% CI 0.41 to 952.8) and 7.53 (95% CI 0.01 to 4503) µM recorded at -50, -80 and -100 mV respectively. The fit however was ambiguous due to the broad confidence intervals. IC_{50}s fitted with the Woodhull equation display voltage-dependency curve although the differences were not statistically significant across all voltages. The δ value obtained from the curve was 1.05. Results are presented in figure 89.



B.

IC_{50} (95% CI) µM	
-50 mV	**64.98** 0.242 to 17290
-80 mV	**19.75** 0.409 to 952.8
-100 mV	**7.534** 0.013 to 4503



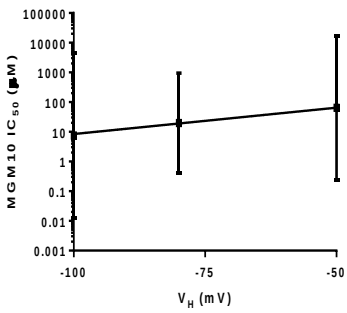
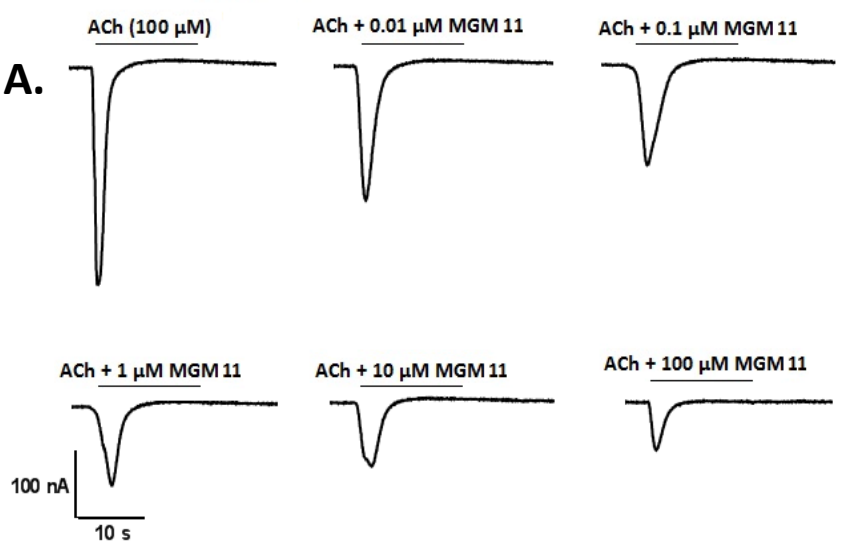


Figure 89: MGM10 block of ACh responses on α7 nicotinic receptor.

(A) Example of TEVC recordings for MGM10 (0.01–100 µM) block of ACh responses at -80 mV on a single oocyte, (B) IC_{50} (95% CI) values for MGM10 recorded at three holding potentials (-50, -80 and -100 mV), (C) Concentration-inhibition curves for MGM10 block. Percentage control response (mean ± SEM, n=3-6) values were plotted, (D) Voltage-dependent inhibition curve for MGM10 block. IC_{50} (95% CI) values plotted and fitted with the Woodhull equation to yield the δ value.

MGM11 was found to be a potent ACh inhibitor in α7 nicotinic receptor. IC_{50}s obtained from the concentration-inhibition curves were $2.261x10^{-3}$ (95% CI $1.815x10^{-6}$ to 2.186), $3.595x10^{-3}$ (95% CI $6.839x10^{-7}$ to 18.9) and $5.167x10^{-3}$ (95% CI $5.219x10^{-6}$ to 5.116) µM recorded at -50, -80 and -100 mV respectively. The IC_{50}s do not show a trend of voltage-dependency and the differences were statistically not significant across all holding potentials. The δ value obtained from the voltage-dependent curve fitted with the Woodhull equation was -0.41 (95% CI -0.94 to 0.13). The results are presented in figure 90.



B.

IC_{50} (95% CI) µM	
-50 mV	**$2.26 x10^{-3}$** $1.82x10^{-6}$ to 2.82
-80 mV	**$3.6x10^{-3}$** $6.84x10^{-7}$ to 18.9
-100 mV	**$5.17x10^{-3}$** $5.22x10^{-6}$ to 5.12

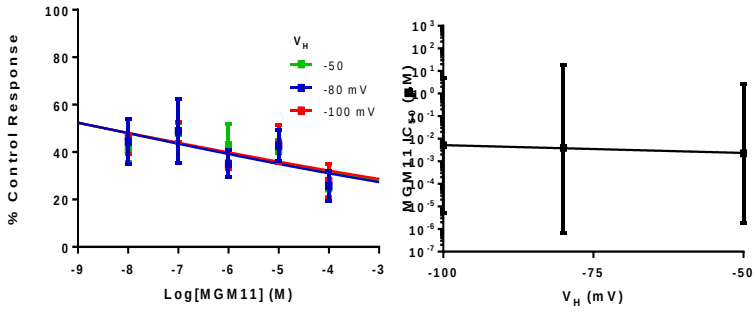
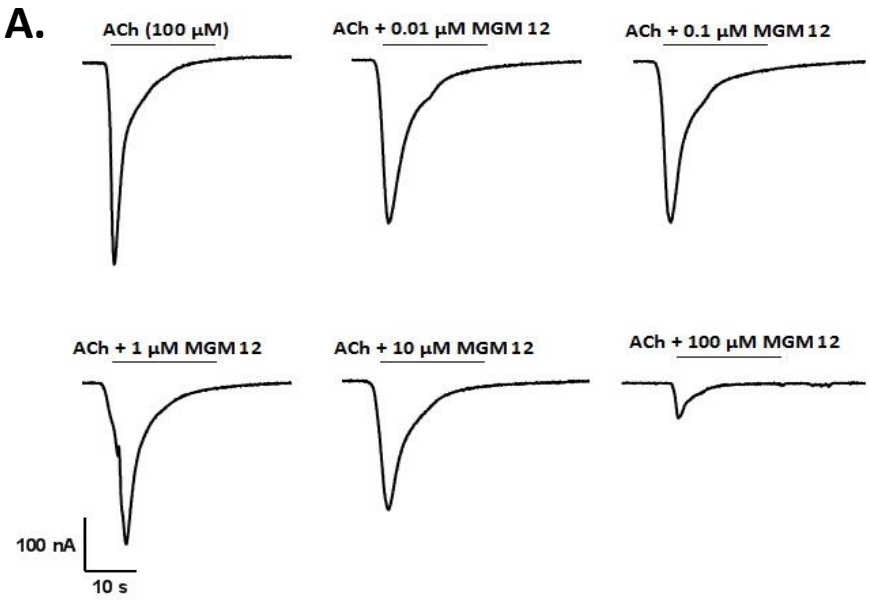


Figure 90: MGM11 block of ACh responses on α7 nicotinic receptor.

(A) Example of TEVC recordings for MGM11 (0.01–100 µM) block of ACh responses at -80 mV on a single oocyte, (B) IC_{50} (95% CI) values for MGM11 recorded at three holding potentials (-50, -80 and -100 mV), (C) Concentration-inhibition curves for MGM11 block of ACh. Percentage control response (mean ± SEM, n=4) values were plotted and fitted with the Hill equation. (D) Voltage-dependent inhibition curve for MGM12 block. IC_{50} (95% CI) values plotted and fitted with the Woodhull equation to yield the δ value.

IC_{50}s obtained from the concentration-inhibition curves for MGM12 were 30.2 (95% CI 7.55 to 121.0), 44.3 (95% CI 0.82 to 2404) and 5.12 (95% CI 1.04 to 25.1) µM recorded at -50, -80 and -100 mV respectively. IC_{50} at -100 mV were particularly low compared to at -75 and -50 mV suggesting voltage-dependency although not statistically significant. The δ value obtained from the voltage-dependent curve fitted with the Woodhull equation was 0.3 (95% CI -8.22 to 8.82). The results are presented in figure 91.



B.

IC_{50} (95% CI) M	
-50 mV	**30.2** 7.55 to 21.0
-80 mV	**44.3** 0.82 to 2404
-100 mV	**5.12** 1.04 to 25.1

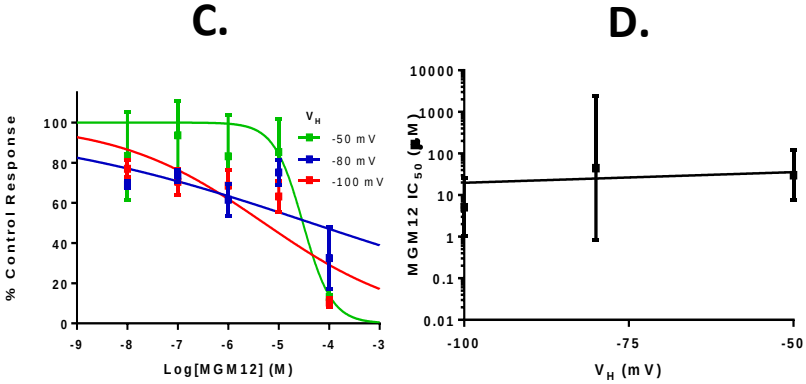


Figure 91: MGM12 block of ACh responses on α7 nicotinic receptor.

(A) Example of TEVC recordings for MGM12 (0.01–100 µM) block of ACh responses at -100 mV on a single oocyte, (B) IC_{50} (95% CI) values for MGM12 recorded at three holding potentials (-50, -80 and -100 mV), (C) Concentration-inhibition curves for MGM12 block. Percentage control response (mean ± SEM, n=3-4) values were plotted and fitted with the Hill equation, (D) Voltage-dependent inhibition curve for MGM12 block. IC_{50} (95% CI) values plotted and fitted with the Woodhull equation to yield the δ value.

5.7 DISCUSSION

Alzheimer is a multifactorial disease with no effective cure. Current available treatments serve only to alleviate the symptoms and suppress neurodegenerative progression and hence improve the quality of life of individuals with AD. Researchers have studied numerous targets and therapeutic strategies in the race to find successful treatments although this goal remains extremely challenging due to the multifactorial nature of dementias. In collaboration with University of Bologna, Italy, this work attempted to develop a new strategy for drug design by creating molecules intended to have multiple functions and targets. In 2012, Rosini and colleagues synthesized a novel dual-target compound by chemically joining memantine and galantamine through different spacers. Each moiety of memantine and galantamine is responsible for activity against NMDAR and AChE respectively. This new chemical entity was able to simultaneously contact both sites of AChE and NMDAR thus retaining their specific pharmacological properties (Rosini et al., 2014).

Due to the promising nature of the compound, this work attempted to further evaluate novel compounds synthesized primarily to act as NMDA blockers but also possessing antioxidant properties to suppress oxidative stress and ability to inhibit Aβ plaque aggregation. The first series of MTDLs consisted of eight MAB compounds derived from memantine, each attached to an antioxidant headgroup. Four of the compounds were linked to methoxyphenol (MAB(23)2, MAB14, MAB2222, MAB30) with varied chain lengths and the other four were incorporated with a derivative of lipoic acid (MAB7, MAB15, MAB21, MAB32). It was predicted that the incorporation of antioxidant pharmacophores would increase the therapeutic potential of this compound in the treatment of Alzheimer's disease (AD) by specifically reducing Aβ-induced oxidative stress.

IC_{50}s for these compounds recorded at -60 mV were in the range between 26.9 to 162.3 μM, much less potent when compared to NMDAR endogenous blocker, Mg^{2+} (IC_{50} = 10.1 μM) and memantine (IC_{50} = 2.28 μM). It was postulated that memantine may have lost its function due to the chain attachment to its amine group which is

likely to be important for memantine function. Consequently, four new compounds were synthesized which had an amide group to the linking chain connecting memantine to antioxidant headgroup hoping that it will increase functionality by freeing the amine group. FC7 and FC12 were incorporated with methoxyphenol while FC17 and FC20 were linked with catechol. One more novel compound, termed GB13 was created similarly to FC20 but with an amine replaced by a sulphide in a shortened chain length. Unfortunately, the findings of this study revealed that this group of MTDLs did not improve potencies of the compounds and instead yielded even higher IC_{50}s compared to the first group of memantine derivatives. GB13 was somewhat potent with an IC_{50} of 68.65 µM, while the FC compounds generated a nearly linear horizontal curve of the concentration-inhibition curves yielding IC_{50}s of more than 100 µM.

The third series of MTDLs investigated in the current study were derived from polyamine spermine, an endogenous modulator of NMDAR responses, with headgroups of varying antioxidant compositions. Spermine is known to antagonize and modulate several ion channels (Williams, 1997a), block in a voltage-dependent manner and possess a rapid binding capacity to the channels (Kashiwagi et al., 1997). CR8 was incorporated with lipoic acid, CR18 with α-tocopherol and melatonin was attached to spermine in CR24. These spermine-derived polyamine compounds proved to be potent NMDA blockers. IC_{50}s obtained from the concentration-inhibition curves were comparable with memantine, with significantly lower IC_{50} for CR18. IC_{50} of CR18 was 0.69 µM, while CR8 and CR24 displayed similar potencies with IC_{50}s of 2.21 and 2.35 µM respectively tested at -60 mV. The results showed that they were more potent than Mg^{2+} (IC_{50} 10.1 µM at -60 mV).

These CR compounds also retained the characteristics of voltage-dependent block similar to Mg^{2+} and memantine which make them ideal candidates for further drug testing. δ values obtained from the Woodhull model (Woodhull, 1973) were for 0.33 (CR8), 0.82 (CR18) and 0.21 (CR24). CR18 probably has the closest binding site to Mg^{2+} (δ = 1.48) which may suggest its relatively higher potency compared to the other two compounds. It is, however, difficult to pinpoint the location of the binding site in the

pore channel due to the varying δ values obtained in this study. However their binding sites are thought to be quite deep within the electric field due to the strong voltage-dependence characteristics. All the CR compounds had δ values of less than 1, as with memantine, suggesting that they may bind to the same or close to the binding site of memantine.

The results of the experiments using CR compounds indicate that this series of compounds should be further investigated as potential AD treatments. Although several clinical investigations have shown that antioxidants provide benefits to attenuate AD-related symptoms or pathogenesis, the results of clinical trials have been disappointing suggesting that single antioxidants may not be adequate for the treatment of neurodegenerative diseases (Liu, 2008). This study suggests an alternative for AD therapy by combining antioxidants and polyamine in a single entity that is able to combat oxidative stress and suppress excitotoxicity at the same time and which therefore might provide a more effective treatment. Furthermore, these antioxidant-containing molecules are proposed to exhibit neuroprotective effects and hence are able to act at different steps in the neurodegenerative process (Bolognesi et al., 2009a). These compounds, however, should also be tested on other receptor channels such as AMPARs and nAChRs to see whether they would exert selectivity and other pharmacological properties against other receptors.

The MTDL concept has thus far led to the development of several potential molecules such as memoquin and lipocrine. Memoquin was formed by incorporating benzoquinone moiety of CoQ into a polyamine chain demonstrating the ability to modulate *in vitro* and *in vivo* molecular targets such as AChE, β-secretase, Aβ, and oxidative processes (Cavalli et al., 2007). Lipocrine was synthesized by coupling the 9-amino-6-chloro-1,2,3,4-tetrahydroacridine moiety with lipoic acid and was shown to exert AChE inhibitory activity and act as a radical scavenger (Rosini et al., 2005). The structures of these two MTDL compounds are shown in figure 92 A and 92 B.

Most recently, the MTDL strategy led to the synthesis of carbacrine, a series of molecules derived from the vasodilating β-blocker, carvedilol and tacrine, an AChEI (as shown in figure 92 C). Despite being developed as a cardiovascular drug, carvedilol was found to possess neuroprotective capacity and exhibit low affinity non-competitive antagonist property on NMDA receptor (Lysko et al., 1998).

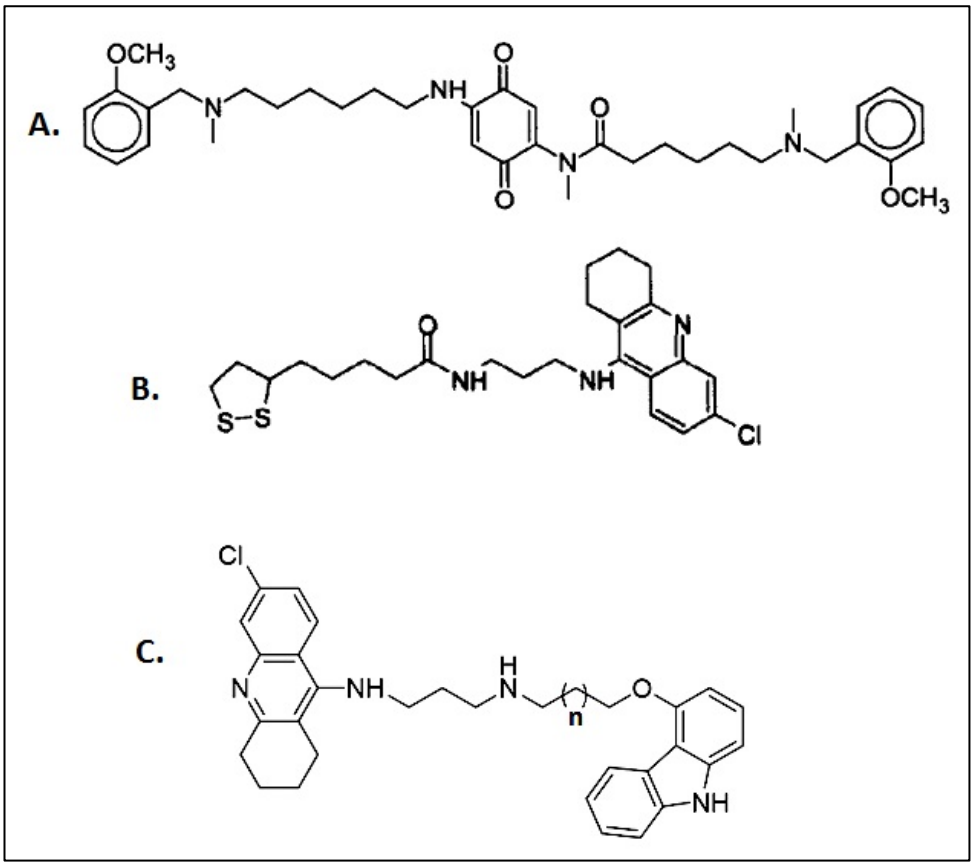


Figure 92: Chemical structures of (A) memoquin, (B) lipocrine and (C) carbacrine.

Memoquin consists of the benzoquinone moiety of CoQ incorporated into a polyamine chain while a 9-amino-6-chloro-1,2,3,4-tetrahydroacridine moiety coupled with lipoic acid led to the formation of lipocrine (Bolognesi et al., 2009a). Carbacrine is derived from carvedilol and tacrine, and designed with increasing chain size (n=3-6) between the two pharmacophores (Rosini et al., 2014).

Evaluation of the carbacrine molecules showed that this MTDL is a potential lead compound endowed with a multifunctional profile as AChEIs and NMDAR antagonist. Carbacrine molecules were found to be effective AChEIs in the nanomolar range, and are able to counteract the formation of ROS in human neuronal-like cells, reduce $A\beta_{1-42}$ self-aggregation and act as non-competitive NMDAR blockers with more efficacy than memantine (Rosini et al., 2014).

Due to the potency of carbacrine, a similar group of molecules termed as MGM compounds were synthesized by integrating AChEI, donepezil with carbazole fragments from carvedilol and evaluated in the present study. Each of these MGM compounds was designed with different methylene chain lengths (n=3-7) between the two pharmacophores. It was hypothesized that these compounds would exhibit NMDAR antagonistic property as well as having the ability to modulate the cholinergic tone.

In contrast to the carbacrine series, these MGM compounds were unfortunately found to be weak NMDAR blockers, particularly MGM11, MGM2 and MGM3 which had the three longest methylene chain lengths existing in that order. At all concentration across all voltages, they managed to only inhibit NMDA responses between 2 to 15%. Even at the highest concentrations tested, the inhibition of control response was minimal. The data obtained were not able to fit or poorly fitted into the Hill equation thus we were unable to generate their IC_{50s}. MGM10 was slightly more potent with IC_{50}s between 230 to 420 µM. MGM12 was the most potent with strong voltage-dependency. However, the IC_{50}s obtained (7.02, 12.6 and 204.9 µM at -100, -75 and -50 mV respectively) were still considered high for use as therapeutics.

Due to the fact that carbacrine molecules were potent NMDAR blockers while MGM compounds were not, it was postulated that the tacrine headgroup may actually be the responsible moiety for the high affinity interaction with NMDAR channel pore rather than carbazole. Results of the present study indicate that the donepezil does not possess affinity towards NMDA receptor. Further work should be aimed at elucidating the structure-activity relationship of these compounds.

Published binding studies that have shown donepezil-derived compounds are able to bind with nAChRs. As nAChR subunits are proposed to have a role in regulating CNS functions (Rammes et al., 2008), activation or inhibition of these receptors may potentially be a relevant target to modulate pathological changes associated with nAChRs. For this reason, MGM compounds were also tested against two nicotinic

receptor subunits, α4β2 and α7 to assess whether they possess agonistic or antagonistic properties.

The agonistic assay revealed that the MGM compounds exert a partial agonistic property on α4β2 nAChR. At 100 µM, MGM compounds diluted in *Xenopus* ringer evoked inward currents of between 15% and 22% compared to the control response induced by 100 µM ACh. The compounds, however, did not exhibit agonistic behaviour when tested against α7 nAChR. The selectivity of this compounds towards α4β2 (although relatively small) but not on α7 subtype might also be a favourable property. α7 nAChR is highly permeable to Ca^{2+} ions, hence activation of this subtype will induce direct Ca^{2+} influx into the channel (Shen and Yakel, 2009) which may contribute to excitotoxicity.

Results of antagonistic assay with MGM compounds revealed that they were weak α4β2 nAChR blockers. This might be explained by the partial agonistic behaviour exerted by the compounds on α4β2 nAChRs. In fact, at maximum concentrations, some of these compounds further potentiated the ACh-induced responses. Inhibition percentages were poorly fitted with the Hill equation and thus IC_{50}s were unable to be calculated. Only MGM12 exhibited slight antagonistic property against α4β2 nAChR with IC_{50}s between 78 to 99 µM at holding potentials between -50 to -100 mV.

Antagonistic assay on α7 nAChRs demonstrated that the MGM compounds were more selective on this nAChR subtype. MGM10 was the most potent with IC_{50}s in the nanomolar range but barely concentration-dependent. Three of the compounds (MGM3, MGM10 and MGM12) recorded IC_{50}s in the range between 2 to 65 µM. MGM2 displayed strong voltage-dependency with huge variation at the three voltages tested. The IC_{50} was extremely high at -50 mV suggesting that this compound is completely inactive at this holding potential. The values however were considered ambiguous due to the poorly fitted data with the Hill equation.

This study provided evidence that the MGM compounds were partially agonistic towards α4β2 nAChRs while selectively antagonize ACh responses in α7 subtypes. The contradicting effects on both nAChR subtypes indicate a non-favourable property of these compounds. Furthermore, this series of compounds also exhibited weak blocking properties on NMDA receptors thus signifying that they are not ideal candidates for development of MTDLs for neurodegenerative disorders.

CHAPTER 6

GENERAL DISCUSSION

6.1 PORE-REGION (M2) MUTATION STUDIES

GluN3 subunits have been frequently reported to exert a negative effect on NMDA-mediated current especially on channel block. This study provided evidence that the modification at the Q/R/N and +1 sites in GluN2A to resemble GluN3 subunits greatly influenced channel block. Double mutations at these sites increased IC_{50}s of open channel blockers in NMDARs and more significantly, the RR mutation (resembling human GluN3B) resulted in greater reduction of channel block compared to GR mutation. This is hypothesized to be the result of increased positive charge at these sites, thus reducing the affinity for Mg^{2+} and other channel blockers.

The present data supported findings by McClymont et al. (2012) that indicated that block by Mg^{2+} and other channel blockers in NMDARs were affected by the incorporation of GluN3 subunits. Furthermore, McClymont and colleagues demonstrated that the sensitivity to channel block was generally further reduced by co-expression of GluN3B than by GluN3A. Since the amino acid occupying the Q/R/N site is identical in the two subunits, the difference might be explained by other differences in their sequences. Numerous studies examining variants outside the selectivity filter region of M2 have been demonstrated to affect block of NMDARs containing GluN1 and GluN2 subunits (Jin et al. 2008; Kashiwagi et al., 2002; Siegler Retchless et al., 2012). Some of these residues are different between GluN3A and GluN3B (highlighted in figure 6) which might explain the differences between receptors containing GluN3A and GluN3B subunits. A study conducted by Wada et al. (2006) demonstrated that a part of the M3 region in both GluN1 and GluN3A forms a narrow constriction in the outer vestibule of the channel thus restricting flux of certain compounds into the pore. The amino acid that was thought to be responsible

for this was identified as the threonine (T) located in the conserved SYTANLAAF motif in the M3 region (shown in figure 93 below). A second amino acid residue located at position +18 (in relation to Q/R/N) in the M3 region is also thought to be responsible for variations in channel properties (Siegler Retchless et al., 2012; Wyllie and Traynelis, 2012). This site is occupied by S in GluN2A and GluN2B, while L occupies the position in GluN2C and GluN2D (figure 93). Combining macroscopic and single channel recordings, this single residue was found to control the three hallmark properties of the NMDA receptor channel; Mg^{2+} block, Ca^{2+} permeability and single-channel conductance (Siegler Retchless et al., 2012). In GluN3, this site is occupied by N, different from all other NMDAR subunits as well as GluA1 and GluA2. It would be interesting to investigate the effects of an amino acid modification at this site on channel properties of GluN3-containing NMDARs.

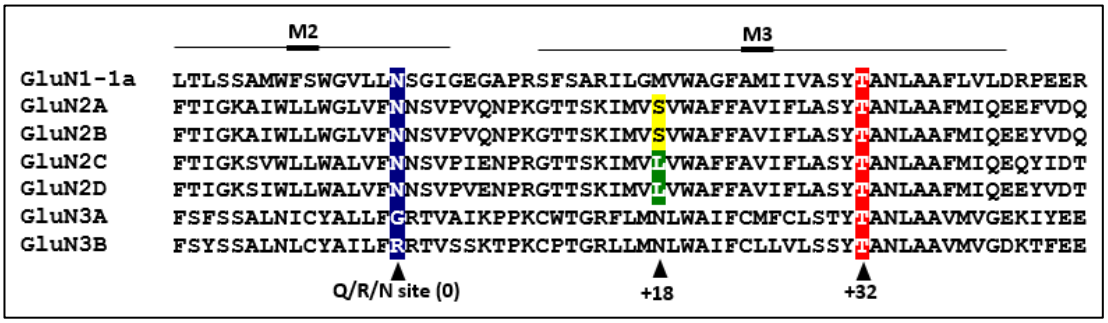


Figure 93: Amino acid sequence alignment for human NMDAR subtypes.

The threonine (T) of GluN1 and GluN3 is in the highly conserved SYTANLAAF motif at position +32 in relation to the Q/R/N site (highlighted in red). It is thought the amino acid forms a narrow constriction in the outer vestibule of the channel thus restricting flux of certain compounds into the pore (Wada et al., 2006). The amino acids serine (S, in GluN2A and GluN2B, highlighted in yellow) and leucine (L, in GluN2C and GluN2D, highlighted in green) were hypothesized to be responsible for NMDAR's important channel properties; Mg^{2+} block, Ca^{2+} permeability and single channel conductance (Siegler Retchless et al., 2012).

The physiological function and effects of GluN3 on the NMDA receptor has not yet been fully elucidated although amino acid changes in the M2 pore region demonstrate that it has a role in Mg^{2+} sensitivity and Ca^{2+} permeability (Paoletti and Neyton, 2007). With these alterations coupled with the fact that GluN3 expression peaks during development, this has led to the hypothesis that the subunit has a

neuroprotective role against excitotoxicity or helps the maturation process at synapses (Henson et al., 2010).

6.2 MTDL AS POTENTIAL THERAPEUTICS FOR AD

NMDAR is considered a potential therapeutic target for AD as its antagonists have been shown not only to be able to block excitotoxicity, but also to suppress synaptic depression induced by Aβ. The deposition of Aβ plaques in the brain has been widely recognized as a primary feature of the disease and NMDARs have been implicated in several roles mediating the Aβ-related mechanism in the pathophysiology of AD (Malinow, 2012) as depicted in figure 94.

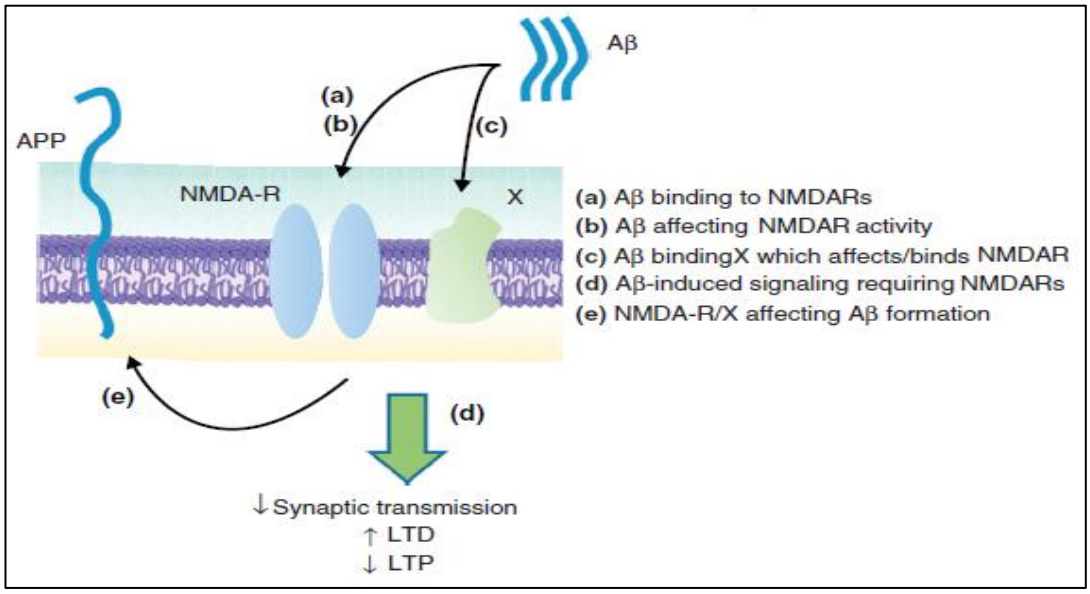


Figure 94: Potential roles of NMDA receptors in Aβ-related mechanism.
Source: Malinow (2012).

Aβ senile plaques have been reported to induce oxidative stress leading to neuronal injury (Varadarajan et al., 2001) while more recent findings have suggested that oxidative stress occurs early in the development of AD prior to cytopathology events (Su et al., 2008). This has been supported by work performed by De Felice and colleagues who postulated that oxidative stress disrupts the molecular mechanisms of plasticity in the early stages of AD, while at a later stage it causes neuronal deterioration and death. Their findings also indicated that over-activity and

excitotoxicity of NMDAR leading to oxidative damage is caused by Aβ oligomers and suggest that this condition could be attenuated by memantine therapy (De Felice et al., 2007). Furthermore, Aβ-induced NMDAR excitotoxicity leading to excess Ca^{2+} influx may also result in neuronal injury contributing to the development of AD (Lipton, 2006). Texido et al. (2011) have shown that NMDA receptors may be activated directly by Aβ oligomers, particularly the GluN1/2A subunit combination. They further demonstrated that drugs possessing NMDAR antagonistic properties such as memantine, MK-801 and AP5 (DL-2-amino-5-phosphonovaleric acid) were able to block high influx of Ca^{2+} and attenuate Aβ-induced damage on neurons in AD. Subsequently, NMDAR antagonists were shown to block the morphological effects of Aβ in pyramidal neurons in rat organotypic slices (Hsieh et al., 2006; Shankar et al., 2007).

The fact that there might be a strong relationship between excitotoxicity, oxidative stress and Aβ formation in the pathogenesis of AD, means that the development of drugs that target all of these components could be of great potential. The MTDL strategy was aimed to design and characterise novel compounds with great potential and ability to (i) block AChE activity in the nanomolar range, (ii) suppress *in vitro* formation of Aβ-plaques, (iii) inhibit NMDA receptors, and (iv) decrease oxidative stress. The present study demonstrated the potency of the CR spermine-derived polyamine compounds which were incorporated with antioxidant moieties. Hence, this body of work should be further investigated and the compounds further characterized for therapeutic impact.

Although NMDARs are traditionally associated with synaptic plasticity in neurons, recent investigations have reported the presence of NMDAR in glial cells and on the myelin sheath of axons (Káradóttir et al., 2005; Micu et al., 2006; Salter and Fern, 2005; Verkhratsky and Kirchhoff, 2007) possibly involved in neuron-to-glia signalling (Lalo et al., 2006). This discovery has increased the potential role of NMDARs in brain disease because NMDAR is now thought to be involved in the pathogeneses of myelin degeneration in multiple sclerosis (MS), cerebral palsy, spinal cord injury and stroke (Bakiri et al., 2008; Karadottir et al., 2005; Paoletti and Neyton, 2007; Stys and Lipton,

2007). Furthermore, the demonstration that NMDAR are involved in central sensitization to noxious stimuli has opened up the possibility of controlling certain types of pain through antagonism of NMDARs.

Other neurological conditions that have been studied and which may benefit from NMDAR antagonism include epilepsy, psychosis, anxiety, amnesia, hyperalgesia and stroke (Meldrum, 2000; Saiki et al., 2013). NMDAR antagonists when administered intracerebroventricularly in mice have been found to be potent anticonvulsants (Meldrum, 1985) and have shown to possess a remarkable neuroprotective role in animal models of cerebral ischemia and hypoglycaemia (Simon et al., 1984). Hence, NMDARs represent a medically relevant target for therapy and therefore it is important to understand the properties of the numerous subtypes that exist for this receptor.

6.3 FUTURE WORKS AND RECOMMENDATIONS

The original objective of this study was to provide a molecular basis as to how GluN3 subunits impart their unique properties to NMDARs that reduce their ability to be blocked and alter their permeability and conductance. The present study demonstrated that the amino acids occupying the Q/R/N and +1 sites play important roles influencing the sensitivity of the NMDA receptors to channel block. GR and more specifically RR as found in human GluN3B at these sites significantly reduced channel block of Mg^{2+}, memantine, MK-801 and CR18. Future works should continue to specifically investigate how these amino acids affect Ca^{2+} permeability and single channel conductance, two other key characteristics of NMDARs.

It is known that GluN3 subunits lower the single channel conductance and reduce Ca^{2+} permeability of an NMDAR (Das et al., 1998; Sasaki et al., 2002). Voltage-clamp and single channel studies using cells expressing NMDAR incorporated with mutant subunits could be employed to see how this affects Ca^{2+} permeability and channel conductance compared to wild type. If the amino acids GR or RR at the Q/R/N and +1 sites do not explain the reduced conductance and Ca^{2+} permeability, a residue in the

cytoplasmic end of the M3 region should be investigated. A previous study by Siegler Retchless et al. (2012) have reported that changes in Mg^{2+} sensitivity, Ca^{2+} permeability and single channel conductance between GluN2A/B versus GluN2C/D are caused by a substitution of this residue.

Another aspect that should be further explored is the difference in properties exerted by GluN3B versus GluN3A. In a study using rat GluN3 RNAs, McClymont et al. (2012) showed that GluN3B consistently provided greater resistance to channel block than GluN3A. Since the amino acids at the Q/R/N and +1 sites are identical in the two subunits in rat, other residues could be responsible for the differences. Therefore, it is recommended that future studies determine which other regions of the GluN3 subunits influence sensitivity to Mg^{2+} and other open channel blockers in order to explain why GluN3B is more resistant than GluN3A. A study by Kashiwagi et al. (2002) demonstrated that channel block by MK-801, memantine and N1,N4,N8-tri-benzyl-spermidine (TB-3-4) in GluN1/2B NMDAR are not only affected by amino acids in the M2 region but also by residues toward the extracellular ends of M1, M3, and M4. Generating chimeric GluN3A/B subunits similar to the strategy used by Wrighton et al. (2008) would be useful to determine the region responsible for changes in Mg^{2+} sensitivity and other channel blockers. Essentially, this would provide important structural and functional information for NMDARs.

Future studies should also examine the neuroprotective role of GluN3 subunits following reports by Nakanishi et al. (2009) that GluN3 may be neuroprotective *in vivo.* The hypothesis to test is whether the neuroprotective effect is mediated by differences in GluN3 at the Q/R/N and adjacent sites. Experiments with cells transfected with GluN1 and GluN2A either without or with GluN3A or GluN3B would be useful to study the excitotoxic insult which could reveal whether the GluN3 subunits provide protection.

The fact that GluN3 subunits containing GR or RR at the Q/R/N and +1 sites render NMDAR less sensitive to open channel block, reduce calcium permeability and exhibit neuroprotective properties, mean that the design of MTDLs should also consider

evaluation on GluN3-containing NMDARs. The molecules designed as NMDAR blockers should display selectivity towards NMDAR subunits that are more permeable to Ca^{2+} while sparing the other subtypes such as GluN3 subunits for normal function.

6.4 CONCLUSION

Characterization of GluN1-1a/GluN2A-containing NMDARs was consistent with previous findings that NMDAR are sensitive to block by Mg^{2+} and other channel blockers in a voltage-dependent manner.

The M2 region of the NMDAR forming the channel pore is responsible for antagonist binding. This study provided further evidence that the Q/R/N and +1 sites in GluN2A and GluN3 subunits located in this region are partly responsible for their specific channel block properties. In humans, the sequence at this locus is NS in GluN1, NN in GluN2A-D, GR in GluN3A and RR in GluN3B. N occupying the Q/R/N site in GluN2A is responsible for providing the binding site for Mg^{2+} and other open channel blockers, and G or R occupying the homologous site in rat GluN3 is partly responsible for the reduced block of Mg^{2+} and other antagonists. The adjacent site (+1) is also postulated to play a role in the binding affinity of open channel blockers. The fact that the double R occupying the Q/R/N and +1 sites significantly increased IC_{50}s for Mg^{2+}, memantine, MK-801 and CR18 compared to wild type suggest that the presence of positively charged amino acids are likely responsible for the specific properties of GluN3-containing NMDARs (Matsuda et al., 2002). The RR mutation also resulted in generally higher IC_{50}s compared to NMDAR assembly containing GR mutation in GluN2A suggesting that sensitivity to block by NMDAR antagonists in human receptor assembly containing GluN3B may be further affected which remain to be tested.

The MTDL study suggested that the spermine-derived polyamine compounds are potent inhibitors of the NMDA receptors particularly CR18. Development of a compound which not only has the ability to block NMDAR excitotoxicity, but also

suppress oxidative stress and formation of Aβ might be the future direction of AD therapeutic strategy.

As shown in this study, CR18 was proven highly potent as a blocker in wild type NMDAR, but less sensitive in recombinant NMDAR containing GR or RR mutation in GluN2A subunits. This characteristic is a favourable property of the compound as an NMDAR blocker since GluN3 subunits containing GR or RR at the Q/R/N and +1 sites are less permeable to Ca^{2+} influx and has been shown to exert neuroprotective effects. Further characterization should be conducted as these compounds showed potential for clinical use in Alzheimer's disease treatment.

Bibliography

Al-Amin HA and Schwarzkopf SB (1996) Effects of the PCP analog dizocilpine on sensory gating: potential relevance to clinical subtypes of schizophrenia. *Biological Psychiatry* **40**:744–754.

Alberdi E, Sanchez-Gomez MV, Cavaliere F, Perez-Samartin A, Zugaza JL, Trullas R, Domercq M and Matute C (2010) Amyloid beta oligomers induce Ca2+ dysregulation and neuronal death through activation of ionotropic glutamate receptors. *Cell Calcium* **47**:264-272.

Allen TD, Rutherford SA, Murray S, Sanderson HS, Gardiner F, Kiseleva E, Goldberg MW and Drummond SP (2007) A protocol for isolating *Xenopus oocyte* nuclear envelope for visualization and characterization by scanning electron microscopy (SEM) or transmission electron microscopy (TEM). *Nature protocols* **2**:1166-1172.

Andersen TF, Tikhonov DB, Bølcho U, Bolshakov K, Nelson JK, Pluteanu F, Mellor IR, Egebjerg J and Strømgaard K (2006) Uncompetitive antagonism of AMPA receptors: Mechanistic insights from studies of polyamine toxin derivatives. *Journal of Medicinal Chemistry* **49**:5414-5423.

Andersson O, Stenqvist A, Attersand A and von Euler G (2001) Nucleotide sequence, genomic organization, and chromosomal localization of genes encoding the human NMDA receptor subunits NR3A and NR3B. *Genomics* **78**:178-184.

Antonov SM, Gmiro VE and Johnson JW (1998) Binding sites for permeant ions in the channel of NMDA receptors and their effects on channel block. *Nature neuroscience* **1**:451-461.

Araujo JA, Studzinski CM and Milgram NW (2005) Further evidence for the cholinergic hypothesis of aging and dementia from the canine model of aging. *Progress in neuro-psychopharmacology & biological psychiatry* **29**:411-422.

Asayama K, Yamadera H, Ito T, Suzuki H, Kudo Y and Endo S (2003) Double blind study of melatonin effects on the sleep-wake rhythm, cognitive and non-cognitive functions in Alzheimer type dementia. *Journal of Nippon Medical School* **70**:334-341.

Atri A, Molinuevo JL, Lemming O, Wirth Y, Pulte I and Wilkinson D (2013) Memantine in patients with Alzheimer's disease receiving donepezil: new analyses of efficacy and safety for combination therapy. *Alzheimer's research & therapy* **5**:6.

Ault B, Evans RH, Francis AA, Oakes DJ and Watkins JC (1980) Selective depression of excitatory amino acid induced depolarizations by magnesium ions in isolated spinal cord preparations. *The Journal of physiology* **307**:413-428.

Bachurin S, Tkachenko S, Baskin I, Lermontova N, Mukhina T, Petrova L, Ustinov A, Proshin A, Grigoriev V, Lukoyanov N, Palyulin V and Zefirov N (2001) Neuroprotective and cognition-enhancing properties of MK-801 flexible analogs. Structure–activity relationships. *Annals of the New York Academy of Sciences* **939**:219-236.

Bähring R and Mayer ML (1998) An analysis of philanthotoxin block for recombinant rat GluR6(Q) glutamate receptor channels. *The Journal of physiology* **509** 635-650.

Bakiri Y, Hamilton NB, Karadottir R and Attwell D (2008) Testing NMDA receptor block as a therapeutic strategy for reducing ischaemic damage to CNS white matter. *Glia* **56**:233-240.

Ballard C, Gauthier S, Corbett A, Brayne C, Aarsland D and Jones E (2011) Alzheimer's disease. *Lancet* **377**:1019-1031.

Bard F, Cannon C, Barbour R, Burke RL, Games D, Grajeda H, Guido T, Hu K, Huang J, Johnson-Wood K, Khan K, Kholodenko D, Lee M, Lieberburg I, Motter R, Nguyen M, Soriano F, Vasquez N, Weiss K, Welch B, Seubert P, Schenk D and Yednock T (2000) Peripherally administered antibodies against amyloid β-peptide enter the central nervous system and reduce pathology in a mouse model of Alzheimer disease. *Nature medicine* **6**:916-919.

Barnard EA, Miledi R and Sumikawa K (1982) Translation of exogenous messenger RNA coding for nicotinic acetylcholine receptors produces functional receptors in *Xenopus* oocytes. *Proceedings of the Royal Society of London B: Biological Sciences* **215**:241-246.

Bats C, Farrant M and Cull-Candy SG (2013) A role of TARPs in the expression and plasticity of calcium-permeable AMPARs: evidence from cerebellar neurons and glia. *Neuropharmacology* **74**:76-85.

Beck C, Wollmuth LP, Seeburg PH, Sakmann B and Kuner T (1999) NMDAR channel segments forming the extracellular vestibule inferred from the accessibility of substituted cycteines. *Neuron* **22**:12.

Berger ML, Bitar AY, Waitner MJ, Rebernik P and O'Sullivan MC (2006) Polyamines and the NMDA receptor: modifying intrinsic activities with aromatic substituents. *Bioorganic & medicinal chemistry letters* **16**:2837-2841.

Bezanilla F (2005) Voltage-gated ion channels. *IEEE Transactions on Nanobioscience* **4**:34-48.

Bhangoo SK and Swanson GT (2013) Kainate receptor signaling in pain pathways. *Molecular Pharmacology* **83**:307-315.

Bi X (2010) Alzheimer disease: Update on basic mechanism. *The Journal of the American Osteopathic Association* **110**:S3-S9.

Bierwirtz A and Schwarz W (2014) Two-electrode voltage-clamp (TEVC).

Birks J and Harvey RJ (2006) Donepezil for dementia due to Alzheimer's disease. *Cochrane Database of Systematic Reviews*:CD001190.

Birks JS, Chong LY and Grimley Evans J (2015) Rivastigmine for Alzheimer's disease. *Cochrane Database of Systematic Reviews* **9**:CD001191.

Bischoff C and Tiedtke PI (1992) Competitive and non-competitive NMDA receptor antagonists in spatial learning tasks. *European Journal of Pharmacology* **213**:269-273.

Blanke ML and VanDongen AMJ (2009) Activation Mechanisms of the NMDA Receptor, in *Biology of the NMDA Receptor* (Van Dongen AM ed), CRC Press/Taylor & Francis, Boca Raton, FL, USA.

Blennow K, de Leon MJ and Zetterberg H (2006) Alzheimer's disease. *The Lancet* **368**:387-403.

Blennow K, Mattsson N, Scholl M, Hansson O and Zetterberg H (2015) Amyloid biomarkers in Alzheimer's disease. *Trends in pharmacological sciences* **36**:297-309.

Boinpally R, Chen L, Zukin SR, McClure N, Hofbauer RK and Periclou A (2015) A novel once-daily fixed-dose combination of memantine extended release and donepezil for the treatment of moderate to severe Alzheimer's disease: two phase I studies in healthy volunteers. *Clinical Drug Investigation* **35**:427-435.

Bolognesi ML, Cavalli A, Bergamini C, Fato R, Lenaz G, Rosini M, Bartolini M, Andrisano V and Melchiorre C (2009a) Toward a rational design of multitarget-directed antioxidants: merging memoquin and lipoic acid molecular frameworks. *Journal of Medicinal Chemistry* **52**:7883-7886.

Bolognesi ML, Cavalli A and Melchiorre C (2009b) Memoquin: a multi-target-directed ligand as an innovative therapeutic opportunity for Alzheimer's disease. *Neurotherapeutics* **6**:152-162.

Bolognesi ML, Matera R, Minarini A, Rosini M and Melchiorre C (2009c) Alzheimer's disease: new approaches to drug discovery. *Current opinion in chemical biology* **13**:303-308.

Bolshakov KV, Kim KH, Potapjeva NN, Gmiro VE, Tikhonov DB, Usherwood PN, Mellor IR and Magazanik LG (2005) Design of antagonists for NMDA and AMPA receptors. *Neuropharmacology* **49**:144-155.

Bowie D (2008) Ionotropic glutamate receptors & CNS disorders. *CNS & Neurological Disorders - Drug Targets* **7**:129-143.

Brackley PT, Bell DR, Choi SK, Nakanishi K and Usherwood PNR (1993) Selective antagonism of native and cloned kainate and NMDA receptors by polyamine-containing toxins. *Journal of Pharmacology and Experimental Therapeutics* **266**:1573-1580.

Bresink I, Benke TA, Collett VJ, Seal AJ, Parsons CG, Henley JM and Collingridge GL (1996) Effects of memantine on recombinant rat NMDA receptors expressed in HEK 293 cells. *British Journal of Pharmacology* **119**:195-204.

Brothwell SL, Barber JL, Monaghan DT, Jane DE, Gibb AJ and Jones S (2008) NR2B- and NR2D-containing synaptic NMDA receptors in developing rat substantia nigra pars compacta dopaminergic neurones. *The Journal of physiology* **586**:739-750.

Buckingham SD, Pym L and Sattelle DB (2006) Oocytes as an expression system for studying receptor/channel targets of drugs and pesticides, in *Methods in Molecular Biology* pp 331-345.

Burnashev N (1998) Calcium permeability of ligand-gated channels. *Cell Calcium* **24**:325-332.

Burnashev N, Schoepfer R, Monyer H, Ruppersberg JP, Günther W, Seeburg PH and Sakmann B (1992) Control by asparagine residues of calcium permeability and magnesium blockade in the NMDA receptor. *Science* **257**:1415-1419.

Cavalli A, Bolognesi ML, Capsoni S, Andrisano V, Bartolini M, Margotti E, Cattaneo A, Recanatini M and Melchiorre C (2007) A small molecule targeting the multifactorial nature of Alzheimer's disease. *Angewandte Chemie International Edition in English* **46**:3689-3692.

Cavara NA and Hollmann M (2008) Shuffling the deck anew: how NR3 tweaks NMDA receptor function. *Molecular Neurobiology* **38**:16-26.

Cavara NA, Orth A and Hollmann M (2009) Effects of NR1 splicing on NR1/NR3B-type excitatory glycine receptors. *BMC neuroscience* **10**:32.

Chaffey H and Chazot PL (2008) NMDA receptor subtypes: Structure, function and therapeutics. *Current Anaesthesia & Critical Care* **19**:183-201.

Chang PK, Verbich D and McKinney RA (2012) AMPA receptors as drug targets in neurological disease--advantages, caveats, and future outlook. *European Journal of Neuroscience* **35**:1908-1916.

Chatterton JE, Awobuluyi M, Premkumar LS, Takahashi H, Talantova M, Shin Y, Cui J, Tu S, Sevarinok KA, Nakanishi N, Tong G, Lipton SA and Zhang D (2002) Excitatory glycine receptors containing the NR3 family of NMDA receptor subunits. *Nature* **415**:793–798.

Chen HS and Lipton SA (1997) Mechanism of memantine block of NMDA-activated channels in rat retinal ganglion cells: uncompetitive antagonism. *The Journal of physiology* **499**:27–46.

Chen HS and Lipton SA (2005) Pharmacological implications of two distinct mechanisms of interaction of memantine with N-methyl-D-aspartate-gated channels. *Journal of Pharmacology and Experimental Therapeutics* **314**:961-971.

Chen HSV, Pellegrini JW, Aggatwal SK, Lei SZ, Warach S, Jensen FE and Lipton SA (1992) Open-channel block of *N*-methyl-D-aspartate (NMDA) responses by memantine: therapeutic advantage against NMDA-receptor mediated neurotoxicity. *The Journal of Neuroscience* **72**:10.

Chen PE, Geballe MT, Katz E, Erreger K, Livesey MR, O'Toole KK, Le P, Lee CJ, Snyder JP, Traynelis SF and Wyllie DJ (2008) Modulation of glycine potency in rat recombinant NMDA receptors containing chimeric NR2A/2D subunits expressed in *Xenopus laevis* oocytes. *The Journal of physiology* **586**:227-245.

Chen PE and Wyllie DJ (2006) Pharmacological insights obtained from structure-function studies of ionotropic glutamate receptors. *British Journal of Pharmacology* **147**:839-853.

Chen Y and Hong X (2016) Effects of carvedilol reduce conjunctivitis through changes in inflammation, NGF and VEGF levels in a rat model. *Experimental and therapeutic medicine* **11**:1987-1992.

Cheng L, Yin WJ, Zhang JF and Qi JS (2009) Amyloid β-protein fragments 25-35 and 31-35 potentiate long-term depression in hippocampal CA1 region of rats in vivo. *Synapse* **63**:206-214.

Ciabarra AM, Sullivan JM, Gahn LG, Pecht G, Heinemann S and Sevarino KA (1995) Cloning and charactrization of χ-1: A developmentally regulated member of a novel class of the ionotropic glutamate receptor. *The Journal of Neuroscience* **15**:6498-6508.

Cole GM, Lim GP, Yang F, Teter B, Begum A, Ma Q, Harris-White ME and Frautschy SA (2005) Prevention of Alzheimer's disease: Omega-3 fatty acid and phenolic anti-oxidant interventions. *Neurobiol Aging* **26 Suppl 1**:133-136.

Collingridge GL and Bliss TVP (1987) NMDA receptors—their role in long-term potentiation. *Trends in Neuroscience* **10**:288-293.

Collingridge GL, Olsen RW, Peters J and Spedding M (2009) A nomenclature for ligand-gated ion channels. *Neuropharmacology* **56**:2-5.

Craig LA, Hong NS and McDonald RJ (2011) Revisiting the cholinergic hypothesis in the development of Alzheimer's disease. *Neuroscience and Biobehavioural Reviews* **35**:1397-1409.

Crews L and Masliah E (2010) Molecular mechanisms of neurodegeneration in Alzheimer's disease. *Human Molecular Genetics* **19**:12-20.

Crofts A (2011) Ion channel block of *N*-methyl-D-aspartate receptors, in *School of Biology* p 80, University of Nottingham, Nottingham, UK.

Crouch PJ, Harding SM, White AR, Camakaris J, Bush AI and Masters CL (2008) Mechanisms of Aβ mediated neurodegeneration in Alzheimer's disease. *International Journal of Biochemistry & Cell Biology* **40**:181-198.

Cull-Candy S, Brickley S and Farrant M (2001) NMDA receptor subunits: diversity, development and disease. *Current opinion in neurobiology* **11**:327-335.

Cull-Candy SG (2007) NMDA Receptors. *eLS* doi: 10.1002/9780470015902.a0000254.pub2.

Dale P, Augustine GJ, Fitzpatrick D, Hall WC, LaMantia A-S, McNamara JO and White LE (2008) *Neuroscience*, Sinauer Associates.

Danysz W and Parsons CG (2012) Alzheimer's disease, β-amyloid, glutamate, NMDA receptors and memantine - searching for the connections. *British Journal of Pharmacology* **167**:324-352.

Danysz W, Zajaczkowski W and Parsons CG (1995) Modulation of learning processes by ionotropic glutamate receptor ligands. *Behavioural Pharmacology* **6**:455-474.

Das S, Sasaki YF, Rothe T, Premkumar LS, Takasu M, Crandall JE, Dikkes P, Conner DA, Rayudu PV, Cheung W, Chen HS, Lipton SA and Nakanishi N (1998) Increased NMDA current and spine density in mice lacking the NMDA receptor subunit NR3A. *Nature* **393**:377-381.

Davies J and Watkins JC (1977) Effects of magnesium ions on the responses of spinal neurones to excitatory amino acids and acetylcholine. *Brain Research* **130**:364-368.

de Carvalho LP, Bochet P and Rossier J (1996) The endogenous agonist quinolinic acid and the non endogenous homoquinolinic acid discriminate between NMDAR2 receptor subunits. *Neurochemistry international* **28**:445-452.

De Felice FG, Velasco PT, Lambert MP, Viola K, Fernandez SJ, Ferreira ST and Klein WL (2007) Aβ oligomers induce neuronal oxidative stress through an *N*-methyl-D-aspartate receptor-dependent mechanism that is blocked by the Alzheimer drug memantine. *The Journal of biological chemistry* **282**:11590-11601.

De La Cruz JP, Ruiz-Moreno MI, Guerrero A, Lopez-Villodres JA, Reyes JJ, Espartero JL, Labajos MT and Gonzalez-Correa JA (2015) Role of the catechol group in the antioxidant and neuroprotective effects of virgin olive oil components in rat brain. *The Journal of nutritional biochemistry* **26**:549-555.

De Strooper B, Saftig P, Craessaerts K, Vanderstichele H, Guhde G, Annaert W, Von Figura K and Van Leuven F (1998) Deficiency of presenilin-1 inhibits the normal cleavage of amyloid precursor protein. *Nature* **391**:387-390.

Delldot (2007) Simplified model of NMDAR activation and various types of NMDAR blockers, in *https://commonswikimediaorg/wiki/File:NMDA_receptor_activation_and_antagonistsPNG* (NMDA_receptor_activation_and_antagonists.PNG ed).

Derkach VA, Oh MC, Guire ES and Soderling TR (2007) Regulatory mechanisms of AMPA receptors in synaptic plasticity. *Nature Reviews Neuroscience* **8**:101-113.

Diamond BJ (2011) Organic Brain Syndrome, in *Encyclopedia of Clinical Neuropsychology* (Kreutzer JS, DeLuca J and Caplan B eds) pp 1825-1828, Springer New York, New York, NY.

Dingledine R, Borges K, Bowie D and Traynelis SF (1999) The glutamate receptor ion channels. *Pharmacological reviews* **51**:7-62.

Dolan H, Crain B, Troncoso J, Resnick SM, Zonderman AB and Obrien RJ (2010) Atherosclerosis, dementia, and Alzheimer disease in the Baltimore Longitudinal Study of Aging cohort. *Annals of Neurology* **68**:231-240.

Dong S, Duan Y, Hu Y and Zhao Z (2012) Advances in the pathogenesis of Alzheimer's disease: a re-evaluation of amyloid cascade hypothesis. *Translational Neurodegeneration* **1**.

Dragicevic N, Copes N, O'Neal-Moffitt G, Jin J, Buzzeo R, Mamcarz M, Tan J, Cao C, Olcese JM, Arendash GW and Bradshaw PC (2011) Melatonin treatment restores mitochondrial function in Alzheimer's mice: A mitochondrial protective role of melatonin membrane receptor signaling. *Journal of Pineal Research* **51**:75–86.

Drake J, Link CD and Butterfield DA (2003) Oxidative stress precedes fibrillar deposition of Alzheimer's disease amyloid β-peptide (1–42) in a transgenic Caenorhabditis elegans model. *Neurobiology of Aging* **24**:415-420.

Dravid SM, Erreger K, Yuan H, Nicholson K, Le P, Lyuboslavsky P, Almonte A, Murray E, Mosely C, Barber J, French A, Balster R, Murray TF and Traynelis SF (2007) Subunit-specific mechanisms and proton sensitivity of NMDA receptor channel block. *The Journal of physiology* **581**:107-128.

Eldar-Finkelman H and Martinez A (2011) GSK-3 inhibitors: preclinical and clinical focus on CNS. *Frontiers in Molecular Neuroscience* **4**:32.

Eldefrawi AT, Eldefrawi ME, Konno K, Mansour NA, Nakanishi K, Oltz E and Usherwood PNR (1988) Structure and synthesis of a potent glutamate receptor antagonist in wasp venom. *Proceedings of the National Academy of Sciences of the United States of America* **85**:4910-4913.

Erreger K, Chen PE, Wyllie DJA and Traynelis PSF (2004) Glutamate receptor gating. *Critical Reviews in Neurobiology* **16**:187-224.

Evans RH, Francis AA and Watkins JC (1977) Selective antagonism by Mg^{2+} of amino acid-induced depolarization of spinal neurones. *Experientia* **33**:489-491.

Farrimond LE, Roberts E and McShane R (2012) Memantine and cholinesterase inhibitor combination therapy for Alzheimer's disease: a systematic review. *BMJ open* **2**.

Fava A, Pirritano D, Plastino M, Cristiano D, Puccio G, Colica C, Ermio C, De Bartolo M, Mauro G and Bosco D (2013) The effect of lipoic acid therapy on cognitive functioning in patients with Alzheimer's disease. *Journal of Neurodegenerative Diseases* **2013**:1-7.

Feng Y and Wang X (2012) Antioxidant therapies for Alzheimer's disease. *Oxidative medicine and cellular longevity* **2012**:472932.

Ferrer-Montiel, V. A, Merino JM, Planells-Cases R, Sun W and Montal M (1998) Structural determinants of the blocker binding site in glutamate and NMDA receptor channels. *Neuropharmacology* **37**:139-147.

Ferrer-Montiel AV, Sun W and Montal M (1995) Molecular design of the *N*-methyl-D-aspartate receptor binding site for phencyclidine and dizolcipine. *Proceedings of the National Academy of Sciences USA* **92**:8021-8025.

Fibiger HC (1991) Cholinergic mechanisms in learning, memory and dementia: a review of recent evidence. *Trends in Neuroscience* **14**:220–223.

Forcina MS, Ciabarra AM and Seravino KA (1995) Cloning of chi-2: a putative member of the ionotropic glutamate receptor superfamily. *Society for Neuroscience Annual Meeting Abstract* **21**:438.433.

Forest Laboratories I (2003) Memantine HCl, Food and Drug Administration, USA.

Foster AC and Wong EHF (1987) The novel anticonvulsant MK-801 binds to the activated state of the *N*-methyl-D-aspartate receptor in rat brain. *British Journal of Pharmacology* **91**:7.

Foy CJ, Passmore AP, Vahidassr MD, Young IS and Lawson JT (1999) Plasma chain-breaking antioxidants in Alzheimer's disease, vascular dementia and Parkinson's disease. *QJM: An International Journal of Medicine* **92**:39–45.

Francis PT (2005) The interplay of neurotransmitters in Alzheimer's disease. *CNS Spectrums* **10**:6-9.

Francis PT, Palmer AM, Snape M and Wilcock GK (1999) The cholinergic hypothesis of Alzheimer's disease: a review progress. *Journal of Neurology, Neurosurgery & Psychiatry* **66**:137–147.

Frankiewicz T, Potier B, Bashir Z, Collingridge GL and Parsons CG (1996) Effects of memantine and MK-801 on NMDA-induced currents in cultured neurons and on synaptic transmission and LTP in area CA1 of rat hippocampal slices. *British Joumal of Pharmacology* **117**:689-697.

Frolund S, Bella A, Kristensen AS, Ziegler HL, Witt M, Olsen CA, Strømgaard K, Franzyk H and Jaroszewski JW (2010) Assessment of structurally diverse philanthotoxin analogues for inhibitory activity on ionotropic glutamate receptor subtypes: discovery of nanomolar, nonselective, and use-dependent antagonists. *Journal of Medicinal Chemistry* **53**:7441-7451.

Fujisawa S, Atsumi T, Ishihara M and Kadoma Y (2004) Cytotoxicity, ROS-generation Activity and Radical-Scavenging Activity of Curcumin and Related Compounds. *Anticancer Research* **24**:563-569.

Fukuzawa K, Kogure K, Morita M, Hama S, Manabe S and Tokumura A (2004) Enhancement of nitric oxide and superoxide generations by alpha-tocopheryl succinate and its apoptotic and anticancer effects. *Biochemistry (Moscow)* **69**:50-57.

Furukawa H, Singh SK, Mancusso R and Gouaux E (2005) Subunit arrangement and function in NMDA receptors. *Nature* **438**:185-192.

Geiger JR, Melcher T, Koh DS, Sakmann B, Seeburg PH, Jonas P and Monyer H (1995) Relative abundance of subunit mRNAs determines gating and Ca^{2+} permeability of AMPA receptors in principal neurons and interneurons in rat CNS. *Neuron* **15**:193-204.

Gielen M, Siegler Retchless B, Mony L, Johnson JW and Paoletti P (2009) Mechanism of differential control of NMDA receptor activity by NR2 subunits. *Nature* **459**:703-707.

Gilgun-Sherki Y, Melamed E and Offen D (2001) Oxidative stress induced-neurodegenerative diseases: the need for antioxidants that penetrate the blood brain barrier. *Neuropharmacology* **40**:959–975.

Gilgun-Sherki Y, Melamed E and Offen D (2003) Antioxidant treatment in Alzheimer's disease: current state. *Journal of Molecular Neuroscience* **21**:1-11.

Gilling KE, Jatzke C, Hechenberger M and Parsons CG (2009) Potency, voltage-dependency, agonist concentration-dependency, blocking kinetics and partial untrapping of the uncompetitive N-methyl-D-aspartate (NMDA) channel blocker memantine at human NMDA (GluN1/GluN2A) receptors. *Neuropharmacology* **56**:866-875.

Goedert M and Ghetti B (2007) Alois Alzheimer: His life and times. *Brain Pathology* **17**:57-62.

Goldin AL (2006) Expression of ion channels in *Xenopus* oocytes, in *Expression and Analysis of Recombinant Ion Channels: From Structural Studies to Pharmacological Screening* (Clare JJ and Trezise DJ eds) p 25, Wiley-VCH Verlag GmbH & Co. KGaA, Weinheim, Germany

Gundersen CB, Miledi R and Parker I (1984) Messenger RNA from human brain induces drug- and voltage-operated channels in *Xenopus* oocytes. *Nature* **308**:421-424.

Gurdon JB, Lane CD, Woodland HR and Marbaix G (1971) Use of frog eggs and oocytes for the study of messenger RNA and its translation in living cells. *Nature* **233**:177-182.

Gutzmann H and Hadler D (1998) Sustained efficacy and safety of idebenone in the treatment of Alzheimer's disease: update on a 2-year double-blind multicentre study. *Journal of Neural Transmission* **54**:301-310.

Henley JM and Wilkinson KA (2016) Synaptic AMPA receptor composition in development, plasticity and disease. *Nature Reviews Neuroscience* **17**:337-350.

Hensley K, Carney JM, Mattson MP, Aksenova M, Harris M, Wu JF, Floyd RA and Butterfield DA (1994) A model for β-amyloid aggregation and neurotoxicity based on free radical generation by the peptide: relevance to Alzheimer disease. *Proceedings of the National Academy of Sciences USA* **91**:3270-3274.

Henson MA, Roberts AC, Pérez-Otaño I and Philpot BD (2010) Influence of the NR3A subunit on NMDA receptor functions. *Progress in Neurobiology* **91**:23-37.

Hirai K, Hayako H, Kato K and Miyamoto M (1998) Idebenone protects hippocampal neurons against amyloid beta-peptide-induced neurotoxicity in rat primary cultures. *Naunyn-Schmiedeberg's Archives of Pharmacology* **358**:582–585.

Hollmann M and Heinemann S (1994) Cloned glutamate receptors. *Annual Review of Neuroscience* **17**:31-108.

Hollmann M, O'Shea-Greenfield A, Rogers SW and Heinemann S (1989) Cloning by functional expression of a member of the glutamate receptor family. *Nature* **342**:643-648.

Holmquist L, Stuchbury G, Berbaum K, Muscat S, Young S, Hager K, Engel J and Munch G (2007) Lipoic acid as a novel treatment for Alzheimer's disease and related dementias. *Pharmacology & therapeutics* **113**:154-164.

Holtmaat A and Svoboda K (2009) Experience-dependent structural synaptic plasticity in the mammalian brain. *Nature Reviews Neuroscience* **10**:647-658.

Howlett DR, George AR, Owen DE, Ward RV and Markwell RE (1999) Common structural features determine the effectiveness of carvedilol, daunomycin and rolitetracycline as inhibitors of Alzheimer *β*-amyloid fibril formation. *Biochemical Journal* **343**:419-423.

Hsieh H, Boehm J, Sato C, Iwatsubo T, Tomita T, Sisodia S and Malinow R (2006) AMPA-R removal underlies Aβ-induced synaptic depression and dendritic spine loss. *Neuron* **52**:831-843.

Hu NW, Klyubin I, Anwyl R and Rowan MJ (2009) GluN2B subunit-containing NMDA receptor antagonists prevent Aβ-mediated synaptic plasticity disruption in vivo. *Proceedings of the National Academy of Sciences USA* **106**:20504-20509.

Huang D, Jiang H, Nakanishi K and Usherwood PNR (1997) Synthesis and pharmacological activity of philanthotoxin-343 analogs: Antagonists of ionotropic glutamate receptors. *Tetrahedron* **53**:12391-12404.

Huang S, Zhang CP, Li GQ, Sun YY, Wang K and Hu FL (2014) Identification of catechol as a new marker for detecting propolis adulteration. *Molecules* **19**:10208-10217.

Huettner JE and Bean BP (1988) Block of *N*-methyl-D-aspartate-activated current by the anticonvulsant MK-801: selective binding to open channels. *Proceedings of the National Academy of Sciences USA* **85**:1307-1311.

Ikeda K, Nagasawa M, Mori H, Araki K, Sakimura K, Watanabe M, Inoue Y and Mishina M (1992) Cloning and expression of the ε4 subunit of the NMDA receptor channel. *FEBS Letters* **313**:34-38.

Imtiaz B, Tolppanen AM, Kivipelto M and Soininen H (2014) Future directions in Alzheimer's disease from risk factors to prevention. *Biochemical Pharmacology* **88**:661-670.

Iqbal K, Liu F and Gong CX (2014) Alzheimer disease therapeutics: Focus on the disease and not just plaques and tangles. *Biochemical Pharmacology* **88**:631-639.

Isaac JT, Ashby MC and McBain CJ (2007) The role of the GluR2 subunit in AMPA receptor function and synaptic plasticity. *Neuron* **54**:859-871.

Ishii T, Moriyoshi K, Sugihara H, Sakurada K, Kadotani H, Yokoi M, Akazawa C, Shigemoto R, Mizuno N, Masu M and Nakanishi S (1993) Molecular characterization of the family of the *N*-methyl-D-aspartate receptor subunits. *The Journal of biological chemistry* **268**:2836-2843.

Jansen M (2016) Jansen Laboratory - Research, Texas Tech University, Texas, USA.

Jonas P and Burnashev N (1995) Molecular mechanisms controlling calcium entry through AMPA-type glutamate receptor channels. *Neuron* **15**:987-990.

Justino GC, Correia CF, Mira L, Borges Dos Santos RM, Martinho Simões JA, Silva AM, Santos C and Gigante B (2006) Antioxidant activity of a catechol derived from abietic acid. *Journal of Agricultural and Food Chemistry* **54**:342-348.

Kachel HS (2014) Inhibition of Mammalian Nicotinic Acetylcholine Receptors by Philanthotoxin Analogues is Strongly Influenced by Subunit Composition, in *School of Life Sciences, Faculty of Medicine and Health Sciences* p 172, University of Nottingham, Nottingham, UK.

Kadoma Y, Atsumi T, Okada N, Ishihara M, Yokoe I and Fujisawa S (2007) Radical-scavenging Activity of Natural Methoxyphenols vs. Synthetic Ones using the Induction Period Method. *Molecules* **12**:130-138.

Karadottir R, Cavelier P, Bergersen LH and Attwell D (2005) NMDA receptors are expressed in oligodendrocytes and activated in ischaemia. *Nature* **438**:1162-1166.

Káradóttir R, Cavelier P, Bergersen LH and Attwell D (2005) NMDA receptors are expressed in oligodendrocytes and activated in ischaemia. *Nature* **438**:1162–1166.

Kashiwagi K, Masuko T, Nguyen CD, Kuno T, Tanaka I, Igarashi K and Williams K (2002) Channel blockers acting at *N*-methyl-D-aspartate receptors: differential effects of mutations in the vestibule and ion channel pore. *Molecular Pharmacology* **61**:533-545.

Kashiwagi K, Pahk AJ, Masuko T, Igarashi K and Williams K (1997) Block and modulation of *N*-methyl-D-aspartate receptors by polyamines and protons: Role of amino acid residues in the transmembrane and pore-forming regions of NR1 and NR2 subunits. *Molecular Pharmacology* **52**:701-713.

Kashiwagi K, Tanaka I, Tamura M, Sugiyama H, Okawara T, Otsuka M, Sabado TN, Williams K and Igarashi K (2004) Anthraquinone polyamines: novel channel blockers to study N-methyl-D-aspartate receptors. *Journal of Pharmacology and Experimental Therapeutics* **309**:884-893.

Kashiwagi K, Williams K and Igarashi K (2007) Anthraquinone polyamines: novel channel blockers of *N*-methyl-D-aspartate receptors. *Amino acids* **33**:299-304.

Kehoe LA, Bernardinelli Y and Muller D (2013) GluN3A: an NMDA receptor subunit with exquisite properties and functions. *Neural plasticity* **2013**:145387.

Kessels HW, Nabavi S and Malinow R (2013) Metabotropic NMDA receptor function is required for β-amyloid-induced synaptic depression. *Proceedings of the National Academy of Sciences USA* **110**:4033-4038.

Khan TR (1994) Action of philanthotoxin on ion channels of arthropod muscle, in *Life Science Department* p 133, University of Nottingham, Nottingham, UK.

Kim AH, Kerchner GA and Choi DW (2002) Blocking Excitotoxicity, in *CNS Neuroprotection* (Marcoux FW and Choi DW eds) pp 3–36, Springer, New York.

Kim JH, Anwyl R, Suh YH, Djamgoz MB and Rowan MJ (2001) Use-dependent effects of amyloidogenic fragments of β-amyloid precursor protein on synaptic plasticity in rat hippocampus *in vivo*. *The Journal of Neuroscience* **21**:1327-1333.

Kleckner NW and Dingledine R (1988) Requirement for glycine in activation of NMDA-receptors expressed in *Xenopus* oocytes. *Science* **241**:835-837.

Klyubin I, Betts V, Welzel AT, Blennow K, Zetterberg H, Wallin A, Lemere CA, Cullen WK, Peng Y, Wisniewski T, Selkoe DJ, Anwyl R, Walsh DM and Rowan MJ (2008) Aβ dimer-containing human CSF disrupts synaptic plasticity: prevention by systemic passive immunization. *The Journal of Neuroscience* **28**:4231-4237.

Klyubin I, Walsh DM, Cullen WK, Fadeeva JV, Anwyl R, Selkoe DJ and Rowan MJ (2004) Soluble arctic amyloid β protein inhibits hippocampal long-term potentiation *in vivo*. *European Journal of Neuroscience* **19**:2839-2846.

Knight HM, Walker R, James R, Porteous DJ, Muir WJ, Blackwood DH and Pickard BS (2012) GRIK4/KA1 protein expression in human brain and correlation with bipolar disorder risk variant status. *American Journal of Medical Genetics Part B, Neuropsychiatric Genetics* **159B**:21-29.

Koek W, Woods JH and Winger GD (1988) MK-801, a proposed noncompetitive antagonist of excitatory amino acid neurotransmission, produces phencyclidine-like behavioral effects in pigeons, rats and rhesus monkeys. *The Journal of pharmacology and experimental therapeutics* **245**:969-974.

Koga K, Sim SE, Chen T, Wu LJ, Kaang BK and Zhuo M (2012) Kainate receptor-mediated synaptic transmissions in the adult rodent insular cortex. *Journal of neurophysiology* **108**:1988-1998.

Korcsmaros T, Szalay MS, Böde C, Kovacs IA and Csermely P (2007) How to design multi-target drugs: Target search options in cellular network. *Expert Opinion on Drug Discovery* **2**:799-808.

Kornhuber J and Quack G (1995) Cerebrospinal fluid and serum concentrations of the *N*-methyl-D-aspartate (NMDA) receptor antagonist memantine in man. *Neuroscience letters* **195**:3.

Kotermanski SE, Wood JT and Johnson JW (2009) Memantine binding to a superficial site on NMDA receptors contributes to partial trapping. *The Journal of physiology* **587**:4589-4604.

Kovacic P and Somanathan R (2010) Clinical physiology and mechanism of dizocilpine (MK-801). *Oxidative medicine and cellular longevity* **3**:13–22.

Kristiansen LV, Huerta I, Beneyto M and Meador-Woodruff JH (2007) NMDA receptors and schizophrenia. *Current opinion in pharmacology* **7**:48-55.

Kumar J and Mayer ML (2013) Functional insights from glutamate receptor ion channel structures. *Annual review of physiology* **75**:313-337.

Kuner T and Schoepfer R (1996) Multiple structural elements determine subunit specificity of Mg^{2+} block in NMDA receptor channels. *The Journal of Neuroscience* **16**:3549-3558.

Kushner L, Lerma J, Zukin RS and Bennett MV (1988) Coexpression of *N*-methyl-D-aspartate and phencyclidine receptors in *Xenopus* oocytes injected with rat brain mRNA. *Proceedings of the National Academy of Sciences USA* **85**:3250-3254.

Kutsuwada T, Kashiwabuchi N, Mori H, Sakimura K, Kushiya E, Araki K, Meguro H, Masaki H, Kumanishi T, Arakawa M and Mishina M (1992) Molecular diversity of the NMDA receptor channel. *Nature* **358**:36-41.

Kvist T, Greenwood JR, Hansen KB, Traynelis SF and Brauner-Osborne H (2013) Structure-based discovery of antagonists for GluN3-containing N-methyl-D-aspartate receptors. *Neuropharmacology* **75**:324-336.

Lacor PN, Buniel MC, Furlow PW, Clemente AS, Velasco PT, Wood M, Viola KL and Klein WL (2007) Aβ oligomer-induced aberrations in synapse composition, shape, and density provide a molecular basis for loss of connectivity in Alzheimer's disease. *The Journal of Neuroscience* **27**:796-807.

Lalo U, Pankratov Y, Kirchhoff F, North RA and Verkhratsky A (2006) NMDA receptors mediate neuron-to-glia signaling in mouse cortical astrocytes. *The Journal of Neuroscience* **26**:2673-2683.

Landgrave-Gomez J, Mercado-Gomez O and Guevara-Guzman R (2015) Epigenetic mechanisms in neurological and neurodegenerative diseases. *Frontiers in cellular neuroscience* **9**:58.

Laurie DJ and Seeburg PH (1994) Ligand affinities at recombinant *N*-methyl-D-aspartate receptors depend on subunit composition. *European Journal of Pharmacology* **268**:335-345.

Lerma J, Kushner L, Spray DC, Bennett MV and Zukin RS (1989) mRNA from NCB-20 cells encodes the *N*-methyl-D-aspartate/phencyclidine receptor: a *Xenopus* oocyte expression study. *Proceedings of the National Academy of Sciences USA* **86**:1708-1711.

Lerma J, Paternain AV, Rodríguez-Moreno A and López-García JC (2001) Molecular physiology of kainate receptors. *Physiological Reviews* **81**:971-998.

Li M (1999) *NMDA Receptor Protocols*, Humana Press.

Liljequist S, Ossowska K, Grabowska-Andén M and Andén NE (1991) Effect of the NMDA receptor antagonist, MK-801, on locomotor activity and on the metabolism of dopamine in various brain areas of mice. *European Journal of Pharmacology* **195**:55-61.

Lipton SA (2006) Paradigm shift in neuroprotection by NMDA receptor blockade: Memantine and beyond. *Nature Reviews Drug Discovery* **5**:160-170.

Liu J (2008) The effects and mechanisms of mitochondrial nutrient alpha-lipoic acid on improving age-associated mitochondrial and cognitive dysfunction: an overview. *Neurochemical research* **33**:194-203.

Liu RY, Zhou JN, van Heerikhuize J, Hofman MA and Swaab DF (1999) Decreased melatonin levels in postmortem cerebrospinal fluid in relation to aging, Alzheimer's disease, and apolipoprotein E-ε4/4 genotype. *Journal of Clinical Endocrinology and Metabolism* **84**:323-327.

Liu XB, Murray KD and Jones EG (2004) Switching of NMDA receptor 2A and 2B subunits at thalamic and cortical synapses during early postnatal development. *The Journal of Neuroscience* **24**:8885-8895.

Liu Y, Hill RH, Arhem P and von Euler G (2001) NMDA and glycine regulate the affinity of the Mg^{2+}-block site in NR1-1a/NR2A NMDA receptor channels expressed in *Xenopus* oocytes. *Life Sciences* **68**:1817–1826.

Llorens-Martin M, Jurado J, Hernandez F and Avila J (2014) GSK-3β, a pivotal kinase in Alzheimer disease. *Frontiers in Molecular Neuroscience* **7**:46.

Lopez-Arrieta JM and Schneider L (2006) Metrifonate for Alzheimer's disease. *Cochrane Database of Systematic Reviews*:CD003155.

Loy C and Schneider L (2006) Galantamine for Alzheimer's disease and mild cognitive impairment. *Cochrane Database of Systematic Reviews*:CD001747.

Lynch MA (2004) Long-term potentiation and memory. *Physiological Reviews* **84**:87–136.

Lysko PG, Lysko KA, Webb CL, Feuerstein G, Mason PE, Walter F and Mason P (1998) Neuroprotective activities of carvedilol and a hydroxylated derivative: Role of membrane biophysical interactions. *Biochemical Pharmacology* **56**:1645–1656.

Lysko PG, Webb CL and Feuerstein G (1994) Neuroprotective effects of carvedilol, a new antihypertensive, as a Na+ channel modulator and glutamate transport inhibitor. *Neuroscience letters* **171**:77-80.

Maczurek A, Hager K, Kenklies M, Sharman M, Martins R, Engel J, Carlson DA and Munch G (2008) Lipoic acid as an anti-inflammatory and neuroprotective treatment for Alzheimer's disease. *Advanced drug delivery reviews* **60**:1463-1470.

Malinow R (2012) New developments on the role of NMDA receptors in Alzheimer's disease. *Current opinion in neurobiology* **22**:559-563.

Martinez-Turrillas R, Puerta E, Chowdhury D, Marco S, Watanabe M, Aguirre N and Perez-Otano I (2012) The NMDA receptor subunit GluN3A protects against 3-nitroproprionic-induced striatal lesions via inhibition of calpain activation. *Neurobiology of Disease* **48**:290-298.

Masuda T, Hidaka K, Shinohara A, Maekawa T, Takeda Y and Yamaguchi H (1999) Chemical Studies on Antioxidant Mechanism of Curcuminoid: Analysis of Radical Reaction Products from Curcumin. *Journal of Agricultural and Food Chemistry* **47**:71−77.

Matsuda K, Kamiya Y, Matsuda S and Yuzaki M (2002) Cloning and characterization of a novel NMDA receptor subunit NR3B: A dominant subunit that reduces calcium permeability. *Molecular Brain Research* **100**:43–52.

Matsui T, Sekiguchi M, Hashimoto A, Tomita U, Nishikawa T and Wada K (1995) Functional comparison of D-serine and glycine in rodents: the effect on cloned NMDA receptors and the extracellular concentration. *Journal of neurochemistry* **65**:454-458.

Matsunaga S, Kishi T and Iwata N (2015) Combination therapy with cholinesterase inhibitors and memantine for Alzheimer's disease: a systematic review and meta-analysis. *International Journal of Neuropsychopharmacology* **18**.

Mattson MP (2004) Pathways towards and away from Alzheimer's disease. *Nature* **430**:631-639.

Mayer ML (2011a) Emerging models of glutamate receptor ion channel structure and function. *Structure* **19**:1370-1380.

Mayer ML (2011b) Structure and mechanism of glutamate receptor ion channel assembly, activation and modulation. *Current opinion in neurobiology* **21**:283-290.

Mayer ML and Westbrook GL (1987) The physiology of excitatory amino acids in the vertebrate central nervous system. *Progress in Neurobiology* **28**:197-276.

Mayer ML, Westbrook GL and Guthrie PB (1984) Voltage-dependent block by Mg^{2+} of NMDA responses in spinal cord neurones. *Nature* **309**:261-263.

McClymont DW (2010) Exploring open channel block of the NMDA receptor, in *School of Biology* p 244, University of Nottingham, Nottingham, UK.

McClymont DW, Harris J and Mellor IR (2012) Open-channel blockade is less effective on GluN3B than GluN3A subunit-containing NMDA receptors. *European Journal of Pharmacology* **686**:22-31.

McShane R, Areosa Sastre A and Minakaran N (2006) Memantine for dementia. *Cochrane Database for Systematic Reviews*:CD003154.

Mecocci P and Polidori MC (2012) Antioxidant clinical trials in mild cognitive impairment and Alzheimer's disease. *Biochimica et Biophysica Acta* **1822**:631-638.

Meguro H, Mari H, Araki K, Kushiya E, Kutsuwada T, M. Y, Kumanishi T, Arakawa M, Sakimura K and Mishina M (1992) Functional characterization of a heteromeric NMDA receptor channel expressed from cloned cDNAs. *Nature* **357**:70-74.

Mehta M, Adem A and Sabbagh M (2012) New acetylcholinesterase inhibitors for Alzheimer's disease. *International Journal of Alzheimer's Disease* **2012**:728983.

Melchiorre C, Antonello A, Banzi R, Bolognesi ML, Minarini A, Rosini M and Tumiatti V (2003) Polymethylene tetraamine backbone as template for the development of biologically active polyamines. *Medicinal research reviews* **23**:200-233.

Meldrum B (1985) Possible therapeutic applications of antagonists of excitatory amino acid neurotransmitters. *Clinical Science* **68**:113–122.

Meldrum BS (2000) Glutamate as a neurotransmitter in the brain- review of physiology and pathology. *Journal of Nutrition* **130**:1007S-1015S.

Mellor IR, Brier TJ, Pluteanu F, Strømgaard K, Saghyan A, Eldursi N, Brierley MJ, Andersen K, Jaroszewski JW, Krogsgaard-Larsen P and Usherwood PNR (2003) Modification of the philanthotoxin-343 polyamine moiety results in different structure-activity profiles at muscle nicotinic ACh, NMDA and AMPA receptors. *Neuropharmacology* **44**:70-80.

Mellor IR and Usherwood PN (2004) Targeting ionotropic receptors with polyamine-containing toxins. *Toxicon : official journal of the International Society on Toxinology* **43**:493-508.

Meltzer CC and Francis PT (2001) Brain aging research at the close of the 20th century: from bench to bedside. *Dialogues in Clinical Neuroscience* **3**:167-180.

Mertz JE and Gurdon JB (1977) Purified DNAs are transcribed after microinjection into *Xenopus* oocytes. *Proceedings of the National Academy of Sciences USA* **74**:1502–1506.

Micu I, Jiang Q, Coderre E, Ridsdale A, Zhang L, Woulfe J, Yin X, Trapp BD, McRory JE, Rehak R, Zamponi GW, Wang W and Stys PK (2006) NMDA receptors mediate calcium accumulation in myelin during chemical ischaemia. *Nature* **439**:988-992.

Miklossy J (2015) Historic evidence to support a causal relationship between spirochetal infections and Alzheimer's disease. *Frontiers in aging neuroscience* **7**:46.

Miledi R (1982) A calcium-dependent transient outward current in *Xenopus* laevis oocytes. *Proceedings of the Royal Society B: Biological Sciences* **215**:491-497.

Miners JS, Baig S, Palmer J, Palmer LE, Kehoe PG and Love S (2008) Aβ-degrading enzymes in Alzheimer's disease. *Brain Pathology* **18**:240-252.

Mirshahi T and Woodward JJ (1995) Ethanol sensitivity of heteromeric NMDA receptors: effects of subunit assembly, glycine and NMDAR1 Mg(2+)-insensitive mutants. *Neuropharmacology* **34**:347-355.

Moeller HB and Fenton RA (2010) Can one Bad Egg' really spoil the batch? *The Journal of physiology* **588**:2283-2284.

Moine G (2008) Xenopus laevis, in *http://wwwflickrcom/photos/gregory-moine/3100727791/* (Xenopus_laevis.png ed), France.

Molino I, Colucci L, Fasanaro AM, Traini E and Amenta F (2013) Efficacy of memantine, donepezil, or their association in moderate-severe Alzheimer's disease: A review of clinical trials. *The Scientific World Journal* **2013**:925702.

Molinuevo JL (2005) Memantine: Targeting glutamate excitotoxicity in Alzheimer's disease and other dementias. *American Journal of Alzheimer's Disease and Other Dementias* **20**:77-85.

Monaghan DT, Irvine MW, Costa BM, Fang G and Jane DE (2012) Pharmacological modulation of NMDA receptor activity and the advent of negative and positive allosteric modulators. *Neurochemistry international* **61**:581-592.

Monyer H, Sprengel R, Schoepfer R, Herb A, Higuchi M, Lomeli H, Burnashev N, Sakmann B and Seeburg PH (1992) Heteromeric NMDA receptors: molecular and functional distinction of subtypes. *Science* **256**:1217-1221.

Moreira PI, Honda K, Liu Q, Santos MS, Oliveira CR, Aliev G, Nunomura A, Zhu X, Smith MA and Perry G (2005) Oxidative stress: the old enemy in Alzheimer's disease pathophysiology. *Current Alzheimer Research* **2**:403-408.

Mori H, Masaki H, Yamakura T and Mishina M (1992) Identification by mutagenesis of a Mg^{2+}-block site of the NMDA receptor channel. *Nature* **358**:673-675.

Moriyoshi K, Masu M, Ishii T, Shigemoto R, Mizuno N and Nakanishi S (1991) Molecular cloning and characterization of the rat NMDA receptor. *Nature* **354**:31-37.

Murphy K, O'Connor DA, Browning CJ, French SD, Michie S, Francis JJ, Russell GM, Workman B, Flicker L, Eccles MP and Green SE (2014) Understanding diagnosis and management of dementia and guideline implementation in general practice: a qualitative study using the theoretical domains framework. *Implementation Science* **9**.

Nakanishi N, Tu S, Shin Y, Cui J, Kurokawa T, Zhang D, Chen HS, Tong G and Lipton SA (2009) Neuroprotection by the NR3A subunit of the NMDA receptor. *The Journal of Neuroscience* **29**:5260-5265.

Nascimento ECM and Martins JBL (2012) Pharmacophoric profile: Design of new potential drugs with PCA analysis, in *Principal Component Analysis: Multidisciplinary Applications* (Sanguansat P ed), InTech.

Nikolaev MV, Magazanik LG and Tikhonov DB (2012) Influence of external magnesium ions on the NMDA receptor channel block by different types of organic cations. *Neuropharmacology* **62**:2078-2085.

Nilsson A, Duan J, Mo-Boquist LL, Benedikz E and Sundström E (2007) Characterisation of the human NMDA receptor subunit NR3A glycine binding site. *Neuropharmacology* **52**:1151–1159.

Nishi M, Hinds H, Lu HP, Kawata M and Hayashi Y (2001) Motoneuron-specific expression of NR3B, a novel NMDA-type glutamate receptor subunit that works in a dominant-negative manner. *The Journal of Neuroscience* **21**:RC185.

Nishida S (2005) Metabolic effects of melatonin on oxidative stress and diabetes mellitus. *Endocrine* **27**:131–135.

Niswender CM and Conn PJ (2010) Metabotropic Glutamate Receptors: Physiology, Pharmacology, and Disease. . *Annual Review of Pharmacology and Toxicology* **50**:295–322.

Nowak L, Bregestovski P, Ascher P, Herbet A and Prochiantz A (1984) Magnesium gates glutamate-activated channels in mouse central neurones. *Nature* **307**:462-465.

Nowotny P, Kwon JM and Goate AM (2001) Alzheimer Disease. *eLS* doi: 10.1038/npg.els.0000228.

Nunomura A, Castellani RJ, Zhu X, Moreira PI, Perry G and Smith MA (2006) Involvement of oxidative stress in Alzheimer disease. *Journal of Neuropathology & Experimental Neurology* **65**:631-641.

Nygaard HB, van Dyck CH and Strittmatter SM (2014) Fyn kinase inhibition as a novel therapy for Alzheimer's disease. *Alzheimer's research & therapy* **6**.

O'Brien RJ and Wong PC (2011) Amyloid precursor protein processing and Alzheimer's disease. *Annual Review of Neuroscience* **34**:185-204.

Olney JW, Labruyere J and Price MT (1989) Pathological changes induced in cerebrocortical neurons by phencyclidine and related drugs. *Science* **244**:1360-1362.

Pachernegg S, Strutz-Seebohm N and Hollmann M (2012) GluN3 subunit-containing NMDA receptors: not just one-trick ponies. *Trends in neurosciences* **35**:240-249.

Paoletti P, Bellone C and Zhou Q (2013) NMDA receptor subunit diversity: impact on receptor properties, synaptic plasticity and disease. *Nature reviews Neuroscience* **14**:383-400.

Paoletti P and Neyton J (2007) NMDA receptor subunits: function and pharmacology. *Current opinion in pharmacology* **7**:39-47.

Paoletti P, Neyton J and Ascher P (1995) Glycine-independent and subunit-specific potentiation of NMDA responses by extracellular Mg^{2+}. *Neuron* **15**:1109-1120.

Parker I, Gundersen CB and Miledi R (1985) A transient inward current elicited by hyperpolarization during serotonin activation in *Xenopus* oocytes. *Proceedings of the Royal Society of London B: Biological Sciences* **223**:279-292.

Parsons CG and Gilling K (2007) Memantine as an Example of a Fast, Voltage-Dependent, Open Channel N-Methyl-d-Aspartate Receptor Blocker, in *Patch-Clamp Methods and Protocols* (Molnar P and Hickman JJ eds) pp 15-36, Humana Press, Totowa, NJ.

Parsons CG, Quack G, Bresink I, Baran L, Przegalinski E, Kostowski W, Krzascik P, Hartmann S and Danysz W (1995) Comparison of the potency, kinetics and voltage-dependency of a series of uncompetitive NMDA receptor antagonists in vitro with anticonvulsive and motor impairment activity in vivo. *Neuropharmacology* **34**:1239-1258.

Patil NA, Somashekar HS, Narendranath S, Prashanth P, Reddy SK and Ramchandra K (2012) NMDA - agonists and antagonists. *Journal of Pharmacy Research* **5**:632-640.

Patneau DK and Mayer ML (1990) Structure-activity relationships for amino acid transmitter candidates acting at *N*-methyl-D-aspartate and quisqualate receptors. *The Journal of Neuroscience* **10**:2385-2399.

Payne HL (2008) The role of transmembrane AMPA receptor regulatory proteins (TARPs) in neurotransmission and receptor trafficking *Molecular Membrane Biology* **25**:353-362.

Petrenko AB, Yamakura T, Baba H and Shimoji K (2003) The role of *N*-methyl-D-aspartate (NMDA) receptors in pain: a review. *Anesthesia & Analgesia*:1108-1116.

Pickard BS, Knight HM, Hamilton RS, Soares DC, Walker R, Boyd JK, Machell J, Maclean A, McGhee KA, Condie A, Porteous DJ, St Clair D, Davis I, Blackwood DH and Muir WJ (2008) A common variant in the 3'UTR of the GRIK4 glutamate receptor gene affects transcript abundance and protects against bipolar disorder. *Proceedings of the National Academy of Sciences USA* **105**:14940-14945.

Piek T, Mantel P and Engels E (1971) Neuromuscular block in insects caused by the venom of the digger wasp *Philanthus triangulum* F. *Comparative and General Pharmacology* **2**:317-331.

Piek T, Mantel P and Jas H (1980) Ion-channel block in insect muscle fibre membrane by the venom of the digger wasp, *Philanthus triangulum* F. *Journal of Insect Physiology* **26**:345-349.

Piek T and Njio KD (1975) Neuromuscular block in honeybees by the venom of the bee wolf wasp (*Philanthus triangulum* F.). *Toxicon : official journal of the International Society on Toxinology* **13**:199-201.

Planells-Cases R, Sun W, Ferrer-Montiel AV and Montal M (1993) Molecular cloning, functional expression and pharmacological characterization of an *N*-methyl-D-aspartate receptor subunit from human brain. *Proceedings of the National Academy of Sciences USA* **90**:5057-5061.

Premkumar LS and Auerbach A (1996) Identification of a high affinity divalent cation binding site near the entrance of the NMDA receptor channel. *Neuron* **16**:869–880.

Prince M, Bryce R, Albanese E, Wimo A, Ribeiro W and Ferri CP (2013) The global prevalence of dementia: a systematic review and metaanalysis. *Alzheimer's & dementia : the journal of the Alzheimer's Association* **9**:63-75 e62.

Prince M, Wimo A, Guerchet M, Ali G-C, Wu Y-T and Prina M (2015) World Alzheimer report 2015: the global impact of dementia, King's College London, London, UK.

Pusch M (2006) Analysis of Electrophysiological Data, in *Expression and Analysis of Recombinant Ion Channels* pp 111-144, Wiley-VCH Verlag GmbH & Co. KGaA.

Qian A, Buller AL and Johnson JW (2005) NR2 subunit-dependence of NMDA receptor channel block by external Mg^{2+}. *The Journal of physiology* **562**:319-331.

Qiu C, Kivipelto M and von Strauss E (2009) Epidemiology of Alzheimer's disease: occurrence, determinants, and strategies toward intervention. *Dialogues in Clinical Neuroscience* **11**:111-128.

Raghava Raju TV, Anil Kumar N, Raja Kumar S, Malleswara Reddy A, Someswara Rao N and Mrutyunjaya Rao I (2013) Development and validation of a stability-indicating RP-HPLC method for the simultaneous estimation of guaifenesin and dextromethorphan iImpurities in pharmaceutical formulations. *Chromatography Research International* **2013**:1-12.

Rammes G, Danysz W and Parsons CG (2008) Pharmacodynamics of memantine: an update. *Current Neuropharmacology* **6**:55-78.

Ransom RW and Stec NL (1988) Cooperative modulation of [^{3}H]MK-801 binding to the N-methyl-D-aspartate receptor-ion channel complex by L-glutamate, glycine, and polyamines. *Journal of neurochemistry* **51**:830-836.

Reitz C and Mayeux R (2014) Alzheimer disease: Epidemiology, diagnostic criteria, risk factors and biomarkers. *Biochemical Pharmacology* **88**:640-651.

Riedel WJ (2014) Preventing cognitive decline in preclinical Alzheimer's disease. *Current opinion in pharmacology* **14**:18-22.

Risgaard R, Hansen KB and Clausen RP (2010) Partial agonists and subunit selectivity at NMDA receptors. *Chemistry* **16**:13910-13918.

Robinson DS (2008) Treating agitation in Alzheimer's disease: efficacy of memantine. *Primary Psychiatry* **15**:28-30.

Roselli F, Tirard M, Lu J, Hutzler P, Lamberti P, Livrea P, Morabito M and Almeida OF (2005) Soluble β-amyloid$_{1-40}$ induces NMDA-dependent degradation of postsynaptic density-95 at glutamatergic synapses. *The Journal of Neuroscience* **25**:11061-11070.

Rosenberg PB (2011) Pilot Trial of Carvedilol in Alzheimer's Disease. Identifier: NCT01354444. In: ClinicalTrials.gov [Internet]. U.S. National Institutes of Health [cited 28 June 2016] Available from: https://clinicaltrials.gov/ct2/show/NCT01354444.

Rosini M, Andrisano V, Bartolini M, Bolognesi ML, Hrelia P, Minarini A, Tarozzi A and Melchiorre C (2005) Rational approach to discover multipotent anti-Alzheimer drugs. *Journal of Medicinal Chemistry* **4**:360-363

Rosini M, Simoni E, Bartolini M, Cavalli A, Ceccarini L, Pascu N, McClymont DW, Tarozzi A, Bolognesi ML, Minarini A, Tumiatti V, Andrisano V, Mellor IR and Melchiorre C (2008) Inhibition of acetylcholinesterase, β-amyloid aggregation, and NMDA receptors in Alzheimer's disease: a promising direction for the multi-target-directed ligands gold rush. *Journal of Medicinal Chemistry* **51**:4.

Rosini M, Simoni E, Minarini A and Melchiorre C (2014) Multi-target design strategies in the context of Alzheimer's disease: Acetylcholinesterase inhibition and NMDA receptor antagonism as the driving forces. *Neurochemical research*.

Rowan MJ, Klyubin I, Cullen WK and Anwyl R (2003) Synaptic plasticity in animal models of early Alzheimer's disease. *Philosophical Transactions of the Royal Society B: Biological Sciences* **358**:821-828.

Rozen S and Skaletsky HJ (2000) Primer3 on the WWW for General Users and for Biologist Programmers, in *Bioinformatics Methods and Protocols: Methods in Molecular Biology* (Krawetz S and Misener S eds) pp 365-386, Humana Press, Totowa, New Jersey, USA.

Saiki R, Yoshizawa Y, Minarini A, Milelli A, Marchetti C, Tumiatti V, Toida T, Kashiwagi K and Igarashi K (2013) In vitro and in vivo evaluation of polymethylene tetraamine derivatives as NMDA receptor channel blockers. *Bioorganic & medicinal chemistry letters* **23**:3901-3904.

Sakai Y, Kimura H and Okamoto K (1986) Pharmacological characterization of serotonin receptor induced by rat brain messenger RNA in *Xenopus* oocytes. *Brain Research* **362**:199-203.

Sakurada K, Masu M and Nakanishi S (1993) Alteration of Ca^{2+} permeability and sensitivity to Mg^{2+} and channel blockers by a single amino acid substitution in the *N*-methyl-D-aspartate receptor. *The Journal of biological chemistry* **268**:410-415.

Salter MG and Fern R (2005) NMDA receptors are expressed in developing oligodendrocyte processes and mediate injury. *Nature* **438**:1167-1171.

Sano M, Ernesto C, Thomas RG, Klauber MR, Schafer K, Grundman M, Woodbury P, Growdon J, Cotman CW, Pfeiffer E, Schneider LS and Thal LJ (1997) A controlled trial of selegiline, alpha-tocopherol, or both as treatment for Alzheimer's disease. *The New England Journal of Medicine* **336**:1216-1222.

Sans N, Vissel B, Petralia RS, Wang YX, Chang K, Royle GA, Wang CY, O'Gorman S, Heinemann SF and Wenthold RJ (2003) Aberrant formation of glutamate receptor complexes in hippocampal neurons of mice lacking the GluR2 AMPA receptor subunit. *The Journal of Neuroscience* **23**:9367–9373.

Sanz-Clemente A, Nicoll RA and Roche KW (2013) Diversity in NMDA receptor composition: many regulators, many consequences. *Neuroscientist* **19**:62-75.

Sasaki YF, Rothe T, Premkumar LS, Das S, Cui J, Talantova MV, Wong HK, Gong X, Chan SF, Zhang D, Nakanishi N, Sucher NJ and Lipton SA (2002) Characterization and comparison of the NR3A subunit of the NMDA receptor in recombinant systems and primary cortical neurons. *Journal of neurophysiology* **87**:2052-2063.

Schenk D, Hagen M and Seubert P (2004) Current progress in beta-amyloid immunotherapy. *Current opinion in immunology* **16**:599-606.

Schneider JA, Arvanitakis Z, Bang W and Bennett DA (2007) Mixed brain pathologies account for most dementia cases in community-dwelling older persons. *Neurology* **69**:2197-2204.

Schofield PR, Darlison MG, Fujita N, Burt DR, Stephenson FA, Rodriguez H, Rhee LM, Ramachandran J, Reale V, Glencorse TA, Seeburg PH and Barnard EA (1987) Sequence and functional expression of the $GABA_A$ receptor shows a ligand-gated receptor super-family. *Nature* **328**:221-227.

Seiler N (2005) Pharmacological aspects of cytotoxic polyamine analogs and derivatives for cancer therapy. *Pharmacology & therapeutics* **107**:99-119.

Selkoe DJ (2004) Alzheimer disease: Mechanistic understanding predicts novel therapies. *Annals of Internal Medicine* **140**:627-638.

Sevarino KA, Ciabarra AM and Forcina MS (1996) x-1 and x-2, members of a novel class of the glutamate receptor superfamily. *Society for Neuroscience Annual Meeting Abstract* **22**:59219.

Shankar GM, Bloodgood BL, Townsend M, Walsh DM, Selkoe DJ and Sabatini BL (2007) Natural oligomers of the Alzheimer amyloid-β protein induce reversible synapse loss by modulating an NMDA-type glutamate receptor-dependent signaling pathway. *The Journal of Neuroscience* **27**:2866-2875.

Shen CJ, Chang CC, Chen YT, Lai CS and Hsu YC (2016) Melatonin suppresses the growth of ovarian cancer cell Lines (OVCAR-429 and PA-1) and potentiates the effect of G1 arrest by targeting CDKs. *International journal of molecular sciences* **17**.

Shen JX and Yakel JL (2009) Nicotinic acetylcholine receptor-mediated calcium signaling in the nervous system. *Acta pharmacologica Sinica* **30**:673-680.

Sheng N, Shi YS, Lomash RM, Roche KW and Nicoll RA (2015) Neto auxiliary proteins control both the trafficking and biophysical properties of the kainate receptor GluK1. *eLife* **4**:e11682.

Shi J, Zhao C, Feng Y and Pan W (2008) Compositions containing coenzyme q-10 and dihydrolipoic acid, Google Patents.

Shi Y, Suh YH, Milstein AD, Isozaki K, Schmid SM, Roche KW and Nicoll RA (2010) Functional comparison of the effects of TARPs and cornichons on AMPA receptor trafficking and gating. *Proceedings of the National Academy of Sciences USA* **107**:16315-16319.

Siegler Retchless B, Gao W and Johnson JW (2012) A single GluN2 subunit residue controls NMDA receptor channel properties via intersubunit interaction. *Nature neuroscience* **15**:406-413, S401-402.

Sigel E (2001) Microinjection into *Xenopus* Oocytes. *eLS* doi: 10.1038/npg.els.0002658.

Simon RP, Swan JH, Griffiths T and Meldrum BS (1984) Blockade of *N*-methyl-D-aspartate receptors may protect against ischemic damage in the brain. *Science* **226**:850-852.

Small G (2011) 18-Month Study of Curcumin (Curcumin). Identifier: NCT01383161. In: ClinicalTrials.gov [Internet]. U.S. National Institutes of Health [cited 27 June 2016] Available from: https://clinicaltrials.gov/ct2/show/NCT01383161

Smith MA, Rottkamp CA, Nunomura A, Raina AK and Perry G (2000) Oxidative stress in Alzheimer's disease. *Biochimica et Biophysica Acta* **1502**:139-144.

Snyder EM, Nong Y, Almeida CG, Paul S, Moran T, Choi EY, Nairn AC, Salter MW, Lombroso PJ, Gouras GK and Greengard P (2005) Regulation of NMDA receptor trafficking by amyloid-β. *Nature neuroscience* **8**:1051-1058.

Sobolevsky AI, Koshelev SG and Khodorov BI (1998) Interaction of memantine and amantadine with agonist-unbound NMDA-receptor channels in acutely isolated rat hippocampal neurons. *The Journal of physiology* **512**:47-60.

Spinney L (2014) Alzheimer's disease: The forgetting gene. *Nature* **510**:26-28.

Stephenson FA (2006) Structure and trafficking of NMDA and $GABA_A$ receptors. *Biochemical Society Transactions* **34**:877-881.

Strømgaard K, Jensen LS and Vogensen SB (2005) Polyamine toxins: development of selective ligands for ionotropic receptors. *Toxicon : official journal of the International Society on Toxinology* **45**:249-254.

Strømgaard K and Mellor I (2004) AMPA receptor ligands: synthetic and pharmacological studies of polyamines and polyamine toxins. *Medicinal research reviews* **24**:589-620.

Stys PK and Lipton SA (2007) White matter NMDA receptors: an unexpected new therapeutic target? *Trends in pharmacological sciences* **28**:561-566.

Su B, Wang X, Nunomura A, Moreira PI, Lee HG, Perry G, Smith MA and Zhu X (2008) Oxidative stress signaling in Alzheimer's disease. *Current Alzheimer Research* **5**:525–532.

Sucher NJ, Akbarian S, Chi CL, Leclerc CL, Awobuluyi M, Deitcher DL, Wu MK, Yuan JP, Jones EG and Lipton SA (1995) Developmental and regional expression pattern of a novel NMDA receptor-like subunit (NMDAR-L) in the rodent brain. *The Journal of Neuroscience* **5**:6509-6520.

Sumikawa K, Houghton M, Emtage JS, Richards BM and Barnard EA (1981) Active multi-subunit ACh receptor assembled by translation of heterologous mRNA in *Xenopus* oocytes. *Nature* **292**:862-864.

Sun L, Margolis FL, Shipley MT and Lidow MS (1998) Identification of a long variant of mRNA encoding the NR3 subunit of the NMDA receptor: its regional distribution and developmental expression in the rat brain. *FEBS Letters* **441**:392–396.

Suzuki Y, Goetze TA, Stroebel D, Balasuriya D, Yoshimura SH, Henderson RM, Paoletti P, Takeyasu K and Edwardson JM (2013) Visualization of structural changes accompanying activation of *N*-methyl-D-aspartate (NMDA) receptors using fast-scan atomic force microscopy imaging. *The Journal of biological chemistry* **288**:778-784.

Swanger SA, Vance KM, Pare JF, Sotty F, Fog K, Smith Y and Traynelis SF (2015) NMDA receptors containing the GluN2D subunit control neuronal function in the subthalamic nucleus. *The Journal of Neuroscience* **35**:15971-15983.

Tabner BJ, El-Agnaf OM, German MJ, Fullwood NJ and Allsop D (2005) Protein aggregation, metals and oxidative stress in neurodegenerative diseases. *Biochemical Society Transactions* **33**:1082-1086.

Tackenberg C, Grinschgl S, Trutzel A, Santuccione AC, Frey MC, Konietzko U, Grimm J, Brandt R and Nitsch RM (2013) NMDA receptor subunit composition determines beta-amyloid-induced neurodegeneration and synaptic loss. *Cell Death and Disease* **4**:e608.

Takatsuki K, Kawahara S, Takehara K, Kishimoto Y and Kirino Y (2001) Effects of the noncompetitive NMDA receptor antagonist MK-801 on classical eyeblink conditioning in mice. *Neuropharmacology* **41**:618–628.

Tamagno E, Bardini P, Obbili A, Vitali A, Borghi R, Zaccheo D, Pronzato MA, Danni O, Smith MA, Perry G and Tabaton M (2002) Oxidative stress increases expression and activity of BACE in NT_2 neurons. *Neurobiology of Disease* **10**:279-288.

Tamburri A, Dudilot A, Licea S, Bourgeois C and Boehm J (2013) NMDA-receptor activation but not ion flux is required for amyloid-beta induced synaptic depression. *PLoS One* **8**.

Texido L, Martin-Satue M, Alberdi E, Solsona C and Matute C (2011) Amyloid beta peptide oligomers directly activate NMDA receptors. *Cell Calcium* **49**:184-190.

Tong G, Takahashi H, Tu S, Shin Y, Talantova M, Zago W, Xia P, Nie Z, Goetz T, Zhang D, Lipton SA and Nakanishi N (2008) Modulation of NMDA receptor properties and synaptic transmission by the NR3A subunit in mouse hippocampal and cerebrocortical neurons. *Journal of neurophysiology* **99**:122-132.

Traynelis SF, Wollmuth LP, McBain CJ, Menniti FS, Vance KM, Ogden KK, Hansen KB, Yuan H, Myers SJ and Dingledine R (2010) Glutamate receptor ion channels: structure, regulation, and function. *Pharmacological reviews* **62**:405-496.

Um JW, Nygaard HB, Heiss JK, Kostylev MA, Stagi M, Vortmeyer A, Wisniewski T, Gunther EC and Strittmatter SM (2012) Alzheimer amyloid-β oligomer bound to postsynaptic prion protein activates Fyn to impair neurons. *Nature neuroscience* **15**:1227-1235.

Urwyler S, Floersheim P, Roy BL and Koller M (2009) Drug design, in vitro pharmacology, and structure-activity relationships of 3-acylamino-2-aminopropionic acid derivatives, a novel class of partial agonists at the glycine site on the N-methyl-D-aspartate (NMDA) receptor complex. *Journal of Medicinal Chemistry* **52**:5093-5107.

Varadarajan S, Kanski J, Aksenova M, Lauderback C and Butterfield DA (2001) Different mechanisms of oxidative stress and neurotoxicity for Alzheimer's Aβ(1-42) and Aβ(25--35). *Journal of the American Chemical Society* **123**:5625-5631.

Vassar R (1999) Beta-secretase cleavage of Alzheimer's amyloid precursor protein by the transmembrane aspartic protease BACE. *Science* **286**:735-741.

Verdoorn TA, Kleckner NW and Dingledine R (1987) Rat brain *N*-methyl-D-aspartate receptors expressed in *Xenopus* oocytes. *Science* **238**:1114-1116.

Verkhratsky A and Kirchhoff F (2007) NMDA receptors in glia. *Neuroscientist* **13**:28-37.

Villarroel A, Burnashev N and Sakmann B (1995) Dimensions of the narrow portion of a recombinant NMDA receptor channel. *Biophysical journal* **68**:866-875.

Vrajova M, Stastny F, Horacek J, Lochman J, Sery O, Pekova S, Klaschka J and Hoschl C (2010) Expression of the hippocampal NMDA receptor GluN1 subunit and its splicing isoforms in schizophrenia: postmortem study. *Neurochemical research* **35**:994-1002.

Wada A, Takahashi H, Lipton SA and Chen HS (2006) NR3A modulates the outer vestibule of the "NMDA" receptor channel. *The Journal of neuroscience : the official journal of the Society for Neuroscience* **26**:13156-13166.

Walsh DM, Klyubin I, Fadeeva JV, Cullen WK, Anwyl R, Wolfe MS, Rowan MJ and Selkoe DJ (2002) Naturally secreted oligomers of amyloid β protein potently inhibit hippocampal long-term potentiation *in vivo*. *Nature* **416**:535-539.

Walsh DM and Selkoe DJ (2004) Deciphering the molecular basis of memory failure in Alzheimer's disease. *Neuron* **44**:181-193.

Wang J, Ono K, Dickstein DL, Arrieta-Cruz I, Zhao W, Qian X, Lamparello A, Subnani R, Ferruzzi M, Pavlides C, Ho L, Hof PR, Teplow DB and Pasinetti GM (2011) Carvedilol as a potential novel agent for the treatment of Alzheimer's disease. *Neurobiology of Aging* **32**:2321.

Washburn MS, Numberger M, Zhang S and Dingledine R (1997) Differential dependence on GluR2 expression of three characteristic features of AMPA receptors. *The Journal of Neuroscience* **17**:9393–9406.

Watkins JC and Jane DE (2006) The glutamate story. *British Journal of Pharmacology* **147 Suppl 1**:S100-108.

Weinreb O, Mandel S, Bar-Am O, Yogev-Falach M, Avramovich-Tirosh Y, Amit T and Youdim MB (2009) Multifunctional neuroprotective derivatives of rasagiline as anti-Alzheimer's disease drugs. *Neurotherapeutics* **6**:163-174.

Weiss JN (1997) The Hill equation revisited: uses and misuses. *The FASEB Journal* **11**:835-841.

Wenthold RJ, Petralia RS, Blahos JI and Niedzielski AS (1996) Evidence for multiple AMPA receptor complexes in hippocampal CA1/CA2 neurons. *The Journal of Neuroscience* **76**:1982-1989.

Williams K (1997a) Interactions of polyamines with ion channels. *Biochemical Journal* **325**:289–297.

Williams K (1997b) Modulation and block of ion channels: A new biology of polyamines. *Cell Signal* **9**:1-13.

Williams K, Pahk AJ, Kashiwagi K, Masuko T, Nguyen ND and Igarashi K (1998) The selectivity filter of the *N*-methyl-D-aspartate receptor: a tryptophan residue controls block andpermeation of Mg^{2+}. *Molecular Pharmacology* **53**:933-941.

Winblad B, Giacobini E, Frölich L, Friedhoff LT, Bruinsma G, Becker RE and Greig NH (2010) Phenserine efficacy in Alzheimer's disease. *Journal of Alzheimer's Disease* **22**:1201-1208.

Wollmuth LP, Kuner T and Sakmann B (1998a) Adjacent asparagines in the NR2-subunit of the NMDA receptor channel control the voltage-dependent block by extracellular Mg^{2+}. *The Journal of physiology* **506.1**:13—32.

Wollmuth LP, Kuner T and Sakmann B (1998b) Intracellular Mg^{2+} interacts with structural determinants of the narrow constriction contributed by the NR1-subunit in the NMDA receptor channel. *The Journal of physiology* **506**:13-32.

Wollmuth LP, Kuner T, Seeburg PH and Sakmann B (1996) Differential contribution of the NR1- and NR2A-subunits to the selectivity filter of recombinant NMDA receptor channels. *The Journal of physiology* **491**:779-797.

Wollmuth LP and Sakmann B (1998) Different mechanisms of Ca^{2+} transport in NMDA and Ca^{2+}-permeable AMPA glutamate receptor channels. *The Journal of general physiology* **112**:623-636.

Wong EH, Kemp JA, Priestley T, Knight AR, Woodruff GN and Iversen LL (1986) The anticonvulsant MK-801 is a potent *N*-methyl-D-aspartate antagonist. *Proceedings of the National Academy of Sciences of the United States of America* **83**:7104-7108.

Wong HK, Liu XB, Matos MF, Chan SF, Perez-Otano I, Boysen M, Cui J, Nakanishi N, Trimmer JS, Jones EG, Lipton SA and Sucher NJ (2002) Temporal and regional expression of NMDA receptor subunit NR3A in the mammalian brain. *The Journal of comparative neurology* **450**:303-317.

Woodhull AM (1973) Ionic blockage of sodium channels in nerve. *The Journal of general physiology* **61**:687-708.

Wrighton DC, Baker EJ, Chen PE and Wyllie DJ (2008) Mg^{2+} and memantine block of rat recombinant NMDA receptors containing chimeric NR2A/2D subunits expressed in *Xenopus laevis* oocytes. *The Journal of physiology* **586**:211-225.

Wyeth MS, Pelkey KA, Petralia RS, Salter MW, McInnes RR and McBain CJ (2014) Neto auxiliary protein interactions regulate kainate and NMDA receptor subunit localization at mossy fiber-CA3 pyramidal cell synapses. *The Journal of Neuroscience* **34**:622-628.

Wyllie DJ, Livesey MR and Hardingham GE (2013) Influence of GluN2 subunit identity on NMDA receptor function. *Neuropharmacology*.

Wyllie DJ and Traynelis SF (2012) NMDA receptor permeation: a light in the tunnel. *Nature neuroscience* **15**:343-344.

Yamakura T, Mori H, Masaki H, Shimoji K and Mishina M (1993) Different sensitivities of NMDA receptor channel subtypes to non-competitive antagonists. *NeuroReport* **4**:687-690.

Yamazaki M, Mori H, Araki K, Mori KJ and M. M (1992) Cloning, expression and modulation of a mouse NMDA receptor subunit. *FEBS Letters* **300**:39-45.

Yang G, Wang Y, Tian J and Liu JP (2013) Huperzine A for Alzheimer's disease: a systematic review and meta-analysis of randomized clinical trials. *PLoS One* **8**:e74916.

Yao Y and Mayer ML (2006) Characterization of a soluble ligand binding domain of the NMDA receptor regulatory subunit NR3A. *The Journal of Neuroscience* **26**:4559-4566.

Youdim MB (2006) The path from anti Parkinson drug selegiline and rasagiline to multifunctional neuroprotective anti Alzheimer drugs ladostigil and m30. *Curr Alzheimer Res* **3**:541-550.

Younkin SG (2006) *PS1, PS2*, and *APP* mutations that cause Alzheimer's disease increase Aβ42, in *Alzheimer: 100 Years and Beyond* (Jucker M, Beyreuther K, Haass C, Nitsch RM and Christen Y eds) pp 189-195, Springer Berlin Heidelberg, Berlin, Heidelberg.

Yuan H, Hansen KB, Vance KM, Ogden KK and Traynelis SF (2009) Control of NMDA receptor function by the NR2 subunit amino-terminal domain. *The Journal of Neuroscience* **29**:12045-12058.

Zhua Y and Auerbacha A (2001) Na^+ occupancy and Mg^{2+} block of the *N*-methyl-D-aspartate receptor channel. *The Journal of general physiology* **117**:275–286.

Zimmer M, Fink TM, Franke Y, Lichter P and Spiess J (1995) Cloning and structure of the gene encoding the human *N*-methyl-D-aspartate receptor (NMDAR1). *Gene* **159**:219-223.

Zini M, Passariello CL, Gottardi D, Cetrullo S, Flamigni F, Pignatti C, Minarini A, Tumiatti V, Milelli A, Melchiorre C and Stefanelli C (2009) Cytotoxicity of methoctramine and methoctramine-related polyamines. *Chemico-biological interactions* **181**:409-416.

Appendix

Abstract presented at the 10th FENS Forum of Neuroscience 2016, Copenhagen, Denmark, 2nd – 6th July 2016.

RR Mutation at the "Q/R/N" and +1 Sites of the NMDA Receptor Channel Reduced the Potencies of Open Channel Blockers

N-methyl-D-aspartate receptors (NMDAR) are ionotropic glutamate receptors which are susceptible to block by Mg^{2+} and are highly permeable to Ca^{2+} hence representing a medically relevant target for neurodegenerative disorders caused by excitotoxicity. Our study focused on the M2 region of the NMDAR which is important in ion selectivity. Previous findings have shown that rat GluN3A and GluN3B subunits containing GR at the "Q/R/N" and +1 position in the M2 region results in reduced potency of channel blockers on NMDAR. In human GluN3B, these sites are occupied by RR which could render even higher resistance to channel block. We tested this hypothesis by mutating NN at the "Q/R/N" and +1 sites in GluN2A subunits to RR and characterised this with several open channel blockers namely Mg^{2+} (endogenous NMDAR blocker), memantine, MK-801 and philanthotoxin-343. Also of significant interest is the -8 position, where W in GluN2A subunits were mutated to N as found in both rat GluN3 and human GluN3B subunits. Wild type and mutated GluN2A were co-expressed with GluN1-1a in *Xenopus* oocytes and responses to NMDA/glycine were recorded using two-electrode voltage clamp. At -75mV, IC_{50}s for Mg^{2+}, memantine and MK-801 were 3.97µM, 1.01µM, 0.033µM, respectively, on wild type NMDAR but increased 27-, 42- and 325-fold for NMDAR containing the RR mutation. W to N mutation at the -8 position resulted in a slight increase (2-fold) of memantine IC_{50} while the blocking potencies of Mg^{2+}, MK-801 and philanthotoxin-343 were not significantly affected. Blocking potency for PhTX-343, however, does not appear to be altered by all mutations as no significant differences were observed across all subunit combinations.

Abstract presented at the 12th International Conference on Alzheimer's and Parkinson's Diseases, AD/PD™ 2015, Nice, France, 18th – 22nd March, 2015.

Evaluation of Novel Polyamine & Memantine-Derivative Compounds Targeting NMDA Receptors for Alzheimer's Disease Treatment.

Objectives: To evaluate novel compounds as potential treatment for Alzheimer's disease targeting *N*-methyl-D-aspartate receptor (NMDAR). These ionotropic glutamate receptors are highly permeable to Ca^{2+}, thus are implicated with excitotoxicity in neurodegenerative disorders.

Methods: The *Xenopus laevis* oocyte expression system was employed in this study where cRNAs for NMDAR subunits were injected into the oocytes and responses to NMDA/glycine and channel blockers were recorded using two-electrode voltage clamp. Three novel polyamine compounds (CR) and eight memantine-derivatives (MAB) incorporated with antioxidant groups (alpha-tocopherol, lipoic acid, melatonin and methoxyphenol) were tested on GluN1/2A NMDAR subunits at -60 mV and compared with Mg^{2+} and memantine.

Results: All spermine-derived CR compounds proved to be highly effective in blocking the NMDAR channel; CR18, CR8 and CR24 recorded IC_{50}s of 0.692, 2.214 and 2.352 µM respectively, all significantly lower than Mg^{2+} (IC_{50} = 10.08 µM). MAB compounds were much less potent; MAB22, MAB30, MAB14 and MAB7 recorded the lowest IC_{50}s (26.90, 38.19, 43.09 and 55.92 µM respectively) versus memantine (IC_{50} = 3.178 µM) while the rest were all higher than 100 µM. This suggests the loss of memantine functionality due to attachment of the antioxidant structure to its amine group. All compounds were also found to act through a voltage-dependent manner assessed via the Woodhull model.

Conclusions: Our data suggests that the CR compounds particularly CR18 (spermine polyamine incorporated with alpha-tocopherol) has the potential for development of Alzheimer's disease treatment which not only can inhibit excitotoxicity, but also suppresses oxidative stress and β-amyloid plaques.